A RESEARCH MONOGRAPH

IDENTIFIABLE BULK GEOMETRY

Dynamical Completion and Observational Limits in Braneworld Cosmology

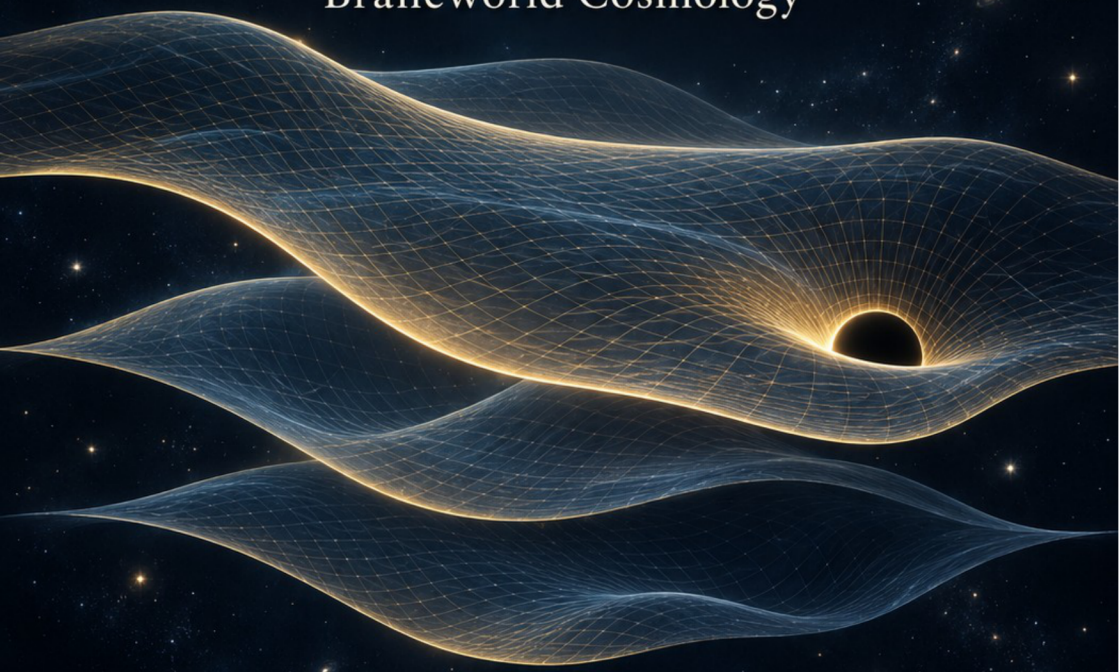

Mohammed F. A. Alghenaim

THIRD EDITION • 2026

Identifiable Bulk Geometry

Dynamical Completion and Observational Limits in Braneworld Cosmology

Mohammed F. A. Alghenaim

Third edition
A5 scientific revision
12 October 2026

Publication and Editorial Note

© 2026 Mohammed F. A. Alghenaim.

Identifiable Bulk Geometry
Dynamical Completion and Observational Limits in Braneworld Cosmology
Third edition, 2026.

This third edition develops the supplied research manuscripts and the subsequent scientific revisions into a connected English monograph. Its nineteen chapters retain the original conventions and add explicit proofs, finite-data certificates, positive-signal calibration and physical comparison results. Numerical examples, synthetic studies and observational comparisons state their separate assumptions and evidence.

AI tools assisted drafting of the third-edition additions, mathematical cross-checks, computational figures, document preparation and conceptual cover artwork. The companion retains the calculations, source records and internal checks. These do not constitute external peer review. Scientific responsibility and any subsequent publication decisions remain with the author.

The book includes linked contents, numbered native equations, figure and table lists, a notation guide, six appendices, an expanded glossary, references and a subject index. The companion preserves the earlier calculations and adds executable certificates, complete production simulation records, exact examples and verification reports for Chapters 15–18.

This third edition adds common-history certificates and correlated geometric bounds, 43,128 nonlinear simulations across a declared finite parameter grid, an observable-equivalence analysis and a complete sound-history classification with free spatial curvature. The original 10,000-draw null experiment is retained. The new simulations add no astronomical observations. Their retrospective design and finite-grid scope are explicit in Chapter 16; Appendix D records reproduction and Appendix E maps contributions and antecedents.

Cover image: conceptual illustration of a brane and surrounding bulk geometry. It is not a numerical spacetime diagram.

Abstract

Cosmological reconstruction constrains a gravitational model without necessarily identifying every parameter or selecting its physical origin. This book studies a conserved barotropic component on a homogeneous brane in a five-dimensional Einstein bulk. With supplied curvature, an exact sound history defines four expansion columns, whose exceptional dependence is classified by a Riccati equation. Releasing spatial curvature adds a fifth column; the third edition classifies its causal exceptional histories by quadratic and shifted-square-root relations.

When the effective vacuum intercept is free, identified coefficients determine a continuous normalization family. Within the stated rank and physical conditions, $L=\beta_1^2/(4\beta_2)-\beta_0$ and d remain constant along that family and determine bulk metric coefficients at fixed reference scales. A new exact example shows that freeing spatial curvature can preserve the entire expansion and sound histories while changing both geometric quantities. A transverse scalar calibration removes the added coefficient freedom precisely when its prediction changes along the null direction.

Finite information is treated through one shared history. A fixed Lipschitz sound class admits finite-mesh outer transport bounds, explicit witnesses and conservative exclusions. The normalized transport error has a sharp $\tanh(r/2)$ envelope under its stated multiplicative bound. Exact convex certificates retain coefficient correlations and can establish positive L when a bounding rectangle cannot. Finite geometric diameter bounds and verified two-model constructions quantify both attainable and unavoidable error.

Reserved fifth- and sixth-epoch contrasts provide exact conditional Gaussian checks when sound, design and covariance are fixed. Simultaneous outer sets propagate specified sound and expansion uncertainty. Selection, unknown covariance, unmeasured calibration and unresolved boxes remain distinct from a validated inverse.

The action analysis separates identical-action vacuum splitting from overall classical scaling, constructs local kinetic realizations and audits the cubic vacuum defect and its canonical repair. A conserved four-dimensional fluid model exactly reproduces the positive dust-branch background. Gaussian comparison theorems state the separation required for discrimination under declared prediction sets, while a signed alternative demonstrates the limitation of pairwise distance alone.

The retained late-time likelihood uses 13 DESI DR2 BAO entries and 1590 Pantheon+ light-curve records with their covariance matrices. Its specified flat

dust branch has a zero-quadratic-correction optimum. The original positive profile crosses $\Delta\chi^2 = 2.7055$ at $\Omega_q = 0.0002534$; that crossing remains a conditional reference value, not a continuous coverage-calibrated bound. The earlier 10,000-draw pointwise null experiment is preserved.

A further 43,128 fully nonlinear simulated fits use eight generating corrections and nine nuisance points, with separate calibration and validation vectors. A Monte Carlo rank construction yields a discrete inversion and a finite-grid coverage theorem for the frozen procedure when the truth lies on its declared grid. Because the grid was selected after examining the historical fit, the observed inversion is explicitly retrospective. No continuous nuisance-space guarantee, new empirical detection or complete brane–bulk perturbation solution is claimed.

Keywords: braneworld cosmology; inverse problems; identifiability; common-history certificates; spatial curvature; vacuum normalization; kinetic scalar fields; Monte Carlo calibration; observable equivalence; bulk geometry.

Scientific Overview

This volume establishes a hierarchy of identifiable quantities in a specified braneworld inverse problem and develops finite certificates for assessing that hierarchy with imperfect information. The assumptions include a homogeneous brane in a five-dimensional Einstein bulk, conserved barotropic matter, fixed reference conventions and stated sign and regularity restrictions. Chapters 5–6 treat the supplied-curvature inverse; Chapters 15–18 develop finite-error certification, positive-signal calibration, physical comparison and the extension to free spatial curvature. Sections E.5–E.6 map the results to their proofs, evidence and antecedents.

The established junction and conservation equations turn a supplied derivative $\chi = d\,p/d\,v$ into a transport coordinate J. With curvature supplied, the expansion has four known columns. Theorem 5.1 gives the complete Riccati criterion for their dependence; Theorem 6.1 gives the full free-vacuum family. Rank four and the AdS conditions identify L and d within that family. When curvature is free, Theorem 18.1 classifies dependence of $1, J, J^2, U, U^2$, where $U = e^{-2s}$. The distinction makes the curvature assumption explicit in every geometric interpretation. Finite design and conditioning remain separate questions.

The literature already contains gravitational dark-sector degeneracies, a brane-tension degeneracy in inflationary reconstruction, fluid–scalar equivalence and kinetic reconstruction. The contribution assessed here is the explicit set of hypotheses, equivalence classes, rank criteria and observation requirements developed in this volume. “Theorem proved in this volume” identifies a proof that readers can examine; it does not assert global priority. Likewise, the Gaussian information split used for selected-mode validation is an application of established statistical methodology. The related-literature section states the nearest verified connections and the distinctions in target and assumptions. [33–35; 51–55; 58]

The dynamical chapters determine what an inverse implies about an action. An unchanged sum $\lambda + U_0$ is an exact relabeling freedom, whereas an overall multiplication of the action is a separate normalization question. The cubic example gives linked conditional predictions $c_\phi^2 = 1/5$ and excitation density proportional to $a^{-18/5}$, while its zero-gradient vacuum has a vanishing quadratic kinetic operator. The canonical repair changes the sound law and follows the joint consistency relations in Proposition 17.4. The quoted temperatures 274.7 and 488.5 GeV are declared radiation benchmarks, not predicted particle thresholds.

The empirical calculation has a narrower target. It fits the unexcited-scalar dust background with 13 DESI DR2 BAO entries and 1590 Pantheon+ light-curve records from 1473 distinct CID labels. In the tested nonnegative branch, the optimum is $\Omega_q = 0$. The original profile crossings are 0.0002534 at level 2.7055 and 0.0003346 at level 3.8415. Chapter 16 adds a frozen finite-grid rank inversion and 43,128 new simulated fits to the earlier null study. The grid is retrospective, the observation model is retained, and no continuous endpoint guarantee follows. Neither distance study measures the dark-fluid sound input. [43; 46–48; 59–62]

Chapter 15 demonstrates finite common-path exclusion with overlapping sound windows and two density drops, and gives a correlated region with exact positive bounds on L. Its upper diameter bound is paired with explicit physical models that establish a lower limit on possible accuracy. Chapter 18 proves that unknown spatial curvature can add ambiguity even when the original four-column inverse has full rank. Both extensions are accompanied by inspectable calculations and complete statements of their domains.

Chapter 17 constructs a positive four-dimensional background competitor and distinguishes equality of expansion histories from equality of complete observation laws. It proves a vacuum-split estimation obstruction, linked kinetic consistency and Gaussian separation criteria. These results determine what a future test must distinguish before a background coefficient can be interpreted as evidence for a particular gravitational origin. [51; 54; 63]

The next empirical advance is a forward model that connects raw distance and perturbation observables to the common sound and expansion inputs, with consistent matter content, local gravitational matching and bulk boundary conditions. The testability register specifies the required inputs, target observables and decision rules. It separates checks already executed from proposed measurements, and it makes the assumptions that would be rejected together explicit. A successful test can restrict this model class and its parameter combinations; comparison with a broader gravitational interpretation requires declared alternative models.

Author's Preface

My aim is to make a demanding question precise: which features of a gravitational model can be learned from cosmological histories? An equation may fit an expansion curve while leaving several physical ingredients interchangeable. Understanding that freedom is part of understanding the theory.

I have organized the account around physical meaning before algebraic technique. A geometrical quantity needs an operational interpretation. A reconstruction needs assumptions, an explicit inverse and a test of uniqueness. A matter history must satisfy conservation throughout one common evolution. Finally, an action must explain what its parameters mean and how a measurement could fix their normalization. Each step deserves its own argument.

The book brings a sequence of research manuscripts into one exposition. Earlier studies investigate finite geometry, matter calibration, sound information and statistical validation. The final study adds covariant normalization, kinetic dynamics and observational scale limits. Their synthesis matters because a weakness at one level can change another result's interpretation. Exact reconstruction can coexist with normalization freedom; local scalar stability can coexist with an unresolved vacuum limit; a precise fit can coexist with an experiment whose statistical calibration remains incomplete.

I want readers to inspect the results and their limits. Definitions and units are collected for reference. Formulas are numbered, worked examples state their inputs, and the computational record distinguishes calculations made for this edition from results reported in its sources. A claim can thus be traced to the hypothesis or calculation on which it depends.

The retained public-data distance calculation has a zero-correction optimum in its specified branch. The third edition expands its statistical assessment through positive generating signals, separate validation draws and an explicit finite-grid procedure. The added calculations clarify the interpretation of the same observations; they do not create a new measurement of the sound history required by the general inverse.

The third-edition additions turn several earlier questions into proved statements and reproducible examples. Shared-path certificates make finite compatibility inspectable. Correlated bounds preserve information lost by independent coefficient intervals. Explicit alternative backgrounds and the free-curvature classification identify limits that must accompany a geometric claim. The

contribution map distinguishes these additions from established methods and from proposed physical measurements.

The purpose is to connect reconstruction with measurable physics through results whose assumptions, derivations and numerical status can be checked. This volume provides a foundation for testing the stated research program and for extending it where a new physical calculation or independent observation supplies the missing information.

Mohammed F. A. Alghenaim

Introduction to the Book

This volume asks how much bulk geometry a cosmological history determines when matter calibration and vacuum normalization are uncertain. The principal inverse uses calculus, ordinary differential equations and linear algebra, together with the Friedmann description of cosmology. The dynamical chapters assume familiarity with general relativity and variational field theory; the statistical chapters require covariance matrices, likelihoods and repeated-sampling inference. Appendix F supplies detailed mathematical arguments that may be read alongside Chapters 4–6.

Chapters 1–3 distinguish observables from parameter labels, state the braneworld conventions and explain finite-epoch reconstruction. Rank supplies a uniqueness condition; projection and short-interval expansions explain why information can remain weak. Chapter 4 requires one common matter history, so finite density values, calibration and sound windows refer to the same conserved fluid.

Chapters 5–6 develop the structural inverse. Sound defines transport functions, making the expansion quadratic in one coordinate plus a dark-radiation term. An exceptional Riccati family marks the failure of complete-history identification. Free vacuum produces a family of physical descriptions. A worked example shows which bulk quantities survive and why one density anchor can be insufficient.

Chapters 7–9 address imperfect information. Sound windows have transfer functions and aliases. Frequency selection changes the statistical problem. Independent training and validation, bounded leakage and covariance calibration give guarantees for specified experiments. Simultaneous outer confidence sets then propagate uncertainty into the physical inverse.

Chapters 10–14 connect the inverse to an action, audit kinetic examples, calculate physical scales and state the links needed to local gravity and perturbations. Chapter 14 retains the earlier testability register. The new synthesis in Chapter 19 incorporates the subsequent mathematical, statistical and physical additions.

Sections 13.7–13.15 preserve the public-data distance fit, sensitivity profiles, pointwise null simulation and local-information diagnostic. Chapter 16 extends this calculation with positive-signal calibration and a discrete inversion under a frozen, retrospective design. Continuous-parameter coverage, a complete early-universe likelihood and local gravitational matching remain distinct tasks.

Chapter 15 gives finite common-history certificates, correlated geometric bounds and upper and lower accuracy statements. Chapter 17 constructs explicit physical comparisons and tests the separation of declared predictions. Chapter 18 classifies the extended inverse when spatial curvature is free. Chapter 19 states the resulting conclusions and the information still required for empirical discrimination.

The appendices provide units, reconstruction procedures, a separate scalar–tensor comparison, the computational record, a source and contribution guide, and complete finite-constraint proofs. The glossary and subject index support later reference. An exact history, finite observations, a noisy window and a normalized action provide different information; retain the hypotheses beside each conclusion.

Contents

Abstract ..... **iii**
Scientific Overview ..... **v**
Author's Preface ..... **vii**
Introduction to the Book ..... **ix**
List of Figures ..... **xviii**
List of Tables ..... **xix**
Notation and Conventions ..... **xxi**
1 Geometry as an Observable **1**
1.1 The question behind reconstruction 1
1.2 What a geodesic triangle measures 2
1.3 Intrinsic and extrinsic curvature 3
1.4 Spatial geometry and optical geometry 4
1.5 The observational interface 6
1.6 Three levels of inference 6
2 The Braneworld Background and Its Conventions **8**
2.1 The model being reconstructed 8
2.2 From the junction condition to expansion 9
2.3 Dimensionless reconstruction variables 11
2.4 What it means to vary tension 12
2.5 Bulk geometry and the horizon 13
2.6 Background closure and dynamical closure 14
3 Identification from Finitely Many Epochs **15**
3.1 A straight line hidden in the background equation 15
3.2 Nuisance directions and exact degeneracy 16
3.3 Correlated errors and projected information 17
3.4 Why a short interval can contain little information 18
3.5 Constant density gain and a tension invariant 20
3.6 Confidence regions for a nonlinear ratio 21
3.7 From a fitted coefficient to a physical claim 22

4 Matter Histories and Common Reconstruction.....24
4.1 What a common history must satisfy.....24
4.2 Density calibration as a functional constraint.....25
4.3 Causal matter on a complete residual curve.....26
4.4 Finite values and exact reachable drops.....27
4.5 Smooth completion and the information in anchors.....30
4.6 Windows constrain integrals of the same history.....32
5 Sound Coordinates and Exceptional Histories.....35
5.1 Conservation supplies a useful coordinate.....35
5.2 A complete classification of rank failure.....36
5.3 Complete histories and finite epochs.....39
5.4 Differential and weak consistency.....40
5.5 A prediction at a reserved expansion epoch.....41
5.6 Numerical conditioning near the exceptional history.....43
6 Uncertain Vacuum and Identifiable Bulk Geometry.....47
6.1 Releasing the vacuum intercept.....47
6.2 The complete physical family.....47
6.3 Geometry that survives the freedom.....49
6.4 Why one density anchor can be insufficient.....51
6.5 From a reconstruction orbit to an action convention.....53
6.6 The limits of the invariant statement.....55
7 Sound Windows and Spectral Recovery.....57
7.1 A logarithmic modulation is a hypothesis.....57
7.2 What a sound window measures.....58
7.3 Multiple modes need additional structure.....59
7.4 Exact blindness and stable design.....61
7.5 When expansion adds independent information.....63
7.6 Unknown frequency and weak signals.....64
8 Selection and Covariance in Statistical Validation.....67
8.1 State the experiment before stating significance.....67
8.2 Calibrating a nonlinear search algorithm.....68

8.3 Independent validation with known covariance....70
8.4 A primary frequency interval leaves bounded leakage....72
8.5 Unknown covariance requires a different observation model....74
8.6 What numerical validation can establish....76
8.7 Allocate the error budget across the scientific claim....78
9 Confidence Sets for Physical Parameters....79
9.1 Retaining everything the observations permit....79
9.2 From window means to a continuous sound band....80
9.3 Propagating uncertainty without linearizing the sound error....81
9.4 A confidence set for the entire fixed-vacuum inverse....82
9.5 The correct extension when the vacuum is free....84
9.6 Rank certification and continuous weak information....85
9.7 What the computational evidence establishes....86
10 Covariant Completion and Vacuum Normalization....88
10.1 From a reconstructed history to a dynamical question....88
10.2 Field equations and the scalar fluid....90
10.3 A constructive local realization theorem....91
10.4 Constant vacuum splitting is an exact redundancy....92
10.5 Overall action scaling is a different freedom....93
10.6 Background coupling and local gravitational matching....93
10.7 Which additional assumptions carry information....95
11 Kinetic Actions and Local Consistency....97
11.1 Constant sound speed and an affine equation of state....97
11.2 What the kinetic signs test....98
11.3 The cubic example has a degenerate zero-gradient vacuum....99
11.4 Adding a canonical term changes the fluid....100
11.5 Evolution from the equation of motion and from the current....101
11.6 What canonical normalization does and does not fix....103
12 Physical Scales, Acceleration, and Varying Tension....105
12.1 The size of the direct quadratic term....105
12.2 A declared present-density benchmark....106

12.3 The early high-density window....109
12.4 An acceleration obstruction....110
12.5 A varying tension must enter a conserved action....111
13 Observational Interfaces....114
13.1 An observable needs a forward model....114
13.2 The local gravitational matching problem....115
13.3 Sound speed does not close the bulk perturbations....116
13.4 What the clock and ranging source actually establishes....117
13.5 A restricted DESI comparison....118
13.6 Reproducible calculations and an observational decision....120
13.7 A specified background from the action....121
13.8 Public observations and retained information....123
13.9 Forward distances and nuisance elimination....124
13.10 Fits and conditional quadratic profiles....126
13.11 Sensitivity and numerical audit....129
13.12 From a distance allowance to a physical scale....133
13.13 Interpretation and the next empirical test....134
13.14 Pointwise plug-in null calibration....136
13.15 Local sensitivity and the efficient-score diagnostic....140
14 What Is Established and What Remains to Be Measured....144
14.1 The result is a hierarchy of identifiable quantities....144
14.2 What the dynamical completion adds....145
14.3 The direct late-time quadratic route is quantitatively restricted....147
14.4 A measurement of the inverse requires its own forward model....148
14.5 Two physically concrete routes beyond the present model....149
14.6 A register of testable claims....151
14.7 Evidence, independent comparisons and scientific responsibility....156
15 Certificates for Finite Observations....158
15.1 The object being certified....158

15.2 A finite mesh enclosing one sound path.....159
15.3 Normalization without losing the useful bound.....161
15.4 An executable witness-or-exclusion procedure.....163
15.5 A finite experiment with genuinely shared constraints.....165
15.6 Correlated finite-error bounds for the invariant.....167
15.7 Quantitative stability and its converse.....170
15.8 Reproduction and the remaining scope.....174
16 Calibration Beyond the Zero Signal.....177
16.1 The experiment and its physical scope.....177
16.2 Upper exclusion and positive detection are different tests.....179
16.3 A finite-grid rank construction.....180
16.4 What is conditional, and what was already selected.....183
16.5 Why the positive-signal critical value can change.....184
16.6 The retrospective inversion on unchanged observations.....186
16.7 Fresh-data coverage and power.....188
16.8 Nuisance control and a quantitative route beyond the grid.....191
16.9 Numerical verification and reproducibility.....193
16.10 What has advanced, and what remains unresolved.....194
17 Observable Equivalence and Physical Discrimination.....197
17.1 The object that a measurement can distinguish.....197
17.2 A conserved effective source for a given background.....198
17.3 An exact positive-fluid competitor to Equation (13.5).....200
17.4 A quantitative no-go for the vacuum split.....202
17.5 Linked consistency relations for the kinetic repair.....204
17.6 Statistical indistinguishability of shared observables.....206
17.7 Exact power for two declared Gaussian predictions.....207
17.8 Composite prediction sets and certified separation.....208
17.9 Executed demonstrations and their scope.....211
17.10 The physical information needed for discrimination.....214
18 Free Spatial Curvature and Exceptional Sound Histories.....216
18.1 The fifth reconstruction column.....216

18.2 Complete classification of rank failure....218
18.3 Constant sound and finite epoch identification....219
18.4 A causal example with changing bulk geometry....221
18.5 The calibration that removes the added freedom....225
18.6 A sixth epoch as a reserved test....227
18.7 What the extension changes....228
19 What the Third Edition Establishes....230
19.1 The exact inverse after its assumptions are exposed....230
19.2 What finite observations can now certify....231
19.3 What the expanded calibration answers....233
19.4 What a future positive coefficient would establish....234
19.5 The remaining research question....236
Appendix A Units and Convention Crosswalk....237
A.1 Natural units and derivative conventions....237
A.2 Split tension and total vacuum stress....239
A.3 Dimensionless reconstruction and physical conversion....239
A.4 Coordinate normalization and SI restoration....240
Appendix B Reconstruction Algorithms....242
B.1 Choose the data problem....242
B.2 Exact sound with supplied vacuum....242
B.3 Exact sound with free vacuum....243
B.4 Finite values with a common matter history....244
B.5 Propagate a common uncertainty event....245
B.6 Report the scope of the result....246
Appendix C Scalar–tensor comparison and finite clock references....247
C.1 A separate four-dimensional model....247
C.2 Weak-source potentials and a common mass standard....248
C.3 Finite-reference identification....249
C.4 A derivative identity is not a unique signature....250
C.5 Higher-order clocks and a stellar precision limit....251

Appendix D Reproducible Calculations.....253
D.1 What the companion calculation contains.....253
D.2 Algebra and evolution checks.....254
D.3 Physical-scale inputs and results.....255
D.4 Figure provenance and interpretation.....257
D.5 Earlier numerical results.....257
D.6 Executed public distance analysis.....258
D.7 Reproducing the pointwise null experiment.....260
D.8 Exact-sound prediction, completion and conditioning.....261
D.9 Reproducing the positive-signal calibration.....262
D.10 Reproducing the new mathematical and physical certificates.....266
Appendix E Source Register and Result Map.....268
E.1 The manuscript sequence.....268
E.2 Relation to the final dynamical paper.....270
E.3 Verification and documentary boundaries.....272
E.4 Relation to established literature.....272
E.5 Contribution map and evidentiary categories.....274
E.6 Contributions and boundaries of the third edition.....278
Appendix F. Finite-constraint completion and recovery certificates.....281
F.1. A right inverse for the finite constraints.....281
F.2. Smooth completion with exact finite data.....283
F.3. Point sound anchors without a derivative budget.....286
F.4. Dense sound windows identify the fixed-vacuum parameter.....289
F.5. A minimal calibration of the free-vacuum orbit.....293
F.6. Finite-error certification of the geometric invariant.....295
Glossary.....297
Terms Added in the Third Edition.....300
References.....302
Subject Index.....309

List of Figures

Figure 1.1 Angular excess and constant curvature.....3
Figure 3.1 Nuisance projection on a short interval.....20
Figure 4.1 Shared histories and incompatible local tests.....29
Figure 5.1. Conditioning near the exceptional sound history.....45
Figure 6.1 Normalization freedom and invariant bulk curvature.....53
Figure 7.1 Window transfer and finite-band visibility.....62
Figure 8.1 Covariance estimation and false-positive rates.....77
Figure 11.1 Kinetic sound and conserved-current evolution.....102
Figure 12.1 Hierarchy of direct quadratic corrections.....108
Figure 13.1. Conditional profiles of the quadratic coefficient.....128
Figure 13.2. Ordered Cholesky-whitened residual diagnostics.....132
Figure 13.3. Pointwise null survival and Monte Carlo uncertainty.....139
Figure 13.4. Nonlinear refitting and the local score approximation.....142
Figure 15.1. Finite-observation witness and exclusion certificates.....166
Figure 15.2. Verified geometric indistinguishability near sound one third.....174
Figure 16.1. Positive-signal upper-statistic calibration.....186
Figure 16.2. Fresh-data power for the zero-correction test.....190
Figure 17.1. Gaussian power and the cost of an unknown alternative direction.....213
Figure 18.1. Free spatial curvature and an exact geometric ambiguity.....224

List of Tables

Table 2.1 Fixed inputs and the consequences of releasing them....12
Table 3.1 Exact nuisance degeneracies for a supplied density normalization....17
Table 4.1 Information inputs and the scope of common-history results....34
Table 5.1. Synthetic conditioning of the exact-sound inverse....44
Table 6.1 Two representatives sharing one density anchor....52
Table 7.1 Source-reported bias from omitting a sound mode....60
Table 7.2 Distinct questions in spectral reconstruction....65
Table 8.1 Statistical experiments and their validation targets....68
Table 10.1 Information needed to fix an action normalization....96
Table 12.1 Physical scales under the stated benchmark inputs....109
Table 13.1 Source-reported compressed-distance comparisons....119
Table 13.2. Data used in the executed likelihood....123
Table 13.3. Executed flat ΛCDM reference minima....126
Table 13.4. Positive Ωq crossings of reference profile levels....127
Table 13.5. Joint sensitivity at the $\Delta\chi^2 = 2.7055$ reference level....130
Table 13.6. Declared stress benchmarks and distance bounds....134
Table 13.7. Conditional null exceedances from simulated data....138
Table 14.1 Established results and the information they require....145
Table 15.1. Effect of the declared density error on the conflicting finite experiment. The sound data and Lipschitz budget stay fixed. An unresolved result is a property of the executed certificate, not a proof of feasibility....166
Table 15.2. Exact bounds from the same constructed coefficient region and its bounding rectangle. Decimal entries are descriptive roundings; the companion records exact fractions....169
Table 15.3. Verified indistinguishable model pairs. The expansion-noise radius is an unweighted Euclidean bound on six dimensionless values. Entries summarize full outward and rational checks stored in the companion....173

Table 16.1. Frozen simulation design; the historical fit was already known.....180
Table 16.2. Retrospective finite-grid acceptance on the historical data; not a prospectively selected continuous 95% confidence limit.....187
Table 16.3. Fresh validation at the central nuisance pair. Each entry is a count out of 200 independent data vectors, conditional on the stored calibration banks.....188
Table 17.1. A four-dimensional positive-fluid representation of the normalized expansion law.....201
Table 17.2. Exact Gaussian decision probabilities and synthetic replication checks at size 0.05.....212
Table 18.1. Exact physical representatives of one free-curvature expansion orbit. Reference scales are fixed; all entries are dimensionless.....222
Table 18.2. Exact projection of the declared curvature-anchor error. These are deterministic allowed ranges under exact expansion and sound, not confidence intervals.....226
Table A.1 Dimensions in the braneworld convention.....238
Table D.1 Declared physical-scale calculations.....255
Table D.2 Provenance of the scientific figures.....257
Table E.1 Source manuscripts and their destinations.....268
Table E.2. Contribution map with evidence and audit locations.....275
Table E.3. Third-edition result map. The evidence category belongs to each stated result and its assumptions.....279

Notation and Conventions

Natural units $c=\hbar=1$ are used unless a numerical conversion states otherwise. The metric signature is ¿ on the brane. The reference epoch is $s=0$, with $s=\log(a/a_{¿})$. A prime on a background function denotes d/ds; a dot denotes proper-time differentiation. Chapter-local indices on statistical matrices do not change these conventions.

Geometry and background reconstruction

Symbol	Meaning and convention
$a, a_{¿}$	Scale factor and its reference value; the convention used to give them length is stated with the bulk metric
H	Hubble expansion rate
k, ℓ, μ_B	Spatial-curvature index, AdS radius and geometric bulk mass coefficient
M_5, M_4	Five-dimensional Planck scale and reduced four-dimensional background scale; local gravitational matching is specified separately
$\lambda=\lambda_{bare}, U_0$	Split brane constant and constant matter vacuum contribution
$\tau=\tau_{vac}=\lambda+U_0$	Total constant vacuum stress entering the vacuum-subtracted background
$g_{ref}=g_{split}$	Reference split coefficient $\lambda_{bare}/(6M_5^6)$
g_{bg}	Vacuum-subtracted background coefficient $\tau_{vac}/(6M_5^6)$
κ_0, S	Reference normalization $g_{ref}/3$ and a fixed positive curvature scale

Symbol	Meaning and convention
h, v, p	Normalized expansion H^2/S, density $\kappa_0 \rho/S$ and pressure $\kappa_0 P/S$ in the inverse chapters
b, u, d	Normalized effective vacuum, spatial curvature and dark-radiation coefficients
η	Inverse split tension $S/\left(2\kappa_0 \lambda_{bare}\right)$
χ	Barotropic derivative $dP/d\rho$; a propagation speed squared only under the declared single-fluid assumptions
q, Q, J	Density decline rate $-v'$, sound transport function and its integrated coordinate
V, C	Density at the reference epoch and the positive transport normalization
α_j, β_j	Fixed-vacuum and free-vacuum expansion coefficients
Σ, L	Free-vacuum discriminant and invariant $L=\Sigma/\left(4\beta_2\right)=1/\left(S\ell^2\right)$

Fields, observations and statistical sets

Symbol	Meaning and convention
X	Scalar kinetic invariant $-h^{\mu\nu}\partial_\mu\phi\,\partial_\nu\phi/2$, using the induced brane metric
$F\left(X\right)$ or $P\left(X\right)$	A kinetic pressure Lagrangian, with its normalization specified locally
c_ϕ^2	Scalar characteristic sound speed on the stated background
ρ_e, p_e	Excitation density and pressure after removal of the constant vacuum
ϵ_{brane}	Direct quadratic-to-linear ratio $\rho_e/\left(2\tau_{vac}\right)$

Symbol	Meaning and convention
Δ, ω, Ω	Window width and frequency variables in logarithmic scale factor
$\operatorname{sinc} z$	$\sin z / z$, extended continuously to one at zero
A	A design matrix or amplitude, explicitly defined in its chapter
U, P_U	Selected orthonormal subspace basis and its orthogonal projector
C, Σ	Observation covariance matrices when used in statistical chapters; distinguish the local matrix Σ from the scalar discriminant in Chapter 6
α	A significance or error-allocation level in statistical statements; elsewhere a positive action-scaling parameter
n, r, N	Number of independent validation vectors, selected rank and number of expansion epochs, respectively
B_β	An outer coefficient confidence region
I	A physically admissible inverse set, with its conditioning assumptions stated

Statistical covariance matrices are distinct from the scalar discriminant of Chapter 6. Appendix A expands the units crosswalk; Appendix C uses a separate four-dimensional scalar–tensor action.

1 Geometry as an Observable

1.1 The question behind reconstruction

An expanding universe presents an inverse problem. A proposed action and a set of initial conditions predict a geometry. An observed geometry must be interpreted in the opposite direction, through the set of actions, matter histories, calibrations, and initial conditions capable of producing it. The inverse direction can retain freedom even when the forward equations are completely deterministic. This distinction is the organizing question of this book. [1; 2; 3; 4]

Consider two models that give exactly the same expansion rate throughout an interval. If their unobserved matter densities differ, an expansion measurement alone has no means of choosing between them. Increasing its numerical precision does not alter that fact. An additional observation becomes useful when its predicted value changes along the family of equivalent backgrounds. Determining which observations have this property requires an explicit model of both the dynamics and the measurement.

The word *geometry* also requires care. The curvature of a spatial slice, the curvature of an optical metric, the bending of a surface in an ambient space, and the curvature of spacetime are distinct quantities. A visual resemblance between two surfaces does not identify their field equations. We begin with this distinction because every later reconstruction depends on knowing what the geometric input actually means. [1]

1.2 What a geodesic triangle measures

In units with the speed of light equal to one, a homogeneous and isotropic spacetime has the local form

$$d s^2 = - d t^2 + a^2(t) \left[\frac{d r^2}{1 - k r^2} + r^2 d \Omega^2 \right]. \tag{1.1}$$

Here the scale factor has dimensions of length and the comoving coordinates are dimensionless. Once their normalization is fixed, the constant k specifies the intrinsic spatial curvature. On a constant-time slice, every sectional curvature is

$$K_{spatial} = \frac{k}{a^2}. \tag{1.2}$$

A geodesic is defined by the intrinsic metric: its tangent is parallel transported along itself. It need not look straight in an external drawing. For a simple triangle whose sides are geodesics in a smooth, totally geodesic two-dimensional section of the slice, Gauss–Bonnet relates its interior angles to the curvature enclosed by the boundary. If the angles are α, β, γ and the intrinsic area is A, the constant-curvature result is

$$\Delta_{\triangle} = \alpha + \beta + \gamma - \pi = \int_A K \, d A = K A. \tag{1.3}$$

The assumptions are part of the measurement. A boundary with nongeodesic sides adds geodesic-curvature terms. A region containing a conical singularity needs its singular contribution. A triangle drawn on a projected image does not automatically have the angles, sides, or area required by this formula. [1, Secs. 2–4]

The small-triangle limit makes the sign of curvature tangible. Let u and v be the orthogonal geodesic legs of a small right triangle and w its geodesic hypotenuse. On a sphere of constant

positive curvature the exact cosine law is $\cos(\sqrt{K}\,w)=\cos(\sqrt{K}\,u)\cos(\sqrt{K}\,v)$. Expanding both sides and solving to fourth order in the lengths gives

$$w^2=u^2+v^2-\frac{K}{3}u^2v^2+O\left(K^2L^6\right). \tag{1.4}$$

Here L bounds the side lengths and the expansion requires $|K|L^2\ll 1$. The hyperbolic cosine law gives the same expression for negative K. Positive curvature decreases the squared hypotenuse relative to its Euclidean value at this order; negative curvature increases it. This is a consequence of the intrinsic metric, independent of how a drawing is arranged on a page. [1, Eq. 7]

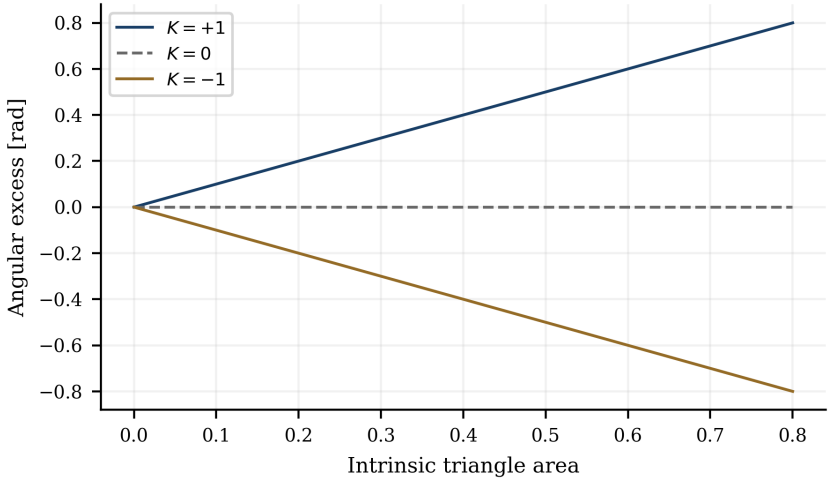

Figure 1.1. Angular excess for three prescribed constant curvatures. The horizontal coordinate is intrinsic triangle area. These exact geometrical relations are illustrations, not astronomical measurements.

1.3 Intrinsic and extrinsic curvature

A cylinder supplies a useful operational example. Its surface bends in ordinary three-dimensional space, yet it can be

unrolled onto a plane without stretching. In local coordinates given by distance around the circumference and distance along the axis, its metric is Euclidean. Small geodesic triangles therefore have zero angular excess. The cylinder has extrinsic curvature while its intrinsic Gaussian curvature vanishes. A sphere, by contrast, cannot be flattened without changing distances. [1]

The reverse inference also fails. A positively curved spatial sphere can be embedded as a chosen surface in a flat ambient spacetime; curvature of that surface does not establish curvature of the ambient spacetime. Likewise, an intrinsically flat brane can be embedded in an anti-de Sitter bulk. The brane's extrinsic curvature and the bulk curvature may be nonzero even though its induced background is flat. These examples show why an intrinsic triangle measurement must enter a specified dynamical model before it can constrain an extra dimension. [1, Secs. 4–6]

There is no contradiction with the usefulness of embedding pictures. Such pictures help explain which manifold carries the observers and which carries the gravitational field. Their role is conceptual. The metric, junction conditions, matter stress, and boundary conditions carry the quantitative content.

1.4 Spatial geometry and optical geometry

For a static metric written as

$$d s^2 = - N^2(x)\, d t^2 + h_{i j}(x)\, d x^i\, d x^j , \tag{1.5}$$

a clock at rest measures $d\tau = N\,dt$. The spatial projection of a null path instead obeys a travel-time problem with optical metric

$$dt^2 = \frac{h_{ij}}{N^2}\,dx^i\,dx^j. \tag{1.6}$$

The optical metric includes the lapse. Its geodesics are therefore generally different from geodesics of h_{ij}. A photographed light-ray triangle and a simultaneous spatial triangle answer different questions. In the Schwarzschild example discussed in the first reference series, the equatorial optical curvature is nonzero and its weak-field behavior is consistent with the usual gravitational deflection. That calculation does not turn every sky triangle into a direct spatial-curvature estimator. [1, Sec. 5]

Even a position-dependent clock rate is insufficient by itself to prove spacetime curvature. Rindler coordinates on a flat spacetime provide a lapse that varies with position for an accelerated congruence. Their Christoffel symbols and relative clock rates can be nontrivial while the Riemann tensor remains zero. The appropriate distinction is between coordinate descriptions, the motion of the observers, and invariant curvature. [1]

These distinctions become especially important in the clock comparisons of Chapter 13 and Appendix C. Clock ratios, orbital accelerations, and lensing can complement one another, but their relation must be derived from the same metric and matter coupling. An approximate potential extracted by one observable cannot silently replace the exact lapse used by another.

1.5 The observational interface

Astronomical observations arrive along our past light cone. A simultaneous spatial slice is a model-dependent reconstruction of those observations. Redshifts, luminosity or angular distances, time delays, and acoustic observables have their own response functions and covariance. A practical analysis must state how those measured quantities constrain H, K, or the residual entering the braneworld equation. [1; 2]

The covariance matters as much as the mean relation. If spatial curvature is inferred from a distance–expansion relation and the same expansion data are then used again in the residual, the resulting quantities are correlated. Treating them as independent adds information that the experiment did not supply. A joint likelihood, or a joint uncertainty region with the appropriate coverage, keeps the dependence explicit. [2, Secs. 2 and 8]

The same discipline applies to sound. The quantity $\chi = d\,p/d\,\rho$ used later belongs to the particular single barotropic fluid entering the adopted background model. A measured acoustic feature in another component is not automatically a measurement of this function. Chapter 7 first studies an explicitly declared window operator; Chapter 13 returns to what an astronomical instrument would have to measure.

1.6 Three levels of inference

We shall distinguish three questions throughout the book. *Compatibility* asks whether at least one allowed model reproduces the data within their uncertainty. *Identification* asks whether the desired parameter or combination has the same value in every compatible model. *Stable recovery* asks whether

small measurement changes lead to controlled changes in the recovered quantity. [5; 6]

These are different mathematical properties. A fit with zero residual proves compatibility. Full column rank can establish identification of regression coefficients. A singular value separated from zero supplies a quantitative route toward stability. Physical interpretation adds another step: the fitted coefficients must map into an admissible action and into the physical parameter of interest. Freeing an effective vacuum term will later leave a family of tensions even when the regression coefficients are uniquely determined.

The succeeding chapters follow this sequence. Geometry supplies a well-defined input. A restricted gravitational model supplies a forward relation. Matter and calibration assumptions define the inverse family. Sound, independent normalization, and uncertainty control then determine which conclusions survive. The final part asks whether the reconstructed histories can arise from a predictive and locally consistent dynamics of sufficient magnitude to test.

2 The Braneworld Background and Its Conventions

2.1 The model being reconstructed

The gravitational setting is a thin brane separating two reflection-related regions of a five-dimensional vacuum spacetime. The bulk obeys Einstein gravity with a negative cosmological constant. The brane carries a positive constant tension and a homogeneous, isotropic matter stress. There is no exchange of energy with the bulk in the reconstruction problem. Induced gravity, a Gauss–Bonnet correction, a second brane, and a bulk scalar are absent from this model. The foundational projected equations and cosmological junction dynamics are established results. [7; 8; 9]

This chapter introduces the convention used by the predecessor papers. The symbol λ denotes the split brane tension, also written λ_{bare} when its separation from matter vacuum energy is important. The density ρ includes the matter assigned to the brane sector under that convention. It may therefore include a constant matter contribution that Chapter 10 will separate explicitly. Until that separation is made, a coefficient defined using λ must not automatically be identified with an independently measured local gravitational coupling. [3; 4]

Use $c=\hbar=1$ unless an SI conversion is stated. The four-dimensional signature is ¿. The five-dimensional reduced gravitational scale is defined by $8\pi G_5=M_5^{-3}$, and $\Lambda_5=-6/\ell^2$. With an appropriate three-dimensional constant-curvature metric $d\Sigma_k^2$, the Schwarzschild–anti-de Sitter bulk takes the form

$$d s_5^2 = -f(r) d T^2 + \frac{d r^2}{f(r)} + r^2 d \Sigma_k^2, f(r) = k + \frac{r^2}{\ell^2} - \frac{\mu_B}{r^2}. \quad (2.1)$$

The brane trajectory is $r = a(t)$, where t is its proper cosmological time. The parameters ℓ and μ_B have dimensions of length and length squared, respectively. We take $\mu_B \geq 0$ and retain a fixed normalization of the spatial coordinates. [1; 5]

2.2 From the junction condition to expansion

On the branch with positive total brane density and the declared normal orientation, the spatial junction condition can be written

$$\sqrt{\dot{a}^2 + f(a)} = \frac{a(\lambda + \rho)}{6 M_5^3}. \quad (2.2)$$

Squaring and dividing by a^2 gives

$$H^2 + \frac{k}{a^2} = \frac{(\lambda + \rho)^2}{36 M_5^6} - \frac{1}{\ell^2} + \frac{\mu_B}{a^4}. \quad (2.3)$$

The unsquared relation records the branch information lost by squaring. A candidate obtained from the algebra must respect the chosen branch and the physical restrictions. Conservation of the brane matter supplies

$$\dot{\rho} + 3 H (\rho + p) = 0. \quad (2.4)$$

The expansion term proportional to ρ^2 and the bulk term proportional to a^{-4} follow from this established system. Combining the spatial curvature measurement of Chapter 1 with Eq. (2.3) supplies an inference equation; it does not create a new gravitational field equation. [1; 2]

Define the split reference coupling and effective constant by

$$g_{ref}=g_{split}=\frac{\lambda}{6M_5^6},\frac{\Lambda_4}{3}=\frac{\lambda^2}{36M_5^6}-\frac{1}{\ell^2}. \tag{2.5}$$

Then

$$H^2+\frac{k}{a^2}=\frac{\Lambda_4}{3}+\frac{g_{ref}\rho}{3}\left(1+\frac{\rho}{2\lambda}\right)+\frac{\mu_B}{a^4}. \tag{2.6}$$

Equivalently, the right side is $\Lambda_4/3+g_{ref}\rho/3+\rho^2/\left(36M_5^6\right)+\mu_B/a^4$. This expanded form makes the dimensions transparent: every term has units of inverse length squared.

The distinction between g_{ref} and a calibrated local $8\pi G_N$ is central to the final manuscript. If a matter constant U_0 is absorbed into the total vacuum stress $\tau=\lambda+U_0$, the vacuum-subtracted background coupling is $g_{bg}=\tau/\left(6M_5^6\right)$. These coefficients coincide in the convention $U_0=0$, but a free vacuum split does not force that convention. Chapters 6 and 10 preserve the predecessor algebra while making the required operational matching explicit. [4, Sec. 4]

2.3 Dimensionless reconstruction variables

Choose fixed reference scales $a_{¿}>0$ and $S>0$, with dimensions of length and inverse length squared. They define coordinates and units for inference. Put $\kappa_0=g_{ref}/3$ and define

$$\begin{aligned} s&=\ln\left(a/a_{¿}\right), h=H^2/S, \\ v&=\kappa_0\rho/S, \eta=\frac{S}{2\kappa_0\lambda}, \\ b&=\frac{\Lambda_4}{3S}, u=\frac{k}{a_{¿}^2 S}, \\ d&=\frac{\mu_B}{a_{¿}^4 S}, E(s)=e^{-4s}. \end{aligned} \tag{2.7}$$

Equation (2.6) becomes

$$h(s)=b-u\,e^{-2s}+v(s)+\eta\,v^2(s)+d\,E(s). \tag{2.8}$$

A prime from this point denotes differentiation with respect to s, not proper time. Thus conservation is $v'+3(v+\varpi)=0$, where $\varpi=\kappa_0 p/S$. In Chapters 4–9, this dimensionless pressure is denoted by p; physical pressure is distinguished explicitly when units are restored. The dimensionless inverse tension is η. We reserve the symbol τ for total vacuum stress and write η^{-1} explicitly when discussing the inverse of inverse tension. This avoids the different uses of τ in the supplied series and the final action analysis.

At fixed κ_0 and S, the reconstruction parameter maps to

$$\lambda=\frac{S}{2\kappa_0\eta}, \ell^{-2}=S\left(\frac{1}{4\eta}-b\right). \tag{2.9}$$

Positive finite tension and a negative bulk cosmological constant require $\eta>0$ and $1/(4\eta)>b$. The boundary $\eta=0$ describes an infinite-tension limit of the effective reconstruction, not an additional finite-tension brane. Positivity

of density and of h must also hold on the interval under consideration. A condition checked only at measured nodes does not prove positivity between them. [10; 11; 5]

Table 2.1. Fixed inputs and the consequences of releasing them. Fixed quantities are assumptions of a calculation, not additional observations. The appropriate row is specified again when a theorem depends on it.

Quantity held fixed	Meaning in the reconstruction	Consequence of releasing it
$a_{¿}$ and S	Coordinate normalization and declared units	Numerical coefficient values and their physical conversion must be transformed consistently
κ_0	The split reference coupling	A new normalization problem enters
b	Effective vacuum contribution under the chosen split	The unique fixed-vacuum tension inverse becomes an equivalence family
u	Spatial-curvature amplitude	An extra nuisance template can absorb a signal direction
d	Bulk term proportional to a^{-4}	Conditional tension sets must be combined through a joint construction or a union

Chapter 18 gives the complete sound-coordinate classification when the spatial-curvature amplitude is released. Its exact example shows why the extra template can change the identifiability of bulk geometry even for a history that has rank four when curvature is supplied.

2.4 What it means to vary tension

Holding the split four-dimensional coefficient fixed while varying λ generally changes M_5. Holding an effective constant

fixed can also change ℓ. The predecessor comparisons are consequently comparisons within a family of parent theories unless additional microscopic constants have been fixed. They are not automatically different solutions of one action with every coupling held constant. [12; 13; 5]

This is useful rather than merely terminological. An inverse theorem states exactly which ingredients can be inferred within the declared family. A microscopic completion then asks which members of that family a physically normalized action permits. An independent calibration may remove a family direction; naming a coefficient of a scalar kinetic term does not by itself provide that calibration. The distinction will become explicit in the action-scaling orbit of Chapter 10.

2.5 Bulk geometry and the horizon

The bulk coefficient μ_B is a parameter of the metric. Converting it into a physical mass requires the gravitational coupling, the horizon topology, and an appropriate normalization or spatial volume. In a planar bulk one usually discusses a mass density after fixing the planar coordinate normalization. A geometrically identified μ_B need not therefore identify a unique physical black-hole mass when G_5 varies. [3; 5]

For $k=0$ and $\mu_B>0$, the horizon radius obeys

$$r_h^4=\mu_B\ell^2. \tag{2.10}$$

Writing $L=\ell^{-2}/S>0$, this gives

$$\frac{r_h}{a_{\dot{c}}}=\left(\frac{d}{L}\right)^{1/4}. \tag{2.11}$$

The planar restriction belongs beside this formula. For other k, one must solve $f\left(r_h\right)=0$ with the corresponding curvature term. For $d=0$ the positive planar Schwarzschild horizon in Eq. (2.10)

is absent; the zero limit should not be described as a detected black hole. Exterior-brane restrictions likewise require checking $a(t) > r_h$ on the stated interval if that is the intended branch.

2.6 Background closure and dynamical closure

Equations (2.3) and (2.4), together with a specified homogeneous matter law, can close a background calculation. They do not supply every boundary condition for the coupled perturbations in the bulk and on the brane. The projected Weyl contribution contains information about the bulk gravitational field, and a prediction for structure or the microwave background needs the relevant bulk boundary problem. [14; 4]

The scope of the book is therefore layered. The first parts establish conditional inverse results. The later parts exhibit explicit scalar actions, distinguish normalization freedoms, and test local kinetic conditions and the magnitude of selected effects. A locally positive scalar sound speed is one requirement in this chain. It does not replace a calculation of the full coupled spectrum.

3 Identification from Finitely Many Epochs

3.1 A straight line hidden in the background equation

Suppose first that curvature, the effective vacuum contribution, and the physical density history under the chosen split are supplied. Write $v = m\,e(s)$, where e is a known dimensionless shape and m is its known normalization. With $q_2 = m^2\eta$, subtract the supplied linear and geometric terms from Eq. (2.8). The remaining response is

$$y(s) = q_2 e^2(s) + d\,e^{-4s}. \tag{3.1}$$

Multiplying by e^{4s} gives a line:

$$z(s) = q_2 x(s) + d\,,\; x(s) = e^{4s}e^2(s)\,,\; z(s) = e^{4s}y(s). \tag{3.2}$$

Two epochs with different x determine the slope and intercept. Any additional epoch supplies a compatibility check. Explicitly,

$$q_2 = \frac{z_j - z_i}{x_j - x_i}\,,\; d = \frac{x_j z_i - x_i z_j}{x_j - x_i}. \tag{3.3}$$

This result requires the denominator to be nonzero. If every sampled x_i is identical, compatible data must have every z_i identical, and only the combination $q_2 x_i + d$ is identified. Determinantal contrasts that vanish automatically at the wrong assumed rank cannot replace this condition. [2, Sec. 3]

The construction is derivative-free at the level of supplied residual values. It says nothing by itself about the measurement procedure used to construct those values. It also exposes a practical limitation: as $x_j - x_i$ becomes small, finite errors can generate large changes in the inferred slope even though the exact two-point formula remains valid.

3.2 Nuisance directions and exact degeneracy

The line is a special case of a linear model with nuisance terms. Write the finite response vector as

$$y = N\,b + q_2 f + \epsilon\,, f = \left(e_i^2\right)_i. \tag{3.4}$$

The columns of N contain the geometric or bulk terms whose amplitudes are free. They are e^{-4s} when only the bulk amplitude is free; $1, e^{-4s}$ when the effective vacuum is also free; and $1, e^{-2s}, e^{-4s}$ when spatial curvature is free as well. A supplied quantity with measurement uncertainty belongs in the joint model or its covariance rather than being treated as exact.

Proposition 3.1. In the interior of the physical domain, the quadratic coefficient is unidentified precisely when its sampled column lies in the span of the nuisance columns.

Proof. Subtract two compatible coefficient representations. If their quadratic coefficients differ, the subtraction expresses f as a nuisance combination. Conversely, any such representation lets a change in q_2 be absorbed by a corresponding change in the nuisance amplitudes. Sufficiently small changes preserve strict physical inequalities at an interior point. Boundary restrictions may need a separate analysis. The same argument works for functions observed throughout an interval. ▫ [2, Proposition 3]

For one conserved fluid with constant $w = p/\rho$, the density behaves as $e = e^{-3(1+w)s}$. Its square has exponent $v = 6(1+w)$. Distinct real exponential functions are linearly independent, and their evaluation matrix has full rank at sufficiently many distinct epochs. One proof divides a supposed linear combination by one exponential, differentiates, and uses Rolle's theorem inductively to bound its number of zeros. The full constant-fluid classification is then immediate. [2, Appendix B]

Table 3.1. Exact nuisance degeneracies for a supplied density normalization. The density normalization is supplied in this table. Exactly enough points to determine all amplitudes leave no residual degree of freedom for a goodness-of-fit test.

Free nuisance templates	Values of w that hide q_2	Generic epochs to fit and to test
e^{-4s}	$-1/3$	2 and 3
$1, e^{-4s}$	$-1, -1/3$	3 and 4
$1, e^{-2s}, e^{-4s}$	$-1, -2/3, -1/3$	4 and 5

A changing equation of state need not restore identification. With a free effective vacuum and bulk amplitude, any positive history satisfying $e^2 = A + B e^{-4s}$ lies in the nuisance span. Conservation gives a generally varying $w(s)$, yet the quadratic term is absorbed exactly into new constant and radiation-like amplitudes. Some such histories fail a barotropic sound condition on part of their domain. Their role at this stage is to demonstrate background degeneracy; Chapter 4 imposes a definite matter class. [2, Sec. 5]

3.3 Correlated errors and projected information

Assume an exact design, a known positive-definite covariance $\Sigma = C C^T$, and Gaussian response errors. Whiten all vectors by C^{-1}. Let P_N and P_X be orthogonal projections onto the whitened nuisance design and the full design $X = [N, f]$, respectively. Define

$$v_f = (I - P_N) C^{-1} f, \quad I_{q_2} = v_f^T v_f. \tag{3.5}$$

When $I_{q_2} > 0$, the unconstrained estimate and its variance are

$$\hat{q}_2 = \frac{v_f^T C^{-1} y}{I_{q_2}}, \quad \mathrm{Var}(\hat{q}_2) = I_{q_2}^{-1}. \tag{3.6}$$

The residual statistic obeys

$$T=\left\|\left(I-P_X\right)C^{-1}y\right\|^2\sim\chi^2_{n-r},r=rank\,X, \tag{3.7}$$

under that unconstrained linear Gaussian model. Whitening turns the noise covariance into the identity, and projection leaves $n-r$ independent standard-normal coordinates. This proves the stated distribution. The information in Eq. (3.5) is the part of the target column that survives nuisance removal. [2, Proposition 2]

A deterministic omitted component can bias a coefficient while remaining completely hidden in the fitted column space. If its whitened vector is in that space, the residual test has no noncentrality from that component. Passing the test establishes compatibility with a finite-dimensional mean model; it does not assign a unique gravitational origin to its coefficients.

The distribution in Eq. (3.7) does not automatically survive positivity constraints, uncertain density regressors, a covariance estimated from the same data, or a frequency selected by searching the data. Chapters 8 and 9 address specific replacements under additional assumptions. Their procedures retain different targets and should not be mixed into one unqualified calibration claim.

3.4 Why a short interval can contain little information

Take fixed sampling coordinates t_i and set $s_i=L\,t_i$. Let the target be $e^{-\nu L t_i}$, with k nuisance exponents $s_1,\dots,s_k$ that are distinct from one another and from ν. For independent absolute response error σ, the leading conditional information is

$$I_{q_2}=\frac{L^{2k}}{\sigma^2\left(k!\right)^2}\prod_{j=1}^{k}\left(\nu-s_j\right)^2\left\|\left(I-P_{k-1}\right)t^k\right\|^2+O\left(L^{2k+1}\right). \tag{3.8}$$

Here P_{k-1} projects onto sampled polynomials through degree $k-1$, and $n \geq k+1$ distinct sampling coordinates are assumed. To see the origin of the result, expand each exponential in powers of L. Interpolation in the exponent variable constructs a nuisance combination matching the target through order $k-1$. The first unmatched coefficient is the product $\prod_j (\nu - s_j)/k!$. Projecting its sampled degree-k polynomial off the lower-degree space and squaring the remaining norm gives Eq. (3.8). [2, Proposition 4 and Appendix C]

One, two, and three nuisance powers therefore suppress the information as L^2, L^4, L^6 under this fixed experiment. An exact exponent collision makes it zero rather than merely smaller. These scalings hold with fixed sample count, sample coordinates, and absolute error; they are not a survey forecast in which exposure, selection, or noise changes with interval length.

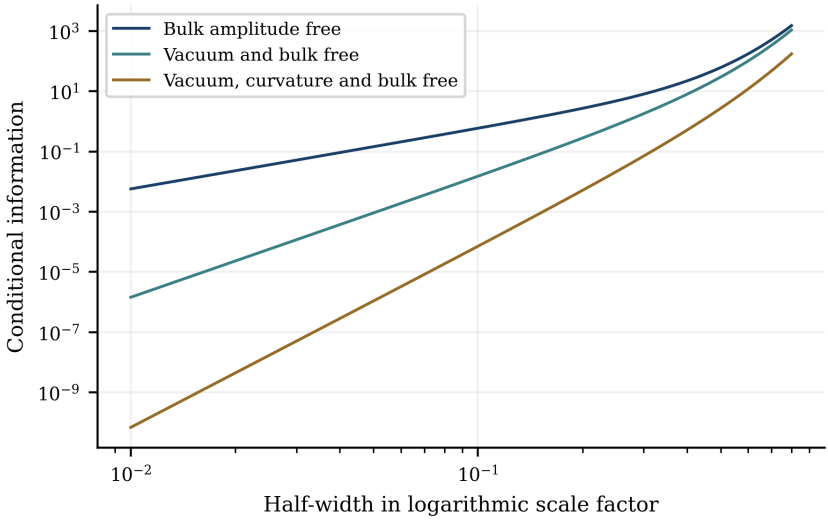

Figure 3.1. Conditional information for a prescribed dust-density template as the logarithmic interval changes. The QR-projected design uses 41 fixed relative epochs and known absolute errors. The curves illustrate information loss from nuisance fitting, not an observational sensitivity forecast.

3.5 Constant density gain and a tension invariant

Now suppose that a positive proxy for the total modeled density has an unknown constant multiplicative gain: $z = g\,v$ with $g>0$. After supplying or fitting the appropriate nuisance terms, the response takes the form

$$y = A\,z + B\,z^{2} + N\,\beta,\; A = g^{-1},\; B = \eta\,g^{-2}. \tag{3.9}$$

If the columns z, z^{2}, N have full rank, the fitted coefficients determine

$$\eta = \frac{B}{A^{2}},\; \lambda = \frac{S}{2\kappa_{0}}\frac{A^{2}}{B}. \tag{3.10}$$

A constant rescaling of the proxy changes A by the inverse scale and B by its inverse square; the ratio is unchanged. This is a conditional algebraic invariant. It is not an assertion that the

ratio of noisy estimates is unbiased. It also requires a proxy for the total density entering the model, not merely the density of a visible tracer or one component of a mixture. [12, Proposition 1]

Unknown gain creates an additional radiation collision. For $w=1/3$, the linear matter term and the free bulk term both vary as e^{-4s}. The coefficient of z^2 can still be separated, but the coefficient of z cannot. A quadratic correction may thus be identified while the tension ratio is not. Fixing the bulk amplitude independently removes that particular coincidence. [12, Sec. 4]

The cancellation is also specific to constant gain. A gain that changes freely with epoch can absorb changes in inverse tension by changing the inferred density history. Chapter 4 considers the intermediate case in which the logarithmic gain has a declared bound on its variation.

3.6 Confidence regions for a nonlinear ratio

The ratio in Eq. (3.10) must be treated globally when its denominator is uncertain. Under the exact-design Gaussian model, a joint confidence ellipse for (A,B) has known coverage. Map its part with $A>0$ and $B>0$ through A^2/B to obtain a tension-scale confidence set. Whenever the joint ellipse contains the true pair, its image contains the true ratio. The projected set therefore has at least the ellipse’s coverage. [12, Sec. 6]

If the ellipse crosses $B=0$ at a point with positive A, its image has no finite upper tension endpoint. A small local error estimate obtained by differentiating the ratio does not contradict this fact. The supplied reference gives a concrete example: a local standard deviation of $\log(A^2/B)$ near 0.0508

coexists with an unbounded upper endpoint of the projected 95 percent set. Both statements describe the same synthetic mean-data design, but only the global set records its denominator uncertainty. [12, Table 3]

Uncertain density measurements introduce another distinction. A joint likelihood can treat the true proxy values as latent quantities, with correlations between geometry and density measurements retained. Its local Schur-complement information is useful, but it is not a substitute for the full nonlinear likelihood or a finite-sample coverage argument. Profiling latent values and integrating them against a population model are different inferential operations. [12, Sec. 7]

3.7 From a fitted coefficient to a physical claim

The results of this chapter identify conditional linear directions and, when the gain assumptions permit it, a ratio. They do not establish a unique higher-dimensional origin. A four-dimensional effective matter description can reproduce the same background terms. For instance, the quadratic contribution of a constant-w fluid has an effective background equation of state $w_Q = 1 + 2w$, while the bulk a^{-4} term behaves like radiation in the background equation. Such a construction need not reproduce every perturbation. Its existence is already enough to delimit what background data alone can prove. [2, Proposition 5]

The next step is to insist that all allowed observations and matter conditions belong to one history. This requirement changes the mathematics. Separate sharp bounds can have an intersection even when no common physical realization exists. Chapter 4 formulates the shared-history problem before Chapters 5 and 6 ask which combinations of the bulk geometry remain identifiable.

4 Matter Histories and Common Reconstruction

4.1 What a common history must satisfy

An expansion curve does not determine its matter interpretation until the gravitational coefficients, the density calibration and the allowed equation of state have been specified. A candidate must satisfy these requirements through one history. Checking each requirement with a different interpolating curve can accept data that no physical history realizes. This chapter develops the distinction first for a complete residual curve and then for finite values and sound windows. [10; 13; 11; 15]

Use the normalization of Chapter 2, with fixed $S, a_{¿}$ and $\kappa_0 = g_{ref}/3$. Throughout this chapter the effective vacuum, curvature and dark-radiation coefficients b, u, d are supplied. Define

$$\begin{aligned} s &= \log(a/a_{¿}), h = H^2/S, \\ B(s) &= b - u e^{-2s} + d e^{-4s}, \\ R &= h - B = \nu + \eta \nu^2, \\ \nu &= \kappa_0 \rho / S, \eta = \frac{S}{2\kappa_0 \lambda_{bare}}. \end{aligned} \tag{4.1}$$

The branch has positive density, positive constant tension, one conserved barotropic fluid and no exchange with the vacuum bulk. Finite physical models have $\eta > 0$ and $\eta b < 1/4$. We sometimes include $\eta = 0$ as the general-relativistic, infinite-tension boundary. It is not an additional finite-tension model. The auxiliary condition $B \geq 0$ guarantees positive expansion for the interpolations below; it is sufficient rather than necessary. Releasing a supplied background coefficient requires a joint

analysis or a union of conditional sets. Chapter 6 treats the distinct free-vacuum problem. [11; 3]

4.2 Density calibration as a functional constraint

For a proposed inverse tension, the positive density is uniquely

$$f_\eta(R)=\frac{2R}{1+\sqrt{1+4\eta R}},\ f_0(R)=R. \tag{4.2}$$

Suppose a proxy measures that same density with log gain γ: $y=\log z=\log v+\gamma$. An external calibration specification supplies $|\gamma(s)-\gamma(t)|\le\delta|s-t|$. The bound controls drift; it leaves the absolute gain free. An arbitrary changing gain can absorb a different density history, whereas a specified drift bound can exclude some histories. [12; 10]

Let $F_\eta(R)=\log f_\eta(R)$. For $X>Y>0$, the contrast $F_\eta(X)-F_\eta(Y)$ decreases strictly as η increases. The key identity is

$$\partial_R\partial_\eta F_\eta(R)=-(1+4\eta R)^{-3/2}<0. \tag{4.3}$$

Integrating over $[Y,X]$ proves the assertion. The contrast decreases from $\log(X/Y)$ to $1/2\log(X/Y)$. If an interior contrast equals c, writing $r=e^c$ gives its unique positive solution

$$\eta=\frac{r(r-1)(X-rY)}{(r^2Y-X)^2}. \tag{4.4}$$

Endpoint contrasts must be handled by limits. The physical upper bound on η, when present, is imposed separately. This monotonicity explains why the calibration-only identified set is an interval; connectedness is not a general property of every later reconstruction problem. [10]

For rectangular residual and proxy bounds, the possible gains at epoch s_i lie in

¿ (4.5)

Proposition 4.1 — Compatible gain values. A gain satisfying all intervals and the drift bound exists exactly when

$$\gamma_i^- - \gamma_j^+ \le \delta\left|s_i - s_j\right| \text{ for all } i, j. \tag{4.6}$$

Proof. Necessity follows by inserting any permitted gain values. For sufficiency, the envelope

$$\gamma(s) = \max_i \left\{\gamma_i^- - \delta\left|s - s_i\right|\right\} \tag{4.7}$$

is δ-Lipschitz and lies in every required gain interval at its node. The monotone inverse then supplies corresponding residual and proxy values. Each inequality in (4.6) is a monotone contrast constraint, so their intersection with the physical domain is an interval. ▫ [10]

All pairs matter when interval values can be selected. At epochs $0,1,2$, take gain intervals $[0,0],[0,2],[2,2]$ and $\delta = 1/2$. Either adjacent pair can be fitted separately. The endpoint gains nevertheless differ by two over a distance of two, exceeding the allowed difference of one. Adjacent inequalities suffice only if they act on one shared vector of unknown gains, or if the exact gains have already been fixed.

4.3 Causal matter on a complete residual curve

For a positive C^2 residual with $R' < 0$, conservation fixes pressure after $v = f_\eta(R)$ is chosen. With $p = \kappa_0 P/S$,

$$\begin{gathered} v' = -3(v+p),\, q = -v' > 0, \\ p = -v + q/3, \\ \chi_\eta = \frac{p'}{v'} = -1 - \frac{R''}{3R'} + \frac{2\eta R'}{3(1+4\eta R)}. \end{gathered} \tag{4.8}$$

Here χ is the squared barotropic sound speed in units $c = 1$. For a mixture with entropy perturbations, the ratio of background

derivatives need not equal a propagation speed. The single-fluid assumption is therefore substantive. [13]

The restrictions $0 \le \chi_\eta \le 1$ become affine inequalities in the candidate parameter:

$$\begin{gathered} A_3 + \eta B_3 \ge 0,\ A_6 + \eta B_6 \le 0, \\ A_j = R'' + j R', \\ B_j = 4 R A_j - 2 (R')^2. \end{gathered} \tag{4.9}$$

The negative sign of R' reverses the inequalities during multiplication. Intersecting these half-lines over the whole interval gives the exact conditional matter set. Moreover, $\partial_\eta \chi_\eta = 2 R' / \left[3 (1 + 4 \eta R)^2 \right] < 0$. A dust-generated residual, $R = e^{-3s} + \eta_0 e^{-6s}$, consequently allows the entire range $0 \le \eta \le \eta_0$ under this matter restriction. Causal matter narrows an ambiguity without necessarily removing it. Differentiating a noisy interpolation and applying (4.9) does not inherit this complete-curve theorem. [13]

4.4 Finite values and exact reachable drops

Finite observations require no measured derivatives. Treat the node decline rates q_i as latent variables and impose the differential inequalities implied by a sound margin:

$$\begin{gathered} m \le \chi \le 1 - m, 0 \le m < 1/2, \\ -B q \le q' \le -A q, A = 3 (1 + m), B = 3 (2 - m). \end{gathered} \tag{4.10}$$

On a cell of length Δ, positive endpoint rates must satisfy $e^{-B\Delta} q_0 \le q_1 \le e^{-A\Delta} q_0$. Every admissible rate lies between

$$q_-(t) = max \{ q_0 e^{-Bt}, q_1 e^{A(\Delta - t)} \}, \tag{4.11}$$

¿

Theorem 4.2 — Reachable density drop. The prescribed transition exists in the class with absolutely continuous $q>0$ exactly when its drop $D=v_0-v_1$ satisfies

$$L_m=\int_0^{\Delta} q_{-}\,dt\le D\le\int_0^{\Delta} q_{+¿}\,dt=U_m.¿ \tag{4.12}$$

Proof. The differential bounds integrated forward and backward give (4.11), proving necessity. Both envelopes satisfy the same linear inequalities and endpoint values. Their convex combination remains admissible and attains every integral between L_m and U_m. Integrating that rate constructs the required positive decreasing density. ▫ [11; 16]

For $m=0$, direct integration yields

$$\begin{aligned} 6L_0&=q_0-2q_1+e^{6\Delta}q_1^2/q_0,\\ 6U_0&=2q_0-q_1-e^{-6\Delta}q_0^2/q_1. \end{aligned} \tag{4.13}$$

Let $Q=\{(a,b,c):a,b\ge0,ab\ge c^2\}$. The drop inequalities are equivalently the two rotated-cone conditions

$$\begin{aligned} &\left(q_0,6D-q_0+2q_1,e^{3\Delta}q_1\right)\in Q,\\ &\left(q_1,2q_0-q_1-6D,e^{-3\Delta}q_0\right)\in Q. \end{aligned} \tag{4.14}$$

For positive margins, the analogous representation uses power cones. One shared q_i must serve both cells meeting at a node. This yields a continuous rate and a C^1 density, hence a single pressure law. At fixed η, residual intervals become density intervals through (4.2), while proxy restrictions become the linear inequalities

$$v_j\le\exp\{\delta|s_i-s_j|-y_i^{-}+y_j^{+¿}\}v_i.¿ \tag{4.15}$$

Together these form a convex feasibility problem in the shared v_i,q_i. Convexity at each fixed η does not establish that its projection over η is one interval. A strictly separated first and

last density interval excludes the zero-rate branch. Without that separation, strict positive enthalpy must be established explicitly. [11; 16]

The need for a common history has an exact counterexample. At spacing $\Delta = \log 2/3$, choose

$$(v_0, v_1, v_2, v_3) = \left(\frac{21}{8}, \frac{13}{8}, \frac{9}{8}, 1\right), (D_0, D_1, D_2) = \left(1, \frac{1}{2}, \frac{1}{8}\right). \tag{4.16}$$

For three equally spaced epochs the necessary and sufficient condition is $e^{-6\Delta} \le D_1/D_0 \le e^{-3\Delta}$. Both adjacent triples in (4.16) pass. The first saturates the upper bound, forcing $q' = -3q$ throughout its two cells; the second saturates the lower bound, forcing $q' = -6q$ throughout its two cells. Their overlap cannot satisfy both with $q > 0$. Matching density values has concealed incompatible pressures. [11]

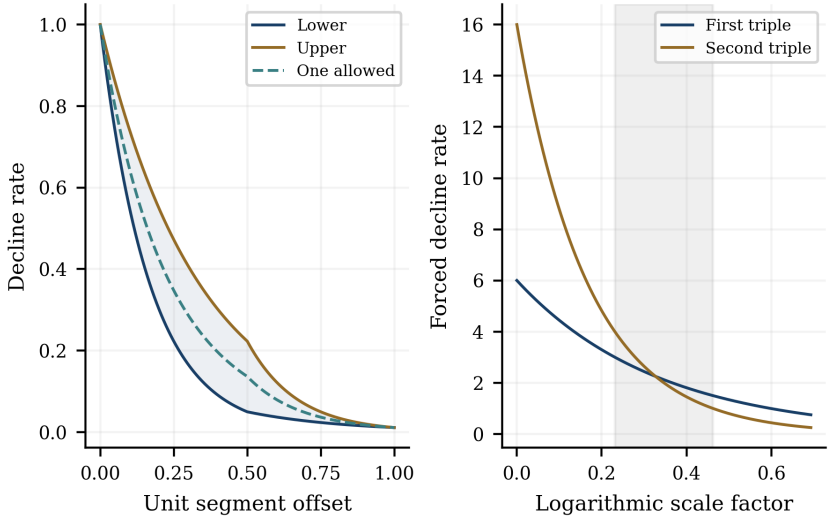

Figure 4.1. Left: exact lower and upper decline-rate envelopes, together with one allowed convex interpolation. Right: the two locally feasible adjacent triples of Equation 4.16 require incompatible rates on their shaded overlap. All curves are constructed examples.

The same example separates marginal from joint calibration tests. Give each density a box of $\pm 20\%$, let the exact proxies equal (4.16), and demand constant gain. Calibration alone fits the central values. Matter alone fits $v(s)=7/8+(7/4)e^{-3s}$. Joint feasibility would force all densities to be one common multiple of (4.16), preserving its contradiction. The intersection of two separately projected parameter sets can therefore be strictly larger than the common-history set. [11]

4.5 Smooth completion and the information in anchors

A weak interpolant can have jumps in its sound profile, so replacing it by a smooth curve requires more than visual interpolation. Theorem F.2 proves an exact finite-constraint completion: if the original positive rate has a uniform margin $m \le \chi \le 1-m$, with $m>0$, then every smaller positive margin $m'<m$ admits a smooth positive rate retaining every density node and every node rate. Including all sound-window endpoints in the node set therefore retains their uniform means exactly. Finite node calibration restrictions can be retained with the same gains.

The proof first uses positive convolution to preserve the differential inequalities, then explicitly constructs a right inverse for the node-value and cell-integral constraints. The resulting correction is small in C^1, while the relaxed margin supplies a strictly positive reserve in the inequalities. This reserve is essential: an extremal reachable drop can force a rate with a derivative jump, so smooth completion at the same margin is not guaranteed. Appendix F gives such a counterexample and the full correction argument. The theorem preserves the finite data, not the original residual curve between nodes, a fixed derivative budget, or the original sound profile. [16; 15]

Every such strictly positive sound history has a local purely kinetic scalar representation. In dimensionless pressure units, set

$$X(s)=X_{¿}\exp\left[-6\int_{s_{¿}}^{s}\chi(t)\,dt\right],$$
$$P(X(s))=p(s),\,P_X=\frac{q}{6X}>0, \tag{4.17}$$
$$2XP_X-P=v,\,P_X+2XP_{XX}=\frac{P_X}{\chi}>0.$$

Strict monotonicity of X makes the definition single valued. The physical pressure Lagrangian is $(S/\kappa_0)P$; $X_{¿}$ sets a field normalization. This construction proves local existence on the sampled kinetic range. It supplies neither a preferred action nor its extension to $X=0$, absolute matter calibration, ultraviolet control or stability of the coupled brane–bulk system. Chapter 10 examines those distinctions at action level. [16; 4]

Without a fixed derivative budget, finitely many point sound values carry less information than a uniform profile restriction. Proposition F.3 proves that any prescribed values in $(0,1)$ at distinct interior epochs can be imposed while retaining the finite density nodes, node rates and included sound-window means, provided the starting history has a positive margin and the final margin is allowed to decrease. The proof controls the integrated effect of narrow sound patches and corrects the finite constraints without changing the imposed derivative-to-rate ratios at the anchors. The statement is false at some boundaries: a continuous nonnegative sound profile with an exactly zero mean on a window must vanish throughout that window. The fixed-Lipschitz problem below is therefore a

different class, not a consequence of arbitrarily narrow smoothing. [17]

For $|\chi(s)-\chi(t)|\le L|s-t|$ and compatible anchors $\chi(r_j)=a_j$, the extremal profiles are

$$\chi_{-}(s)=max\{m,\underset{j}{max}(a_j-L|s-r_j|)\}, \tag{4.18}$$

Writing $Q_\chi(s)=\exp\left[-3(s-s_0)-3\int_{s_0}^{s}\chi\right]$, three density nodes are compatible exactly when their drop ratio lies between the ratios of $\int_{s_1}^{s_2}Q_\chi$ to $\int_{s_0}^{s_1}Q_\chi$ for $\chi_{+¿¿}$ and χ_{-}, respectively. If one sound profile is larger, the ratio of its Q to the other decreases with s, reducing this later-to-earlier integral ratio. Convex interpolation of the envelopes covers the intermediate ratios continuously. This result applies to three nodes; additional nodes must still share one profile. [17]

Appendix F supplies a self-contained proof of the envelope ordering and the sufficiency construction in this three-node class.

4.6 Windows constrain integrals of the same history

A uniform sound mean over $[a,b]$ has an exact endpoint interpretation:

$$\overline{\chi}_{[a,b]}=-1-\frac{\log q(b)-\log q(a)}{3(b-a)}. \tag{4.19}$$

Thus a mean interval $[l,u]$ gives linear rate-ratio bounds $e^{-3(1+u)(b-a)}q(a)\le q(b)\le e^{-3(1+l)(b-a)}q(a)$. Add every window endpoint to the common node set and retain the same density, rate and gain variables. Two adjacent equal-width means of 0.2

and 0.4 force the union mean to be 0.3; a reported union mean of 0.5 cannot be repaired by another matter interpolation. [15]

Exact adjacent sound means determine all node-rate ratios up to one common positive amplitude. At a proposed η, the corresponding density drops must still satisfy the common-history constraints. Their projection should be retained as a compatible set unless connectedness has been established separately.

Theorem F.4 proves the limiting identification statement without presuming that these sets are intervals. Keep $b, u, d, S, \kappa_0, a_{¿}$ fixed and restrict η to a fixed compact physical search set. For exact residual samples generated by one admissible positive decreasing history, meshes whose maximum spacing tends to zero recover its unique parameter if the valid adjacent-sound-mean interval widths also tend to zero. With exact means on nested meshes, the compatible sets are nested and contract to that parameter. The proof uses the uniform bound $\left|\log\left(q/\left(C Q_{¿}\right)\right)\right| \le 3\delta/2$ inside a cell of width at most δ, followed by a polynomial uniqueness argument; it does not differentiate measured residual samples.

This conclusion requires both increasingly informative sampling and shrinking measurement uncertainty. Proposition F.5 constructs an interior class in which a fixed nonzero sound-mean tolerance preserves a neighborhood of parameters on every mesh. Neither result supplies a finite-sample confidence level or permits the background coefficients to change during refinement. [15]

Table 4.1. Information inputs and the scope of common-history results.

Input	Exact conclusion in its stated class	Essential qualification
Complete residual and matter inequalities	Conditional interval of inverse tensions	Requires control between all epochs
Finite values with shared rates and gains	Exact common-history feasibility at fixed η	Its parameter projection need not be an interval
Smoothness and isolated sound anchors	Local smooth completions remain plentiful	No fixed derivative budget
Finite sound windows	Shared endpoint constraints on q	The mean is of χ in $\log a$
Simultaneous measurement region	Coverage transfers through feasible histories	A deterministic box alone has no probability level

These sets describe identification under the stated inputs. Confidence coverage additionally requires a simultaneous measurement event; tension in physical units requires matched density and gravitational conventions. The following chapters retain these requirements while parametrizing the sound history.

5 Sound Coordinates and Exceptional Histories

5.1 Conservation supplies a useful coordinate

Sound information changes the reconstruction problem because it constrains how a conserved fluid moves through its possible density states. The relevant quantity is the barotropic derivative $\chi = d\,p/d\,v$. It is not the ratio p/v, and it is not the sound horizon inferred from baryon acoustic oscillations. Throughout this chapter there is one conserved barotropic component, positive density and enthalpy, constant positive brane tension, and no energy exchange with the vacuum bulk. The reference scales $S, a_{¿}$ and coefficient $\kappa_0 = g_{ref}/3$ remain fixed. The effective vacuum amplitude b is initially supplied; the next chapter releases it. [13; 18; 19]

Let $I = ¿$ be a compact interval containing zero, with $s = \log(a/a_{¿})$. Conservation and the definition $q = -v' > 0$ give

$$v' = -3(v+p),\; p = -v + \frac{q}{3},\; q' = -3(1+\chi)q. \tag{5.1}$$

For continuous $0 < \chi < 1$, introduce

$$\begin{gathered} Q(s) = \exp\left[-3s - 3\int_0^s \chi(t)\,dt\right], \\ J(s) = -\int_0^s Q(t)\,dt, \\ q(s) = C\,Q(s),\; v(s) = V + C\,J(s),\; C > 0. \end{gathered} \tag{5.2}$$

Here $Q(0) = 1$, $J(0) = 0$, and $V = v(0)$. Since $J' = -Q < 0$, the sound history provides a one-to-one coordinate on the interval. It determines the shape of the transport, while V and C remain

free. In particular, specifying $d\,p/d\,v$ leaves an additive pressure constant undetermined.

Write $E=e^{-4s}$ and remove the supplied vacuum and curvature terms from the dimensionless expansion:

$$\begin{aligned} F=h-b+u\,e^{-2s}=v+\eta\,v^2+d\,E,\\ \eta=\frac{S}{2\kappa_0\lambda_{bare}}>0,\\ F=\alpha_0+\alpha_1 J+\alpha_2 J^2+d\,E,\\ \alpha_0=V+\eta\,V^2,\alpha_1=C(1+2\eta\,V),\alpha_2=\eta\,C^2. \end{aligned} \tag{5.3}$$

This is the four-column inverse: the nonlinear matter history enters through the known coordinate J, leaving a linear coefficient problem. Its fixed-vacuum physical inverse is

$$\begin{aligned} \Delta_\alpha=\alpha_1^2-4\,\alpha_0\alpha_2=C^2,\\ C=\sqrt{\Delta_\alpha},\eta=\frac{\alpha_2}{\Delta_\alpha},\\ V=\frac{2\,C\,\alpha_0}{\alpha_1+C},\lambda_{bare}=\frac{S\,\Delta_\alpha}{2\kappa_0\alpha_2}. \end{aligned} \tag{5.4}$$

The positive branch requires $\alpha_0,\alpha_1,\alpha_2,\Delta_\alpha>0$, $d\geq 0$, positive density and expansion throughout I, and $1/(4\eta)-b>0$. Algebraic uniqueness is therefore separate from physical existence. These conditions also identify what is held fixed when the word *tension* is used in this reconstruction. The physical vacuum convention is revisited in Chapters 6 and 10. [18; 3; 4]

5.2 A complete classification of rank failure

Assume now $\chi\in C^1(I)$. Define

$$D_\chi=3\,\chi'+18\,\chi^2-2. \tag{5.5}$$

This expression diagnoses a precise obstruction: the dark-radiation column can become a quadratic function of the sound coordinate. It is not a new field equation. [19]

Theorem 5.1 — Exceptional sound histories. The functions $1, J, J^2, E$ are linearly dependent on I if and only if $D_\chi \equiv 0$. In the range $0<\chi<1$, all such histories are

$$\chi(s)=\frac{1-\zeta e^{-4s}}{3\left(1+\zeta e^{-4s}\right)}, -\frac{1}{2}<\zeta e^{-4s}<1 \left(s\in I\right), \tag{5.6}$$

for a real constant ζ.

Proof. Put $x=J(s)$, and denote composition with the inverse map by a tilde. Since $d/dx=-Q^{-1}d/ds$, repeated differentiation gives

$$\begin{aligned}\tilde{f}_{xxx}=&-Q^{-3}\{f'''+9(1+\chi)f''\\&+\left[18(1+\chi)^2+3\chi'\right]f'\}.\end{aligned} \tag{5.7}$$

Using $E'=-4E$, $E''=16E$, and $E'''=-64E$, this reduces to

$$\widetilde{E}_{xxx}=\frac{4E}{Q^3}D_\chi, W_s\left(1, J, J^2, E\right)=8EQ^3D_\chi. \tag{5.8}$$

Here W_s is the determinant with these four functions as columns and derivative orders zero through three as rows. A zero of the diagnostic at one epoch does not make it vanish on the whole interval.

The first three functions are independent because $J(I)$ contains an interval. Dependence of all four is thus equivalent to $\widetilde{E}$ being a quadratic polynomial. Its third derivative vanishes exactly when $D_\chi \equiv 0$. This uses the polynomial structure directly; it does not assume a general converse from a vanishing Wronskian.

The remaining differential equation is $\chi' = 2/3 - 6\chi^2$. The substitution

$$z = \frac{1-3\chi}{1+3\chi} \Rightarrow z' = -4z \Rightarrow z = \zeta e^{-4s} \tag{5.9}$$

gives (5.6). Solving $0 < \chi < 1$ on this branch gives precisely $-1/2 < \zeta E < 1$. The negative stationary solution $\chi = -1/3$ is excluded; $\zeta = 0$ includes $\chi = 1/3$. This proves completeness. ▫

For $\zeta \neq 0$, direct integration makes the dependence explicit:

$$\begin{aligned} Q &= \frac{\sqrt{1+\zeta}\,E}{\sqrt{1+\zeta E}}, \\ J &= \frac{\sqrt{1+\zeta}}{2\zeta}\left(\sqrt{1+\zeta E} - \sqrt{1+\zeta}\right), \\ E &= 1 + 4J + g_\zeta J^2, \; g_\zeta = \frac{4\zeta}{1+\zeta}. \end{aligned} \tag{5.10}$$

Consequently the coefficient change

$$\left(\alpha_0, \alpha_1, \alpha_2, d\right) \mapsto \left(\alpha_0 - t, \alpha_1 - 4t, \alpha_2 - g_\zeta t, d + t\right) \tag{5.11}$$

preserves the complete expansion and sound histories. At an interior physical model, sufficiently small changes remain admissible and change d. At a boundary, admissibility must be checked rather than inferred from the null direction alone.

For $\zeta = 0$, $Q = E$ and $J = (E-1)/4$. This familiar radiation-shaped exception permits an affine equation of state; sound one third does not force its constant offset to vanish. For nonzero ζ, the shifted pressure has a modified-Chaplygin form. This connection identifies a known equation-of-state family, not an independently established cosmological matter component. The negative-ζ branch is allowed by the inverse theorem even though its shifted density variable need not be positive. [18; 19]

5.3 Complete histories and finite epochs

Outside the exceptional family, complete exact histories determine at most one coefficient vector. Finite measurements require their own rank condition. At distinct epochs $s_0<\cdots<s_3$, define $x_i=J(s_i)$ and the matrix A with rows $(1, x_i, x_i^2, E_i)$. The divided-difference identity gives, for an intermediate epoch s_ξ,

$$\det A=\frac{2E(s_\xi)D_\chi(s_\xi)}{3Q(s_\xi)^3}\prod_{0\le i<j\le 3}(x_j-x_i). \tag{5.12}$$

Indeed, dividing the determinant by the Vandermonde product gives the third divided difference of $\widetilde{E}$, equal to $\widetilde{E}_{xxx}(x_\xi)/3!$. Thus a nowhere-zero diagnostic makes every four distinct epochs nonsingular. If the diagnostic is merely nonzero somewhere, suitable four-epoch designs exist in a neighborhood of that point. A diagnostic that changes sign does not guarantee every chosen design. [19]

For example, constant $\chi=0.2$ gives $D_\chi=-1.28$; any four distinct epochs have exact coefficient rank four. Constant $\chi=1/3$ gives rank failure for every design, regardless of the number of repeats. These statements concern exact rank, not achievable accuracy.

The distinction becomes sharp near an exception. If $\chi_\varepsilon=\chi_0+\varepsilon r$, where χ_0 is exceptional and $r\in C^1(I)$ is fixed, then

$$D_{\chi_\varepsilon}=\varepsilon(3r'+36\chi_0 r)+18\varepsilon^2 r^2. \tag{5.13}$$

The definitions of Q, J imply $A_\varepsilon-A_0=O(|\varepsilon|)$ for fixed epochs. Applying this difference to a unit null vector of A_0 proves $\sigma_{min}(A_\varepsilon)=O(|\varepsilon|)$. This is an upper bound; some perturbations remain exceptional. A small departure may restore uniqueness while leaving the inverse extremely sensitive to noise.

5.4 Differential and weak consistency

Define the differential operator

$$L_\chi F = F''' + 9(1+\chi) F'' + \left[18(1+\chi)^2 + 3\chi'\right] F'. \tag{5.14}$$

For $F \in C^3(I)$, a fixed constant d admits a four-column representation exactly when

$$L_\chi F + 4\, d\, E\, D_\chi = 0 \text{ throughout } I. \tag{5.15}$$

The proof follows from (5.7): the identity is equivalent to a vanishing third J-derivative of $F - d\,E$, hence to one quadratic on the connected interval. Where $D_\chi \neq 0$, it yields $d = -L_\chi F / (4\,E\,D_\chi)$. Its constancy on only part of the interval does not replace the global condition. [19]

A weak inverse moves derivatives from the measured expansion to a chosen test function. On the increasing interval $J = ¿$, choose $\phi \in C^3$ with ϕ, ϕ', ϕ'' zero at both endpoints. Set

$$A_\phi = \int_J \widetilde{F}\, \phi'''\, dx, \quad B_\phi = \int_J \widetilde{E}\, \phi'''\, dx. \tag{5.16}$$

Three integrations by parts annihilate every quadratic, proving $A_\phi = d\, B_\phi$. If $B_\phi \neq 0$, then

$$d = \frac{A_\phi}{B_\phi}, \quad \left|\hat{d} - d\right| \leq \frac{\varepsilon_F \left\| \phi''' \right\|_1}{\left|B_\phi\right|} \tag{5.17}$$

when the expansion error is uniformly at most ε_F, with exact sound and integration. Moreover,

$$B_\phi = -\int_J \frac{4\,E}{Q^3}\, D_\chi \phi\, dx. \tag{5.18}$$

A nonnegative test supported where the diagnostic has one nonzero sign gives a nonzero denominator. All denominators vanish for an exceptional history. Conversely, equality for

every compactly supported smooth test means that the distributional third derivative of $\widetilde{F}-d\,\widetilde{E}$ vanishes, so the continuous function is a quadratic. Agreement for finitely many tests is only a necessary screen.

The integrals can be evaluated in increasing s using the kernel $\phi'''(J(s))Q(s)$. An alternative is to project E off $span(1, J, J^2)$ in $L^2(I)$: if $R_E = E - \Pi E \neq 0$, then $d = \langle R_E, F \rangle / \| R_E \|^2$. Both versions reveal why proximity to an exceptional history magnifies error. Both require full functions or justified integral enclosures. Four expansion samples do not supply a continuous band. Chapter 9 extends the uncertainty accounting when the sound coordinate itself is uncertain. [3; 20]

5.5 A prediction at a reserved expansion epoch

The four-column representation can be tested on an expansion value that was not used to determine its coefficients. This gives a concrete consequence of the inverse once the sound history and the observational covariance have been specified. The following result is elementary linear prediction applied to the representation in Section 5.2; its value is to state precisely what a prospective check would require.

Proposition 5.2 Reserved-epoch consistency. Fix the sound history, the curvature convention and five distinct epochs before inspecting the expansion observations. Write the mean corrected expansion as $y(s) = a(s)^T \beta$, where the first four rows form an invertible matrix A_T. Let the five observed values have jointly Gaussian errors with known covariance Σ. No independence between training and reserved observations is required.

$$a(s)=\left(1, J(s), J(s)^2, e^{-4s}\right)^T,$$
$$A_T=\begin{pmatrix} a(s_1)^T \\ a(s_2)^T \\ a(s_3)^T \\ a(s_4)^T \end{pmatrix}. \tag{5.19}$$

The four training values determine the linear prediction and its coefficient-free residual:

$$\omega=A_T^{-T}\,a(s_¿),\ \hat{y}_¿=\omega^T y_T,$$
$$r_¿=y_¿-\hat{y}_¿,\ h=\left(-\omega^T, 1\right). \tag{5.20}$$

If $h\Sigma h^T>0$, its standardized squared residual has an exact reference distribution:

$$Z_¿=\frac{r_¿}{\sqrt{h\Sigma h^T}}\sim N(0,1),$$
$$Z_¿^2\sim \chi_1^2. \tag{5.21}$$

Proof. Stack the five design rows into A. The definition of ω gives $hA=0$, so $r_¿=h\varepsilon$. A fixed linear contrast of a jointly Gaussian vector is Gaussian, with mean zero and variance $h\Sigma h^T$. Dividing by its positive standard deviation proves the assertion. The result holds for every fixed coefficient vector for which the mean representation is correct.

This is an unconditional sampling statement for the specified contrast. It is not a conditional probability given the realized training vector. Estimating the sound history from these same observations, selecting the epochs after examining residuals, replacing the known covariance by an estimate, or using a constrained nonlinear training fit changes the experiment and requires additional calibration. A rejection tests the combined

sound, expansion and covariance model; it does not isolate an extra dimension as its cause.

A constructed example fixes $\chi = 0.2$ and training epochs $s = (-0.5, -0.25, 0, 0.25)$, with $s_{¿} = 0.5$ reserved. The transport coordinate is $J = (e^{-3.6s} - 1)/3.6$. The weights, rounded below for display, depend on these design choices and not on β. The computation retains full precision.

$$\hat{y}_{¿} \simeq -0.0247235265\, y_1 + 0.3023077211\, y_2 - 1.2173321837\, y_3 + 1.9397479891\, y_4. \tag{5.22}$$

Using the coefficients of Equation 6.16 to generate all five means gives $y_{¿} = 8.8320623309$, recovered by the four training means to numerical precision. For the declared synthetic covariance $\Sigma_{ij} = 10^{-8} \exp(-|s_i - s_j|/0.25)$, the residual standard deviation is $1.83251219 \times 10^{-4}$. These are generated values for a test design, not observations or forecasts for a measured cosmological fluid. An empirical implementation must first supply the observation model discussed in Section 14.4.

5.6 Numerical conditioning near the exceptional history

A full-rank design can contain little usable information about the physical invariants. The synthetic diagnostic here uses 21 equally spaced epochs in $[-0.5, 0.5]$, an exact constant sound history, independent errors of standard deviation $\sigma_y = 10^{-4}$, and the coefficient vector in Equation 6.16. For each chosen χ, the mean is regenerated as $A(\chi)\beta$; no common fixed data vector is silently fitted to different sound histories.

To compare rank conditioning, each column is divided by its Euclidean length before singular values are calculated. Coefficient covariance is then transformed back to the original units. With the stated independent Gaussian errors, the

unrestricted linear estimator has covariance $V_\beta = \sigma_y^2 \left(A^T A \right)^{-1}$. Singular-value decomposition evaluates this expression without forming an inverse of the normal matrix.

$$\begin{aligned} L &= \frac{\beta_1^2}{4\beta_2} - \beta_0, \\ \nabla L &= \left(-1, \frac{\beta_1}{2\beta_2}, -\frac{\beta_1^2}{4\beta_2^2}, 0 \right)^T, \\ \sigma_{L,lin}^2 &= (\nabla L)^T V_\beta \nabla L. \end{aligned} \tag{5.23}$$

The last line is a first-order uncertainty diagnostic evaluated at the supplied coefficients. It is not an exact confidence interval for the nonlinear invariant. In particular, values of $\sigma_{L,lin}/L$ near or above unity signal that a local Gaussian interpretation is inadequate. Appendix F supplies an interval enclosure that remains valid when coefficient errors are too large for linearization, provided the lower bound on β_2 stays positive.

Table 5.1. Synthetic conditioning of the exact-sound inverse.

Sound χ	Smallest singular value	$\sigma_{L,lin}/L$
0.2000	0.00477449	0.9501
0.3000	0.00132495	6.6898
0.3300	0.000135879	72.8272
0.3330	0.0000136204	733.5911
1/3	zero in exact arithmetic	not identifiable

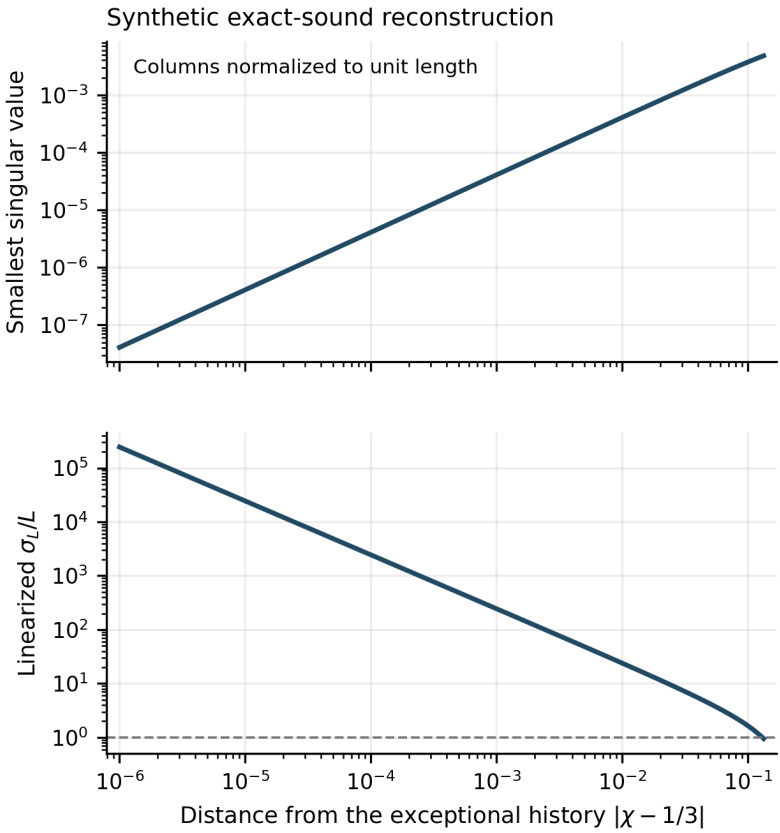

Figure 5.1. Synthetic conditioning for 21 fixed epochs and exact constant sound. The upper panel uses unit-length design columns. The lower panel gives only the first-order fractional uncertainty in L for the declared noise scale; it is not a confidence interval when large. At $\chi = 1/3$ the dark-radiation column is exactly 1 + 4J and the four-column rank drops to three.

For these coefficients, $L = 1/75$ is obtained by subtracting two much larger terms. This cancellation contributes to the sensitivity even at $\chi = 0.2$. The reported noise level is a chosen numerical input, not an estimate of achievable observational precision; scaling it by a factor scales the linearized standard deviations by the same factor. The experiment separates a

structural failure at the Riccati history from the continuous loss of precision as that history is approached. Neither a small fit residual nor exact coefficient identifiability certifies a precise bulk curvature measurement.

Third-edition extension. The preceding Riccati classification assumes that the spatial-curvature contribution has already been supplied. Chapter 18 classifies the five-column problem in which that amplitude is unknown, and identifies the independent calibration that can remove the added freedom.

6 Uncertain Vacuum and Identifiable Bulk Geometry

6.1 Releasing the vacuum intercept

The fixed-vacuum inverse answers a conditional question. If the effective vacuum amplitude is unknown, the expansion coefficients still may be identifiable, but their interpretation changes. Keep the reference $\kappa_0 = g_{ref}/3$, S, a_i, supplied spatial curvature u, and exact sound history fixed. Remove only the known curvature term:

$$\begin{aligned} y = h + u\, e^{-2s} &= \beta_0 + \beta_1 J + \beta_2 J^2 + d\, E, \\ \beta_0 &= b + V + \eta V^2, \\ \beta_1 = C(1 + 2\eta V),\ &\beta_2 = \eta C^2. \end{aligned} \tag{6.1}$$

Rank four identifies $(\beta_0, \beta_1, \beta_2, d)$, provided the observations are represented by these columns. It does not identify the five quantities (b, V, C, η, d). Counting alone suggests a freedom; the following result finds every allowed representative and shows which geometric quantities survive. [3]

6.2 The complete physical family

Define

$$\Sigma = \beta_1^2 - 4\beta_0\beta_2,\ T(s) = \beta_1 + 2\beta_2 J(s),\ C_{max} = \min_I T(s). \tag{6.2}$$

Theorem 6.1 — Free-vacuum equivalence class. Suppose the identified coefficients satisfy $\beta_2>0$, $d\geq 0$, and the common expansion is positive. Every positive-density, positive-tension realization has the unique parameterization

$$\begin{aligned} \eta_C &= \frac{\beta_2}{C^2}, \\ V_C &= \frac{C\left(\beta_1 - C\right)}{2\beta_2}, \\ b_C &= \frac{C^2 - \Sigma}{4\beta_2}, 0<C<C_{max}. \end{aligned} \tag{6.3}$$

The family is nonempty when $C_{max}>0$, and is anti-de Sitter precisely when $\Sigma>0$. A separate prior $b\geq 0$ restricts it to $C^2\geq\Sigma$.

Proof. Solve $\beta_2=\eta C^2$ for η, then $\beta_1=C+2\beta_2 V/C$ for V, and finally the intercept for b. These steps give (6.3) and prove necessity. Conversely, define

$$v_C(s)=\frac{C\left[T(s)-C\right]}{2\beta_2}, p_C=-v_C+\frac{CQ}{3}. \tag{6.4}$$

Substitution recovers all three coefficients. Since $T'=-2\beta_2 Q<0$, positivity throughout I is equivalent to $0<C<C_{max}=T$¿. Differentiation gives $-v_C'=CQ$ and $dp_C/dv_C=\chi$; conservation and positive enthalpy follow. Finally,

$$\frac{1}{4\eta_C}-b_C=\frac{\Sigma}{4\beta_2}, \tag{6.5}$$

which proves the AdS condition. The zero-density endpoint is excluded. ▫

At a supplied b, this reduces to

$$C=\sqrt{\Sigma+4\beta_2 b}\,,\eta=\frac{\beta_2}{\Sigma+4\beta_2 b}, \tag{6.6}$$

subject to the same physical domain. Thus the earlier fixed-vacuum result remains valid. Replacing its discriminant by Σ while treating b as unknown would give a false unique tension.

6.3 Geometry that survives the freedom

Define the dimensionless curvature combination

$$L=\frac{1}{S\ell^2}=\frac{\Sigma}{4\beta_2}=\frac{\beta_1^2}{4\beta_2}-\beta_0. \tag{6.7}$$

Theorem 6.2 — Invariant bulk metric. Under Theorem 6.1, rank-four identification and $L>0$ determine

$$\ell=(SL)^{-1/2},\mu_B=a_i^4 Sd\,,f_k(r)=k+\frac{r^2}{\ell^2}-\frac{\mu_B}{r^2} \tag{6.8}$$

throughout the equivalence class. This follows immediately from (6.5) and the identified d. The bulk metric function is fixed although the matter normalization and split tension vary. On a chosen expanding branch, equal expansion and equal initial scale factor also fix the brane trajectory. [3]

Geometrically, $-L$ is the vertex value of the reconstructed quadratic in J. An affine relabeling $\hat{J}=a_J J+c_J,\ a_J\neq 0$, transforms its coefficients but preserves the vertex value. This is a useful coordinate check. If the vertex lies beyond the visited matter interval, evaluating it remains a model-dependent extrapolation of the quadratic, not a measurement of that unvisited state.

For a planar bulk, $d>0$ gives

$$\frac{r_h}{a_¿}=\left(\frac{d}{L}\right)^{1/4}. \tag{6.9}$$

An exterior brane on the whole interval requires $r_h/a_¿<e^{s_-}$. For supplied nonzero k, the candidate positive metric root is

$$r_h^2=\frac{\ell^2}{2}\left[-k+\sqrt{k^2+\frac{4\mu_B}{\ell^2}}\right]. \tag{6.10}$$

A root and its spacetime interpretation must satisfy the chosen bulk domain. For $k=0, d=0$, zero is not a finite-radius black-hole horizon.

The invariant μ_B has units of length squared. A dimensional bulk mass is proportional to μ_B/G_5, with an additional spatial-volume convention in the planar case. In this family,

$$\lambda_{bare,C}=\frac{SC^2}{2\kappa_0\beta_2}, G_{5,C}=2G_{4,ref}\sqrt{\frac{\eta_C}{S}}, 8\pi G_{4,ref}=g_{ref}. \tag{6.11}$$

Thus invariant geometric mass coefficient does not mean invariant physical mass. Nor does a planar bulk horizon determine the shadow or ringdown of a localized astrophysical black hole.

For smooth exact histories, set $g=y-dE$. The invariant also obeys

$$L=\frac{g'^2}{2\left[g''+3(1+\chi)g'\right]}-g, g''+3(1+\chi)g'=2\beta_2Q^2>0. \tag{6.12}$$

Constancy of this expression is a consistency check within the quadratic model. Its derivative form does not justify twice differentiating noisy distances without an observation and error model.

6.4 Why one density anchor can be insufficient

At an anchored epoch s_a, equation (6.4) gives

$$C^2 - T_a C + 2\beta_2 v_a = 0, T_a = T(s_a). \tag{6.13}$$

A quadratic can have two physical roots. An absolute density measurement therefore need not select one representative. By contrast, two densities at distinct epochs give

$$C = \frac{v_a - v_b}{J_a - J_b}, V = v_a - C J_a, \tag{6.14}$$

and one calibrated enthalpy gives

$$C = \frac{3(v_a + p_a)}{Q_a}. \tag{6.15}$$

The proofs are respectively the difference of two linear density equations and conservation. Every resulting candidate still must obey the full data and physical constraints. Unknown-gain proxies do not supply these anchors. The densities refer to the stated vacuum convention; the argument does not make two indistinguishable constant vacuum terms separately observable. [3; 4]

The information requirement can be stated more economically than two separate absolute density measurements. One absolutely calibrated density difference between distinct epochs already fixes C, because the additive term in $v = V + C J$ cancels and J is strictly monotone. The identified coefficients then determine V through Equation 6.3. A common unknown additive density offset does not obstruct this step; an unknown multiplicative gain does. Proposition F.6 proves this statement and gives finite-error outer bounds when both the density difference and the sound transport are uncertain. Every

candidate remains subject to the physical-domain and joint-data checks.

An exact worked counterexample makes the two-root issue tangible. Take the planar case $k=u=0$ and choose

$$I=[-0.5,0.5],\chi=0.2,$$
$$Q=e^{-3.6s},J=\frac{e^{-3.6s}-1}{3.6},\tag{6.16}$$
$$(\beta_0,\beta_1,\beta_2,d)=(9.5632,3.216,0.27,10^{-4}).$$

Then $\Sigma=0.0144$, $L=1/75$, and $C_{max}\simeq 3.090794833$. The anchor $v(0)=1.2$ admits $C=0.216$ and $C=3$.

Table 6.1. Two representatives sharing one density anchor.

Quantity	First representative	Second representative
C	0.216	3.000
$v(0)$	1.200	1.200
η	5.787037037	0.030000000
b	0.029866667	8.320000000
L	0.013333333	0.013333333
$r_h/a_¿$	0.294283096	0.294283096

Both have positive density, enthalpy, expansion and vacuum amplitude. Their common horizon lies below the earliest brane radius $e^{-0.5}\simeq 0.606530660$. Their split tensions differ by $(3/0.216)^2\simeq 192.90$. This is an analytic construction, with rounded table entries, illustrating identical restricted information rather than two observed universes. [3]

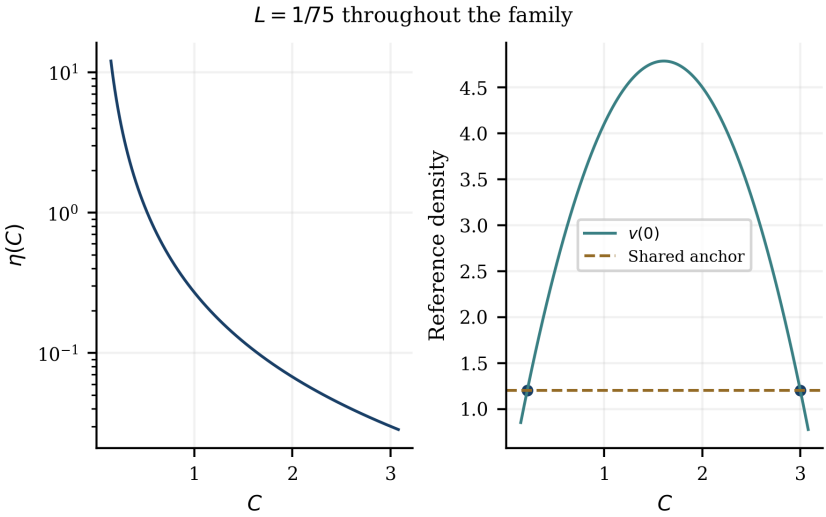

Figure 6.1. The equivalence class of Equation 6.16. The inverse tension and density normalization vary with C, while the bulk curvature combination remains 1/75. The two marked representatives share the density anchor v(0)=1.2. The figure uses the planar example and its stated physical interval.

6.5 From a reconstruction orbit to an action convention

The physical meaning of this family requires more care than its algebra. Relative to one representative, let $\alpha = C_{new}/C > 0$. Equations (6.3)–(6.4) give

$$
\begin{aligned}
v_\alpha &= \alpha\, v + \frac{\alpha(1-\alpha)}{2\eta}, \\
p_\alpha &= \alpha\, p - \frac{\alpha(1-\alpha)}{2\eta}, \\
\eta_\alpha &= \frac{\eta}{\alpha^2}, b_\alpha = b + \frac{\alpha^2-1}{4\eta}, \\
\lambda_{bare,\alpha} &= \alpha^2 \lambda_{bare}, G_{5,\alpha} = \frac{G_5}{\alpha}.
\end{aligned}
\tag{6.17}
$$

If the microscopic matter action may change, this transformation can multiply the entire classical action by α. For the scalar realization $F(X)-U_0$, with $8\pi G_5=M_5^{-3}$, one implementation is

$$\begin{aligned} M_{5,\alpha}^3=\alpha M_5^3, F_\alpha=\alpha F, \\ U_{0,\alpha}=\alpha U_0-(\alpha^2-\alpha)\lambda_{bare}, \\ \tau_{vac}=\lambda_{bare}+U_0, \tau_{vac,\alpha}=\alpha\tau_{vac}. \end{aligned} \tag{6.18}$$

With geometric bulk cosmological constant fixed, the bulk, boundary and brane actions scale together. Classical stationary configurations are unchanged. Scaling a whole action at fixed $\hbar$ is not generally a quantum equivalence, and the full transformation is unavailable if other matter sectors have independently fixed absolute normalizations. [3; 4]

After subtracting the declared constant vacuum, the coefficient of linear excitation density is different from the reference split coefficient:

$$\begin{aligned} g_{ref}=g_{split}=\frac{\lambda_{bare}}{6M_5^6}, \\ g_{bg}=\frac{\tau_{vac}}{6M_5^6}, \\ (g_{split})_\alpha=g_{split}, (g_{bg})_\alpha=\frac{g_{bg}}{\alpha}. \end{aligned} \tag{6.19}$$

An exact nonzero absolute determination of g_{bg} can therefore select at most one member of this orbit. Identifying it with locally measured $8\pi G_N$ needs low-energy localization, fixed stress standards and negligible extra scalar or bulk contributions. Chapter 10 supplies the action-level account; a local source matching calculation has not been completed for

every cosmological scalar state. This conditional route does not contradict the earlier inverse at fixed g_{ref}.

There is also a separate, exact parameter redundancy:

$$\lambda_{bare} \mapsto \lambda_{bare} + \Delta, U_0 \mapsto U_0 - \Delta. \tag{6.20}$$

Only their sum occurs in the action. No observable of that identical action can distinguish the two labels without additional structure. An absolute gravitational calibration removes the stated scaling orbit under its matching conditions; it does not remove this vacuum-split redundancy. The distinction is already rooted in the brane stress decomposition and becomes decisive when a reconstructed history is promoted to a dynamical model. [7; 4]

6.6 The limits of the invariant statement

The Riccati exceptions of Chapter 5 survive the release of b. At $\chi = 1/3$, changing the coefficients by $t(-1, -4, 0, 1)$ preserves complete histories while changing d and generally L. Bulk invariance is therefore conditional on coefficient identification, not guaranteed by any expansion-plus-sound pair. [19; 3]

Outside that exception, finite measurements still require informative epochs, adequate precision and a validated sound model. Additional density differences must give one common C, and calibrated enthalpies must make $3(v + p)/Q$ constant. These are operational restrictions on the declared model. Chapter 9 propagates uncertainty through the joint sets so that neither a spurious unique tension nor an artificially precise bulk geometry is created by substituting fitted sound values as though they were exact.

An invariant can nevertheless be poorly conditioned. In the example of Equation 6.16, $L = 9.576533333\ldots - 9.5632 = 1/75$ is a small difference of larger quantities. Its response to

coefficient errors is governed locally by Equation F.29, and a small first-order uncertainty is not guaranteed by rank alone. Proposition F.7 gives an exact finite-error enclosure of L for a rectangular coefficient region. A finite upper bound on the AdS radius follows from that certificate only when the enclosed L values are separated from zero. Correlations and further physical constraints should be retained when the joint region supplies more information than its bounding rectangle.

Third-edition extension. The invariance just established applies to the declared normalization family with supplied curvature. Chapter 18 constructs an enlarged coefficient family in which curvature is free and the bulk geometric quantities vary despite identical expansion and sound. Chapter 15 treats finite correlated coefficient uncertainty, and Chapter 17 addresses competing physical origins.

7 Sound Windows and Spectral Recovery

7.1 A logarithmic modulation is a hypothesis

The conservation coordinate of Chapter 5 makes prescribed sound histories tractable. It does not select their functional form. One candidate is a sinusoid in logarithmic scale factor,

$$\chi(s)=\chi_0+A\cos(\omega s+\delta),\ 0<|A|<min(\chi_0,1-\chi_0). \tag{7.1}$$

The inequality supplies a strict sound margin. Choosing $\omega=2\pi/\log\varphi$, where $\varphi=(1+\sqrt{5})/2$, inserts a golden-ratio period into the matter model. Neither the Einstein equations nor a drawing of an expanding spiral derives that choice. A monotone scale factor can be displayed on a logarithmic spiral with a freely assigned angular coordinate. Such a display changes the representation of a history rather than its dynamics. [21]

For (7.1), conservation gives

$$\begin{aligned} Q(s)&=\exp\{-3(1+\chi_0)s \\ &\quad -3A/\omega[\sin(\omega s+\delta)-\sin\delta]\}, \\ J(s)&=-\int_0^s Q(t)\,dt,\ v=V+CJ. \end{aligned} \tag{7.2}$$

Every nonconstant finite sum of distinct positive-frequency harmonics is outside the complete-history exception of Chapter 5. Indeed, let ω_K be its highest frequency with amplitude $A_K\neq 0$. The diagnostic $3\chi'+18\chi^2-2$ contains a harmonic at $2\omega_K$ with amplitude $9A_K^2$. No derivative term or product of lower frequencies can cancel it. Consequently $1, J, J^2, e^{-4s}$ are functionally independent. This proof works for arbitrary distinct positive frequencies; it grants no special dynamical status to the golden choice. [22]

Functional independence does not guarantee a well-conditioned sampled matrix. For example, when the mean sound is $1/3$, expansion epochs taken at one repeated modulation phase can make the sampled dark-radiation column affine in J. The sampled rank then falls even though the continuous functions are independent. More observations at the same aliased phases do not repair that design. [21; 23]

7.2 What a sound window measures

Assume an observation is a uniform average of χ over a width $w>0$ centered at c, both measured in $s=\log(a/a_{¿})$. For a harmonic its response is

$$W_w\chi(c)=\chi_0+A\,m_w(\omega)\cos(\omega c+\delta),\qquad m_w(\omega)=sinc(\omega w/2),\ sinc\,x=\frac{\sin x}{x}. \tag{7.3}$$

These are stipulated effective-fluid sound observations. The operator averages χ itself in logarithmic scale factor. Averaging its square root, using cosmic time, or interpreting it as the baryon acoustic sound horizon would change the measurement. An astronomical application needs a forward model connecting perturbation measurements to this operator and its joint errors. The results below begin after that observation model has been supplied. [15; 21]

Two widths can recover an unknown single frequency without fitting the gravitational sector. Measure widths Δ and 2Δ at common centers, and remove each vector's constant component with $P_N=I-11^T/N$. Let $U=P_N\,y^{(1)}$ and $Z=P_N\,y^{(2)}$. The identity $sinc(2x)=\cos x\,sinc\,x$ gives

$$Z=r\,U,\ r=\frac{U^TZ}{U^TU}=\cos(\omega\Delta/2),\ \omega=\frac{2}{\Delta}\arccos r. \tag{7.4}$$

This inverse requires $U \neq 0$ and a declared frequency branch inside $(0, 2\pi/\Delta)$. Frequency recovery requires calibrated relative gains and window widths. Centering can protect the frequency ratio against constant channel offsets; it does not remove an unknown relative multiplicative gain. Once the frequency is known, three distinct phases permit recovery of the physical sound baseline χ_0 and both quadratures, provided the absolute gain and zero point are also calibrated. [23]

The inverse also displays its instability. With deterministic centered errors of norms at most ϵ_1, ϵ_2, an observed ratio formed from $\widetilde{U}, \widetilde{Z}$ obeys

$$|\hat{r} - r| \leq \frac{\epsilon_1 + \epsilon_2}{\|\widetilde{U}\|}, \widetilde{U} \neq 0. \tag{7.5}$$

Intersect this enclosure with the cosine image of the allowed branch before applying the decreasing arccosine. An empty intersection indicates incompatibility with the assumed signal and error bounds. A small centered response yields a broad enclosure even if the algebraic ratio can be computed. Near a branch endpoint, arccosine further amplifies error. [23]

7.3 Multiple modes need additional structure

A second oscillation changes the paired-width ratio: it is generally no longer the cosine of either frequency. Nor is it necessarily a positive weighted average of their cosines; that interpretation requires orthogonal centered mode responses. Omitting a mode can bias the inferred gravitational coefficients while all final coefficients remain physically admissible. [22]

Three commensurate widths provide an exact two-mode construction. Assume $0<\omega_1<\omega_2<2\pi/\Delta$, so both frequencies lie on the same injective cosine branch. Set $c_j=\cos(\omega_j\Delta/2)$, with $c_1\neq c_2$, and let z_j be their centered first-width responses. For widths $n\Delta$, define $H_n=n\,P_N\,y^{(n)}$. The Chebyshev identity gives

$$\begin{aligned} H_n&=\sum_{j=1}^{2} U_{n-1}(c_j)\,z_j,\\ H_3&=2t\,H_2-(4\,p_f+1)\,H_1,\\ t&=c_1+c_2,\ p_f=c_1c_2. \end{aligned} \tag{7.6}$$

If z_1, z_2 are independent, the recurrence determines t, p_f; the roots of $x^2-t\,x+p_f$ give the two cosines. A single arccosine branch removes the branch ambiguity, and a separate rank-five condition on the uncentered design recovers the constant and four quadratures. Two real roots from noisy data alone do not establish two physical modes. Close roots, nearly dependent response vectors and an omitted third mode all undermine interpretation. [22]

One synthetic example in the source makes the risk concrete:

Table 7.1. Source-reported bias from omitting a sound mode.

Model used to fit two-mode truth	Recovered η	Recovered d
Generating values	0.030000	0.150000
Misspecified single mode	0.027485	0.116383

The single-mode coefficients pass the stated physical screen. Their disagreement is therefore model error, not a violation that a positivity filter necessarily detects. These are source-reported synthetic calculations under supplied b, u and scales; they are neither astronomical estimates nor new numerical reruns for this chapter. [22, Table 3]

7.4 Exact blindness and stable design

An integer number of periods within every window erases a harmonic exactly. For widths $w_j = j\Delta$, the frequency $2\pi/\Delta$ has $m_{w_j} = 0$ for every j. An irrational ratio between two widths removes such common zeros. For complete center functions on an open interval, this suffices for injectivity on finite trigonometric sums: linear independence of distinct harmonics forces any invisible harmonic to vanish in every channel. [24]

Two qualifications are essential. First, finitely many measurements cannot identify an unrestricted number of modes. If the number of unknown real coefficients exceeds the number of observations, a linear null direction exists; a small perturbation in that direction can preserve a strict sound margin. Second, absence of exact zeros says nothing by itself about noise amplification. Define

$$T_w(\omega) = \left[\sum_j m_{w_j}(\omega)^2\right]^{1/2}, \gamma_\Omega = \min_{0 \le \omega \le \Omega} T_w(\omega). \tag{7.7}$$

The positive floor on a declared compact band quantifies transfer visibility. Every fixed collection of positive widths still has $T_w(\omega) = O\left(|\omega|^{-1}\right)$ as frequency grows, so no all-frequency positive floor exists. With widths $(\Delta, 2\Delta, \varphi\Delta)$, the Fibonacci frequencies $\omega_n = 2\pi F_n/\Delta$ satisfy

$$T_w(\omega_n) = \frac{\sin\left(\pi\varphi^{-n}\right)}{\pi\varphi F_n}, F_n^2 T_w(\omega_n) \to \frac{1}{\sqrt{5}\varphi}. \tag{7.8}$$

Golden widths remove common zeros but retain increasingly weak responses. This is a property of the chosen averaging design, not evidence for Fibonacci dynamics in the Universe. [24]

A usable numerical design criterion needs an enclosure between grid points. Since $|sinc'x| \le 1/2$, the transfer norm is Lipschitz with constant $L_\omega = \|w\|_2/4$. A frequency grid of maximum spacing h_ω, including both band endpoints, supplies

$$\max\{0, g_{grid} - L_\omega h_\omega/2\} \le \gamma_\Omega \le g_{grid}, \tag{7.9}$$

where g_{grid} is the smallest grid response. Width uncertainty further reduces the guaranteed floor by at most $\Omega\|\delta w\|_2/4$. Rounding error requires separate control if a formally certified computational bound is claimed. [24]

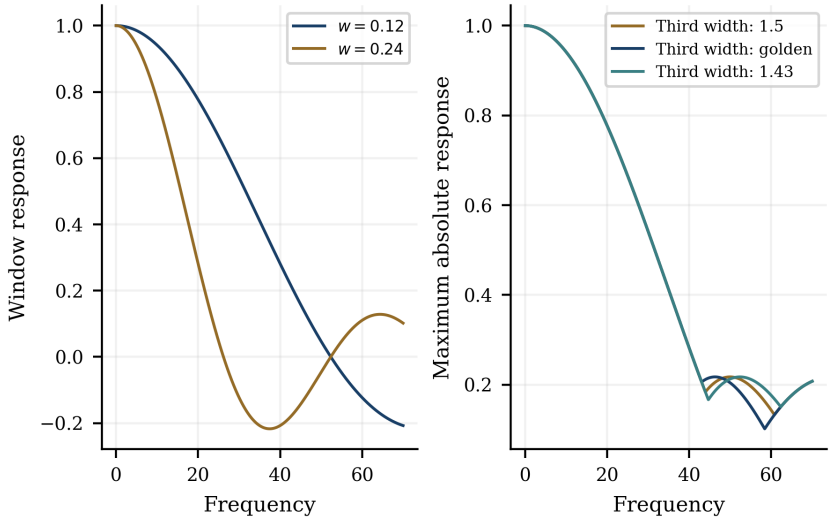

Figure 7.1. Uniform sound-window transfer on the declared frequency band. Left: the signed responses of widths 0.12 and 0.24. Right: their combined magnitude with a third width of ratio 1.5, the golden value, or 1.43. A finite-band design comparison does not establish an all-frequency stability guarantee.

For the source's declared band $[0, 70]$ and $\Delta = 0.12$, the grid lower bounds from (7.9) are approximately 0.20709 for width ratio 1.5, 0.16421 for φ, and 0.21684 for the selected ratio 1.43, each used alongside $\Delta, 2\Delta$. A rational design can therefore

outperform a golden design on a finite band even though it has a common zero elsewhere. The criterion and frequency band determine the comparison. Finite-center conditioning, covariance and the final physical target must also enter an actual design decision. [24, Table 2]

7.5 When expansion adds independent information

For a supplied sound parameter vector, expansion retains the linear four-column form of Chapter 5. That physical inverse assumes fixed b; its coefficient precision cannot be transferred unchanged to the free-vacuum tension family of Chapter 6.

The statistical information statements in Sections 7.5 and 7.6 assume Gaussian errors with fixed known covariance and independent sound and expansion blocks. The Jacobian rank identity itself is deterministic and does not require that probability law. In the corresponding whitened coordinates, let $\overline{A}$ be the expansion matrix, X the sound Jacobian and D the expansion derivatives with respect to sound parameters. The combined Jacobian is

$$G=\begin{pmatrix} X & 0 \\ D & \overline{A} \end{pmatrix}, P_A^{\perp}=I-\overline{A}\,\overline{A}^{+¿.¿} \tag{7.10}$$

Proposition 7.1 — Independent expansion information. If $\overline{A}$ has rank four, the joint Jacobian has full column rank exactly when

$$ker\,X \cap ker\left(P_A^{\perp} D\right)=\{0\}. \tag{7.11}$$

Proof. A null perturbation must satisfy $X\,\delta\theta_s=0$ and $D\,\delta\theta_s+\overline{A}\,\delta\alpha=0$. The second equation has a solution precisely when its sound perturbation lies in the gravity-column span, equivalently when $P_A^{\perp} D\,\delta\theta_s=0$. Full rank of $\overline{A}$ then eliminates any remaining pure gravity null vector. ▫ [25]

This explains why expansion can help with a sound-blind mode. It also explains why four expansion epochs are insufficient to guarantee that help: an invertible square A can absorb small sound changes by changing its four coefficients. At an interior physical model, sufficiently small perturbations preserve the strict physical inequalities, so this coefficient freedom gives nearby physical alternatives. More generally, if sound leaves r_0 first-order directions undetermined, at least r_0 expansion residual dimensions beyond the four gravity columns are necessary. Several hidden directions must remain jointly independent after projection; checking each column separately is insufficient.

Even when rank is restored, information can be small. For an infinitesimal high-frequency mode added to a fixed smooth base history, integration by parts gives $\| P_A^{\perp} D_{\Omega} \| = O\left(\Omega^{-2}\right)$ at fixed epochs and noise. Leading terms lie in the gravity-column span and disappear on projection. At a sound common zero, the resulting local amplitude information can decay as Ω^{-4}. This is a local derivative statement around the specified base, not a bound on every finite nonlinear modification. [25]

7.6 Unknown frequency and weak signals

An unknown upper frequency introduces another distinction. Let G_v contain the nuisance derivatives, including its two amplitude quadratures, and let h_{Ω} be the frequency derivative of the full whitened mean. If G_v has full column rank, the effective local frequency information is

$$I_{\Omega} = ¿¿ \tag{7.12}$$

Positive I_{Ω} gives a regular local inverse direction. The associated local standard-deviation scale is $I_{\Omega}^{-1/2}$; it is not a guarantee that a nonlinear search finds the correct frequency

globally. At a window zero, the amplitude response may vanish while its frequency derivative remains nonzero. At zero physical amplitude, however, the entire mean is independent of that frequency. [26]

On a bounded interval, the derivative of a harmonic with respect to frequency is proportional to its amplitude magnitude. Here $A \geq 0$ denotes the Euclidean norm of the upper harmonic's two quadrature coefficients. The corresponding conservation and expansion derivatives obey the same amplitude scaling. Consequently

$$\| h_{\Omega} \| \leq A\, C_{\Omega}, I_{\Omega} \leq A^{2} C_{\Omega}^{2}, \tag{7.13}$$

for a constant determined by the fixed physical and observation bounds. Nearby frequency models therefore approach the same probability law as $A \to 0$. Reporting a precise frequency when the component itself is absent cannot be justified by optimization alone. Separated bands and nonzero signal assumptions should be visible whenever regular frequency errors are quoted. [26]

Table 7.2. Distinct questions in spectral reconstruction.

Question	Required control	What it does not establish
Is a harmonic visible?	Window transfer and finite design rank	Adequate precision
Can sound and expansion recover local parameters?	Joint projected Jacobian rank	A global unique solution
Is an added frequency estimable?	Nonvanishing effective information	Detection of an added component
Is a selected mode significant?	Calibration of the actual search and null	A cosmological interpretation

These distinctions determine the statistical problem. A frequency chosen because it gives the largest apparent improvement is no longer a prespecified frequency. Its reference distribution must account for that search, the nuisance family and the covariance assumptions. Chapter 8 develops those controls before any spectral claim is carried into physical reconstruction.

8 Selection and Covariance in Statistical Validation

8.1 State the experiment before stating significance

A fitted oscillation, a rejected null hypothesis and a confidence interval answer different questions. Their guarantees also depend on different observation models. Series II moves from a nonlinear joint sound–expansion search to sound-only validation, then from known covariance to independent complete repeats with unknown covariance. These transitions add useful results by changing assumptions or statistical targets. They cannot be compressed into one unrestricted claim that a detected frequency has been validated. [27; 28; 29; 30]

In the known-covariance experiment, a specified fixed whitening gives $z=\left(z_s, z_F\right) \sim N_N\left(g, I_N\right)$. The source design has 51 sound means and 41 expansion coordinates, with known sound covariance and independent known-variance expansion errors. Other designs require their own matrices. The theoretical guarantees do not attach to the number 92; they attach to the stated mean, covariance and independence conditions.

Table 8.1. Statistical experiments and their validation targets.

Procedure	Observation requirement	Statistical target
Calibrated nonlinear joint search	Known Gaussian covariance; declared null references	Improvement produced by the specified fitting algorithm
Selected sound validation	Known Gaussian covariance; independent information split	A component in a selected sound subspace
Validation with uncertain primary frequency	Previous conditions and fixed bounds on the primary family	An added projected component after bounded primary leakage
Validation with unknown covariance	Independent, identically distributed complete Gaussian repeats	The same selected component with covariance uncertainty included

The sound-only null permits an arbitrary expansion mean. Expansion may guide selection without supplying the held-out validation statistic. This enlarged null covers the inherited physical nulls but changes what is being tested. Its sound guarantee can survive a change to the gravity intercept when the sound and noise assumptions remain valid. A joint search calibrated for a fixed-vacuum physical null requires renewed calibration if that null or its score changes. [28; 30; 3]

8.2 Calibrating a nonlinear search algorithm

Let a fully specified fitting procedure return residual sums R_0, R_1 for the null and alternative. Define

$$T_A(z) = max\{0, R_0(z) - R_1(z)\}. \tag{8.1}$$

The procedure includes frequency bands, initializations, stopping rules, parameter screens and a rule for failures.

Without certified global minima, this is an algorithm-defined improvement score. A local optimizer can nevertheless yield a valid test if its complete score distribution is calibrated under the null. It does not yield a certificate excluding every unvisited parameter value. [27]

For a specified null $g_0(v)$, independently generate B observations from the same Gaussian law and apply the identical procedure. The Monte Carlo p-value is

$$p_B(v;z)=\frac{1+\sum_{b=1}^{B}1\{T_A(z_b)\geq T_A(z)\}}{B+1}. \tag{8.2}$$

Proposition 8.1 — Specified-null calibration. Under that null,

$$Pr\{p_B\leq\alpha\}\leq\frac{\lfloor\alpha(B+1)\rfloor}{B+1}\leq\alpha. \tag{8.3}$$

Proof. The observation and calibration scores are exchangeable. Without ties, the observed descending rank is uniform on $1,\ldots,B+1$. Counting ties with “greater than or equal” only increases the reported p-value. Counting the ranks that permit rejection proves the bound. ▫ [27]

A shorter search on simulated data, a frequency band chosen from the observation but held fixed in simulation, or selective removal of failed observed fits breaks that exchangeability argument. Increasing the number of simulations cannot repair a mismatch in the procedure.

Unknown null parameters need additional treatment. A maximum $p_V=max_{v\in V}\,p_B(v;z)$ controls every member of a fixed finite reference set V, since it dominates the p-value at the true reference. No multiplicity factor over these references is needed. A supremum over the complete null family would similarly be valid, but an attained local maximum is a lower

bound on that supremum and cannot certify rejection. A finite reference grid does not establish continuum coverage merely by being dense. [27]

One explicit extension uses distances between whitened Gaussian means. Their total variation distance is

$$v_{TV}(r)=2\Phi(r/2)-1,\ p_{cover}=min\{1,\ p_V+v_{TV}(r)\}. \tag{8.4}$$

If every allowed null mean lies within distance r of a reference, this correction controls that covered family. For $0<\alpha<1$, if $\alpha\le v_{TV}(r)$, rejection is impossible for the finite Monte Carlo p-value. Otherwise, rejection under the nearby reference has probability at most $\alpha-v_{TV}(r)$; changing only the observation law increases it by at most the total variation distance. The simulations remain independent with their original law. Coverage of the mean-space neighborhood is an assumption to establish, not a consequence of plotting reference fits. [27]

A fitted-null bootstrap uses $\hat{v}(z)$ to generate its calibration law. The observed vector is then not an independent draw from a null fixed at that estimate. Such a bootstrap may have validity under additional conditions, but the rank proof above does not establish it. The +1 correction addresses simulation rank, not estimated-null dependence.

8.3 Independent validation with known covariance

Suppose the primary frequency is supplied. Let X_0 contain the whitened constant and two primary quadratures, and let

$$P=I-X_0X_0^{+¿.¿} \tag{8.5}$$

Under the enlarged sound null $g_s\in col(X_0)$, the projected mean vanishes exactly. A prespecified finite-frequency scan of projected noise can therefore be calibrated by the same exchangeability argument without estimating physical

nuisance parameters. Selection using the same residual still has to be included in that scan; a fixed-frequency chi-squared reference does not calibrate a maximum over frequencies. [28]

An alternative reserves independent information for validation. For a fixed fraction $0<f<1$ and independent $\xi \sim N_N(0, I_N)$, set

$$z^{tr} = z + \sqrt{(1-f)/f}\,\xi, \qquad z^{va} = z - \sqrt{f/(1-f)}\,\xi. \tag{8.6}$$

Their cross covariance is zero; joint Gaussianity makes them independent. Their covariances are I/f and $I/(1-f)$, and $z = f\,z^{tr} + (1-f)\,z^{va}$. Thus randomization partitions information without creating another observation. The selector may inspect training sound and expansion, but not validation, the original vector or the randomization separately. Either of the latter, together with training, can reveal held-out information. [28]

This Gaussian construction is an instance of established information splitting and data fission. The choice $\tau_{split} = \sqrt{(1-f)/f}$ translates the usual fission parameterization into Equation (8.6). The result developed below applies it to the selected, primary-residualized sound subspace and its stated nuisance model. [52; 55]

Let training choose an orthonormal basis U in the primary-residualized upper-mode space, of rank $r \le 2$. Conditional on training,

$$T_{va} = (1-f)\,\| U^T P\, z_s^{va} \|^2 \sim \chi^2_r \tag{8.7}$$

under the null. The proof is immediate: the projected validation vector has zero mean and identity covariance after multiplication by $\sqrt{1-f}$. Rank zero abstains. An inaccurate

training fit reduces usefulness or power; it does not change this conditional Gaussian law.

For a training-chosen unit direction q, the corresponding interval targets $\psi = q^T P g_s$, the total projected sound mean. It does not cover an unprojected amplitude, true frequency, tension or bulk mass. Furthermore, if the upper harmonic is exactly erased by every sound window, the validation mean is unchanged under its presence. Expansion may identify a promising frequency during training while sound validation remains at null-level power. That statement concerns this sound-only route, not every joint test. [28]

Known covariance is essential to the artificial split. If the actual covariance of z is $I + E$, the cross covariance of the two components is E. Nominal whitening with an estimated or incorrect covariance therefore does not inherit independence.

8.4 A primary frequency interval leaves bounded leakage

If the primary frequency lies in an externally supplied interval, no fixed linear contrast can remove every primary harmonic in that interval while retaining other harmonic means. To see why, associate a finite-window contrast with its compactly supported kernel $k_q(t)$. Its Fourier transform

$$F_q(v) = \int k_q(t) e^{i v t} d t \tag{8.8}$$

is entire. Removing both quadratures on a nonempty open frequency interval makes this function vanish there, hence everywhere by the identity theorem. This obstructs exact linear removal; it does not rule out nonlinear nuisance inference or controlled approximate removal. [29]

A practical construction projects the constant and the first K frequency derivatives at a nominal ω_c. The primary-only sound

mean is $g_{s,0}=\chi_0 c+X_\omega a$, where c is the constant column and X_ω contains the two harmonic columns in the whitened sound coordinates. Restrict $|\omega-\omega_c|\le h_\omega$, $0\le\chi_0\le 1$, and $\|a\|\le A_{max}$, while leaving the expansion mean unrestricted. For any selected orthonormal U, define $d_j=\|U^T X_{\omega_c}^{(j)}\|_{op}$ and a uniform derivative bound M_{K+1}. The window kernels provide such a bound through their absolute moments. Taylor's theorem gives

$$\begin{aligned} R_U &\le \sum_{j=0}^{K} \frac{h_\omega^j d_j}{j!}+\frac{h_\omega^{K+1} M_{K+1}}{(K+1)!}, \\ R_U &= ¿\omega \|U^T X_\omega\|_{op}, \\ B_U &= \|U^T c\|+A_{max} R_U, \|U^T g_{s,0}\|\le B_U. \end{aligned} \tag{8.9}$$

Here c is the transformed constant column and $g_{s,0}$ the primary-only mean. In implementation, replace R_U by its computable upper bound. A grid can tighten it only with a justified between-grid derivative correction. Small residual derivative columns must be retained when exact annihilation is not achieved numerically. [29]

Training may choose the frequency and projection order. Under known covariance, $Z=\sqrt{1-f}\,U^T z_s^{va}$ has identity covariance and null mean norm at most $b_U=\sqrt{1-f}\,B_U$. Its squared norm therefore has noncentrality no larger than b_U^2. Comparing $\|Z\|^2$ with the upper tail of $\chi_r^2(b_U^2)$ is conservative because that family is stochastically increasing in noncentrality. This yields conditional control over the bounded primary family without assuming that a fitted primary projector exactly removes the truth. [29]

The interval, amplitude bound and covariance must be justified independently of the tested observation. The source's amplitude bound of one half follows for a globally causal single

sinusoid; it does not follow from causality only on a finite observed segment. With primary leakage retained, the confidence target is now the projected added component, rather than the total projected mean of the previous section.

8.5 Unknown covariance requires a different observation model

Let L_0 be a fixed invertible nominal transformation of the sound block. The complete vectors Y_j below are already expressed in those coordinates, with $c = L_0 1$ and $X_v = L_0 W_v$, where W_v contains the untransformed window responses of Chapter 7. The unknown covariance Σ refers to these same coordinates; L_0 need not whiten it. The unknown-covariance construction assumes complete repeats

$$Y_j \overset{iid}{\sim} N_N(g, \Sigma), \Sigma \succ 0 \text{ unknown}. \tag{8.10}$$

Within a repeat, sound and expansion coordinates may have arbitrary correlations. Across repeats, independence, common mean and common covariance are essential. Distinct redshift bins, overlapping windows, or repeated readouts sharing calibration error are not automatically independent complete vectors. A common cosmic-variance component also violates this contract. [30]

Disjoint repeat groups provide independent training and validation without knowing Σ. Training chooses U and a valid primary radius B_U using the same transformed window columns. In n validation repeats let $V_i = U^T Y_{i,s}$, with sample mean $\overline{V}$ and usual unbiased covariance S_V. For $n > r > 0$, form

$$D = n \min_{\|m\| \le B_U} (\overline{V} - m)^T S_V^{-1} (\overline{V} - m). \tag{8.11}$$

Theorem 8.2 — Hotelling domination. Write $a_{n,r}=(n-r)/[r(n-1)]$. Rejecting when $a_{n,r}D$ exceeds the $(1-\alpha)$ quantile of $F_{r,n-r}$ has conditional null probability at most α.

Proof. The true projected primary mean m_0 belongs to the nuisance ball. Hence, pointwise,

$$D\le n(\overline{V}-m_0)^T S_V^{-1}(\overline{V}-m_0)=T_0^2,$$
$$a_{n,r}T_0^2\sim F_{r,n-r}. \tag{8.12}$$

The second line is the classical Gaussian one-sample Hotelling law, conditional on training. The rejection event for D is contained in the corresponding level-α event for T_0^2. Integrating over training preserves the bound. ▫ [30]

The minimized statistic $a_{n,r}D$ does not generally have an exact F distribution. The reference dominates it. The proof integrates over the validation mean and covariance estimate together; it is not conditional on the realized S_V. Only an at-most-two-dimensional covariance is estimated, so one requires $n>r$, not $n>N$. Rank zero or $n\le r$ requires abstention for this construction.

The ball minimization is a convex problem. If $\overline{V}$ lies in the ball, $D=0$. Otherwise, diagonalize $S_V=O\,diag(s_j)O^T$ and write $z=O^T\overline{V}$. For $B_U>0$, its unique solution is

$$m_{¿}=O\left(\frac{z_j}{1+\lambda_{opt}s_j}\right)_j,\ \sum_j\frac{z_j^2}{(1+\lambda_{opt}s_j)^2}=B_U^2. \tag{8.13}$$

The multiplier $\lambda_{opt}>0$ is a numerical optimization variable, unrelated to brane tension. The left side decreases continuously to zero, so a bracketed scalar solve determines it. At $B_U=0$, the only possible nuisance mean is zero. [30]

For component confidence statements, assume the alternative mean decomposes as $g_s = g_{s,0} + g_{s,add}$, with the primary contribution satisfying the same family bounds. The target is $U^T g_{s,add}$. Subtracting a proposed added component before applying (8.11) gives a confidence region: the Minkowski sum of $\overline{V}$, the nuisance ball and the centered Hotelling ellipsoid. It simultaneously covers all directional contrasts within the training-selected subspace. A direction chosen after validation may be reported from that whole region. A smaller scalar Student interval instead requires the direction to have been chosen using training alone. [30]

For that scalar route, let the primary contrast lie in $\left[l_q, u_q\right]$, and let $\overline{Z}, s_q$ be the validation mean and standard deviation. The added contrast has the interval

$$\left[\overline{Z} - u_q - t_{¿} s_q/\sqrt{n}, \overline{Z} - l_q + t_{¿} s_q/\sqrt{n}\right], t_{¿} = t_{n-1,1-\alpha/2}. \tag{8.14}$$

It follows by applying the centered Student law to the total mean and subtracting every allowed primary contribution. Neither this interval nor the projected region identifies a physical frequency or the complete matter history. Rejecting whenever either a directional test or the ball test is significant also needs multiplicity control.

8.6 What numerical validation can establish

The cost of covariance estimation is visible even without frequency selection or primary leakage. With $r = 2$, $B_U = 0$ and $n > 2$, inserting sample covariance into a chi-squared reference gives null rejection probability

$$Pr\{T_0^2 > \chi^2_{2,0.95}\} = \left(1 + \frac{\chi^2_{2,0.95}}{n-1}\right)^{-(n-2)/2}. \tag{8.15}$$

It is approximately 33.4 %, 15.6 % and 8.5 % at $n = 4, 8, 20$, respectively, instead of 5 %. This classical finite-sample effect explains why an estimated covariance cannot simply replace a known covariance while leaving the reference law unchanged. [30]

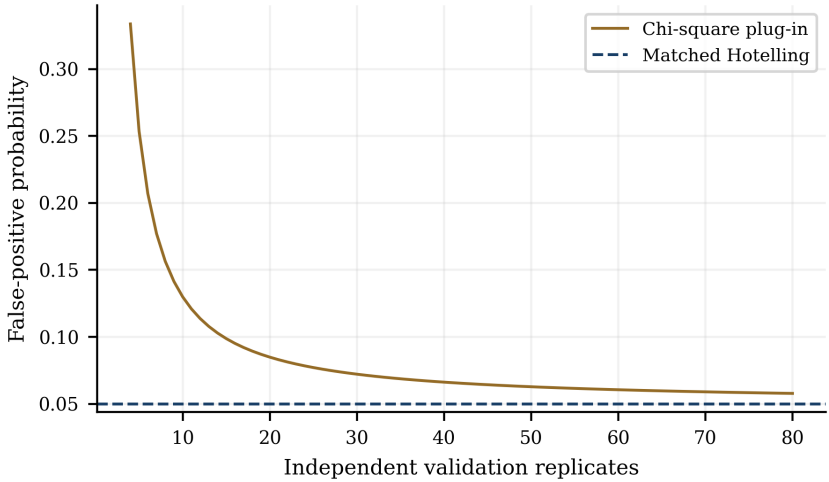

Figure 8.1. Exact null rejection probabilities for a rank-two Gaussian validation mean. A chi-squared threshold with an estimated covariance exceeds its nominal five-percent size. The matched Hotelling reference retains five-percent size in the same independent-replicate experiment. This is an analytical calculation, not a new simulation ensemble.

The source simulations also distinguish formula validity from implementation evidence. Paper VII reports naive nonlinear-search rejection rates of 25.2 %–30.4 % in its chosen null cells; these rates belong to that algorithm and experiment. Paper X retains a lowest corrected directional coverage of 91.5 % in its small main cells. A later 20,000-batch diagnostic for one fixed training choice gives 94.93 % directional and 95.04 % region coverage. The latter check does not replace the original shortfall or establish uniform empirical coverage. These figures

are source-reported synthetic results, not newly reproduced runs or observations of the Universe. [27; 30]

8.7 Allocate the error budget across the scientific claim

A validated sound contrast is not a uniform band for $\chi(s)$. It cannot directly replace the upstream function uncertainty required to reconstruct J, the expansion matrix and the entire physical identified set. Chapter 9 builds that separate route. Likewise, a local frequency error bar should not be relabeled as evidence for an added mode when its amplitude can vanish. [26; 20]

Suppose a test controls false rejection at α_T, and a compatible physical confidence construction controls noncoverage at α_C, under common assumptions. Then

$$Pr\{\text{false rejection or physical noncoverage}\} \le \alpha_T + \alpha_C. \tag{8.16}$$

No independence is required. Two separate five-percent guarantees yield a ten-percent union bound, not an automatic joint ninety-five-percent statement. Moreover, unconditional physical coverage need not remain ninety-five percent after restricting reports to datasets with a discovery. Conditional reporting needs its own coverage argument. [6]

The defensible sequence is therefore explicit: state the physical family and observation model, specify what selection may inspect, calibrate the resulting statistic, name its exact confidence target, and propagate a justified common uncertainty event to the physical quantities. Stronger claims require stronger premises at the step where they enter, rather than a more impressive significance number at the end.

9 Confidence Sets for Physical Parameters

9.1 Retaining everything the observations permit

A fitted sound curve is an uncertain input to the gravitational inverse. Treating it as exact can make a coefficient estimate look precise while ignoring the uncertainty that changes its design matrix. A second issue is structural: different physical models may produce the same observation mean. A valid confidence procedure should retain that entire identified set on one coverage event. More repeated measurements can reduce statistical uncertainty without resolving an exact equivalence. [20; 6]

The construction below has a specific observation contract. There are $n \geq 2$ independent, identically distributed complete Gaussian measurement vectors,

$$Y^{(r)} \sim N_p\left(g, \Sigma_Y\right), r = 1, \ldots, n, \tag{9.1}$$

with a common unknown positive-definite covariance. Each vector contains the same sound-window and expansion measurements. Correlation inside a vector may be arbitrary. Different cosmological epochs are coordinates, not independent repeats of the complete experiment. A common cosmic-variance contribution across repeats would require a different model. Gaussianity is assumed for the supplied expansion coordinate; it does not follow automatically by squaring noisy measurements of H. [30; 20]

Let $\overline{Y}$ and S_Y denote the sample mean and covariance. Coordinatewise Student intervals with a Bonferroni allocation give

$$r_j = t_{n-1,1-\alpha/(2p)} \sqrt{\frac{(S_Y)_{jj}}{n}}, E = \{ |\overline{Y}_j - g_j| \le r_j \text{ for all } j \}. \tag{9.2}$$

Each marginal Student pivot is exact under (9.1), and a union bound proves $Pr_g(E) \ge 1 - \alpha$. Independence between coordinates is unnecessary. This approach sacrifices precision to avoid estimating and inverting the full covariance matrix. The resulting probability statement concerns repeated complete experiments under the declared model; it is not a posterior probability assigned to the fixed physical parameters.

9.2 From window means to a continuous sound band

Let sound centers cover I, with maximum spacing h_s, and let the largest centered uniform window have width w. The centers, widths and gains are calibrated inputs. Suppose

$$\chi \in C^2(I_{ext}), \| \chi'' \|_\infty \le M_\chi, \tag{9.3}$$

on the interval enlarged to contain the complete windows. Interpolate the measured sound means linearly to obtain $\hat{\chi}$. Centered averaging differs from the central value by at most $M_\chi w^2/24$, while linear interpolation between exact node values contributes at most $M_\chi h_s^2/8$. Consequently, on the same event E

,

$$\| \chi - \hat{\chi} \|_\infty \le \varepsilon_\chi, \varepsilon_\chi = \max_{j \in sound} r_j + \frac{M_\chi w^2}{24} + \frac{M_\chi h_s^2}{8}. \tag{9.4}$$

These terms are respectively measurement uncertainty, averaging bias and interpolation bias. More repeats shrink the first term. Finer centers and narrower windows can shrink the

last two, subject to their actual measurement errors. The bound M_{χ} defines the model class and is not established merely because the fitted curve is smooth. [20]

The dependence on regularity matters for combining earlier chapters. For a finite harmonic family,

$$\chi(s)=\chi_0+\sum_k A_k\cos(\omega_k s+\delta_k)\Rightarrow \|\chi''\|_\infty\le\sum_k |A_k|\omega_k^2. \tag{9.5}$$

At $\omega_g=2\pi/\log\varphi$, amplitude 0.005 contributes approximately 0.852427 to this bound; amplitude 0.08 contributes approximately 13.638831. The source experiment with $M_{\chi}=1$ covers the first example, not the second. Detecting a higher-frequency component therefore does not automatically supply a valid physical confidence set under an earlier, smaller regularity budget. [20; 6]

9.3 Propagating uncertainty without linearizing the sound error

Define $\hat{Q},\hat{J}$ from $\hat{\chi}$ as in Chapter 5. The exact exponential relation implies

$$e^{-a(s)}\le\frac{Q(s)}{\hat{Q}(s)}\le e^{a(s)},\quad a(s)=3\,\varepsilon_{\chi}|s|. \tag{9.6}$$

Integration in either direction from zero gives

$$\left|J(s)-\hat{J}(s)\right|\le\left|\hat{J}(s)\right|\left[e^{a(s)}-1\right]. \tag{9.7}$$

If a numerical value $\widetilde{J}_i$ has a justified quadrature error ζ_i, use

$$R_i=\left(\left|\widetilde{J}_i\right|+\zeta_i\right)\left[e^{3\varepsilon_{\chi}|s_i|}-1\right]+\zeta_i. \tag{9.8}$$

The expansion design and its entrywise uncertainty are then

$$\widehat{A}_i=\left(1,\widetilde{J}_i,\widetilde{J}_i^2,E_i\right),$$
$$B_i=\left(0,R_i,2\left|\widetilde{J}_i\right|R_i+R_i^2,0\right), \tag{9.9}$$
$$\left|A_\chi-\widehat{A}\right|\le B.$$

The first and last columns are exact because the reference epochs and scales are supplied. The quadratic-column bound follows from $\left|x^2-y^2\right|\le 2|y||x-y|+|x-y|^2$. No first-order approximation in ε_χ has been made. A quadrature truncation bound and a comparison between two integration grids are different forms of evidence; a fully rigorous numerical enclosure must also account for the numerical errors its guarantee claims to cover. [20]

9.4 A confidence set for the entire fixed-vacuum inverse

For known b and supplied u, let $f_i=h_i^{obs}-b+u\,e^{-2s_i}$ be the measured expansion residual, and let e be its simultaneous error radii from (9.2). The physical coefficient vector is $\theta=\left(\alpha_0,\alpha_1,\alpha_2,d\right)\ge 0$. Define the outer polyhedron

$$P_b=\{\theta\ge 0:\left|\widehat{A}\,\theta-f\right|\le e+B\,\theta\}. \tag{9.10}$$

Equivalently, its absolute-value condition is the pair of linear inequalities $\left(\widehat{A}-B\right)\theta\le f+e$ and $\left(-\widehat{A}-B\right)\theta\le -f+e$. Nonnegative coefficients make this a linear feasibility problem even though the underlying sound uncertainty is functional. [20]

Let $\Theta_b(g)$ contain every coefficient vector whose one common sound history obeys the regularity and physical assumptions and reproduces the true observation mean g. It may contain one vector or many.

Theorem 9.1 — Same-event coverage. Under the observation and enclosure assumptions,

$$\Pr_{g}\{\Theta_b(g)\subseteq P_b\}\geq 1-\alpha. \tag{9.11}$$

Proof. On E, every admissible history sharing the true sound means lies in the band (9.4), hence satisfies (9.9). For any $\theta\in\Theta_b(g)$, choose its witnessing history. Then

$$\begin{aligned}\left|\widehat{A}\,\theta-f\right| &\leq \left|g_F-f\right|+\left|\left(\widehat{A}-A_\chi\right)\theta\right| \\ &\leq e+B\theta.\end{aligned} \tag{9.12}$$

Thus all such vectors are retained together on E. The probability bound follows from (9.2), without assuming rank four or selecting a single true parameter. ▫

The set is deliberately outer. It forgets that the entries of A_χ must arise from the same integrated sound path, so some admitted coefficients may have no common-history witness. Physical filtering and additional valid anchors can tighten it, provided they retain every compatible history. Testing only the nominal fitted sound path would not have that property.

Intersect the set with the positive physical branch and map it through (5.4). This preserves simultaneous coverage of the entire physical identified set. For simple computable bounds, linear programs give coordinate intervals $l_j\leq\theta_j\leq u_j$. A conservative discriminant enclosure is

$$\Delta_L=max\left(0,l_1^2-4\,u_0\,u_2\right),\Delta_U=u_1^2-4\,l_0\,l_2. \tag{9.13}$$

Whenever the box contains a physical vector,

$$\frac{l_2}{\Delta_U} \le \eta \le \frac{u_2}{\Delta_L},$$
$$\frac{S\Delta_L}{2\kappa_0 u_2} \le \lambda_{bare} \le \frac{S\Delta_U}{2\kappa_0 l_2}, \tag{9.14}$$
$$l_d \le d \le u_d.$$

A zero denominator in an upper bound means no finite upper bound from that formula. The AdS condition and other prior information remain separately identifiable restrictions. Marginal endpoints need not occur at one jointly feasible vector. These intervals condition on the supplied conversion scales; uncertainty in those scales needs its own joint enlargement.

9.5 The correct extension when the vacuum is free

Freeing b changes the intercept domain and the physical map. With measured $y = h + u e^{-2s}$, use

$$¿\, y_i - \beta_0 - \beta_1 \tilde{J}_i - \beta_2 \tilde{J}_i^2 - d\, E_i \vee ¿ \le e_i + R_i \beta_1 + \left(2\left|\tilde{J}_i\right| R_i + R_i^2\right)\beta_2 \tag{9.15}$$
$$\beta_0 \in R, \beta_1, \beta_2, d \ge 0.$$

The physical branch requires $\beta_2 > 0$. The unrestricted sign of β_0 causes no difficulty because its column has no sound error. Imposing $\beta_0 \ge 0$ would exclude some free negative-vacuum models without justification. The proof of simultaneous coefficient retention is otherwise identical. [3]

The physical image now contains every admissible C from (6.3), not one tension obtained from a discriminant. Formally, take the union over retained coefficients and common sound histories in the band, retaining their allowed C intervals. That union includes the full physical identified set on E. A necessary physical enclosure can replace the exact common-history

search when computing conservative bounds; a check against only $\hat{J}$ cannot silently replace it.

For coefficient bounds with $0 \le l_1 \le u_1$ and $0 < l_2 \le u_2$, the geometric invariant obeys

$$L_{-} = \frac{l_1^2}{4u_2} - u_0, L_{+¿=\frac{u_1^2}{4l_2}-l_0.¿} \tag{9.16}$$

If $L_{-} > 0$ and $0 \le d_{-} \le d_{+¿¿}$, then

$$¿ \tag{9.17}$$

The horizon expression requires a positive-radius physical branch. If L approaches zero at positive d, no finite upper horizon bound follows without an additional restriction, such as the exterior-brane condition. Even sharply determined L, d can coexist with the free C family and an unbounded relative uncertainty in split tension. Total vacuum stress τ_{vac} requires the physical normalization discussed in Chapter 10; it is not obtained by renaming $1/\eta$.

9.6 Rank certification and continuous weak information

Assume at least four expansion epochs. For any positive diagonal 4×4 column scaling W, define

$$\gamma = \sigma_{min}\left(\hat{A}\, W\right) - \| B\, W \|_F. \tag{9.18}$$

On E, $\gamma > 0$ implies every admissible sound history has a full-rank sampled matrix, since $\| A_\chi W z \| \ge \gamma$ for every unit vector z. This certifies separation from exact Riccati dependence without estimating χ'. A nonpositive margin is inconclusive. A positive margin identifies coefficients at each fixed history; it does not make different uncertain histories share one coefficient vector, and it does not remove the free-vacuum C orbit. [20]

Continuous weak information is a separate observation setting. Suppose simultaneous continuous bands supply $|y-\hat{y}|\le \varepsilon_y(s)$ and the sound bound. Choose a test ϕ supported strictly inside every allowed $J(I)$, with $M_3=\|\phi'''\|_\infty$ and Lipschitz constant L_3 for ϕ'''. For exact nominal integrals, define

$$\begin{aligned} \widehat{K}&=\phi'''(\hat{J})\widehat{Q},\\ R_J&=|\hat{J}|(e^a-1),\\ R_K&=\widehat{Q}\{e^a L_3 R_J+M_3(e^a-1)\},\\ \widehat{A}_\phi&=\int_I \hat{y}\,\widehat{K}\,ds,\ \widehat{B}_\phi=\int_I E\,\widehat{K}\,ds. \end{aligned} \tag{9.19}$$

The kernel difference is bounded by R_K. Therefore, with

$$\begin{aligned} r_A&=\int_I \varepsilon_y|\widehat{K}|\,ds+\int_I (|\hat{y}|+\varepsilon_y)R_K\,ds,\\ r_B&=\int_I E\,R_K\,ds, \end{aligned} \tag{9.20}$$

every compatible nonnegative d satisfies

$$|\widehat{A}_\phi-d\,\widehat{B}_\phi|\le r_A+d\,r_B. \tag{9.21}$$

This follows by perturbing the exact weak identity $A_\phi=d\,B_\phi$. It remains valid with free vacuum because the constant intercept is annihilated. It is two linear inequalities in d, avoiding division by an uncertain denominator. Valid integration errors can be added to r_A, r_B. Several tests can be intersected on the same continuous-band event without a new multiplicity charge. Four expansion values alone do not provide that event. [19; 20; 3]

9.7 What the computational evidence establishes

Series II XI reports 4,800 synthetic datasets using 24 complete repeats, 65 sound centers and four expansion epochs. Its full outer sets retained the generating coefficients in every reported

trial. A conditional comparison that omitted sound uncertainty sometimes retained them much less often, although both procedures' broad marginal boxes covered the generating mass and tension. These results illustrate conservatism and the cost of ignored uncertainty. They establish neither a measured tension nor sharp or uniform empirical coverage; the theorem follows from its observation assumptions and set-inclusion proof. [20]

A projected-sound interval does not supply the uniform sound band needed by the inverse. Combining discovery-error allowance α_T and physical noncoverage allowance α_C guarantees only $1-\alpha_T-\alpha_C$ by a union bound. Unconditional coverage need not survive selection. Every report therefore needs its observation model, regularity bounds and exact confidence target. [28; 29; 6]

10 Covariant Completion and Vacuum Normalization

10.1 From a reconstructed history to a dynamical question

An inverse reconstruction determines what a chosen class of histories permits us to infer. A dynamical completion asks a further question: which action produces those histories, and which additional predictions follow once its parameters, matter standards, and boundary conditions have been fixed? The distinction matters because a sufficiently adjustable action can reproduce a supplied history without explaining why that history occurs. The final research memorandum makes this distinction explicit and supplies the completion examined in this chapter. [3] [4]

The preceding reconstruction kept the algebraic coefficient $g_{ref}=g_{split}=\lambda/\left(6\,M_5^6\right)$ fixed. That coefficient must now be compared with the response to excitations after all constant matter vacuum terms have been removed. The comparison changes the interpretation of a possible gravitational calibration. It leaves the predecessor’s algebraic equivalence class intact within its declared normalization convention.

We use $c=\hbar=1$, the brane signature ¿, and a five-dimensional Lorentzian bulk. The induced brane metric is $h_{\mu\nu}$. The brane separates two reflection-related regions $M_{+¿¿}$ and M_{-}. A minimal completion is

$$
\begin{aligned}
S &= S_{bulk} + S_{GHY} + S_{\Sigma}, \\
S_{bulk} &= \frac{M_5^3}{2} \sum_{\sigma=\pm} \int_{M_\sigma} d^5x \sqrt{-g_5} \left(R_5 - 2\Lambda_5 \right), \\
S_{\Sigma} &= \int_{\Sigma} d^4x \sqrt{-h} \left[-\lambda + F(X) - U_0 + L_{SM} + L_{DM} \right], \\
X &= -\frac{1}{2} h^{\mu\nu} \partial_\mu \phi \, \partial_\nu \phi \, , \Lambda_5 = -\frac{6}{\ell^2}.
\end{aligned}
\tag{10.1}
$$

The boundary action contains the Gibbons–Hawking–York terms on both sides with consistent normal orientations. The convention $8\pi G_5 = M_5^{-3}$ fixes the gravitational normalization. For a scalar assigned its usual mass dimension, $[\phi]=E$, while $[X]=[F]=[U_0]=[\lambda]=E^4$, $[M_5]=E$, and $[\ell]=E^{-1}$. Constant vacuum contributions from the other brane sectors are included in the declared renormalized constant λ; their excitations remain explicit. This choice organizes the terms in the action. It does not explain their renormalized magnitudes. [4]

No induced brane Einstein term, Gauss–Bonnet term, bulk scalar, or direct scalar–Standard Model coupling is present. The resulting junction dynamics therefore belongs to the stated Randall–Sundrum type model. The symmetry content consists of five-dimensional covariance, the Z_2 reflection, the matter gauge symmetries, and the scalar shift $\phi \mapsto \phi + constant$. The shift symmetry permits a function of X; it does not select a particular power or a cosmological charge. [7] [8] [31] [4]

10.2 Field equations and the scalar fluid

Bulk variation and the brane junction condition give

$$G_{AB}^{(5)} + \Lambda_5 g_{AB} = 0 , \tag{10.2}$$

Here $T_{\mu\nu}$ is the full brane stress, including its constant part. The sign of $K_{\mu\nu}^{+¿¿}$ follows the specified normal convention; the reflection condition supplies the factor of one half. These are established junction equations. [7] [8]

For the scalar, integration by parts in its variation and variation with respect to $h^{\mu\nu}$ yield

$$\begin{aligned} \nabla_\mu \left(F_X \nabla^\mu \phi \right) &= 0 , \\ T^{\phi}_{\mu\nu} &= F_X \partial_\mu \phi \, \partial_\nu \phi + \left(F - U_0 \right) h_{\mu\nu} . \end{aligned} \tag{10.3}$$

On a homogeneous timelike branch, $X = \dot{\phi}^2 / 2 > 0$, this stress has perfect-fluid form. Its density, pressure, and local scalar kinetic coefficients are

$$\begin{aligned} p_\phi &= F - U_0 , \rho_\phi = 2 X F_X - F + U_0 , \\ K &= F_X + 2 X F_{XX} , c_\phi^2 = \frac{F_X}{K} . \end{aligned} \tag{10.4}$$

The homogeneous equation is $K \ddot{\phi} + 3 H F_X \dot{\phi} = 0$, and the conserved shift charge is $a^3 F_X \dot{\phi}$. Positivity of F_X and K gives the local spatial and temporal kinetic signs on this background. The identification with an irrotational barotropic fluid and the distinction between an adiabatic sound speed and the propagation speed of a general scalar are established results. For a purely kinetic action the relevant speeds agree on the branch under consideration. [32] [33]

10.3 A constructive local realization theorem

The availability of a scalar action is a weak selection criterion for the histories used in the inverse problem. The following construction demonstrates why. Let $s=\ln(a/a_{¿})$, with $s=0$ chosen inside the interval of interest. Suppose a differentiable barotropic history satisfies positive density, positive enthalpy $W=\rho+p$, conservation $\rho'=-3W$, and a continuous sound history $0<\chi=dp/d\rho\le 1$ on a compact interval.

Proposition 10.1. For every $X_{¿}>0$, the assignments

$$X(s)=X_{¿}\exp\left[-6\int_0^s \chi(t)\,dt\right], \qquad P(X(s))=p(s) \tag{10.5}$$

define a local purely kinetic action reproducing that density and sound history, with positive local kinetic coefficients. [4]

Proof. Since $X'=-6\chi X<0$, the map from s to X is invertible on the interval. Conservation gives $p'=-3\chi W$, so differentiation along the trajectory gives

$$P_X=\frac{p'}{X'}=\frac{W}{2X}>0, \qquad 2XP_X-P=\rho, \qquad P_X+2XP_{XX}=\frac{P_X}{\chi}>0. \tag{10.6}$$

For the last identity, differentiate the reconstructed density with respect to X and use $dp/d\rho=\chi$. Finally, $W'=-3(1+\chi)W$, and the logarithmic derivative of $a^3W/\sqrt{2X}$ vanishes. This quantity equals $a^3P_X\sqrt{2X}$, so the homogeneous scalar equation holds as well.

The construction fixes the action only on the visited interval of X. It supplies neither an extension to a zero-gradient vacuum

nor a principle selecting the observed history. The freedom in $X_{¿}$ also exposes field normalization: choosing a coordinate on scalar-field space is not an absolute density measurement. The broader relation between kinetic fields and barotropic fluids predates this construction; the point here is its consequence for the inverse research program. [33] [34] [35]

10.4 Constant vacuum splitting is an exact redundancy

Separate the total constant vacuum stress from its excitations:

$$\begin{aligned} \tau &= \lambda + U_0 > 0, \\ \rho_e &= 2X F_X - F + \rho_{SM} + \rho_{DM}, \\ p_e &= F + p_{SM} + p_{DM}. \end{aligned} \tag{10.7}$$

The scalar τ denotes a vacuum stress, not the tensor often denoted by that letter in brane references. If the action extends to a zero-gradient vacuum, we adopt $F(0)=0$ by absorbing its constant into U_0. A local action supplied by Proposition 10.1 need not admit that extension.

Proposition 10.2. For any allowed constant Δ, the transformation

$$\lambda \mapsto \lambda + \Delta, U_0 \mapsto U_0 - \Delta \tag{10.8}$$

leaves the full action unchanged.

Proof. Its only dependence on these constants is through $-\lambda - U_0 = -\tau$. Every field variation is therefore identical before and after the relabeling.

No observable of this identical action separates the two constants. A microscopic model might distinguish their origins through additional structure, but the present parameterization contains no such information. This exact statement makes concrete the vacuum–matter split ambiguity noted in the

foundational brane analysis. It is a redundancy of description, not a newly discovered physical symmetry. [7] [4]

10.5 Overall action scaling is a different freedom

For the predecessor's one-fluid realization, let $\alpha>0$ label the normalization orbit:

$$\begin{aligned} \lambda_\alpha=\alpha^2\lambda, M_{5,\alpha}^3=\alpha M_5^3, \\ F_\alpha=\alpha F, U_{0,\alpha}=\alpha U_0-\left(\alpha^2-\alpha\right)\lambda. \end{aligned} \tag{10.9}$$

It follows that $\tau_\alpha=\alpha\tau$ and $\rho_{e,\alpha}=\alpha\rho_e$. With geometric Λ_5 fixed, all bulk, boundary, and one-sector brane terms scale together, giving $S_\alpha=\alpha S$. The classical stationary configurations are unchanged because multiplying an action by a nonzero constant leaves its Euler–Lagrange equations unchanged. [3] [4]

This transformation differs from Equation 10.8: the action is multiplied, rather than left identical. At fixed $\hbar$, its quantum phase changes. Furthermore, an orbit that scales all brane matter does not remain available unchanged when independently normalized Standard Model or other matter sectors are held fixed. A physical energy standard can consequently obstruct this particular scaling. That observation does not establish identifiability across every enlarged dark-sector action.

10.6 Background coupling and local gravitational matching

The homogeneous junction equation, written in the vacuum-subtracted variables, is

$$H^2+\frac{k}{a^2}=\frac{\left(\tau+\rho_e\right)^2}{36M_5^6}-\frac{1}{\ell^2}+\frac{\mu_B}{a^4}, \mu_B\geq 0. \tag{10.10}$$

Expanding the square defines a background response coefficient and an effective vacuum curvature:

$$g_{bg}=\frac{\tau}{6\,M_5^6}=M_4^{-2},$$
$$\frac{\Lambda_{eff}}{3}=\frac{\tau^2}{36\,M_5^6}-\ell^{-2}. \tag{10.11}$$

M_4 here is defined by a background coefficient. Identifying g_{bg} with locally measured $8\pi G_N$ additionally requires a localized gravitational response, calibrated matter standards, and negligible extra scalar or bulk contributions in the measurement regime. The tuned weakly curved vacuum supplies the familiar localization limit; a rolling scalar cosmology requires its own matching calculation. The present source has not solved that localized-source problem. [31] [4]

The two coefficients transform differently:

$$g_{ref}=g_{split}=\frac{\lambda}{6\,M_5^6},$$
$$\left(g_{split}\right)_\alpha=g_{split},\left(g_{bg}\right)_\alpha=\frac{g_{bg}}{\alpha}. \tag{10.12}$$

Thus an exact nonzero determination of g_{bg} in fixed absolute stress units selects at most one member of this orbit, provided the matching just described is justified. It cannot distinguish λ from U_0 under the identical-action transformation. The conserved split coefficient used in Chapters 2–9 and the operationally matched coefficient answer different questions once a separate constant matter vacuum term is present.

If ℓ, Λ_{eff}, and a matched M_4 are independently supplied, algebra gives

$$\tau = 6\,M_4^2\left(\ell^{-2} + \frac{\Lambda_{eff}}{3}\right), \qquad M_5^6 = \frac{\tau\,M_4^2}{6}. \tag{10.13}$$

The bracket must be positive. These three inputs have not been jointly measured for the model studied here; an effective vacuum term from a different cosmological fit cannot be imported without its assumptions. The result identifies the extra information needed to determine the total vacuum stress, while leaving the separation of its constant pieces redundant. It supplies a precise interface between the formal inverse result and a possible experiment. [4]

10.7 Which additional assumptions carry information

The different normalization choices can now be compared without treating every supplied constant as a new measurement.

Table 10.1. Information needed to fix an action normalization.

Supplied information	What it fixes	What remains
A sound history $\chi(s)$	The allowed fluid shape	Density normalization and vacuum offset
Existence of a kinetic $P(X)$	A local field realization	Choice of action outside the sampled interval
A named cubic coefficient	A field-coordinate convention unless other couplings are fixed	Charge and absolute stress calibration
A matched nonzero g_{bg}	At most one representative of the stated scaling orbit	Other action families and the constant split
Matched M_4, ℓ, and Λ_{eff}	Total τ and M_5	Separate values of λ and U_0

This separation also disciplines proposed additional principles. None of the symmetries listed in Section 10.1 selects a golden-ratio frequency, a preferred kinetic power, or the Noether charge. A proposed numerical relation would have to follow from additional dynamics or independently specified boundary data. Reproducing a chosen relation by adjusting an otherwise unrestricted function leaves the selection problem unanswered. The completion establishes what is dynamically possible within the class; a predictive restriction must further explain which members are admitted before the target history is imposed. [4]

11 Kinetic Actions and Local Consistency

11.1 Constant sound speed and an affine equation of state

A kinetic realization should first reproduce the intended fluid and then be examined on backgrounds different from the one used to construct it. The constant-sound example makes both steps explicit. Choose $F(X)=AX^{n}$ with $A>0$, $n\geq 1$, and a homogeneous timelike field. The coefficient has dimension $[A]=E^{4-4n}$. Substitution into the density and pressure gives

$$\begin{aligned}\rho_{\phi}&=(2n-1)AX^{n}+U_{0},\\ p_{\phi}&=AX^{n}-U_{0}=\frac{\rho_{\phi}-2nU_{0}}{2n-1},\\ c_{\phi}^{2}&=\frac{1}{2n-1}.\end{aligned}\tag{11.1}$$

The excitation density $\rho_{\phi,e}=(2n-1)AX^{n}$ has pressure $p_{\phi,e}=AX^{n}$. Conservation therefore makes it redshift as $a^{-3(1+c_{\phi}^{2})}$. The constant U_{0} supplies the affine intercept; it does not alter the kinetic sound speed. This established field–fluid relation realizes the predecessor's $\chi=0.2$ example with $n=3$ and $A=M^{-8}$. [34] [4]

The conserved current also determines the background normalization. For a chosen sign of $\dot{\phi}$, $a^{3}nAX^{n-1}\sqrt{2X}$ is constant. Consequently $X\propto a^{-6/(2n-1)}$, and raising it to the power n reproduces the density law. The current's value is independent initial information. Giving the coefficient the name M^{-8} does not fix that information or attach an external energy calibration to the field.

The radiation-like case illustrates a connection with the rank exceptions of the inverse reconstruction. At $\chi=1/3$, one has $n=2$, and the excitation density scales as a^{-4}. Its linear

background dependence can overlap the dark-radiation column of the reconstruction. Rewriting the fluid as a scalar does not create a new independent column or remove this structural degeneracy. [3] [4]

For the pure cubic branch, $\chi = 1/5$ denotes a squared sound speed: $c\varphi = c/\sqrt{5}$, approximately 0.447c. Conservation gives $\rho_{exc} \propto a^{-18/5}$ for the excitation above the constant vacuum offset. These are linked consequences of one kinetic ansatz. They are not the matter inputs used in the distance fit of §§13.7–13.13, which uses a canonical unexcited scalar and separately conserved dust. Its quadratic dust term scales as $(1 + z)^6$; a pure cubic excitation squared would instead scale as $(1+z)^{7.2}$.

11.2 What the kinetic signs test

Consider a small fluctuation π about a local slowly varying background $\bar{\phi}$, so that $\phi = \bar{\phi} + \pi$. In a local inertial patch with homogeneous background gradient $v = \dot{\bar{\phi}}$ and $X_0 = v^2/2$, the kinetic invariant changes by

$$X = X_0 + v\dot{\pi} + \frac{1}{2}\left[\dot{\pi}^2 - (\nabla\pi)^2\right]. \tag{11.2}$$

At the order relevant to the principal kinetic terms, background derivatives and metric mixing are held aside. Expanding a general F gives

$$L_2 = \frac{1}{2}\left[\left(F_X + 2X_0F_{XX}\right)\dot{\pi}^2 - F_X(\nabla\pi)^2\right]_{X_0}. \tag{11.3}$$

The local Fourier equation consequently has $\omega^2 = (F_X/K)|k|^2$. A positive temporal coefficient avoids a negative kinetic energy for this scalar fluctuation; a positive spatial coefficient avoids the corresponding short-wavelength gradient instability. Requiring their ratio not to exceed one imposes the stated

subluminal condition relative to the local brane metric in this timelike setting. These are tests of a particular local principal part, rather than a proof about every state of the coupled five-dimensional system. [32] [4]

This distinction is useful even for a spatially homogeneous cosmology. Positive coefficients do not tell us whether nonlinear waves form caustics, whether all admissible initial data evolve globally, or whether the scalar couples to an unstable bulk mode. Those questions require equations and boundary conditions beyond the frozen-background diagnostic. Studies of nonlinear kinetic theories make the need for additional control clear, although their different actions and applications cannot be imported as solutions of the present model. [36]

11.3 The cubic example has a degenerate zero-gradient vacuum

For $F = X^3/M^8$, $F_X = 3X^2/M^8$ and $K = 15X^2/M^8$. Both are positive for every $X > 0$, while both vanish at zero. The behavior at that endpoint can be seen without relying on the ratio of two vanishing coefficients.

Write $\delta X_1 = v\dot{\pi}$ and $\delta X_2 = \left[\dot{\pi}^2 - (\nabla\pi)^2\right]/2$. In the expansion of $\left(X_0 + \delta X_1 + \delta X_2\right)^3$, the quadratic terms are $3X_0^2\delta X_2 + 3X_0\delta X_1^2$. The cubic terms are $6X_0\delta X_1\delta X_2 + \delta X_1^3$. Using $v = \sqrt{2X_0}$ yields

$$L_2 = \frac{X_0^2}{2M^8}\left[15\dot{\pi}^2 - 3(\nabla\pi)^2\right], \qquad L_3 = \frac{X_0\sqrt{2X_0}}{M^8}\left[5\dot{\pi}^3 - 3\dot{\pi}(\nabla\pi)^2\right]. \tag{11.4}$$

At $X_0 = 0$, the action begins at sixth order in derivatives of the fluctuation amplitude, since X itself is quadratic in $\partial\pi$. There is

no quadratic operator to invert into a Gaussian scalar propagator in the pure cubic truncation. A finite limiting value of $F_X/K=1/5$ does not repair the missing kinetic normalization. [4]

For $X_0>0$, canonical normalization of the temporal term gives

$$\pi_c=\frac{\sqrt{15}\,X_0}{M^4}\pi\,,$$
$$L_3\sim\frac{M^4}{X_0^{3/2}}\left(\partial\pi_c\right)^3,\Lambda_{int}\sim\frac{X_0^{3/4}}{M^2}. \tag{11.5}$$

The last relation is dimensional power counting for the displayed interaction, with numerical and angular coefficients suppressed. It is not a completed unitarity calculation, particularly once gravity and other operators are included. It shows why no background-independent weak-coupling scale extending to $X_0=0$ has been established. [4]

The implication for a finite-density universe is narrower. A background-dependent scale can remain above the frequencies of a particular cosmological calculation even as it tends to zero in a different limit. The correct comparison is between the frequencies and gradients actually used, the background-dependent interactions, and the operators retained in the action. The local-vacuum defect therefore defeats an unqualified claim of a regular perturbative vacuum theory, without by itself disproving every finite-density solution.

11.4 Adding a canonical term changes the fluid

A simple comparison restores a nonzero quadratic operator at zero gradient:

$$P\left(X\right)=X+\frac{X^3}{M^8}-U_0\,,x=\frac{X}{M^4}. \tag{11.6}$$

The excitation density, pressure, and kinetic coefficients become

$$\rho_{\phi,e}=M^4\left(x+5x^3\right),\ p_{\phi,e}=M^4\left(x+x^3\right),$$
$$P_X=1+3x^2,\ K=1+15x^2,$$
$$c_\phi^2=\frac{1+3x^2}{1+15x^2},\ \frac{1}{5}<c_\phi^2\le 1. \tag{11.7}$$

Here $x\ge 0$ describes the homogeneous timelike branch and its zero-gradient limit. At zero, the scalar fluctuation has a canonical kinetic term and luminal local propagation. The fluid four-velocity, which divides by $\sqrt{2X}$, need not be used at that endpoint. At large positive x, the squared sound speed approaches $1/5$, but it is no longer the exact constant history of the cubic model. [4]

The equation-of-state ratio of the excitations also changes: $w_e=\left(1+x^2\right)/\left(1+5x^2\right)$. At small x, both the pressure–density ratio and the propagation speed approach the canonical stiff-fluid limit. The system therefore interpolates between two kinetic regimes rather than preserving a single affine history. Repairing a local property of an action can alter the inverse data it was designed to reproduce.

11.5 Evolution from the equation of motion and from the current

Since $\dot{X}=\dot{\phi}\ddot{\phi}$, the homogeneous scalar equation implies $dX/ds=-6XP_X/K$. For the canonical-plus-cubic action this gives two equivalent descriptions:

$$\frac{dx}{ds}=-6x\frac{1+3x^2}{1+15x^2},$$
$$a^3\left(1+3x^2\right)\sqrt{2x}=constant. \tag{11.8}$$

An overall factor M^2 has been absorbed into the charge constant. On the positive branch, squaring the current relation between $s=0$ and s gives the useful algebraic form

$$x(s)\left[1+3\,x(s)^2\right]^2 = x(0)\left[1+3\,x(0)^2\right]^2 e^{-6s}. \tag{11.9}$$

The left-hand side increases strictly for $x>0$, so this equation selects a unique positive root. It offers a numerical comparison independent of integrating the differential equation for $\ln x$. In the small-x regime, x approximately redshifts as a^{-6}; in the cubic-dominated regime it approximately redshifts as $a^{-6/5}$. Their corresponding excitation densities approach a^{-6} and $a^{-18/5}$.

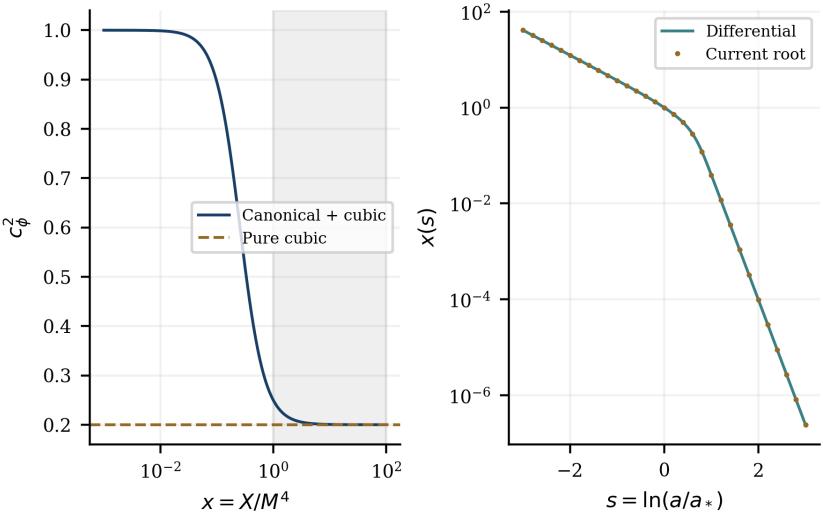

Figure 11.1. Left: the canonical-plus-cubic sound speed and the positive-X pure-cubic limit. The shaded x>1 range needs separate effective-theory justification. Right: homogeneous evolution from x(0)=1, computed by differential integration and an independent conserved-current root. These are model calculations, not fitted observations.

The figure compares the two sound-speed functions and a current-conserving trajectory initialized with $x(0)=1$. The

original book calculation compares differential evolution with an independent current-root solution on $-3 \le s \le 3$. Their maximum difference in $\ln x$ is approximately 1.48×10^{-11}, with relative current drift 1.91×10^{-11}; Appendix D records the program and its scope. The final source paper reports its own comparison over $-3 \le s \le 3$, with maximum difference 6.91×10^{-10} and relative drift 3.90×10^{-10}. Those separate source-reported diagnostics are retained as such. [4]

11.6 What canonical normalization does and does not fix

Setting $P_X(0) = 1$ fixes a useful field-coordinate convention around the vacuum. It does not by itself determine the physical value of M, the cosmological charge, or the gravitational normalization. The action remains a model family until those parameters are attached to declared measurements or theoretical restrictions.

The normalization freedom has a concrete expression. Multiply the scalar action by the positive orbit factor α and introduce $\psi = \sqrt{\alpha}\,\phi$, so that $X_\psi = \alpha X$. Its Lagrangian can again have a unit canonical coefficient:

$$\alpha\left(X + \frac{X^3}{M^8} - U_0\right) = X_\psi + \frac{X_\psi^3}{\alpha^2 M^8} - \alpha U_0 . \tag{11.10}$$

The higher-order scale has changed to $\alpha^{1/4} M$. Thus canonical field normalization alone does not prohibit the overall classical rescaling when the other parameters are free to transform with it. Fixing a higher-order coefficient through an independent physical process, or fixing matter interactions that do not admit this rescaling, supplies information of a different kind. This algebra illustrates the distinction in Chapter 10 rather than claiming that every possible dark-sector degeneracy has the same form.

Shift symmetry permits X^2/M^4 and higher powers as well as the terms retained here. If M is interpreted as a generic expansion scale, the large-x region needed to approximate the pure cubic response is not controlled merely by truncating that series. A theory with a justified resummation or a different background cutoff might support such a regime; neither has been derived in the sources used here. [4]

The completed local result is therefore specific. A pure cubic action realizes the constant-sound background and has positive coefficients on its positive-X branch. Its zero-gradient vacuum lacks a quadratic propagator. A canonical addition restores that operator while changing the sound history. These conclusions identify which further dynamics must be supplied before the same model can be used for a full perturbation calculation or an observational likelihood.

12 Physical Scales, Acceleration, and Varying Tension

12.1 The size of the direct quadratic term

A background correction can be mathematically identifiable and still be far below an observationally useful scale. The junction equation provides a direct comparison once the total vacuum stress and the matter normalization are fixed. Expanding Equation 10.10 gives

$$H^2+\frac{k}{a^2}=\frac{\Lambda_{eff}}{3}+\frac{\rho_e}{3M_4^2}\left(1+\frac{\rho_e}{2\tau}\right)+\frac{\mu_B}{a^4}. \tag{12.1}$$

Define the excitation contribution $H_\rho^2=\rho_e/\left(3M_4^2\right)$. The ratio of the direct quadratic density term to the corresponding linear term is

$$\begin{aligned}\epsilon_{brane}&=\frac{\rho_e}{2\tau}\\ &¿\frac{H_\rho^2\ell^2}{4\left(1+\Lambda_{eff}\ell^2/3\right)}.\end{aligned} \tag{12.2}$$

The second line follows by substituting Equation 10.13; it introduces no additional gravitational law. In SI units, the numerator contains $\left(H_\rho\ell/c\right)^2$. The denominator is positive in the declared $\tau>0$ domain. This relation connects the scale of the correction with the bulk curvature and the vacuum-subtracted gravitational response. [4]

The denominator contains $\tau=\lambda+U_0$. Using a freely split bare λ here would attach an apparent effect size to a quantity that changes under an identical-action relabeling. The bare tension can replace τ only after adopting a convention in which all constant brane vacuum terms have been absorbed into it.

For a precise comparison of expansion rates, let H_{lin} denote the rate in the same flat background with the quadratic term omitted and all other contributions held fixed. If the effective vacuum and dark-radiation contributions are nonnegative, define $f_\rho = H_\rho^2 / H_{lin}^2 \le 1$. Then

$$\frac{H - H_{lin}}{H_{lin}} = \sqrt{1 + f_\rho \epsilon_{brane}} - 1$$
$$¿ \frac{f_\rho \epsilon_{brane}}{\sqrt{1 + f_\rho \epsilon_{brane}} + 1} \le \frac{\epsilon_{brane}}{2}. \tag{12.3}$$

The rationalized expression also avoids subtracting nearly equal numbers when the correction is tiny. A background with negative compensating contributions does not satisfy this particular bound. Neither does the calculation bound every scalar, dark-radiation, or bulk perturbation effect.

12.2 A declared present-density benchmark

Use the reference inputs $H_0 = 70\, km\, s^{-1}\, M\, pc^{-1}$ and $M_4 = 2.435 \times 10^{18}\, GeV$, with the matching assumptions of Chapter 10. They give $H_0 = 2.26855 \times 10^{-18}\, s^{-1}$ and the conventional density scale $3 M_4^2 H_0^2 = 3.96594 \times 10^{-47}\, GeV^4$. Setting the excitation density equal to that scale and choosing $\tau^{1/4} = 1\, TeV$ gives

$$\epsilon_{brane} = 1.983 \times 10^{-59}, \frac{H - H_{lin}}{H_{lin}} \le 9.915 \times 10^{-60}. \tag{12.4}$$

These numbers are evaluations of declared inputs, not estimates of a measured scalar density. The choice of critical-density scale does not simultaneously fit all other terms in the cosmological equation. With independently fixed nonnegative contributions it is a useful upper reference scale; arbitrarily

large excitation densities hidden by negative cancellations require a different analysis. [4]

The TeV value denotes the fourth root of the total vacuum stress. It is neither the five-dimensional Planck mass M_5 nor the kinetic interaction scale M introduced in Chapter 11; those quantities enter different operators and have different matching relations.

The vacuum-tuned conversion $\Lambda_{eff}=0$ gives $\ell=\sqrt{6}\,M_4/\sqrt{\tau}$. A TeV tension scale corresponds to $\ell\simeq 1.177\,mm$, while the illustrative choice $\ell=0.1\,mm$ corresponds to $\tau^{1/4}\simeq 3.431\,TeV$. These are conversions between parameters. Compatibility with a laboratory experiment requires the force profile predicted by the specified model, convolved with the experiment's source and detector geometry.

For example, Lee and collaborators tested separations from $52\,\mu m$ to $3.0\,mm$ and reported a limit for gravitational-strength Yukawa interactions. Their smallest separation is not itself a bound on an AdS radius; a Yukawa profile and the Randall–Sundrum correction are different response functions. The experimental result is evidence about its stated force model and statistical analysis. [37]

The reverse calculation is informative. Requiring $\epsilon_{brane}=0.01$ at the same density gives $\tau^{1/4}\simeq 6.673\,meV$. Under the zero-effective-vacuum conversion, this corresponds to $\ell\simeq 2.643\times 10^{25}\,m$, or about $0.86\,Gpc$. Such a scale is incompatible with treating laboratory and ordinary astrophysical gravity as the conventional short-distance localization limit of this simple model. The calculation isolates the difficulty with this direct late-time quadratic route; modifications of the bulk or brane action change the question. [4]

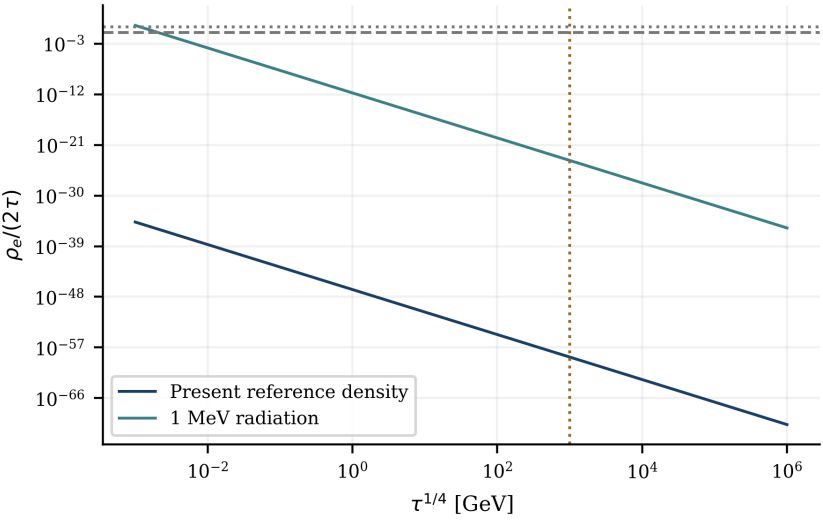

Figure 12.1. The direct quadratic-to-linear ratio as the total vacuum energy scale varies, at two fixed reference densities. The present-density and MeV-radiation curves use the explicit Appendix D inputs. The horizontal ratios are diagnostic levels and the vertical tension mark is a benchmark; none is a fitted exclusion boundary.

The hierarchy plot shows the direct ratio at two fixed reference densities as the total vacuum energy scale varies. Its curves are generated consequences of Equation 12.2. The benchmark and diagnostic tolerance lines identify chosen inputs, not fitted exclusion boundaries.

12.3 The early high-density window

Radiation at temperature T has the idealized density $\rho_r = \pi^2 g_¿ T^4/30$. For a fixed effective relativistic degree count $g_¿$, imposing a diagnostic maximum ratio or solving for the temperature of a chosen ratio gives

$$\rho_r(T) = \frac{\pi^2}{30} g_¿ T^4,$$
$$\tau \geq \frac{\pi^2 g_¿ T^4}{60 \epsilon_{max}}, \tag{12.5}$$
$$T(\epsilon) = \left(\frac{60 \epsilon \tau}{\pi^2 g_¿} \right)^{1/4}.$$

At $T = 1\,MeV$, $g_¿ = 10.75$, and $\epsilon_{max} = 0.1$, the resulting tension energy scale is $2.051\,MeV$. It is a radiation-density exercise with an assumed tolerance, rather than a nucleosynthesis likelihood. The MeV scale associated with this requirement must be distinguished from the much stronger scales motivated by short-distance gravity in a conventional RSII interpretation. [38] [4]

Table 12.1. Physical scales under the stated benchmark inputs.

Declared calculation	Result
Present reference density $3 M_4^2 H_0^2$	$3.966 \times 10^{-47}\,GeV^4$
Present direct ratio at $\tau^{1/4} = 1\,TeV$	1.983×10^{-59}
Ratio at $T = 1\,MeV$ and TeV tension	1.768×10^{-24}
Tension scale for the stated BBN tolerance	$2.051\,MeV$

Declared calculation	Result
Temperature for $\epsilon = 0.1,\ g_{¿} = 106.75$	$274.7\,GeV$
Temperature for $\epsilon = 1,\ g_{¿} = 106.75$	$488.5\,GeV$
Tuned AdS radius at TeV tension	$1.177\,mm$

The several-hundred-GeV values locate a regime where a high-density correction can matter. They do not determine a primordial spectrum. In such a regime, thermal production of bulk gravitons can carry energy away from the brane, so the vacuum-bulk, no-exchange model may cease to supply the correct background equations. This energy-transfer issue has been studied in the early brane-cosmology literature and must be incorporated in any proposed application of the window. [38]

12.4 An acceleration obstruction

For constant τ and no bulk exchange, the total excitation stress obeys $\dot{\rho}_e + 3H\left(\rho_e + p_e\right) = 0$. Differentiate Equation 12.1 on an interval where $H \neq 0$ and use this conservation equation. The result is

$$\dot{H} - \frac{k}{a^2} = -\frac{\rho_e + p_e}{2M_4^2}\left(1 + \frac{\rho_e}{\tau}\right) - \frac{2\mu_B}{a^4}. \tag{12.6}$$

Adding H^2 eliminates spatial curvature and gives

$$\frac{\ddot{a}}{a} = \frac{\Lambda_{eff}}{3} - \frac{\rho_e + 3p_e + \left(\rho_e/\tau\right)\left(2\rho_e + 3p_e\right)}{6M_4^2} - \frac{\mu_B}{a^4}. \tag{12.7}$$

Proposition 12.1. If $\tau > 0$, $\rho_e \geq 0$, $p_e \geq 0$, $\mu_B \geq 0$, and $\Lambda_{eff} \leq 0$, then $\ddot{a} \leq 0$. The inequality is strict whenever a negative contribution is nonzero. [4]

Proof. Each term on the right-hand side of Equation 12.7 is nonpositive under the premises. The curvature term has cancelled, so choosing a different spatial curvature does not reverse the conclusion. At an isolated point with $H = 0$, the expression applies by continuity where the complete field equations admit that extension.

Both kinetic examples in Chapter 11 have nonnegative excitation pressure. Ordinary radiation and pressureless baryonic or dark matter preserve the premise. Their positive quadratic correction therefore cannot supply acceleration without a positive effective vacuum contribution or a change in some other premise. A constant U_0 can affect Λ_{eff}, but this is the already declared vacuum sector, rather than acceleration generated by positive-pressure kinetic energy.

Negative pressure in another sector, negative dark radiation, induced gravity, a bulk field, or energy exchange would change the assumptions and require new equations. The proposition is an obstruction for the model actually derived, not a classification of all higher-dimensional cosmologies.

12.5 A varying tension must enter a conserved action

Replacing a constant by a chosen function of time does not complete a covariant mechanism. Within a restricted scalar-dependent brane action, write

$$\begin{aligned} L_\Sigma &= F(X) - U(\phi) - \lambda(\phi) + L_{other}, \\ V_{eff}(\phi) &= U(\phi) + \lambda(\phi). \end{aligned} \tag{12.8}$$

The homogeneous scalar equation depends on the sum: $K\ddot{\phi}+3HF_X\dot{\phi}+V_{eff,\phi}=0$. Calling one part of this potential a varying tension creates no extra dynamical degree of freedom when the action supplies no additional coupling that distinguishes the functions. It also changes the scalar shift symmetry unless the sum is constant. [4]

Suppose the quantity called matter includes $F-U+L_{other}$ but excludes λ. Its pressure and density then satisfy

$$\dot{\rho}_m+3H\left(\rho_m+p_m\right)=-\dot{\lambda} \tag{12.9}$$

in the vacuum bulk without exchange. The total density includes λ, its pressure includes $-\lambda$, and total conservation directly produces the right-hand side. Imposing separate conservation on the same ρ_m while varying λ would remove the energy needed for this identity. A covariant model can include the appropriate exchange; it must declare it. Variable-tension brane models have established antecedents and do not inherit the constant-tension inverse unchanged. [39]

The term $-\dot{\lambda}$ in this definition is an exchange between the parts of the brane stress called matter and vacuum. It does not require a flux into the bulk: that flux was excluded when deriving the equation. If the functions U and λ are relabeled while keeping their sum fixed, the total stress remains the same even though the bookkeeping of this internal exchange changes. A separately modeled bulk flux would add further terms and physical information. This distinction prevents a change of parameter names from being mistaken for a mechanism of energy loss.

Likewise, a fixed M_5 and a varying split λ imply a varying algebraic g_{split}. Calling it an instantaneous Newton constant does not solve the response of a localized source in the rolling background. The resulting research choice is concrete: determine that local response with normalized matter, or formulate an early high-density model with its energy transfer and perturbations. Neither route follows from an arbitrary time dependence inserted into the background equation.

13 Observational Interfaces

13.1 An observable needs a forward model

The inverse results specify information that would identify particular mathematical quantities. An experiment supplies a different starting point: photon arrival times, frequency ratios, angular positions, forces, or statistical correlations in a catalogue. A physical conclusion requires a forward map connecting the action and its boundary data to those recorded quantities. Calibration, source structure, nuisance parameters, and covariance belong to that map. [3] [40] [4]

This distinction separates three questions. Structural identifiability asks whether ideal data determine a parameter within a declared model class. Statistical inference asks how well finite, noisy data determine it. Physical interpretation asks whether the selected parameterization corresponds to a distinguishable interaction or merely another representation of the same predictions. The finite-reference scalar example in Appendix C and the brane equivalence family answer different versions of these questions.

For the brane reconstruction, a supplied continuous sound history is part of the mathematical input. A distance survey does not automatically supply that function. For the kinetic completion, an action specifies a relation between pressure, density, and scalar perturbations, but its normalizations and initial charge must still be fixed. These two levels become an observational theory only after the source and measurement models are joined.

13.2 The local gravitational matching problem

The definition $g_{bg}=M_4^{-2}$ in Chapter 10 is the coefficient of the vacuum-subtracted linear density term. Even the homogeneous response away from the vacuum contains another density-dependent factor:

$$\left.\frac{\partial H^2}{\partial \rho_e}\right|_{a,\tau}=\frac{1}{3M_4^2}\left(1+\frac{\rho_e}{\tau}\right), \tag{13.1}$$

with the other background terms held fixed. This derivative is not a Poisson equation for an isolated mass. It illustrates why reading a coefficient from the homogeneous Friedmann equation does not, by itself, complete a Cavendish or orbital calibration. [4]

In the standard single positive-tension brane vacuum, localization recovers four-dimensional gravity at leading order. The explicit weak-field analysis of Garriga and Tanaka treats isolated matter and the bulk gravitational response, including its leading Kaluza–Klein corrections. That calculation supplies an appropriate antecedent for local matching; it does not automatically solve the same problem on an arbitrary rolling $P(X)$ background. [41]

A matching calculation for the present completion would specify the background scalar and vacuum state, introduce a normalized localized source, solve the coupled linearized bulk and brane equations with physical boundary conditions, and extract the force and clock response in an overlap region. The source mass must be expressed in the same matter standards used by the experiment. Only then can a parameter inferred from those responses be compared with g_{bg}.

If the required matching reduces the local coefficient to g_{bg}, an absolute calibration can select a representative of the scaling

orbit. If additional scalar or bulk contributions remain, the response involves further parameters. In either case, no local measurement distinguishes the identical-action split $\lambda+\Delta$, $U_0-\Delta$. The distinction between these two normalization questions survives every improvement in instrumental precision. [4]

13.3 Sound speed does not close the bulk perturbations

For a purely kinetic scalar on its timelike branch, the pressure and density functions determine its intrinsic scalar sound speed. They do not determine all gravitational degrees of freedom outside the brane. The projected brane equations contain the bulk Weyl contribution, whose evolution generally requires bulk information. An initially homogeneous dark-radiation coefficient does not specify all of its inhomogeneous perturbations. [7]

The limitation should be stated precisely. Some large-scale curvature evolution can be obtained from brane conservation equations without solving the entire bulk. Langlois, Maartens, Sasaki, and Wands show how this works and also identify the remaining difficulty: relating the curvature perturbations to metric potentials requires Weyl anisotropic stress, which is not determined by the brane equations alone. That missing information matters for cosmic microwave background predictions. [14]

A prospective cosmological calculation must therefore choose the matter content and initial perturbations, specify the allowed bulk modes and boundary conditions, and evolve the observables appropriate to the data set. Multiple separately normalized fluids may also introduce relative perturbations beyond the one-fluid reconstruction. The local fluid–scalar equivalence of Chapter 10 is valuable within this calculation,

but it does not supply its missing gravitational boundary problem.

13.4 What the clock and ranging source actually establishes

The longer scalar–tensor manuscript develops a separate four-dimensional model with matter coupled to a conformally related physical metric. Its clocks, lenses, and massive tracers probe that metric and its source-dependent scalar field. The brane scalar in Equation 10.1 has a different action and coupling structure. The shared subject is inference from calibrated observables; no common dynamical embedding has been derived. [40] [4]

The scalar–tensor source contains a finite-reference inverse theorem, higher-order clock and propagation calculations, synthetic experiments, and limited analyses of published data. Appendix C gives the central equations and the calibration restrictions. Its scalar–matter coupling is denoted here by α_{ST}, to distinguish it from the normalization-orbit label in Chapter 10.

For a massless constant-coupling submodel, the source combines the Cassini summary for $\gamma - 1$ with one selected lunar-ranging summary. Under its uniform prior in $t = 1 - \gamma$, assumed zero cross-experiment covariance, and weak-body mapping, it reports $\left|\alpha_{ST}\right|_{95} = 0.003959254$. This is a conditional summary-data posterior, not a bound on brane tension. The selected Ke et al. lunar result is itself conditioned on fixed ephemerides and uses conservative expanded uncertainty scales. Its alternative ephemeris reductions are not additional independent experiments to multiply into the same likelihood. [40] [42]

The same manuscript audits thirteen APOLLO normal-point records from two dates in August 2019. Parsing those records and converting their quoted timing uncertainties is useful provenance work. It does not fit a gravitational signal, derive a scalar range, or replace the orbital, clock, reflector, atmosphere, and station models needed to predict a ranging observation. Raw photon records and a complete observation normal matrix were not fitted in that calculation. [40]

13.5 A restricted DESI comparison

BAO measurements constrain combinations of cosmological distances and a sound-horizon scale. In a flat geometry the relevant model distances can be expressed as

$$\begin{aligned} \frac{D_H(z)}{r_d} &= \frac{A}{E(z)}, \\ \frac{D_M(z)}{r_d} &= A\int_0^z \frac{du}{E(u)}, \\ A &= \frac{c}{H_0 r_d}, E(z) = \frac{H(z)}{H_0}. \end{aligned} \tag{13.2}$$

Here r_d concerns the photon–baryon acoustic history. It is not a measured value of the dark-fluid function $dp/d\rho$ used in the brane inverse theorem. A free A also does not determine H_0 and r_d separately. [43]

The scalar–tensor source reports a calculation with a thirteen-component DESI DR2 compressed distance vector and its full covariance. For a shape vector $f(\vartheta)$ and covariance C, the fitted scale is obtained from

$$\begin{aligned} \chi^2(A,\vartheta) &= (d - Af)^T C^{-1}(d - Af), \\ \widehat{A}(\vartheta) &= \frac{f^T C^{-1} d}{f^T C^{-1} f}. \end{aligned} \tag{13.3}$$

This profiling retains the correlations; using only marginal errors would define a different statistic. The historical source describes manually transcribed inputs, and its supplied manuscript did not include an executable likelihood archive. Table 13.1 records its reported values. In this observational revision, the control calculations are independently re-executed from downloaded public bytes; Sections 13.8–13.10 give the new provenance and numerical comparison. [40; 47]

The native branch tested there is a flat, massless, zero-vacuum dust solution of the four-dimensional scalar–tensor model:

$$E(z)=(1+z)^{\nu},\nu=\frac{3-\alpha_{ST}^{2}}{2\left(1-\alpha_{ST}^{2}\right)},0\le\alpha_{ST}^{2}<1. \tag{13.4}$$

Its scalar-free limit has $\nu=1.5$. The manuscript separately fits a free power-law control and a flat ΛCDM control. [40]

Table 13.1. Source-reported compressed-distance comparisons.

Distance-shape model	Reported shape result	Reported χ^2
Native scalar-free flat dust	$\nu=1.5$ fixed	1420.183
Native dust, $0\le\alpha_{ST}\le0.1$	Optimum at $\alpha_{ST}=0$	1420.183
Independent power-law control	$\nu=1.095896$	96.966
Separate flat ΛCDM control	$\Omega_m=0.297462$	10.271

Each fit profiles the same free BAO scale. The large discrepancy of the native dust branch is a useful negative result for that branch under the compressed likelihood. Adding a vacuum component in the ΛCDM control changes the model. Its better fit cannot be transferred to the zero-vacuum branch, the full

scalar–tensor action, or the five-dimensional inverse theorem. Nor does the extreme dust statistic justify an extrapolation to a spectacular far-tail significance without validating that use of the compressed likelihood. [40]

The predecessor's reuse of the scalar-free dust comparison is reuse of the same data and control, rather than independent observational confirmation. The final dynamical memorandum itself performed no DESI, Planck, supernova, or nuclear-reaction likelihood. The present revision adds a separate, newly executed background-distance calculation after Section 13.6; the memorandum's physical-scale results retain their original benchmark status. [3; 4]

13.6 Reproducible calculations and an observational decision

The final memorandum reports thirty-three named checks, including the action-scaling identities, kinetic coefficients, acceleration equation, and numerical reconstruction of a prescribed nonconstant sound history. Its illustrative profile is $\chi(s)=0.22+0.07\sin(1.7\,s)$ on $[-1,1]$, with $\rho(0)=3$, $\rho(0)+p(0)=2.6$, and $X(0)=1$ in model units. The reported recovery error from independently differentiated interpolants is 5.92×10^{-8} in the interval interior. These are generated-model tests, not observations of a sound history. [4]

The book's direct evaluations of the scale formulas are distinct from those source-reported verification records. Reproducing the full source suite requires its programs, inputs, tolerances, environment, and output logs. A count of passed names demonstrates what the document claims; actual execution evidence requires the executable materials.

An observational extension must fit the recorded quantities with their calibration and trajectory nuisances. Signal injection should test attenuation; joint covariance should test agreement across channels. A scalar-free null has an unidentified range, so its detection statistic requires separate calibration. [40]

13.7 A specified background from the action

The observational extension asks a narrow question: do present distance data prefer a positive quadratic density term in a flat, constant-total-tension braneworld? The test uses the Einstein bulk and junction conventions of Chapter 10, a positive total vacuum stress, no brane–bulk energy exchange, and a homogeneous nonnegative bulk mass. Baryons and cold dark matter are conserved pressureless components whose sum is the matter density. A constant effective vacuum is allowed.

For the scalar sector choose the regular canonical action F(X) = X in its unexcited state X = 0, with constant vacuum U_0. Dust belongs to the separately specified matter sector. This avoids invoking the positive-sound reconstruction theorem to represent exact zero-sound dust and avoids the cubic vacuum defect. It is a consistent background specialization, not a uniqueness statement about scalar completion or a proof of full coupled perturbation stability.

Set $x = a_0/a = 1 + z$ and $E = H/H_0$. Conservation gives dust density proportional to x^3. Substitute into Equation 12.1, set spatial curvature to zero, divide by H_0^2, and use E(0) = 1. The normalized braneworld expansion relation used in the distance likelihood is

$$E^2(z) = 1 + \Omega_m\left(x^3 - 1\right) + \Omega_q\left(x^6 - 1\right) + \Omega_{dr}\left(x^4 - 1\right), x = 1 + z. \tag{13.5}$$

Here Ωm weights conserved dust, Ωq its quadratic density correction, and Ωdr geometric dark radiation. The dimensionless definitions and physical ratio are

$$\Omega_m=\frac{\rho_{m0}}{3M_4^2H_0^2},\Omega_q=\frac{\rho_{m0}^2}{36M_5^6H_0^2},$$
$$\Omega_{dr}=\frac{\mu_B}{a_0^4H_0^2},\Omega_\Lambda=\frac{\Lambda_{eff}}{3H_0^2}, \tag{13.6}$$
$$\epsilon_0=\frac{\Omega_q}{\Omega_m}=\frac{\rho_{m0}}{2\tau},\tau=\lambda+U_0.$$

The factor a_0 is retained because the book uses a length-valued scale factor. Each Ω is dimensionless; ρ and τ have energy dimension four, while H, M_4 and M_5 have energy dimension one. The background identity $M_4^2 = 6M_5^6/\tau$ yields the ratio in Equation 13.6. These definitions do not identify M_4 with a measured local gravitational coupling without the matching discussed earlier.

The expanding AdS branch used here additionally requires

$$\Omega_\Lambda=1-\Omega_m-\Omega_q-\Omega_{dr}>0,$$
$$\frac{\ell^{-2}}{H_0^2}=\frac{\Omega_m^2}{4\Omega_q}-\Omega_\Lambda>0\left(\Omega_q>0\right). \tag{13.7}$$

The second line follows by subtracting the effective vacuum term from $\tau^2/(36M_5^6)$. The code enforces it at positive Ω_q. The $\Omega_q = 0$ boundary is the formal general-relativistic control limit; it is not a finite-tension parameter estimate. The search domain is $0.05 \le \Omega_m \le 0.70$, $0 \le \Omega_q \le 0.05$ and $0 \le \Omega_{dr} \le 0.20$, with the two conditions above. A negative-dark-radiation branch is not tested.

Equation 13.5 is a normalized specialization of the established braneworld Friedmann law. Supernova tests also have

established antecedents. Its role here is a reproducible distance model with an explicit physical-scale audit, not a new law or a unique signature of extra dimensions. Setting $\Omega q = \Omega dr = 0$ recovers the flat ΛCDM background. Total vacuum stress $\tau = \lambda + U_0$ enters through Equation 13.6; this parameterization preserves, rather than breaks, the exact vacuum-relabeling redundancy. [8; 9; 49]

13.8 Public observations and retained information

The data are the public DESI DR2 compressed BAO means and covariance distributed in the Cobaya BAO data repository, and the Pantheon+ magnitude table with its statistical-plus-systematic covariance. Repository commits, immutable source URLs, file sizes and SHA256 hashes are archived. The data were downloaded as bytes, not transcribed from a plot or table. Retrieval and calculation were performed on 10 October 2026. [43; 46–48]

Table 13.2. Data used in the executed likelihood.

Input	Selection and size
DESI DR2 BAO	13 distance entries; $0.295 \le z \le 2.33$; full 13×13 covariance
Pantheon+	1701 original light-curve rows; retain $zHD > 0.01$
Retained supernova data	1590 light-curve rows from 1473 distinct CID labels; full selected covariance
Supernova redshifts	$0.01016 \le zHD \le 2.26137$; separate zHEL retained
Absolute calibration	No Cepheid distance, SH0ES modulus or H_0 prior used

The supernova selection and observables follow the collaboration's SN-only likelihood: use m_b_corr, zHD in the radial integral, and zHEL in the luminosity prefactor. Repeated

light-curve records are retained with their covariance; they are not counted as distinct supernovae or deduplicated. Ten retained rows carry a calibrator flag, but the flag does not introduce a Cepheid calibration into this likelihood. The SH0ES label in the input filename is not itself a likelihood term. [48]

Cross-survey covariance is assumed zero. Within each survey the published full covariance is used, and both selected matrices are symmetric and Cholesky positive definite. The calculation does not refit light curves, the galaxy correlation function, selection corrections, or the collaboration's systematic-error construction. Its validity is conditional on the published compressed observation models.

13.9 Forward distances and nuisance elimination

Let I be the dimensionless radial integral and A = c/(H_0r_d). In the flat geometry the BAO predictions are

$$I(z)=\int_0^z \frac{du}{E(u)}, D_M/r_d = A\,I(z),$$
$$D_H/r_d = A/E(z), \tag{13.8}$$
$$D_V/r_d = A\left[\frac{z\,I^2(z)}{E(z)}\right]^{1/3}.$$

The appropriate expression is selected for each row of the public vector. The scale A is profiled with Equation 13.3 and stays positive in every reported fit. It does not measure H_0 and r_d separately. For the supernova apparent magnitudes, an additive intercept absorbs the absolute magnitude and Hubble scale:

$$\begin{gathered} m_i^{th} = M + g_i, \\ g_i = 5\log_{10}\left[\left(1+z_{HEL,i}\right) I\left(z_{HD,i}\right)\right], \\ \widehat{M} = \frac{1^T C_{SN}^{-1}(m-g)}{1^T C_{SN}^{-1} 1}. \end{gathered} \tag{13.9}$$

The observed vector m contains m_b_corr. The vector of ones has the same dimension. This formula follows by differentiating the Gaussian quadratic form with respect to the intercept. Because the covariance is fixed, integrating that intercept with a constant flat measure adds a parameter-independent factor for the SN-only calculation. Profiling the BAO scale is not generally equivalent to marginalizing it with a flat prior: its curvature depends on the cosmological shape.

$$\begin{gathered} r_B = d - \widehat{A} f, r_S = m - g - \widehat{M} 1, \\ \chi^2_{prof}(\theta) = r_B^T C_{BAO}^{-1} r_B + r_S^T C_{SN}^{-1} r_S, \\ \theta = \left(\Omega_m, \Omega_q, \Omega_{dr}\right). \end{gathered} \tag{13.10}$$

Cholesky whitening evaluates the quadratic forms and scalar nuisance solutions without explicitly inverting the covariance. The primary analysis uses frequentist profile curves. No Markov chain, posterior for Ω_q, Bayes factor, or prior-independent model probability is inferred from them. Low-dimensional profiling is sufficient for this stated calculation; it is not a substitute for a full perturbation likelihood.

Distances are integrated with 64-point Gauss–Legendre quadrature at each observed redshift. Scalar bounded optimization or multistart constrained optimization handles the remaining parameters, explicitly retaining the nested zero-correction edge. The analysis specification was recorded before these fits, but was not externally preregistered or blinded; published cosmological summaries and historical control values were already known.

13.10 Fits and conditional quadratic profiles

The flat ΛCDM control fixes both extra coefficients to zero. Its separately fitted matter coefficients and minimum statistics are shown below. The joint data vector has 1603 entries and three fitted parameters, including the two profiled distance nuisances. The covariance and systematic construction make a reduced statistic a diagnostic, not an independent cosmological validation.

Table 13.3. Executed flat ΛCDM reference minima.

Data	Ω_m	χ^2 minimum
DESI BAO	0.297462	10.271041
Pantheon+	0.331576	1402.919128
Joint	0.304214	1416.139173

At the joint minimum, A = 29.678604 and the magnitude intercept is 23.798362. The BAO and SN contributions to χ^2 are 10.869899 and 1405.269274. The Ω_m profile reaches $\Delta\chi^2 = 1$ at 0.296378 and 0.312255. These values refer to the specified flat control, with freely profiled calibration scales.

Allowing $\Omega_q \geq 0$ gives $\Omega_q = 0$ and the same minimum to numerical precision. Allowing nonnegative dark radiation as well gives $\Omega_{dr} = 0$ at the minimum. Thus the fits find no improvement from either positive addition within the tested

domain. The edge optimum leaves finite positive values admissible at nonzero profile cost; it does not prove infinite physical tension or rule out braneworld gravity as a class.

For each fixed q, nuisance matter and any allowed dark radiation are reoptimized. In the baseline Ω_{dr} is held at zero; in the dark-radiation sensitivity it is varied. Define

$$\Delta\chi^2(q) = \chi^2_\star(q) - \chi^2_{min},$$
$$\chi^2_\star(q) = \min_{\Omega_m, \Omega_{dr}} \chi^2_{prof}(\Omega_m, q, \Omega_{dr}). \tag{13.11}$$

Table 13.4. Positive Ω_q crossings of reference profile levels.

Data or variant	$\Delta\chi^2 = 2.7055$	$\Delta\chi^2 = 3.8415$
BAO only	0.0004738	0.0005852
SN only	0.0080329	0.0104220
Joint	0.0002534	0.0003346
Joint with Ω_{dr} free	0.0002534	0.0003346

The levels 2.7055 and 3.8415 are one-parameter reference thresholds. Section 13.14 calibrates a zero-correction test at one fitted nuisance point with 10,000 conditional simulations and fixed zero dark radiation. Chapter 16 adds a separate positive-signal finite-grid inversion. Neither calculation changes the original profile crossings into continuous upper bounds with guaranteed coverage. The table retains its profile-level labels; its minima and crossings do not touch the stated upper search boundaries. [56; 57; 59; 60]

At the joint second crossing, the fitted matter coefficient is 0.294185 and the AdS curvature condition is comfortably positive. The nonnegative dark-radiation profile remains at its zero edge over the reported curve and has the same crossings. This says nothing about cancellation by an allowed negative dark-radiation branch.

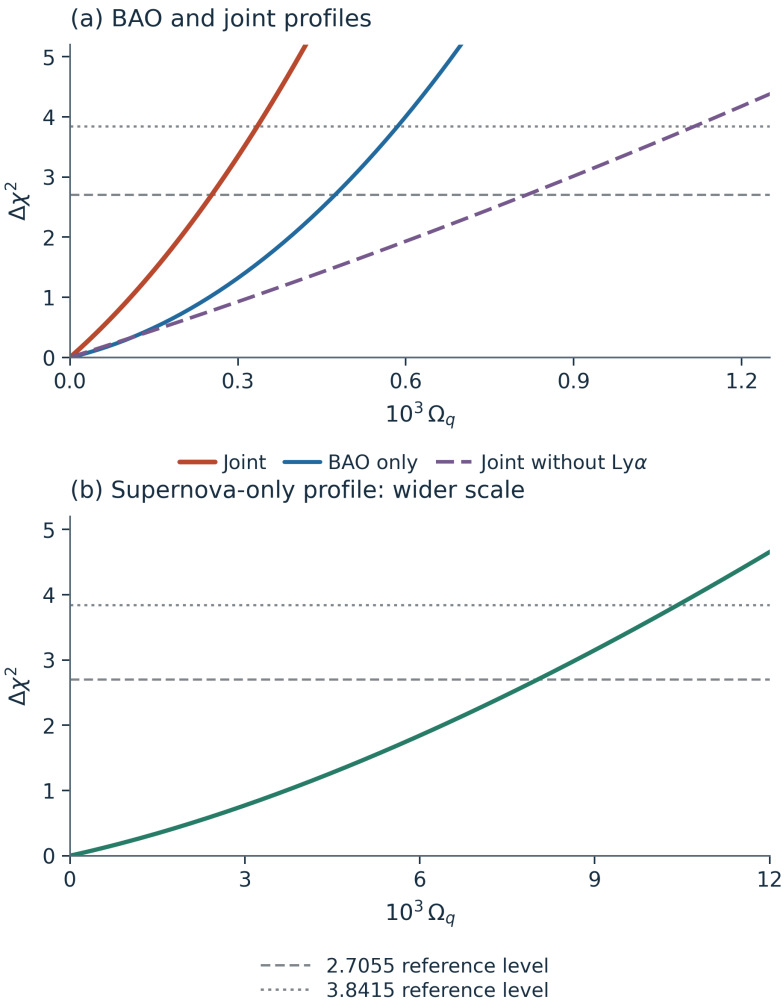

Figure 13.1. Conditional Ω_q profiles with nuisance parameters reoptimized and Ω_{dr} = 0. Panel (a): BAO only, joint BAO + SN, and joint without the z = 2.33 Lyα block. Panel (b): SN only on a wider scale. Both horizontal axes show 10^3 Ω_q; each curve uses its own minimum. The guides are $\Delta\chi^2$ = 2.7055 and 3.8415 reference levels. The first joint crossing is 0.0002534. Statistical scope is defined in Sections 13.10 and 13.14.

The independently executed DESI control reproduces the historical Ω_m = 0.297462 and χ^2 = 10.271. The free power-law control gives exponent 1.095896 and χ^2 = 96.965522; scalar-free dust gives χ^2 = 1420.183280. Agreement verifies these compressed-distance computations, not a new independent observation or a far-tail significance.

Pantheon+ alone gives profile mode 0.331576. Direct one-dimensional marginalization with a uniform Ω_m measure on [0.05, 0.70] and a constant intercept measure gives mean 0.332258 and standard deviation 0.018210. The published summary is 0.334 ± 0.018. The mean difference is −0.001742, about −0.097 of the published standard deviation. It is small, but remains unreconciled with the complete original pipeline. Comparing like statistics does not remove it. This is close consistency, not exact reproduction of that published posterior. [46]

13.11 Sensitivity and numerical audit

Three variations test specific analysis choices. A higher supernova cut removes the nearest retained records. Omitting the z = 2.33 Lyα BAO block leaves eleven BAO entries. Finally, a fixed ordinary-radiation-to-matter ratio r = 1/3400 is inserted in both the linear density term and its square:

$$t(x)=x^3+r\,x^4,\ t_0=1+r,$$
$$E^2(z)=1+\Omega_m\left(t-t_0\right)+\Omega_q\left(t^2-t_0^2\right)+\Omega_{dr}\left(x^4-1\right). \tag{13.12}$$

The radiation ratio is a declared benchmark, not a measured value obtained from these distances. In this variation the vacuum condition uses $1-\Omega_m\,t_0-\Omega_q\,t_0^2-\Omega_{dr}$. Squaring only the

dust term would omit the dust–radiation cross term and would not implement the same junction law.

Table 13.5. Joint sensitivity at the $\Delta\chi^2 = 2.7055$ reference level.

Selection	SN rows	Ω_q crossing
Baseline	1590	0.0002534
zHD > 0.023	1371	0.0002726
No Lyα BAO	1590	0.0008164
Radiation benchmark	1590	0.0002514

The higher supernova cut changes the crossing by about 7.6 percent. Removing the highest-redshift BAO block weakens it by a factor of 3.22. The radiation benchmark changes it by less than one percent. All three optima remain at zero quadratic correction. The redshift leverage is expected for a term growing as x^6, but the size of that leverage also shows why robustness to the high-redshift compressed likelihood matters.

The new numerical audit records 16 passed checks. They cover input integrity, matrix properties, reference controls, quadrature, analytical nuisance elimination, an independent optimizer, and nested model identities. At three declared test points, including positive corrections, the largest χ^2 change between 64- and 128-point quadrature is 3.0×10^{-12}. Adaptive quadrature independently agrees with radial integrals within 1.2×10^{-16}. Numerical nuisance fitting agrees with analytical profiling within 9×10^{-12} in χ^2.

The audit preserves two initial failures. A Pantheon-summary tolerance of 0.001 failed and remains an unresolved external-summary difference. Powell first stopped 0.000811 above the boundary minimum; bounded Nelder–Mead and SLSQP recovered that minimum. Figures 13.1–13.2 show the profiles

and ordered whitened residuals. The archive retains the original failure records and the later numerical resolution.

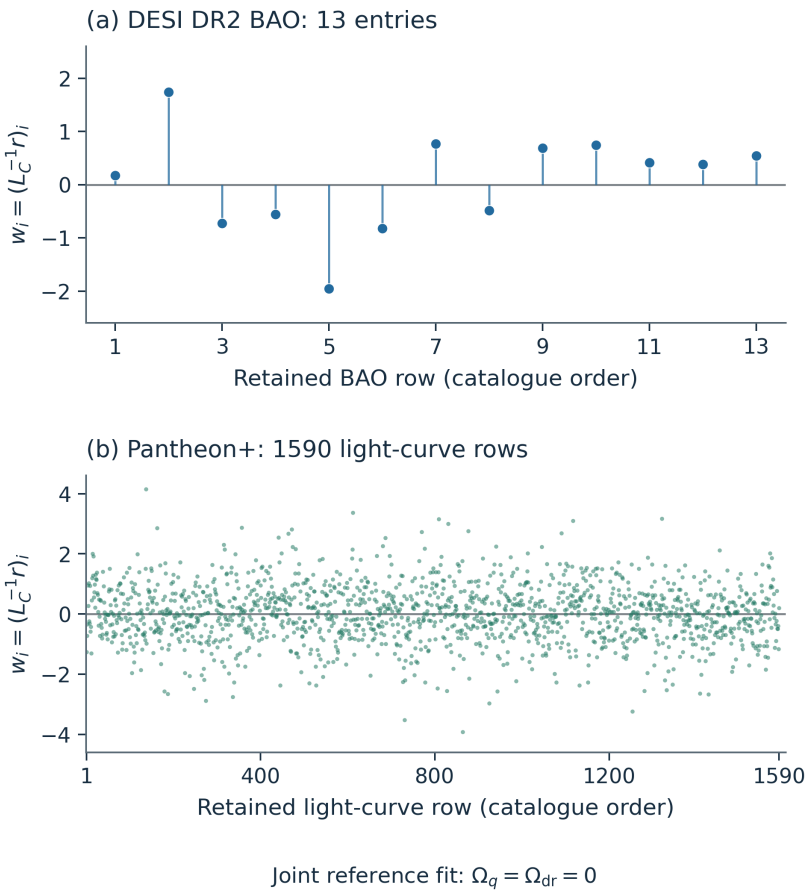

Figure 13.2. Ordered Cholesky-whitened residuals at the joint flat reference fit, $\Omega_q = \Omega_{dr} = 0$. For each survey, $w = L_C^{-1} r$ with $C = L_C L_C^T$ and r = observed − fitted prediction. Panel (a) retains all 13 BAO entries; panel (b) retains 1590 Pantheon+ light-curve rows from 1473 distinct CID labels. The row order is unchanged from the archived derived catalogues. Cholesky components combine correlated catalogue residuals and depend on the ordering; they are not independent per-object errors or individual significance tests. Repeated light-curve entries remain in the covariance-aware calculation. The zero line is a diagnostic reference; the fitted model also imposes constraints on the residual vector.

13.12 From a distance allowance to a physical scale

A distance-level coefficient must be compared with the action's normalized density scale. For a flat dust reference with the same Ω_m and H_0, zero dark radiation, and $0 < \Omega_m < 1$, let E_0 denote the zero-quadratic model. Define the fractional addition to E_0^2 by

$$u(z)=\frac{\Omega_q\left(x^6-1\right)}{E_0^2(z)}\le\epsilon_0 x^3,$$
$$E_0^2(z)=\Omega_m x^3+1-\Omega_m. \tag{13.13}$$

The inequality follows because $E_0^2 \ge \Omega_m x^3$ and $x^6 - 1 \le x^6$ for $z \ge 0$. If u_{max} bounds u over the observed interval, the integrands and radial inverse expansion are bounded between their reference values and those values divided by $\sqrt{(1 + u_{max})}$. Integration preserves the bounds. The geometric mean defining D_V and the common luminosity prefactor preserve them as well. Thus, for D equal to D_M, D_H, D_V or D_L,

$$\frac{\left|D-D_0\right|}{D_0}\le 1-\left(1+u_{max}\right)^{-1/2}$$
$$\le\frac{\epsilon_0}{2}\left(1+z_{max}\right)^3, \tag{13.14}$$
$$\left|\Delta m\right|\le\frac{5\epsilon_0}{2\ln 10}\left(1+z_{max}\right)^3.$$

The final magnitude inequality uses $\ln(1 + u_{max}) \le u_{max}$. These are elementary conditional bounds, not a new dynamical law. They avoid loss of numerical precision from subtracting cosmological distances whose relative difference is vastly below machine epsilon. They hold before nuisance refitting and hence provide a conservative sensitivity screen; they do not bound independent scalar, dark-radiation or bulk perturbation effects.

For illustration only, set H_0 = 70 km s^{-1} Mpc^{-1}, M_4 = 2.435 × 10^{18} GeV, and Ω_m = 0.304214 from the reference shape fit. The first two quantities are external benchmark inputs, not measurements in this likelihood. The corresponding present dust density is 1.2065 × 10^{-47} GeV^4. Applying Equation 13.14 up to z_{max} = 2.33 gives

Table 13.6. Declared stress benchmarks and distance bounds.

Stress scale	Ω_q	Maximum $\lvert\Delta D\rvert/D_0$
1 MeV	1.835 × 10^{-36}	1.114 × 10^{-34}
1 TeV	1.835 × 10^{-60}	1.114 × 10^{-58}

The corresponding absolute magnitude bounds are 2.419 × 10^{-34} and 2.419 × 10^{-58}. Converting the joint first profile crossing at the fixed benchmark matter coefficient gives a total-stress energy scale near 9.23 meV. This is an illustrative parameter conversion, not a measured tension limit with local-gravity or nucleosynthesis validity. Its contrast with the MeV and TeV benchmarks quantifies the gap between late-time distance sensitivity and the physically small direct correction.

A MeV total-stress benchmark and a TeV total-stress benchmark are not universal empirical lower limits. Published nucleosynthesis work constrains the five-dimensional Planck scale jointly with dark radiation under its own abundance assumptions; those units and parameters cannot be replaced by τ to the one-quarter power. A current BBN likelihood and the localized force response would require their own models and data. [37; 50]

13.13 Interpretation and the next empirical test

The executed result is a covariance-aware distance constraint on a specified background coefficient, with no preference for a positive correction in the tested branch. It supplies the practical

application missing from the earlier book edition at the background level. It does not identify a bulk black hole, measure the dark-fluid sound history, distinguish an identical-action vacuum split, or establish a new gravitational interaction.

The highest-q profiles are late-time phenomenological comparisons. Allowing r_d to float removes an imposed numerical sound-horizon calibration; it does not make an arbitrary early universe consistent with the BAO template or with recombination. A constant x^6 contribution can radically change the early expansion. No acoustic-horizon integral, nuclear network, transfer function, CMB spectrum, or full-shape galaxy likelihood has been solved here. Large allowed distance coefficients must not be advertised as globally viable braneworld parameters.

The mathematical inverse remains conditional on sound and expansion information that these catalogues do not provide. Conversely, an identical-action transformation that preserves τ leaves this likelihood unchanged exactly. More data or an MCMC sampler cannot separate physically identical labels. Absolute calibration can address a different normalization freedom only when the corresponding forward measurement is specified.

The next defensible extension is to close the bulk and brane perturbation boundary problem, propagate a conserved multi-component matter model, compute the early acoustic scale, and validate the compressed approximation or use the collaboration likelihood appropriate to the predicted observables. Signal-injection experiments should then calibrate coverage at physical boundaries. Local-force and BBN constraints should be joined only through consistent parameter matching. Those steps may strengthen exclusions or reveal a distinguishable effect; the present calculations do not prejudge their outcome.

13.14 Pointwise plug-in null calibration

The profile crossings in Section 13.10 and the sampling distribution of a discovery statistic are different questions. This extension addresses the latter for the baseline branch with dark radiation fixed at zero. It asks how often Gaussian data generated at the fitted zero-quadratic control would produce an apparent preference for a positive quadratic term. Define

$$T = \min_{\Omega_m, A, M} \chi^2\left(\Omega_q = 0, \Omega_{dr} = 0\right) - \min_{\Omega_m, \Omega_q \geq 0, A, M} \chi^2\left(\Omega_{dr} = 0\right). \tag{13.15}$$

The two calibration nuisances and the matter coefficient are fitted under both hypotheses. The alternative includes the zero-correction edge, so the statistic is nonnegative. For the real DESI–Pantheon+ data, the statistic is zero to numerical precision, with a residual below 4×10^{-14} in magnitude. The positive correction provides no improvement in this branch.

The null generating point is the observed joint control fit, $\Omega_{m0} = 0.3042141978$, $A_0 = 29.678604089$ and $M_0 = 23.798361833$, with $\Omega_{q0} = \Omega_{dr0} = 0$. These are plug-in generating values for this

experiment, not externally known calibrations. Using the original mean functions f and g and the original covariance Cholesky factors, the simulated vectors are

$$\begin{aligned} d_B^{¿} &= A_0 f(\theta_0) + L_B \epsilon_B, \\ m_S^{¿} &= M_0 1 + g(\theta_0) + L_S \epsilon_S, \end{aligned} \tag{13.16}$$

where $\epsilon_B \sim N(0, I_{13})$ and $\epsilon_S \sim N(0, I_{1590})$ are independent. Thus the simulations preserve the published within-survey covariance, including its off-diagonal terms, at exactly its stated scale. No residual-variance rescaling is fitted. Cross-survey covariance remains zero. The covariance matrices and their systematic-error construction are conditioned upon; uncertainty in their estimation and non-Gaussian survey errors are not simulated.

A total of 10,000 independent vectors were generated with NumPy Generator(PCG64), seed 20261012. The original data selection, redshift conventions, flatness restriction, positive-total-tension branch and parameter bounds are unchanged. Every simulated data set was fitted to the full nonlinear distance model with dark radiation fixed at zero. The BAO amplitude and supernova intercept were profiled analytically, while the matter and quadratic coefficients were optimized numerically. Analytical derivatives and a Fisher starting value accelerate the calculation; no surrogate expansion replaces the nonlinear likelihood. Every alternative was optimized, including draws whose solution lies on the zero edge. Unsuccessful or insufficiently stationary optimizations were retried with bounded Nelder–Mead.

With a single regular nonnegative coefficient and identifiable interior nuisance parameters, the familiar asymptotic boundary reference is [56; 57]

$$T \overset{reference}{\sim} 1/2\,\delta_0 + 1/2\,\chi^2_1,$$
$$P(T>t) = 1/2\,P\left(\chi^2_1>t\right), t>0. \tag{13.17}$$

Here δ_0 is a point mass at zero. The AdS and effective-vacuum inequalities are inactive locally at the generating point; dark radiation is fixed, so this experiment does not introduce a second active nonnegative parameter. The simulation tests this reference at one specified nuisance point rather than asserting a uniform asymptotic result over the full model.

The fitted boundary mass was 4974/10000, or 0.4974. Its Monte Carlo standard error was 0.0050, and its exact binomial 95% Monte Carlo interval was [0.4876, 0.5072]. A tolerance of $T \le 10^{-8}$ defines numerical zero for this summary. The threshold results are:

Table 13.7. Conditional null exceedances from simulated data.

Threshold / reference tail	**Simulated tail**	**Exact 95% MC interval**
1.6424 / 0.100	989/10000 = 0.0989	[0.0931, 0.1049]
2.7055 / 0.050	515/10000 = 0.0515	[0.0472, 0.0560]
3.8415 / 0.025	259/10000 = 0.0259	[0.0229, 0.0292]
5.4119 / 0.010	91/10000 = 0.0091	[0.0073, 0.0112]

The asymptotic reference lies inside each reported pointwise Monte Carlo interval, including the boundary-mass interval. These intervals describe uncertainty from a finite simulation count. They are not intervals for a cosmological parameter. In particular, $t = 2.7055$ corresponds to a 5% tail of the one-boundary null reference, while $t = 3.8415$ corresponds to a 2.5% tail. Neither statement assigns coverage to an upper endpoint of the existing q profile. The empirical 95th percentile of T was

2.7503, with a 95% order-statistic Monte Carlo interval [2.5836, 2.8705]; the half-mixture reference gives 2.7055. Figure 13.3 displays the empirical survival curve and a labelled pointwise Monte Carlo band.

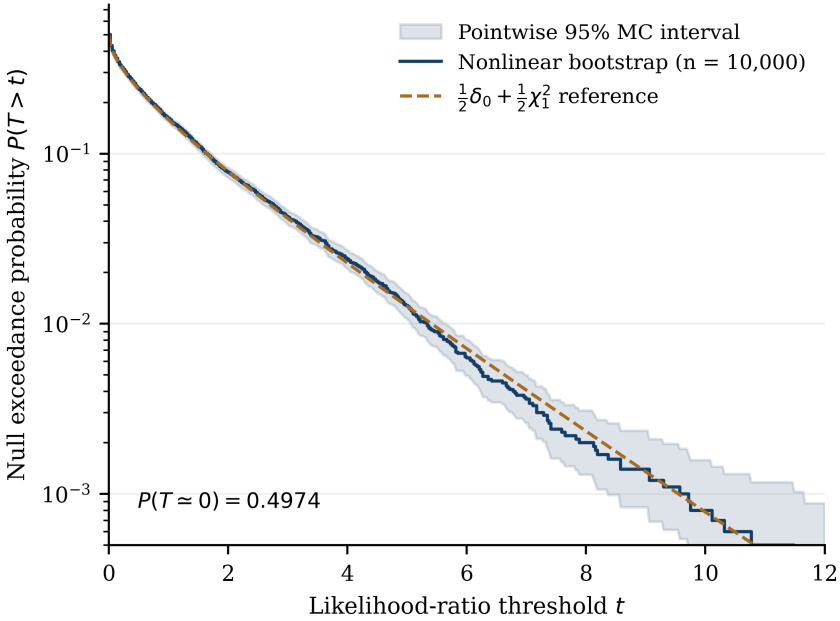

Figure 13.3. Pointwise null calibration of the positive-quadratic test. Empirical survival probability from 10,000 simulated Gaussian DESI–Pantheon+ vectors generated at the fitted $q = 0$, dark-radiation-zero control, compared with the $\frac{1}{2}\delta_0 + \frac{1}{2}\chi^2_1$ reference. The shaded region is a pointwise 95% Wilson Monte Carlo interval, not a cosmological confidence region or a simultaneous band. Every simulated vector is refitted with the original nonlinear distance model. The estimated zero-statistic mass is 0.4974. This calibrates a test at one null point and does not establish coverage of a positive-q upper profile endpoint.

The simulation is reproducible from the included raw inputs. The accelerated likelihood agrees with the original implementation at specified zero and positive corrections; its derivatives were checked by finite differences. A multistart

audit includes ordinary draws, the largest test statistics and draws nearest the reference thresholds. Independently, 40 selected draws were fitted using the original book likelihood and its numerical-derivative multistart optimizer; the largest change in T was below 4×10^{-8}. The new runner's 7 specified checks passed. These checks are additional to, and distinct from, the original sixteen numerical observational checks and twenty-five analytical companion checks.

This is a pointwise calibration result at the fitted zero-correction control. It does not convert $\Omega_q=0.0002534$ into a continuous coverage-calibrated upper limit. Chapter 16 now supplies a separately defined finite-grid rank inversion, simulations at positive coefficients and nuisance-grid maximization, with explicit retrospective-selection and off-grid limitations. Coverage with free nonnegative dark radiation, covariance-construction uncertainty, non-Gaussian errors and a completed early-universe likelihood remains outside the executed calibration.

13.15 Local sensitivity and the efficient-score diagnostic

The same calculation exposes the local information that distinguishes matter evolution from the quadratic correction within this specified background. Let $\tilde{f}=L_B^{-1}f$ and $\tilde{g}=L_S^{-1}g$. Let P_B remove the BAO amplitude direction $\tilde{f}_0$, and let P_S remove the whitened supernova constant direction $L_S^{-1}1$. The two nuisance-projected tangent columns are

$$j_a=\begin{pmatrix} A_0 P_B \partial_a \tilde{f} \\ P_S \partial_a \tilde{g} \end{pmatrix}_{\theta_0}, a\in\{m,q\}, \qquad F_{ab}=j_a^T j_b. \tag{13.18}$$

Projecting the quadratic column off the matter column gives

$$j_{q\mid m}=j_q-j_m\frac{j_m^T j_q}{j_m^T j_m},$$
$$Z=\frac{j_{q\mid m}^T \epsilon}{\| j_{q\mid m}\|}, \tag{13.19}$$
$$T_{lin}=\left[max\left(0,Z\right)\right]^2.$$

For the Gaussian tangent experiment, Z is standard normal and the half-mixture follows directly. The nonlinear simulation uses the same noise vectors, allowing a paired comparison without extra sampling variability. The mean nonlinear-minus-score difference was 0.00354 in T, its root-mean-square difference was 0.01487, and its largest absolute difference was 0.25248. Figure 13.4 shows all paired draws. This diagnostic evaluates the size of the local approximation; the reported bootstrap statistic always comes from the nonlinear fit.

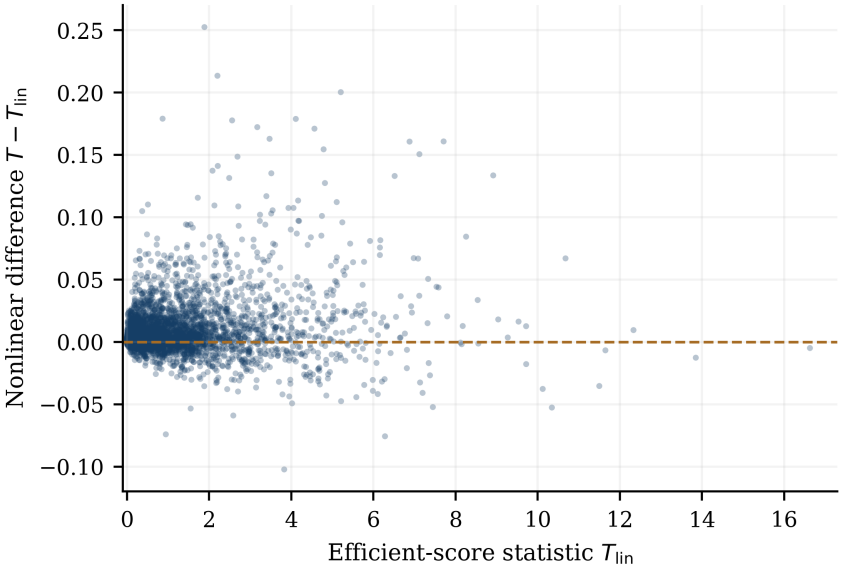

Figure 13.4. Nonlinear fit versus the tangent-score experiment. For all 10,000 identical Gaussian noise draws, the ordinate shows $T - T_{lin}$, where T is obtained by nonlinear refitting and $T_{lin} = \left[max\left(0, Z\right) \right]^2$ uses the normalized nuisance-projected quadratic score at the null. The dashed line denotes exact agreement. The score approximation is used for diagnosis and starting values; it does not replace the full likelihood in the bootstrap. The horizontal and vertical axes contain simulated quantities, not extra astronomical observations.

With the calibration nuisances projected out, the local unconstrained standard deviation of q after matter profiling is 0.0003204. The local matter standard deviation is 0.0078526 if q is fixed, and 0.0126445 if both tangent coefficients vary. The corresponding local parameter correlation is -0.78379. After normalizing the tangent columns to unit length, the information condition number is 8.2503; this normalization prevents a numerical change of parameter units from masquerading as physical degeneracy.

These are local sensitivity diagnostics, not a boundary confidence region or a posterior. They show that the matter and quadratic shapes are correlated but locally distinguishable within this two-coefficient experiment. They do not remove the identical-action vacuum-split redundancy or identify a five-dimensional origin. The observed efficient score is -1.31070; its negative sign is consistent with the constrained optimum remaining on $q=0$ and supplies no evidence for a positive correction.

14 What Is Established and What Remains to Be Measured

14.1 The result is a hierarchy of identifiable quantities

The central result is conditional but substantive. With supplied spatial curvature, a declared five-dimensional Einstein-bulk model and an exact barotropic sound history, cosmological reconstruction has four expansion columns. Their independence identifies the coefficients. A free effective vacuum then leaves an equivalence class of matter normalizations and split tensions, along which the stated bulk combinations remain constant. Chapter 18 extends this hierarchy when spatial curvature is unknown; Chapter 19 synthesizes the third-edition results. [18; 19; 3]

The Riccati classification marks the exact boundary of the structural result. At an exceptional sound history, the dark-radiation column is already quadratic in the sound coordinate. Complete expansion and sound histories can then agree while the bulk metric changes. Away from the exception, carefully chosen finite epochs may identify coefficients, but small singular values can still make numerical reconstruction uninformative. Uniqueness, stability and measurement precision are separate accomplishments.

Table 14.1. Established results and the information they require.

Established statement	Information and model on which it depends
A sound coordinate linearizes the conserved density history	One conserved barotropic component and the supplied sound function
The Riccati family exhausts full-history column dependence	Exact differentiable sound on the whole stated interval
Free vacuum leaves a complete normalization family	Identified coefficients, physical interior and the declared reference convention
Bulk curvature and geometric mass survive that family	Rank four, positive quadratic coefficient and the AdS branch
Finite uncertainties admit simultaneous outer confidence sets	A valid observation model, calibrated windows and a justified regularity class
A local scalar action can realize the history	Positive enthalpy and sound, over the visited field interval

This hierarchy explains why a geometric reconstruction can be informative without establishing a unique microscopic theory. It also makes failure interpretable. An inconsistent overdetermined design, incompatible anchors, or an empty properly calibrated confidence set rejects at least one premise of the combined model and measurement procedure; it need not identify which premise failed.

14.2 What the dynamical completion adds

The action analysis moves beyond curve reconstruction by identifying which freedoms have physical content. A conserved barotropic history with positive enthalpy and sound admits a

local purely kinetic representation. The construction proves existence and supplies the homogeneous equation of motion. It does not select one kinetic law from all the laws that could reproduce the chosen history. Shift symmetry permits many functions of X and selects no golden-ratio frequency. [4]

Two normalization issues remain distinct. The change $\lambda_{bare} \mapsto \lambda_{bare} + \Delta$, $U_0 \mapsto U_0 - \Delta$ leaves the action identical because only $\tau_{vac} = \lambda_{bare} + U_0$ occurs. No observation of that action separates the two labels. The classical scaling orbit instead multiplies the action by a positive constant. It preserves the reference split coefficient but changes the vacuum-subtracted background coefficient in fixed stress units. A justified absolute measurement of the latter can select one orbit representative, while the exact split redundancy remains. [7; 3; 4]

The constant-sound example also demonstrates why a local action needs a dynamical audit. The pure cubic kinetic law has positive scalar kinetic coefficients at every strictly positive X, yet they vanish at its zero-gradient vacuum. It has no quadratic scalar propagator there. Adding a canonical term makes that vacuum locally regular but changes the sound speed:

$$F(X) = X + \frac{X^3}{M^8}, c_\phi^2 = \frac{1+3x^2}{1+15x^2}, x = \frac{X}{M^4}. \tag{14.1}$$

The sound approaches one fifth only at large x. If the polynomial is interpreted as an ordinary small-x expansion, that regime is not controlled without further justification. A finite-background effective theory could have a different cutoff, but positive sound speed alone neither supplies it nor proves coupled brane–bulk stability. The demonstrated repair resolves a specific local defect; it does not complete the ultraviolet theory. [4]

14.3 The direct late-time quadratic route is quantitatively restricted

Once the total constant vacuum stress and low-energy gravitational matching are declared, the direct quadratic-to-linear density ratio is

$$\epsilon_{brane}=\frac{\rho_e}{2\tau_{vac}}=\frac{H_\rho^2\ell^2}{4\left(1+\Lambda_{eff}\ell^2/3\right)},H_\rho^2=\frac{\rho_e}{3M_4^2}. \tag{14.2}$$

At the source's benchmark $H_0=70\,km\,s^{-1}\,M\,pc^{-1}$, $M_4=2.435\times10^{18}\,GeV$ and excitation density equal to the corresponding critical-density scale, a total tension scale $\tau_{vac}^{1/4}=1\,TeV$ gives $\epsilon_{brane}\simeq1.983\times10^{-59}$. This is a declared scale calculation. It provides no practical late-time expansion signal from this direct correction at those inputs. [4]

A one-percent ratio at the same density instead requires a tension scale of approximately $6.67\,meV$. With zero effective vacuum in the conversion, its AdS radius is approximately $0.86\,Gpc$. The resulting scale conflict concerns the standard localized-gravity interpretation. It does not show that all dark radiation, scalar clustering or higher-dimensional effects are too small.

The acceleration conclusion is comparably precise. Positive total tension, nonnegative excitation density and pressure, nonnegative dark radiation, and nonpositive effective vacuum give $\ddot{a}\leq0$. The positive quadratic correction cannot accelerate that matter content. Adding a constant scalar vacuum may change the effective vacuum term, but does not turn the kinetic correction into a new source of negative pressure. Extensions with other matter stresses or different gravitational terms constitute different hypotheses. [4]

The executed distance study tests the normalized relation (13.5). The joint minimum lies at the zero-correction boundary of its flat dust branch. The original profile reaches $\Omega_q = 0.0002534$ at level 2.7055, a conditional reference crossing. Chapter 16 adds a retrospective finite-grid calibration, with no continuous endpoint guarantee or evidence for extra dimensions. The declared MeV and TeV total-stress benchmarks predict coefficients far below this distance sensitivity. Early-universe, perturbation and local-gravity tests remain separate.

14.4 A measurement of the inverse requires its own forward model

The first observational task is to connect measured quantities to the information assumed by the inverse. Distances are not an exact table of H^2, and BAO measurements do not supply a continuous dark-fluid $d\,p/d\,\rho$. Their acoustic scale involves the baryon–photon history. Extracting the dark-fluid sound information would require a perturbation model that specifies matter content, entropy and anisotropic stresses, its gravitational coupling, and the relevant bulk boundary conditions. The same model must propagate calibration and covariance into the sound windows and expansion coordinates. [15; 3; 4]

A concrete test can then be defined. With independently supplied exact sound and more than four suitable expansion epochs, let A be the four-column design and C the known Gaussian expansion covariance. In the unrestricted coefficient model,

$$T = \min_{\beta} (y - A\beta)^T C^{-1} (y - A\beta) \sim \chi^2_{N - \operatorname{rank} A}. \tag{14.3}$$

This checks the quadratic-plus-dark-radiation representation. Estimated sound, frequency selection, unknown covariance and

physical-boundary fitting change the calibration; the procedures in the statistical chapters address particular versions of those problems. Rejecting the representation does not uniquely diagnose an extra dimension. Accepting it does not exclude a sufficiently flexible four-dimensional effective stress model. [27; 6; 3]

Absolute matter information gives a complementary test. Two calibrated density differences must select the same transport normalization, and calibrated enthalpy divided by Q must be constant. The vacuum convention and stress units must be explicit. Their uncertainties belong in the joint set, not in independent substitutions of central values. This would make the proposed reconstruction an observation-level inverse with stated alternatives; the supplied research does not yet contain that combined cosmological experiment.

14.5 Two physically concrete routes beyond the present model

One route is a local gravitational matching calculation for a fully normalized scalar sector. The action, its matter standards and a background solution define the problem. A localized source then determines the induced metric response on the brane, including the scalar and bulk contributions under declared boundary conditions. The resulting force and clock observables establish when the cosmological coefficient g_{bg} agrees with locally measured $8\pi G_N$. This calculation would test the operational calibration used in the hierarchy estimates and identify the parameter combinations actually fixed by local gravity. Its result cannot be assumed for every rolling-scalar background merely because the background Friedmann equation has a familiar linear term. [4]

A second route is an early high-density model. For a radiation benchmark,

$$T(\epsilon)=\left(\frac{60\,\epsilon\,\tau_{vac}}{\pi^{2}\,g_{¿}}\right)^{1/4}. \tag{14.4}$$

At the TeV tension benchmark and fixed $g_{¿}=106.75$, ratios 0.1 and 1 occur near 274.7 and 488.5 GeV. These temperatures locate a regime where the quadratic term is no longer negligible. They do not predict a spectrum. Bulk-graviton production and energy transfer can invalidate the vacuum-bulk and no-exchange assumptions, requiring an enlarged background and perturbation system. A nuclear-reaction or CMB calculation would then use that system, rather than importing the constant-tension inverse unchanged. [4]

Varying the tension also changes the conservation problem. In the limited scalar action where $U(\phi)$ and $\lambda_{bare}(\phi)$ enter only through their sum, renaming part of the potential adds no new degree of freedom. If matter excludes the variable tension, vacuum-bulk conservation reads

$$\dot{\rho}_{m}+3H(\rho_{m}+p_{m})=-\dot{\lambda}_{bare}. \tag{14.5}$$

Imposing separate conservation of the same matter while varying that tension would contradict this equation unless additional transfer terms are included. A viable extension needs dynamics and observable couplings that distinguish its ingredients. [4]

The reserved-epoch construction in Section 5.5 and the test register below sharpen the next experimental question. A useful new datum must test an overdetermined representation or constrain an otherwise free normalization, with its covariance and physical conversion supplied. Increasing

numerical precision alone cannot distinguish parameter labels that produce the same complete action.

14.6 A register of testable claims

Each entry states the premise before the target and separates an algebraic calculation from a cosmological measurement. A test is complete only when the measured quantity, forward model, covariance and decision rule are specified. The same observation must not be counted twice merely because a model links two derived quantities.

T1. $c_\phi^2 = 1/5$

Premise and prediction. $F(X) = X^3/M^8$, positive X, a homogeneous shift-symmetric scalar and the stated background/perturbation conventions. $F_X/(F_X + 2XF_{XX})$ = 1/5. The propagation speed is c/√5, not 0.2c.

Measurement and decision. First close the coupled scalar–brane–bulk perturbation problem; then predict scale- and redshift-dependent clustering or lensing observables for this component, including its abundance and its covariances with other matter. Compare the fixed cubic model with a declared kinetic alternative using a calibrated likelihood. A mismatch rejects the combined cubic realization and its auxiliary assumptions; it does not independently falsify the five-dimensional background law.

Present status. The algebra and kinetic signs are checked. No observed dark-fluid sound measurement is supplied. The X = 0 quadratic kinetic operator vanishes, so the finite positive-X sound-speed ratio is not evidence for a regular vacuum propagator. §§11.1–11.4; [32–35]

T2. $\rho_{exc} \propto a^{-18/5} = a^{-3.6}$

Premise and prediction. The same cubic positive-X model and a conserved shift current $a^3 F_X \dot{\phi}$. A constant vacuum contribution is kept separate. $X \propto a^{-6/5}$ and $\rho_{exc} = 5X^3/M^8 \propto a^{-18/5}$. The exponent follows from $\chi = 1/5$ and conservation.

Measurement and decision. Build a common multi-component background and perturbation likelihood with an explicitly normalized excitation density. Fit that component across redshift, rather than labeling the total cosmic density or a generic reconstructed H(z) with this exponent. Test the joint sound-and-density relation against a specified broader kinetic family. Count the linked restrictions consistently; $c\varphi^2$ and the density exponent are consequences of the same power law and are not independent empirical discoveries.

Present status. Analytic and equation-of-motion checks are available. The canonical repair changes the exact relation to $c_\phi^2 = (1+3x^2)/(1+15x^2)$, $x = X/M^4$. A cubic-dominated approximation needs its own range of validity. §§11.1, 11.4–11.6

T3. 274.7 and 488.5 GeV

Premise and prediction. $\tau^{1/4} = 1$ TeV for total vacuum stress, $\rho_r = (\pi^2/30) g_¿ T^4$, fixed $g^* = 106.75$, and $\varepsilon = \rho r/(2\tau)$. The chosen levels are $\varepsilon = 0.1$ and $\varepsilon = 1$. $T_\epsilon = \left[60\,\epsilon\,\tau/(\pi^2 g_¿)\right]^{1/4}$, giving approximately 274.7 and 488.5 GeV. Changes in τ or g* change these temperatures.

Measurement and decision. Specify g*(T), the thermal history, brane–bulk energy transfer and perturbation boundary conditions. Compute the corresponding abundance, acoustic or particle-production observable before comparing with an appropriate dataset. Use the predicted observable and a

declared likelihood to test a normalized high-density model. A benchmark temperature by itself has no detection or exclusion threshold.

Present status. The scale conversion is executed; an early-universe likelihood and a spectrum at these temperatures are not. $\tau^{1/4}$, M_5 and the kinetic scale M are different parameters. §§12.3, 14.5; Appendix D; [38; 50]

T4. Observed Ω_q distance profile

Premise and prediction. $E^2(z) = 1 + \Omega_m(x^3 - 1) + \Omega_q(x^6 - 1) + \Omega_{dr}(x^4 - 1)$, $x = 1 + z$; the stated flat dust specialization, physical branch and search domain; 13 BAO entries and 1590 correlated light-curve rows; profiled BAO scale and SN intercept. The best fit in the tested nonnegative branch is $\Omega_q = 0$. The original joint crossings are 0.0002534 at $\Delta\chi^2 = 2.7055$ and 0.0003346 at $\Delta\chi^2 = 3.8415$. Ω_q is a constant coefficient; its contribution to E^2 varies with redshift.

Measurement and decision. Reproduce the archived profiles and use each calibration for its specified purpose. Chapter 16 executes positive-signal injections, nuisance-grid maximization and discrete inversion with the same deterministic fitting procedure. A continuous confidence statement requires additional control between grid points and over its nuisance and selection domain. Competing physical models require their own forward observables and consistent early-universe and normalization assumptions.

Present status. The distance likelihood, numerical audit and original 10,000-draw null calibration are executed. Chapter 16 adds 43,128 production simulated fits under a frozen finite-grid procedure. The same observations, covariance and fixed dark-radiation assumption are retained. This is not the cubic sound

example and does not identify bulk geometry from measured sound. Sections 13.7–13.15 and Chapter 16; [43; 46–48; 56–57; 59–62]

T5. The invariant L and common four-column representation

Premise and prediction. A measured common sound history and expansion model, the homogeneous conserved-barotropic assumptions, positive enthalpy, declared curvature and reference scales, rank four, $\beta_2 > 0$ and $L > 0$ for the AdS interpretation. $L = \beta_1^2 / (4\beta_2) - \beta_0$ and d are constant along the free-vacuum orbit. The corresponding quantities are $\ell = (SL)^{-1/2}$ and $\mu_B = a_c^4 S d$.

Measurement and decision. Use a joint forward model to infer sound and expansion with their covariance. Fit the common representation across well-conditioned, overlapping intervals, or predict reserved epochs after fitting the coefficients. Compare the resulting invariant estimates in the common reference convention. For independently supplied exact sound, known Gaussian expansion covariance and unrestricted coefficients, the residual quadratic form has χ^2 with N − rank(A) degrees of freedom. Estimated sound, selected windows, fitted covariance or physical boundaries require recalibration. Test goodness of fit and precision; agreement of an underdetermined four-point interpolation alone is not a consistency test.

Present status. The invariant is proved under the model; current distance catalogues do not supply the sound input. A fitted vertex outside the visited interval is a model-based extrapolation. Rejection concerns the combined representation and measurement assumptions, and acceptance does not

uniquely identify extra dimensions. Proposition 5.2 and Figure 5.1 make the reserved-epoch test and conditioning diagnostic explicit. Theorems 5.1 and 6.1–6.2; §§6.3, 14.4; [51; 54]

T6. Absolute normalization within the C-family

Premise and prediction. The same J and Q, independently calibrated matter stress or enthalpy in a declared physical convention, and a joint uncertainty model for the anchors and expansion. A calibrated density difference at distinct J values determines C through $\Delta v = C\,\Delta J$; enthalpy gives $C = 3(v+p)/Q$. Multiple anchors or windows must select one common C. One absolute density value alone can retain two branches.

Measurement and decision. Specify how an actual independent matter observable measures the relevant component and its absolute units; combine all anchors with the common transport and cosmological fit. Test whether a common C lies in the joint allowed set. If it does not, reject the combined matter calibration and transport model. Quote the surviving normalization set rather than choosing a central branch by hand.

Present status. The uniqueness and two-root statements are mathematical results; the proposed matter measurement is not supplied. Fixing this normalization does not distinguish the identical-action relabeling $\lambda \to \lambda + \Delta$, $U_0 \to U_0 - \Delta$. Proposition F.6 supplies the density-difference proof and finite-error bounds. §§6.4–6.5, 10.4–10.6, 14.4

A practical extension should preserve this sequence: specify the normalized action and alternatives; solve the relevant background and perturbations; map them to raw or validated compressed observables; declare the selection, nuisance and covariance treatment; calibrate the complete fitting procedure;

then report the parameter combinations and assumptions actually tested. This register is a plan for those measurements, not a claim that they have already been carried out.

14.7 Evidence, independent comparisons and scientific responsibility

The source calculations occupy several evidentiary levels: exact derivations, synthetic numerical checks, conditional analyses of observation summaries, and proposed applications. Counts of passed checks assess specified implementations; they are not counts of independent confirmations of a gravitational law. Reproducing a source table also differs from independently deriving its observation likelihood or comparing against new measurements. The book's provenance and computational records preserve these distinctions.

The retained analysis includes catalogue-level distance fitting with public covariance matrices and archived raw inputs. Its numerical record reports both the successful reference reproduction and the small unresolved Pantheon-summary difference. These results belong to the preserved background-distance analysis; they do not turn earlier synthetic studies into observed detections.

The separate clock–lensing–dynamics study uses a four-dimensional massive scalar–tensor action. Its finite-reference inverse and source-calibration issues illuminate the same general problem of identifying parameters from observables. Its scalar range, charges and physical metric are not the brane tension, dark-radiation coefficient or five-dimensional coupling. Its compressed-distance comparison tests a specified cosmological branch, not the bulk-identification theorem proved here. Keeping that study in a separate appendix makes

the common inferential lesson useful without asserting an undeveloped unification. [40; 3]

A complete account can establish a mathematical result and document its physical limitations while leaving future measurements open. Responsible authorship requires the derivations, references, numerical status and claim boundaries to remain inspectable. AI assistance supplies no independent peer review, and a coherent synthesis does not certify historical priority. The meaningful next advance would be a calibrated observation or a dynamically justified restriction that excludes members of the present equivalence class for a stated physical reason. That advance has a defined target: identifying what nature fixes after the mathematical freedoms, measurement errors and action conventions have been accounted for.

Third-edition continuation. The following chapters add completed proofs and computational studies to this earlier register. Their conclusions, implementation records and remaining physical questions are integrated in Chapter 19 and Section E.6.

15 Certificates for Finite Observations

A reconstruction becomes useful when another investigator can check why a proposed history is permitted, why a class of histories is excluded, and how far the remaining geometries can differ. A fitted curve alone answers none of these questions. This chapter develops finite, inspectable certificates for the transport problem and its geometric image. Each numerical example is a constructed experiment; the examples do not constitute additional astronomical observations.

The starting points are the shared-history requirements of Chapter 4, the sound-coordinate inverse of Chapter 5, the invariant of Chapter 6, the simultaneous outer sets of Chapter 9, and the completion and error results of Appendix F. The additions here are a quantitative treatment of a fixed Lipschitz class, a sharper normalization bound, an exact way to retain coefficient correlations, and explicit upper and lower bounds on geometric recovery. The statements are proved under their declared hypotheses. Their inclusion is not a claim of priority over all work on inverse problems or validated numerics.

15.1 The object being certified

Translate the left endpoint to zero and write $I=[0,T]$. Fix a sound margin $0<m<1/2$ and a Lipschitz budget $M_{\chi}\geq 0$. A candidate sound belongs to the class $m\leq \chi\leq 1-m$ with $|\chi(s)-\chi(t)|\leq M_{\chi}|s-t|$. These are assumptions on one specified barotropic component. Neither a distance likelihood nor the baryon-photon sound horizon supplies these assumptions or measures this sound automatically.

$$Q_{\chi}(s)=\exp\left[-3s-3\int_{0}^{s}\chi(t)\,dt\right]$$
$$q(s)=C\,Q_{\chi}(s),C>0 \tag{15.1}$$
$$v(s)=v_{0}-C\int_{0}^{s}Q_{\chi}(t)\,dt$$

The finite inputs considered first are calibrated density differences $D_{i}=v_{0}-v(s_{i})$, intervals for sound values at specified epochs, and intervals for finitely many sound means. A mean may use a nonnegative weight on an arbitrary window, normalized to have integral one. Overlapping windows remain constraints on the same function. A supplied positive compact interval bounds C; the candidate terminal density must remain positive. These hypotheses define a useful restricted problem rather than the most general observation model in the book.

In a fixed-background search, uncertain residual samples can first be transformed to density intervals using the monotone map f_{η} in Equation F.14, separately for each retained value or box of the background parameters. Unknown calibration gains, curvature coefficients, and physical-domain constraints must be carried with those same candidates. The program accompanying this chapter executes the calibrated-density problem just stated. It does not advertise a solution of the entire joint cosmological inverse.

15.2 A finite mesh enclosing one sound path

Let $0=s_{0}<\cdots<s_{N}=T$, with $h_{j}=s_{j+1}-s_{j}$, contain all point anchors. Suppose the nodal values of a candidate belong to a box. Its midpoint values are $\acute{c}_{j}$ and its largest half-width is ρ. Let $\acute{\chi}$ be the piecewise linear interpolant of the midpoint values. The midpoint need not satisfy the Lipschitz budget to serve as an

outer reference; it must satisfy that budget before it can serve as a witness.

Theorem 15.1 — Finite-mesh transport enclosure. Every sound in the declared Lipschitz class whose node values lie in the box satisfies

$$\left|\log \frac{Q_{\chi}(s)}{Q_{\acute{\chi}}(s)}\right| \le r_N(s \in I)$$
$$r_N = 3\rho T + \frac{3M_{\chi}}{4}\sum_{j=0}^{N-1} h_j^2 \tag{15.2}$$

Its pointwise distance from the midpoint interpolant is at most $\rho + M_{\chi} h_{max}/2$. Consequently every normalized nonnegative weighted sound mean differs from the corresponding midpoint mean by at most that quantity. The transport bound is uniform and requires no differentiation of an observed expansion history.

Proof. First interpolate the actual node values, calling the resulting function χ_h. On a cell of length h, with endpoint values a, b, the Lipschitz property bounds the true sound between the two endpoint cones:

$$\begin{aligned} &max\{a - M_{\chi} t, b - M_{\chi}(h - t)\} \\ &\qquad \le \chi(t) \le \\ &min\{a + M_{\chi} t, b + M_{\chi}(h - t)\} \end{aligned} \tag{15.3}$$

The upper cone envelope lies above the line joining a to b; the lower envelope lies below it. For $M_{\chi} > 0$, either enclosed triangular area equals $M_{\chi} h^2/4 - (b-a)^2/(4M_{\chi})$, which is nonnegative and at most $M_{\chi} h^2/4$. On any prefix of the cell, the signed integral of $\chi - \chi_h$ is bounded in absolute value by the

complete triangular area. Summing complete cells and the final partial cell therefore gives

$$\begin{aligned} &¿_{s\in I}\left|\int_{0}^{s}\left(\chi-\chi_{h}\right)dt\right| \\ &\leq\frac{M_{\chi}}{4}\sum_{j}h_{j}^{2} \end{aligned} \tag{15.4}$$

Linear interpolation preserves the maximum nodal error, so $\left|\chi_{h}-\acute{\chi}\right|\leq\rho$. Its integrated contribution is at most ρT. Multiplication by three in the exponent of Equation 15.1 proves Equation 15.2. Each triangular height is at most $M_{\chi}h/2$, proving the pointwise claim. Integration against a normalized nonnegative weight proves the mean claim. When $M_{\chi}=0$, every admissible path is constant and the interpolation error vanishes. This also proves that limiting case.

For an equal mesh, the second term in r_{N} is $3M_{\chi}Th_{max}/4$. It shrinks with the numerical mesh, but the first term does not shrink unless the nodal box narrows. Adding computational nodes is not equivalent to obtaining new measurements at those nodes: their allowed values must be inherited from the original observations and the Lipschitz constraints. This distinction prevents a mesh refinement from manufacturing information.

15.3 Normalization without losing the useful bound

The rate normalization C disappears from a ratio of cumulative density drops. Let $\acute{F}(s)$ be the normalized integral of the midpoint transport, and let $F_{\chi}(s)$ be the corresponding quantity for the actual sound:

$$\acute{F}(s)=\frac{\int_0^s Q_{\acute{\chi}}(t)\,dt}{\int_0^T Q_{\acute{\chi}}(t)\,dt} \qquad F_{\chi}(s)=\frac{v_0-v(s)}{v_0-v(T)} \tag{15.5}$$

Proposition 15.2 — Sharp normalized transport enclosure. If $\left|\log\left(Q_{\chi}/Q_{\acute{\chi}}\right)\right|\le r$, then, for $x=\acute{F}(s)$,

$$\frac{x}{x+e^{2r}(1-x)}\le F_{\chi}(s) \qquad F_{\chi}(s)\le\frac{e^{2r}x}{1-x+e^{2r}x} \tag{15.6}$$

$$\underset{s\in I}{¿}\left|F_{\chi}(s)-\acute{F}(s)\right|\le\tanh(r/2) \tag{15.7}$$

Proof. Regard normalized $Q_{\acute{\chi}}$ as a probability weight. The interval $[0,s]$ has mass x. Reweighting it by a factor between e^{-r} and e^{r} makes its new mass smallest by assigning the lower factor inside and the upper factor outside; reversing those choices makes it largest. This gives Equation 15.6. Maximizing the difference between either endpoint and x over $0\le x\le 1$ gives $\left(e^{r}-1\right)/\left(e^{r}+1\right)=\tanh(r/2)$. The endpoint choices attain the bound in the unrestricted multiplicative-envelope class. They need not belong to the narrower Lipschitz class.

Equation F.21 used the simpler bound $e^{2r}-1$. Equation 15.7 remains below one and is asymptotic to $r/2$ for small r. The pointwise interval in Equation 15.6 is often tighter still, especially when most of the cumulative drop has occurred

before the chosen epoch. Keeping the denominator and numerator linked is responsible for this improvement.

With positive measured drop intervals $D_i \in ¿$ and $D_T \in ¿$, every common history must also put its normalized drop in ¿. Disjointness from Equation 15.6 excludes the entire nodal box, regardless of which common C it uses. Overlap is only a necessary condition. Several overlapping interval projections can still correspond to different paths.

15.4 An executable witness-or-exclusion procedure

Theorem 15.3 — Soundness of finite box certificates. Cover every nodal vector allowed by the finite sound data with finitely many closed boxes contained in $\left[m, 1-m\right]^{N+1}$. For each box, use outward numerical enclosures of Equations 15.2 and 15.6 and of the midpoint window integrals. Discard a box only when one required observation interval is disjoint from a necessary outer enclosure, or when a necessary nodal Lipschitz inequality fails. If every covering box is discarded, no history in the declared class satisfies all the inputs. If one interpolant passes the range, Lipschitz, window, density, normalization and terminal-positivity checks, it is a common-history witness.

Proof. A true history has one nodal vector in the initial cover. Its box passes every necessary test by Theorem 15.1 and Proposition 15.2. Bisection replaces a box by two children whose union contains it, so this retention property survives any finite sequence of subdivisions. A discarded cover therefore cannot contain a true nodal vector. Conversely, an accepted piecewise linear sound is a single explicitly defined function. Equation 15.1 constructs its positive rate and density, and the checked intervals contain all their required measurements. Define the pressure by $p = -v + q/3$ along the path. Strictly

decreasing v permits inversion on the visited density interval. Differentiation gives $d\,p/d\,v=\chi$ for the resulting barotropic pressure law, which meets the declared conditions.

The returned states are deliberately different. A witness proves existence for the tested inputs. Exclusion proves absence within the stated class and covering domain. An unresolved box proves neither. The implementation can bisect retained boxes, but it has no asserted bound on the number of subdivisions needed, and the example runs use one initial box. Boundary equalities and persistent observational uncertainty can keep a calculation unresolved. Smooth completion from Appendix F does not justify silently increasing the fixed Lipschitz budget; the reported witnesses already satisfy that budget directly.

The numerical certificate uses 70-digit decimal interval arithmetic. Addition, multiplication and division are rounded outward. Decimal exponential and square root evaluations are widened after the correctly rounded operation. Transport integrals use composite Simpson quadrature on each affine-sound cell, including an analytic remainder. Within such a cell put $r_q=3(1+\chi)$ and $b_q=3\chi'$. Then

$$\begin{aligned} Q^{(4)}&=\left(r_q^4-6r_q^2b_q+3b_q^2\right)Q\\ \left|Q^{(4)}\right|&\le 1296+216\left|b_q\right|+3b_q^2 \end{aligned} \tag{15.8}$$

Here $0\le\chi\le1$, $0<Q\le1$, and the normalization is $Q(0)=1$. For a cell segment of length a and an even number n of equal Simpson subintervals, the absolute remainder is at most $a(a/n)^4\max\left|Q^{(4)}\right|/180$. Integrating separately across sound-slope changes is essential. These analytic error allowances, rather than agreement between two ordinary floating-point runs, support the numerical inclusion decisions.

15.5 A finite experiment with genuinely shared constraints

Consider $I=[0,1]$, $m=0.1$, $M_{\chi}=0.3$, $v_0=2$, and $0.9\le C\le 1.1$. At the seventeen epochs $j/16$, each sound interval has center $0.25+0.2\,j/16$ and half-width 0.002. Two uniform mean intervals use the overlapping windows $[0,1/2]$ and $[1/4,3/4]$. A third uses the normalized weight $w(s)=2s$ on $[0,1]$. Each mean interval has half-width 0.002 about its value for the same reference path.

$$\begin{aligned}\chi_{¿}(s)&=0.25+0.2\,s\\ Q_{¿}(s)&=e^{-3.75\,s-0.3\,s^{2}}\end{aligned}\tag{15.9}$$

For $C=1$, outward quadrature gives cumulative drops approximately 0.222538041 at $s=1/2$ and 0.252614026 at $s=1$. Intervals of half-width 0.0002 around those rounded values have a verified joint witness. To construct a conflicting experiment, multiply the first central drop by 1.006 and the terminal central drop by 0.994, retaining nine decimal places. The new centers are 0.223873269 and 0.251098342.

Each changed density datum, considered separately with every sound constraint, admits a witness: the common sound can remain the reference path while its normalization changes. The pair of changed density data asks for two incompatible normalizations. This claim is checked without inferring infeasibility from an optimizer failure. The sound box has $r_N=0.0200625$, and all admissible normalized half-epoch drops lie in the outward interval $[0.876667,0.885086]$. At density half-width 0.0002, the measured ratio lies in $[0.890070,0.893084]$. Their positive separation excludes the entire common-path class.

Table 15.1. Effect of the declared density error on the conflicting finite experiment. The sound data and Lipschitz budget stay fixed. An unresolved result is a property of the executed certificate, not a proof of feasibility.

Drop half-width	Result	Reason
0.00001	Excluded	Disjoint ratio enclosures
0.0002	Excluded	Disjoint ratio enclosures
0.0005	Excluded	Disjoint ratio enclosures
0.001	Unresolved	Outer overlap; no accepted witness
0.002	Witness	One path and one normalization pass

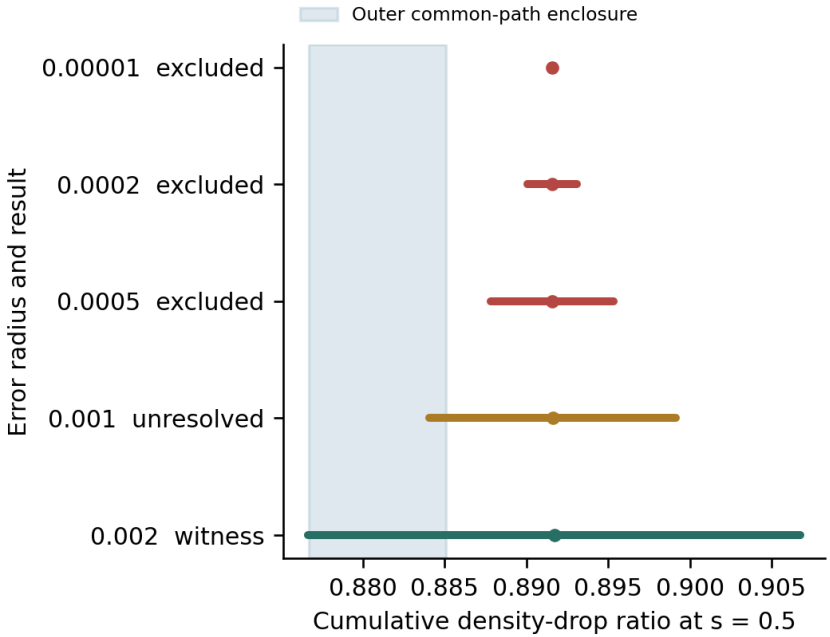

Figure 15.1. Constructed finite-observation experiment. The shaded band contains the normalized density-drop ratios permitted by every sound in the declared box and Lipschitz class. Horizontal intervals come from the two conflicting density observations. The widest interval admits a directly verified common-path witness; the intermediate overlap remains unresolved by the executed one-box calculation.

Wider observational intervals can erase a previously certifiable inconsistency. They do not make the original narrow-interval contradiction disappear; they define a different information set. The example also shows why a collection of successful marginal fits is insufficient. A joint test must retain one normalization and one path throughout the calculation. No probability such as 95% is attached to these deterministic intervals unless a separate observation model establishes their simultaneous coverage.

15.6 Correlated finite-error bounds for the invariant

Proposition F.7 exactly projects a rectangular coefficient region. A rectangle can nevertheless discard the directions along which an experiment is informative. Retain instead a nonempty compact convex polytope K, given by its complete vertex set, in the coefficient variables. Require $\beta_2 \geq a > 0$ throughout it; β_0 may have either sign. The invariant remains

$$L(\beta) = \frac{\beta_1^2}{4\beta_2} - \beta_0 \tag{15.10}$$

Theorem 15.4 — Correlated polytope certificates. The maximum of L on K is attained at a vertex. Its minimum is the optimum of the convex epigraph problem

$$\min_{\beta \in K,\, t \in R} t \qquad \begin{pmatrix} \beta_0 + t & \beta_1/2 \\ \beta_1/2 & \beta_2 \end{pmatrix} \succcurlyeq 0 \tag{15.11}$$

For any supplied real z, a lower certificate needing only affine optimization is

$$\min_{\beta \in K} L(\beta) \geq \min_{\beta \in K} \{ z\beta_1 - z^2\beta_2 - \beta_0 \} \tag{15.12}$$

If a point of K attains that lower certificate, it is a globally minimizing point. A floating-point epigraph solver by itself does not establish a rigorous lower bound; an outward or exact affine/dual certificate, and the feasibility of the attaining point, must be checked.

Proof. Completing the square gives the identity

$$L(\beta) = \sup_{z \in R} \{ z\beta_1 - z^2\beta_2 - \beta_0 \} \tag{15.13}$$

Thus L is a supremum of affine functions of the coefficients and is convex. Every point in K is a convex combination of its vertices, so its value cannot exceed the largest vertex value. Positivity of β_2 makes the two-by-two positive-semidefinite condition equivalent, by its Schur complement, to $t \geq L(\beta)$. This proves the epigraph statement. Fixing one z in the supremum proves Equation 15.12, and an attaining feasible point proves equality. All statements are valid for lower-dimensional polytopes as well.

A rational example illustrates the improvement using the reference coefficients of Equation 6.16. Define the complete correlated region by

$$\begin{gathered} \beta_2 = 0.27, d = 10^{-4} \\ \beta_1 = 3.216 + t, |t| \leq 0.02 \\ \beta_0 = 9.5632 + \frac{268}{45} t + u \\ |u| \leq 0.001 \end{gathered} \tag{15.14}$$

The four sign choices for t and u are its vertices. Substitution, performed with exact rational arithmetic in the companion, gives

$$L=\frac{1}{75}+\frac{t^2}{1.08}-u$$
$$\min_K L=\frac{37}{3000},\max_K L=\frac{397}{27000} \tag{15.15}$$

The supporting value $z=268/45$ makes Equation 15.12 equal to $1/75-u$. Its smallest value is attained at $t=0,u=0.001$, certifying the minimum. A vertex with $|t|=0.02,u=-0.001$ certifies the maximum. Both arguments are finite and exact; no numerical optimizer is used.

Table 15.2. Exact bounds from the same constructed coefficient region and its bounding rectangle. Decimal entries are descriptive roundings; the companion records exact fractions.

Region retained	Minimum L	Maximum L
Correlated polytope	0.0123333333	0.0147037037
Bounding rectangle	−0.2255185185	0.2529259259

The correlated set certifies a positive AdS invariant, whereas its bounding rectangle crosses zero. For a supplied exact $S>0$, the correlated certificate gives

$$\sqrt{\frac{27000}{397}}\le\sqrt{S}\,\ell$$
$$\sqrt{S}\,\ell\le\sqrt{\frac{3000}{37}} \tag{15.16}$$

The endpoints are approximately 8.24682 and 9.00450. This gain comes from retaining coefficient correlations, not from adding observations. The region is constructed and has no asserted confidence level. If a similarly constructed outer

polytope retained the full physical set on the simultaneous event of Theorem 9.1, its geometric image would retain that same event coverage. Whether an outer coefficient point has a common physical sound history remains a separate check.

15.7 Quantitative stability and its converse

The transport certificate can be connected directly to the sampled design. With the left-endpoint normalization used here, $J(s)=-\int_0^s Q(t)\,dt$. Put $\acute{J}$ for its midpoint-path value. Equation 15.2 gives an error enclosure without differentiating any measured quantity:

$$\begin{aligned} \left|J(s_i)-\acute{J}(s_i)\right| &\le R_i \\ R_i &= \left|\acute{J}(s_i)\right|\left(e^{r_N}-1\right) \end{aligned} \tag{15.17}$$

The intercept and $E=e^{-4s}$ columns do not change when only the sound changes. The two remaining columns have errors bounded by R_i and $2\left|\acute{J}(s_i)\right|R_i+R_i^2$. Therefore the following computable quantity is a valid matrix error bound:

$$\begin{aligned} B_i &= 2\left|\acute{J}(s_i)\right|R_i+R_i^2 \\ \delta_A^2 &= \sum_i \left(R_i^2+B_i^2\right) \end{aligned} \tag{15.18}$$

This uses the Frobenius norm to dominate the operator norm. It intentionally allows more matrices than one physical sound can generate; it therefore remains an outer bound. A sharper correlated matrix enclosure may reduce it. An uncertain curvature column or an uncertain conversion scale is a different source of error and must be included explicitly if present. These two equations connect finite sound anchors and a declared derivative budget to the stability hypotheses below.

A full-rank nominal design supports a finite deterministic diameter bound once its units and error norm are fixed. Write $\beta=(\beta_0,\beta_1,\beta_2,d)$. Suppose every admitted candidate satisfies

$$\begin{aligned}\hat{y}&=(A+\Delta A)\beta+e\\ \|e\|_2&\le\varepsilon,\|\Delta A\|_2\le\delta_A\\ \|\beta\|_2&\le M,\sigma_{min}(A)\ge\sigma>0\end{aligned}\tag{15.19}$$

Different candidates may use different admissible sound histories and hence different ΔA. The norms refer to the declared column and observation scaling. A numerical singular value must be enclosed or otherwise lower-bounded if σ is to be used as a rigorous certificate.

Proposition 15.5 — Finite geometric diameter. If the coefficient region also has $\beta_2\ge a>0$ and $|\beta_1|\le B$, any two candidates satisfy

$$\begin{aligned}\|\beta-\tilde{\beta}\|_2&\le\frac{2(\varepsilon+\delta_A M)}{\sigma}\\ |L(\beta)-L(\tilde{\beta})|&\\ &\le\frac{2G(\varepsilon+\delta_A M)}{\sigma}\end{aligned}\tag{15.20}$$

$$G=\sqrt{1+\frac{B^2}{4a^2}+\frac{B^4}{16a^4}}\tag{15.21}$$

If all the candidates additionally have $L\ge l>0$, their AdS radii differ by at most their L-diameter divided by $2\sqrt{S}\,l^{3/2}$. If $\delta_A<\sigma$, one may obtain a valid coefficient norm bound directly from the data:

$$M=\frac{\|\hat{y}\|_2+\varepsilon}{\sigma-\delta_A}\tag{15.22}$$

Proof. The two nominal residuals $A\beta-\hat{y}$ and $A\widetilde{\beta}-\hat{y}$ each have norm at most $\varepsilon+\delta_A M$. Subtraction and the lower singular-value bound prove the first inequality. The gradient of L is $\left(-1,\beta_1/(2\beta_2),-\beta_1^2/(4\beta_2^2),0\right)$, whose norm on the segment joining the candidates is at most G. The segment preserves $\beta_2\ge a$ and $|\beta_1|\le B$, so integration of this derivative proves the second inequality. The radius bound follows by differentiating $(SL)^{-1/2}$ on $L\ge l$. Finally, every $A+\Delta A$ has lower singular value at least $\sigma-\delta_A$, proving Equation 15.22.

This is an explicit finite-error continuation of the rank statement in Section 9.6. A positive rank margin alone does not give one coefficient vector for all uncertain sounds. Equation 15.20 bounds how different those vectors and their invariants may be. The bound can be conservative; the correlated optimization of Section 15.6 can exploit information that the three scalar quantities M,a,B discard.

A small observed residual also cannot establish that a much narrower error bar is achievable. The following converse uses two complete candidate models instead of a first-order condition number.

Theorem 15.6 — Two-model indistinguishability bound. In the exact-design experiment $y=A\beta+e$, with $\|e\|_2\le\varepsilon$, suppose two physically admitted coefficients satisfy

$$\| A ¿ \tag{15.23}$$

There is one observed vector compatible with both. For any estimator of L evaluated at that vector, at least one of the two models has absolute estimation error at least

$$\frac{1}{2} ¿ \tag{15.24}$$

Proof. Choose the observed vector halfway between $A\beta^{+¿¿}$ and $A\beta^{-}$. Its two error vectors have norm at most ε. A single reported number cannot lie at distance less than half the separation from both invariant values, by the triangle inequality. The claim requires no distributional assumption. It is a worst-case deterministic statement, not a posterior interval or a frequentist power calculation.

The executed pairs use the six epochs $0, 0.2, \dots, 1$, the unscaled four-column design, and a known constant sound $\chi = 1/3 - \delta$. The reference coefficient vector is $(9.5632, 3.216, 0.27, 0.001)$. A numerical singular vector proposes two nearby coefficient vectors; their printed decimal coordinates are then treated as exact rational inputs. Interval forward evaluation verifies Equation 15.23 independently of the singular-value estimate. The code also verifies $L > 0$, $d > 0$, positive density and expansion, positive vacuum amplitude at $C = 0.2$, and the planar exterior condition $d < L$ on $[0, 1]$.

Table 15.3. Verified indistinguishable model pairs. The expansion-noise radius is an unweighted Euclidean bound on six dimensionless values. Entries summarize full outward and rational checks stored in the companion.

Sound offset δ	Sufficient noise radius	Minimum worst-case L error
0.1	9.23254×10^{-7}	0.00624262
0.01	1.08295×10^{-7}	0.00400781
0.001	1.09455×10^{-8}	0.00524048
0.0001	1.09564×10^{-9}	0.00536535
0.00001	1.09575×10^{-10}	0.00537785

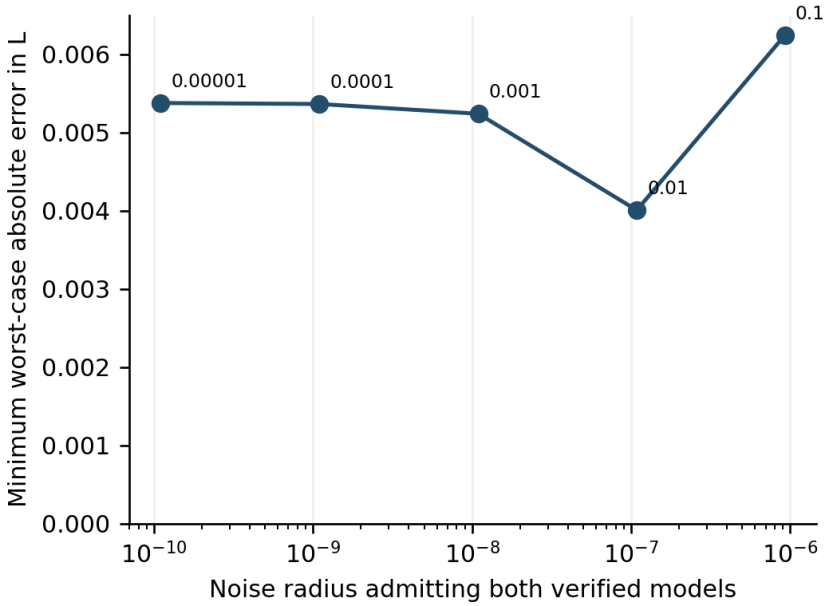

Figure 15.2. Constructed two-model lower bounds near the constant-sound exception. Each label gives the offset below sound one third. The horizontal coordinate is a noise radius sufficient to admit both interval-verified models; the vertical coordinate is half their exact invariant separation. Singular vectors only propose the pairs. The verified forward differences, rather than floating-point singular values, establish the plotted indistinguishability statements.

In the last pair, an expansion-noise radius below 1.1×10^{-10} still permits invariant values approximately 0.00795630 and 0.01871202. Exact rank has not failed at that nonzero sound offset, yet a uniformly accurate reconstruction is impossible at the stated noise level. At sound exactly one third, Theorem 5.1 already supplies an exact null direction. The present calculation quantifies how the obstruction persists in finite-error experiments near that boundary.

15.8 Reproduction and the remaining scope

The accompanying script math/reproduce_certificates.py generates the complete finite-observation inputs, interval

quadratures, witnesses, box exclusions, exact rational polytope certificates, and two-model forward checks. The JSON records retain more digits than the printed tables; the CSV files are intended for inspection and plotting. The figures can be regenerated without reading or changing the original astronomical input files. The authoring source and integration blocks are included alongside the calculations.

The executable enforces its arithmetic domain: input decimals, mesh preprocessing, exact box midpoints and quadrature grids must be representable without rounding at the configured precision. An inexact preprocessing operation returns an unresolved status without issuing a certificate. Only outward interval primitives and explicitly declared choices of a point inside an interval permit rounding. Window endpoints must lie in the domain, and affine weights must be nonnegative with positive integral. An additional standard-library verifier uses exact rational Taylor brackets to check both transport integrals and every two-model forward difference independently of Simpson quadrature and singular-value calculations.

These results strengthen three links in the argument. Finite sound and density constraints can now carry an explicit shared witness or a conservative exclusion. Correlated coefficient information can certify a positive AdS invariant when a rectangle cannot. A finite-error geometric recovery claim can be compared with both an upper bound and a concrete pair that obstructs a tighter guarantee. Each conclusion has a directly inspectable mathematical or computational certificate.

The outstanding physics remains substantial. The required sound information must be linked to an observable of the intended component; a selected perturbation problem must be completed before it supplies that link. The certificate does not

separate vacuum terms that occur only through their sum, choose a unique higher-dimensional origin among matching backgrounds, or turn a synthetic experiment into a detection. Those limits define where a further physical test is needed and where additional computation alone cannot supply the missing information.

16 Calibration Beyond the Zero Signal

A parameter limit needs a sampling experiment that matches the claim attached to it. Chapter 13 established a useful pointwise check: simulated data generated at one fitted zero-correction model reproduced the expected behaviour of a detection statistic. That experiment did not determine how often an upper procedure would retain a true positive correction. The distinction matters because the physical boundary, nuisance dependence and direction of rejection change the problem. This chapter supplies the missing positive-signal experiment for a precisely delimited version of the distance model.

The completed extension comprises 43,128 fully nonlinear simulated-data fits at 72 generating points, including separate calibration and validation draws. It also supplies a discrete test inversion on the historical observations and a complete numerical audit. The statistical machinery is established; the contribution here is its explicit implementation, verification and application to this book's specified branch. The result is a reproducible finite-grid calibration. It does not establish confidence coverage over a continuous cosmological parameter space, and it does not convert an inserted signal into an astronomical detection.

16.1 The experiment and its physical scope

Write $m=\Omega_m$ and $q=\Omega_q$. The branch is the dust-background model used in the main distance analysis, with dark radiation and the ordinary radiation ratio fixed at zero:

$$E^2(z)=1+m\left[(1+z)^3-1\right] +q\left[(1+z)^6-1\right]. \tag{16.1}$$

The numerical parameter region is $0.05 \le m \le 0.70$ and $0 \le q \le 0.05$, with positive effective vacuum and the original AdS-branch inequality. The generating grid lies well inside the additional physical restrictions. Every fit profiles the matter coefficient and both distance-calibration nuisances. The nonnegative correction is fitted under the alternative; it is held at the tested value under the restricted hypothesis. The dark-radiation parameter is never freed in this experiment.

The data vector retains the same 13 BAO observables and 1590 selected supernova light-curve rows as Chapter 13. Supernova rows are not reinterpreted as 1590 independent objects: their published covariance is retained. The Gaussian likelihood conditions on the full within-survey covariance matrices, their stated normalization, the existing data selection and the redshift conventions. Cross-survey covariance remains zero, exactly as in the baseline likelihood. Redshift errors, covariance-estimation error and non-Gaussian survey systematics are not newly simulated.

$$\begin{aligned} d_B^{¿} &= A\, f(m,q) + L_B \epsilon_B, \\ d_S^{¿} &= g(m,q) + M\,1 + L_S \epsilon_S, \\ \epsilon_B &\sim N(0, I_{13}), \epsilon_S \sim N(0, I_{1590}). \end{aligned} \tag{16.2}$$

Here $L_B L_B^T = C_B$ and $L_S L_S^T = C_S$ are the covariance factorizations. Independent whitened Gaussian coordinates therefore regenerate the original correlated error experiment. The BAO amplitude A is a nuisance parameter rather than an externally supplied sound-horizon calibration. The supernova intercept M absorbs an arbitrary common magnitude shift. Its analytic profiling makes the ideal statistic independent of that shift, so an additional grid in M is unnecessary. The stored generating

intercept is 23.8; no local-distance-ladder measurement is thereby introduced.

Equation (16.1) is not the cubic-field evolution of Chapter 12. A conserved dust density has an a^{-3} term and a quadratic a^{-6} correction. The cubic kinetic example instead has its own field density and sound evolution. Substituting the cubic example's interpretation for the dust coefficient would require a new mean function and a new calibration. The results in this chapter concern only the displayed background-distance experiment, including its freedom in A.

16.2 Upper exclusion and positive detection are different tests

Let $\chi^2_p(q;Y)$ denote the minimum at fixed q after profiling m, A, M in a data vector Y, and let $\chi^2_{min}(Y)$ be the minimum over the physical nonnegative branch. Define the constrained best-fitting correction $\hat{q}(Y) \geq 0$. These are fits to the nonlinear distance integrals, not to a tangent expansion:

$$\chi^2_p(q;Y) = \min_{m,A,M} \chi^2(m,q,A,M;Y),$$
$$\chi^2_{min}(Y) = \min_{q \geq 0} \chi^2_p(q;Y). \tag{16.3}$$

For upper exclusion, a fluctuation that favours a larger correction is not evidence that the tested correction is too large. We therefore use the bounded one-sided profile statistic of the standard likelihood construction [60]:

$$U_q(Y) = \begin{cases} \chi^2_p(q;Y) - \chi^2_{min}(Y), & \hat{q} \leq q, \\ 0, & \hat{q} > q. \end{cases} \tag{16.4}$$

A positive-detection statistic asks the opposite directional question: how much does allowing the correction improve the fit over the zero edge? It is

$$D(Y)=\chi^2_p(0;Y)-\chi^2_{min}(Y). \tag{16.5}$$

These definitions make U_0 identically zero, whereas D can be positive. Thus an upper construction always retains the physical zero value; that is not a claim of successful zero-signal detection. Discovery power is measured separately with D and with calibration banks generated at $q=0$. Using the same symbol or the same reference percentile for these two questions would obscure which error probability has been controlled.

The implementation uses the same deterministic global and zero-edge fits for every data vector, independently of the tested q. Restricted positive-q fits supply U_q but cannot change the discovery statistic. Additional multistarts belong to the separate numerical audit and are not selectively applied only to the observations. This detail ensures that a comparison of observed and simulated ranks uses a common numerical statistic, as required by the sampling argument.

16.3 A finite-grid rank construction

The nuisance grid contains nine pairs, formed from three matter values and three amplitudes. The central values come from the already examined second-edition fit. The eight correction values include the zero edge and seven positive signals. The grid is an explicit finite statistical model for this calculation; there is no certified interpolation between its points.

Table 16.1. Frozen simulation design; the historical fit was already known.

Item	Specification
q grid	$\{0, 10^{-4}, 2\times10^{-4}, 2.5\times10^{-4},$ $3\times10^{-4}, 4\times10^{-4}, 6\times10^{-4}, 10^{-3}\}$

Item	Specification
m grid	0.28; 0.3042142049; 0.33
A grid	28.5; 29.6786042519; 31.0
Generating cells	8 corrections × 9 nuisance pairs = 72
Calibration draws	399 per cell; 28,728 total
Fresh validation draws	200 per cell; 14,400 total
Completed inferential draws	43,128
Rank denominator	400; minimum p-value 0.0025
Rejection rule	$p_{max} \le 0.05$

At each candidate q and nuisance pair $\eta_j = (m_j, A_j)$, generate $B = 399$ independent calibration statistics. For any separate data vector, calculate the conservative rank p-value

$$p_j(q;Y) = \frac{1 + R_j(q;Y)}{B+1},$$
$$R_j(q;Y) = \sum_{b=1}^{B} 1\{U_q(Y_{jb}^{*}) \ge U_q(Y)\}. \tag{16.6}$$

The observed vector counts as one member of the exchangeable collection; the numerator and denominator therefore both contain the additional one. Counting all ties in the upper tail makes the test conservative. A tail with no simulated exceedance produces $1/400$, not zero [62]. The nuisance-protected p-value takes the maximum over the nine specified pairs:

$$p_{max}(q;Y) = \max_{1 \le j \le 9} p_j(q;Y). \tag{16.7}$$

Proposition 16.1 (Error control for the frozen grid). Suppose the covariance model is correct, the procedure and grid are fixed, and the true (q, m, A) is one of the 72 generating points. With independent calibration draws, rejection by $p_{max} \le 0.05$ has probability at most 0.05 jointly over a fresh data vector and the calibration randomness. This is the finite-grid application of the maximized Monte Carlo test principle [59].

Proof. At the true nuisance point, the test vector and its 399 calibration vectors are exchangeable. Their conservative upper rank is stochastically no smaller than the discrete uniform rank. Since 20 of 400 ranks are at most 0.05, the rejection probability for that point is at most 0.05. The maximum p-value is at least the p-value at the true point, so its rejection event is a subset of that event. Ties can only reduce rejection. This proves the stated bound.

$$P_{q,\eta_j}\{p_{max}(q;Y) \le \alpha\} \le \frac{\lfloor \alpha(B+1) \rfloor}{B+1} \le \alpha. \tag{16.8}$$

Inversion retains every grid correction whose upper hypothesis is not rejected:

$$C_G(Y) = ¿ \{q \in G_q : p_{max}(q;Y) > 0.05\}. \tag{16.9}$$

For the frozen finite model, this set covers the true grid correction with probability at least 0.95. No multiplicity correction over the eight tested corrections is needed for that single-parameter coverage statement: excluding the true value is precisely its own rejection event. This does not give simultaneous coverage for eight distinct scientific claims, nor permit choosing a favourable test after examining the ranks.

The set need not be an interval, and its largest retained point is not a calibrated endpoint for an underlying continuum.

16.4 What is conditional, and what was already selected

There are three different probability statements. First, Proposition 16.1 describes the fixed numerical grid and repeats both the data experiment and the Monte Carlo calibration. Second, the validation study keeps the realized calibration banks fixed and draws new data from each cell. It estimates the conditional coverage and detection probability of those particular banks. Third, the historical observations are processed after the grid has been chosen with knowledge of their earlier fit. The last calculation is retrospective; it is not a prospectively preregistered confidence statement.

The selection distinction is substantive. A confidence set constructed for a frozen grid cannot acquire an unconditional post-selection guarantee merely because that grid has now been written to a file. The observed-data table is therefore labelled a retrospective finite-grid acceptance calculation. The mathematical coverage bound describes fresh repeated data under the fixed procedure. An application seeking an unconditional historical cosmological confidence bound must also address how the nuisance set was selected, or establish a valid continuous nuisance treatment.

The validation experiment uses 200 independent fresh vectors per cell. Conditional on fixed banks, each cell's retained/not-retained decisions are independent Bernoulli outcomes. Their Clopper–Pearson intervals [61] describe Monte Carlo uncertainty in that cell's conditional probability. They do not quantify uncertainty in a cosmological parameter. Nor are the 72 intervals simultaneous: several cells share the same

calibration banks, and inspecting their extrema after simulation changes the interpretation of a selected worst cell.

A small minimum validation fraction does not contradict the rank theorem by itself. The theorem averages over calibration randomness, while a particular finite bank can yield a lower or higher conditional acceptance probability. Conversely, a collection of attractive validation fractions cannot prove a stronger continuous theorem. The exact claim rests on exchangeability and nuisance inclusion, and the numerical experiment checks its realized behaviour and implementation in the declared model.

16.5 Why the positive-signal critical value can change

A simple scalar experiment explains why calibrating the zero signal alone is insufficient. Let $X = q + \sigma Z$, with $Z \sim N(0,1)$, known σ, and the constrained fit $\hat{q} = max(0, X)$. This is an illustrative Gaussian model, not a substitute for the distance likelihood. Set $a = q/\sigma$. Direct substitution into the upper statistic gives

$$U_q = \begin{cases} 0, & Z > 0, \\ Z^2, & -a \le Z \le 0, \\ -a^2 - 2aZ, & Z < -a. \end{cases} \tag{16.10}$$

For $q > 0$, the 95th percentile is obtained by inserting the lower 5% normal quantile. If $z_{.95} = \Phi^{-1}(0.95)$, it is

$$c_{.95}(q) = \begin{cases} 2a z_{.95} - a^2, & 0 < a < z_{.95}, \\ z_{.95}^2, & a \ge z_{.95}. \end{cases} \tag{16.11}$$

At the exact zero edge the upper statistic is identically zero. For a small positive signal its critical value can be much smaller than 2.7055; only the more interior regime reaches that familiar

reference. The physical boundary changes the denominator of the likelihood ratio on downward fluctuations. This elementary derivation explains why a fixed threshold can be conservative for upper exclusion near zero without being a universal confidence prescription. It also explains how a calibrated upper procedure can reject a candidate that an uncalibrated fixed-reference crossing retained, while the data still show no preference for a positive signal.

The nonlinear calibration does not assume this scalar formula or infer its accuracy from a Fisher matrix. It estimates the actual cell distributions by refitting the distance integrals. Figure 16.1 shows the empirical 95th percentiles, including their variation across the nine nuisance points. These descriptive percentiles are not themselves the rank decision rule: the published decisions use the exact integer exceedance counts and the maximum p-value.

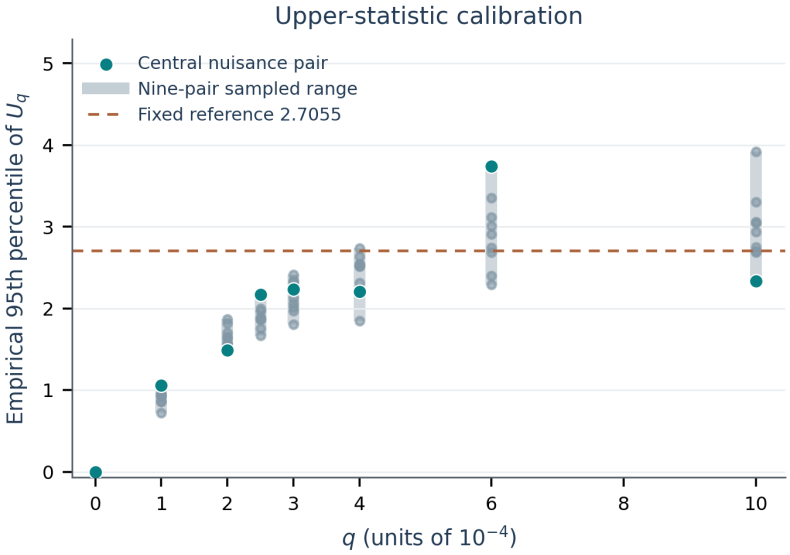

Figure 16.1. Positive-signal upper-statistic calibration. Points show empirical 95th percentiles from 399 nonlinear calibration draws at each of the 72 stated generating points. The central nuisance pair is highlighted; vertical ranges summarize only the nine sampled pairs at a given correction. The dashed 2.7055 line is a reference, not a fitted critical curve. The zero upper statistic at $q=0$ follows from its definition. No continuous-nuisance or inter-grid coverage is implied.

16.6 The retrospective inversion on unchanged observations

The historical data retain $\hat{q}=0$ and $D=0$ at the numerical precision of the likelihood. Their finite-grid detection p-value is 1, because every simulated detection statistic is at least zero. The new calculation therefore supplies no positive-correction evidence. It asks instead which specified positive corrections are incompatible in the upper direction under the frozen simulation procedure.

Table 16.2. Retrospective finite-grid acceptance on the historical data; not a prospectively selected continuous 95% confidence limit.

q tested	U_q observed	p_{max}	Grid decision
0	0.0000	1.0000	Retained
0.0001	0.9165	0.0725	Retained
0.0002	2.0301	0.0450	Rejected
0.00025	2.6611	0.0275	Rejected
0.0003	3.3417	0.0200	Rejected
0.0004	4.8520	0.0100	Rejected
0.0006	8.4710	0.0050	Rejected
0.001	18.1101	0.0025	Rejected

The retained grid values are 0, 0.0001. The rejected grid values are 0.0002, 0.00025, 0.0003, 0.0004, 0.0006, 0.001. All nine nuisance-specific ranks are preserved for every row, so the reported maximum can be checked without rerunning a likelihood fit. The resolution of each p-value is 0.0025. A value at the lower resolution limit cannot support a claim of an arbitrarily small tail probability; no extra digits of significance are supplied by the number of printed decimals.

No line is drawn between the retained and rejected grid points to announce a continuous upper endpoint. Such interpolation would require additional control of the statistic's distribution between correction values and over nuisance parameters omitted from the finite set. The older profile crossing near $q = 0.0002534$ remains a reference crossing in Chapter 13. This table reports a different, explicitly directional, simulation-calibrated construction. It cannot retroactively give that old crossing an unproved confidence interpretation.

The observed grid was centred using an earlier analysis of the same historical measurements. Its numerical acceptance decisions are fully reproducible, but they are not evidence of an untouched external prediction test. Their value is that the rule, model and limits are now explicit. A future application could freeze the rule before accessing a new data vector; alternatively, a valid nuisance confidence region with its own error allocation could replace the selected finite nuisance list. Neither additional step is claimed here.

16.7 Fresh-data coverage and power

Table 16.3. Fresh validation at the central nuisance pair. Each entry is a count out of 200 independent data vectors, conditional on the stored calibration banks.

q true	Grid retained	Zero rejected	Reference retained
0	200/200	5/200	200/200
0.0001	196/200	19/200	200/200
0.0002	190/200	26/200	198/200
0.00025	194/200	37/200	199/200
0.0003	195/200	39/200	197/200
0.0004	190/200	50/200	190/200
0.0006	196/200	98/200	193/200
0.001	194/200	177/200	189/200

“Grid retained” records whether the upper construction contains the true grid correction. “Zero rejected” records positive detection using the separate zero-signal calibration banks. “Reference retained” uses the fixed rule $U_q \le 2.705543454$ for comparison only. An accepted true correction and a rejected zero model can occur together

without inconsistency. They answer whether an upper procedure retains the generating correction and whether the same data provide evidence against the absence of a correction.

For example, at the central pair the conditional detection estimate at q= 0 is 0.025 [0.008, 0.057]; at q= 0.00025 it is 0.185 [0.134, 0.246]; and at q= 0.001 it is 0.885 [0.832, 0.926]. Brackets are pointwise 95% exact binomial Monte Carlo intervals. These probabilities are properties of simulated data under the stated model. They do not add observations to the original surveys or increase the evidence in the observed vector.

At q= 0.0001, central-pair upper retention is 0.980 [0.950, 0.995]. At q= 0.001 it is 0.970 [0.936, 0.989]. Across all 72 cells the empirical retention fractions range from 0.925 to 1.000. This range describes sampled cells and finite validation noise; it is neither a confidence band nor a certificate for unsampled nuisance values. Full cell counts and their conditional intervals are retained in the companion.

Figure 16.2 displays the separate detection-power experiment. Its error bars describe the central cell's 200 validation draws; the spread across the other nuisance points is shown independently. Reusing the same zero banks makes this a fixed-test power comparison. The threshold is not recalibrated at a positive signal so as to make detection easier. All 72 cells use the same zero-hypothesis rejection rule, and no cell is dropped because it has low power or an inconvenient conditional coverage fraction.

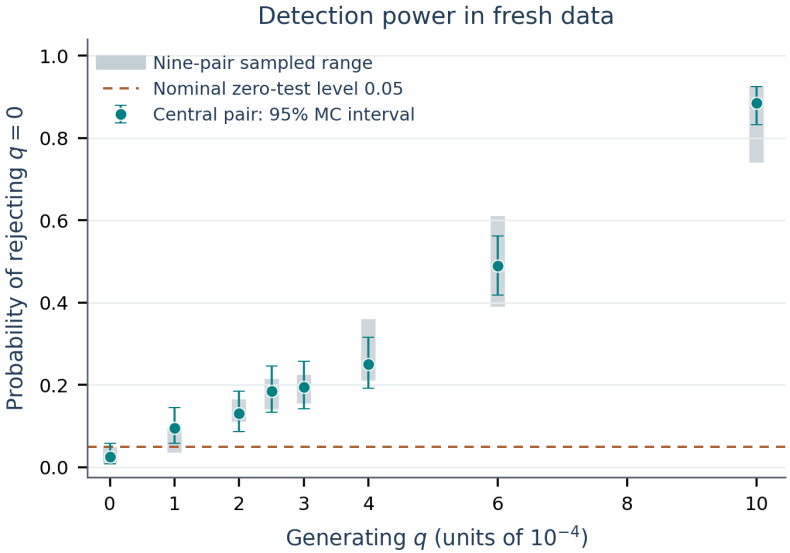

Figure 16.2. Conditional probability of rejecting the zero correction in fresh simulated data. Central markers and pointwise 95% Clopper–Pearson intervals use 200 validation draws per correction at the central nuisance pair; the pale vertical ranges show the extrema among the nine sampled nuisance pairs. The same stored zero-signal calibration banks and maximum-p rejection rule are used throughout. These are power estimates for the specified Gaussian distance experiment, not probabilities that the historical Universe has a positive correction.

The power calculation gives a more useful interpretation of an inserted number than a successful fit to its mean vector alone. It asks how often a noisy realization survives nuisance refitting and actually triggers the fixed decision rule. A signal with modest power can easily remain undetected; a high-power synthetic example can demonstrate sensitivity within this experiment without identifying the physical origin of the signal. The result remains conditional on the released covariance, background branch and nuisance values.

16.8 Nuisance control and a quantitative route beyond the grid

It is useful to distinguish two operations that are often both described as accounting for nuisance parameters. Profiling chooses the nuisance values that fit a particular data vector best. Calibration specifies the law that generated that vector and asks how often the resulting fitted statistic rejects. The first operation belongs to the definition of the statistic. The second concerns its distribution. They coincide only in special circumstances, and no distribution-free profiling theorem has been established for the present nonlinear distance problem.

The supernova intercept illustrates a nuisance that really can disappear. In whitened coordinates, let $u = L_S^{-1} 1$ and let $P_S = I - u\,u^T / \left(u^T u\right)$. Profiling the intercept replaces the supernova residual by its projection through P_S. A change $d_S \mapsto d_S + c\,1$ is annihilated by that projection. This conclusion holds for the complete nonlinear mean function, so it does not depend on approximating the correction by a small perturbation. A known linear group action has removed an entire continuous nuisance direction.

The BAO amplitude behaves differently. At fixed nonlinear parameters, its unconstrained least-squares solution is $\widehat{A} = f_w^T d_w / \left(f_w^T f_w\right)$, where $f_w = L_B^{-1} f$ and $d_w = L_B^{-1} d_B$. The realized fits all have positive amplitude. However, changing the generating A while holding the released covariance fixed changes the signal-to-noise ratio of shape variations. In particular the mean derivative with respect to q contains $A\,\partial_q f_w$. Refitting the amplitude therefore does not prove that the sampling law of the profiled correction statistic is

independent of its generating value. This is why three amplitude values, as well as three matter values, are simulated.

There is a mathematically explicit way to describe the gap between a tested nuisance point and an untested nearby one. It supplies a useful target for a future continuous calibration, although it is not used to alter the published decisions. Keep the tested correction fixed at a grid value and compare two Gaussian data laws with the same covariance C, means μ and μ_j, and the same supernova-intercept convention. Define their whitened mean separation by

$$r_j = \| C^{-1/2} (\mu - \mu_j) \|_2 . \tag{16.12}$$

The total-variation distance between these two Gaussian laws is exactly

$$\delta_j = 2\,\Phi(r_j/2) - 1 . \tag{16.13}$$

To see this, whiten the data and rotate the mean difference onto one coordinate. The likelihood comparison between the two simple Gaussian laws changes sign at the midpoint between their means. Integrating the probability difference over that half-space reduces the calculation to two one-dimensional normal tails; all orthogonal coordinates integrate to one. The resulting expression bounds the difference in probability of any measurable rejection event. The Monte Carlo banks can be included as an independent common auxiliary random variable, so the same bound applies to the randomized rank procedure.

Consequently, if one grid nuisance point is within whitened mean distance r_j of a continuous nuisance alternative, the frozen rule satisfies

$$P_{q,\eta}\{p_{max}(q;Y)\le 0.05\} \le min\{1,0.05+\delta_j\}. \tag{16.14}$$

This bound states exactly what a finite neighborhood can cost in error control. It does not preserve 95% coverage automatically. For example, a separation of 0.1 gives $\delta_j \simeq 0.0399$, leaving only a 91.0% lower coverage bound from this general transfer argument. That calculation is an analytic illustration, not a measured property of the present nuisance rectangle. A procedure targeting 95% throughout certified neighborhoods could reserve an error budget: a 4% grid test together with a verified variation bound of 1% is one possible allocation. The completed experiment in this chapter instead uses the predeclared 5% grid rule.

To turn this observation into a continuous result, one must bound the mean separation throughout the proposed nuisance region, not merely evaluate a few additional points. Adaptive subdivisions, derivative bounds or another rigorous enclosure could do that work. The present grids are too sparsely described to supply such a certificate without further analysis, and no certified maximum separation over the full box is reported. Nor does this fixed-q argument fill the gaps between tested corrections. The value of the bound is to identify a precise quantity that a continuous extension would have to control, and to make the possible coverage loss explicit instead of hiding it in the word “nearby”.

16.9 Numerical verification and reproducibility

The accelerated objective agrees with the baseline likelihood at the declared control and positive points, with maximum absolute chi-square discrepancy 2.00e-11. Analytic derivatives passed finite-difference checks. Raising the distance quadrature

from 64 to 128 nodes changed the tested shape values by at most 2.66e-15. An explicit arbitrary supernova-intercept shift check confirmed the expected profiled invariance at the tested numerical tolerance. These address likelihood translation and numerical integration risks; they do not test the adequacy of the astronomical error model.

All 43,128 production fits reported successful optimization. The largest scaled projected-gradient diagnostic was 1.78e-05; 478 fits used the declared fallback. The constrained and unrestricted objective values satisfied the checked nesting tolerance, and no fit reached the artificial upper search boundaries. A deterministic audit refitted 556 ordinary and extreme draws from the calibration and validation stages with additional starts; the maximum change in either statistic was 1.19e-12. A further 15 selected draws were evaluated with the original likelihood and its original optimizer, with maximum statistic difference 1.15e-09.

The statistical and computational records are separate. The companion preserves the protocol, its documented implementation amendment, all per-cell JSONL checkpoints, a 43,128-row replicate CSV, validation decisions, nuisance-specific observed ranks, source code and immutable raw-input hashes. CSV and checkpoint contents were compared field by field. The earlier 10,000-draw null experiment remains intact. A short superseded implementation prefix is preserved as an excluded audit record because a common-statistic issue was corrected; it contributes to none of the tables, calibration banks or reported production totals.

16.10 What has advanced, and what remains unresolved

The advance is a completed inference experiment beyond the zero edge: positive signals are generated and refitted; nuisance

variation is declared; finite-grid upper tests are inverted; conditional coverage and power are measured on fresh data; and the scope of the mathematical guarantee is written beside the result. The confidence language now has a concrete procedure to which it can refer. A continuous upper claim, a second free nonnegative correction and a new physical interpretation remain separate research tasks.

In particular, maximizing over nine nuisance points is not maximizing over all admissible m and A. Profiling nuisances in each likelihood fit does not remove their possible influence on the sampling distribution. A valid continuous extension would need certified control of that influence, or another construction whose theorem covers the full nuisance region. It would also need a stated treatment of the historical selection step. Merely making the grid denser would be useful numerically but would not by itself prove either requirement.

An eventual positive detection in this background branch would still have to be compared with physically distinct models that produce the same distance evolution. A quadratic dust term does not uniquely label a higher-dimensional mechanism. Growth, lensing, local gravity and early-universe observables must be connected through a specified dynamical completion before such an interpretation can be tested. The present experiment neither supplies those missing perturbation equations nor calibrates a sound-history inverse problem.

The deterministic certificates in Chapter 15 retain their own interpretation. They establish existence, exclusion or uncertainty bounds for explicitly supplied input sets. This distance-only simulation does not provide a simultaneous 95% input event for an unmeasured sound history or for the geometric inverse coefficients. Attaching a probability to those

certificates would require a correct joint observation model and a stated allocation of error probabilities. No coverage label is transferred from this chapter to a different inverse problem merely because both calculations appear in the same book.

The resulting statement is consequently precise: this chapter provides a verified finite-grid calibration of the stated Gaussian distance experiment and a transparent retrospective application to unchanged observations. It yields no positive-correction detection. It supplies the code, counts and proof needed to distinguish an actual calibrated finite procedure from a suggestive profile crossing, while preserving the physical and statistical questions that this procedure does not settle.

17 Observable Equivalence and Physical Discrimination

17.1 The object that a measurement can distinguish

The inverse developed in this book identifies combinations of geometric parameters within a specified class of solutions. An additional question concerns the class itself: could another physical description generate the same measurements? A unique coefficient vector inside one family does not settle that question. This chapter makes the distinction operational by constructing an explicit four-dimensional competitor, proving an estimation obstruction for the vacuum split, and deriving quantitative discrimination conditions for declared prediction sets.

Three forms of equivalence must be kept separate. Background equivalence means that two solutions have the same expansion history and spatial geometry over the interval considered. Observable equivalence means that the stated observation map, including calibration and noise, gives the same probability distribution. Identical-action equivalence means that the action and other ingredients of the physical specification are unchanged by a relabeling. Background equivalence can be broken by additional observables. An exact redundancy of an unchanged physical specification cannot be broken by observing that specification more accurately.

The general dark-sector degeneracy is established: gravitational measurements constrain total stress-energy without necessarily fixing its decomposition. Kunz's analysis supplies a direct antecedent [51]. The contribution here is an explicit construction for Equation (13.5), its restrictions, and a set of finite-noise decision statements linked to the book's inference

targets. The construction neither introduces a new Friedmann law nor proves worldwide priority for the underlying statistical method.

In particular, the bulk invariant L retains its conditional meaning. Once the geometric family and junction assumptions have been adopted, suitable data may determine L sharply. Interpreting that estimate as evidence for extra dimensions requires a further comparison: can the same observation law arise outside the adopted family? The coefficient inverse addresses the first question. A justified separation certificate for physically completed prediction sets addresses the second. A number derived by inserting a four-dimensional competitor's background into the brane inverse is not, by that substitution alone, the measurement of a bulk possessed by the competitor.

17.2 A conserved effective source for a given background

Consider a spatially flat, expanding Friedmann background on an interval. Write $s=\ln(a/a_{\circ})$, assume $H>0$, and let a conserved source with density ρ and pressure p satisfy

$$H^2=F(s,\rho)>0,\qquad \rho'=-3(\rho+p). \tag{17.1}$$

Here a prime denotes d/ds and F is continuously differentiable on the visited domain. Its explicit dependence on s can include other specified homogeneous components. Choose a constant positive four-dimensional reference mass M_{ref}. Choosing this normalization is part of the comparison; this chapter does not identify it with a measured local Newton constant without gravitational matching.

Proposition 17.1 (conserved effective-source representation). On this interval define

$$\begin{aligned} \rho_E &= 3M_{ref}^2 F, \\ p_E &= -3M_{ref}^2 F - M_{ref}^2 F_s \\ &\quad + 3M_{ref}^2 F_\rho(\rho + p). \end{aligned} \tag{17.2}$$

Then this density and pressure satisfy the flat four-dimensional Friedmann, continuity, and acceleration equations for the original scale factor.

Proof. The total derivative of F is $F_s - 3F_\rho(\rho + p)$. Substituting it into Equation (17.2) gives $p_E = -\rho_E - \rho_E'/3$. The Friedmann equation holds by definition. Since $d/dt = H\, d/ds$ and $H > 0$, differentiating H^2 gives $\dot{H} = (H^2)'/2$. Therefore

$$\begin{aligned} \rho_E' + 3(\rho_E + p_E) &= 0, \\ -2M_{ref}^2 \dot{H} &= \rho_E + p_E. \end{aligned} \tag{17.3}$$

These are the required equations. If the original ρ, p describe a separately conserved retained matter sector, the residual $\rho_D = \rho_E - \rho$, $p_D = p_E - p$ is also conserved. This follows by subtracting the two continuity equations, without assigning a microscopic identity to that residual.

For the polynomial background used throughout the book, the effective pressure can be written explicitly:

$$\begin{aligned} F &= A + B\rho + C\rho^2 + V, V = De^{-4s}, \\ \frac{p_E}{3M_{ref}^2} &= -A + Bp \\ &\quad + C(\rho^2 + 2\rho p) + \frac{V}{3}. \end{aligned} \tag{17.4}$$

This formula preserves the conservation equation rather than matching only one algebraic Friedmann value. For a source

with constant $p=w\rho$, its quadratic contribution redshifts as $a^{-6(1+w)}$ and has effective equation-of-state ratio $1+2w$. The effective ratio need not equal the original source's propagation speed. It is a property of a background stress representation, not a derivation of the quadratic contribution's independent fluctuation dynamics.

The proposition has explicit limits. Although the total effective density is positive by construction, its residual or individual components may violate positivity or other matter restrictions. A pressure defined along one trajectory need not extend to a stable local action or to an admissible equation of state away from that trajectory. No entropy perturbation, anisotropic stress, bulk boundary condition, or quantum state has been supplied. Consequently the construction proves background representability in an unrestricted effective-source class; it does not prove equivalence between every fully specified microscopic theory.

17.3 An exact positive-fluid competitor to Equation (13.5)

The normalized dust branch admits a particularly transparent comparison. Put $x=1+z=a_0/a$ and $\Omega_\Lambda=1-\Omega_m-\Omega_q-\Omega_{dr}$. Equation (13.5) is exactly

$$E^2=1+\Omega_m\left(x^3-1\right)+\Omega_q\left(x^6-1\right)+\Omega_{dr}\left(x^4-1\right) \quad (17.5)$$
$$¿\,\Omega_m x^3+\Omega_q x^6+\Omega_{dr}x^4+\Omega_\Lambda .$$

Proposition 17.2 (four-component background equivalence). Suppose the four coefficients in the last line are nonnegative. Four-dimensional general relativity with the same H_0, flat spatial geometry, and the separately conserved components in

Table 17.1 has precisely this background. The critical reference density is $\rho_{c0}=3M_{ref}^{2}H_{0}^{2}$.

Table 17.1. A four-dimensional positive-fluid representation of the normalized expansion law.

Component	ρ_i/ρ_{c0}	w_i
Dust	$\Omega_m x^3$	0
Stiff component	$\Omega_q x^6$	1
Radiationlike component	$\Omega_{dr} x^4$	$1/3$
Vacuum	Ω_Λ	-1

Proof. Each row obeys $\rho_i'=-3\left(1+w_i\right)\rho_i$. Adding the four densities and applying the flat Einstein Friedmann equation gives the final line of Equation (17.5). The first equality then recovers the original normalized relation. The pressures also agree with Proposition 17.1 for dust. A positive stiff component can be realized at the homogeneous level by a free canonical scalar: its conserved momentum gives $\dot{\phi}\propto a^{-3}$ and $\rho_\phi=p_\phi=\dot{\phi}^2/2\propto a^{-6}$.

This is a positive-component counterexample on the stated coefficient domain. If one coefficient is negative, the algebraic effective representation still exists, but the positive-fluid proposition no longer applies. The comparison also does not certify viability through nucleosynthesis, recombination, or structure formation. The numerical illustration below is deliberately restricted to a late-time interval, and its chosen coefficients are not reported as a new fit.

With a shared photon propagation law and distance calibration, the luminosity distance and redshift drift are identical:

$$\frac{H_0 D_L(z)}{c} = (1+z)\int_0^z \frac{dt}{E(t)}, \qquad \dot{z} = (1+z)H_0 - H(z). \tag{17.6}$$

Any additional background observable that depends only on this same geometry remains matched. For BAO ratios, the ruler r_d must also be assigned the same value or be given a mutually consistent early-time calculation. Matching $E(z)$ over a late-time interval alone does not establish that ruler equality. Similarly, a common supernova distance law requires common luminosity calibration assumptions. These conditions prevent a background identity from being misdescribed as equality of an entire cosmological likelihood.

The implication for a future positive Ω_q is exact but limited: detecting the x^6 contribution in this background law would distinguish it from the zero-correction subfamily, while leaving the positive stiff-fluid construction as a background competitor. To discriminate its physical origin, a proposed measurement must separate predictions that the two completed models actually make.

17.4 A quantitative no-go for the vacuum split

The vacuum freedom in Chapter 10 is stronger than a similarity of expansion histories. Assume that the only dependence on the two constants is the brane term

$$S_{vac} = -\int d^4x\sqrt{-h}\,(\lambda + U_0), \qquad \tau = \lambda + U_0. \tag{17.7}$$

Keep all other couplings, admissible conditions, and the rule for selecting the physical state fixed. For any allowed Δ, the transformation

$$\begin{aligned} \lambda &\mapsto \lambda + \Delta, \\ U_0 &\mapsto U_0 - \Delta \end{aligned} \tag{17.8}$$

leaves the entire action identical. Every field variation is unchanged. With the same state and observation prescription, the distributions of all observables described by that specification are consequently identical. An extra coupling that separately depends on one constant would change this premise and would constitute an enlarged model.

Proposition 17.3 (irreducible split-estimation risk). Consider two allowed representatives related by a nonzero Δ, and any estimator $\hat{\lambda}$ formed from any amount of data generated by this identical specification. Let R_0 and R_1 denote its mean squared errors for the two respective values of λ. Then

$$max\left(R_0, R_1\right) \geq \frac{\Delta^2}{4}. \tag{17.9}$$

Proof. The estimator has the same distribution at both representatives. Put $m = \lambda + \Delta/2$. Under that common distribution,

$$\begin{aligned} &\frac{R_0 + R_1}{2} \\ &¿\, E\left[\left(\hat{\lambda} - m\right)^2\right] + \frac{\Delta^2}{4}. \end{aligned} \tag{17.10}$$

The nonnegative first term proves the claim. If either risk is infinite the inequality remains valid. The result applies at every sample size; hence an estimator cannot be uniformly consistent at these two representatives. An estimator also cannot be unbiased for both distinct values because its expectation is the same under both laws.

The measurable target can instead be τ, or another function constant on the relabeling orbit. A restrictive prior may select a preferred representative, but the data likelihood has not supplied that selection. This statement is distinct from multiplying an action by a positive constant. Overall action scaling preserves classical stationary equations while changing the action itself, its fixed-$\hbar$ quantum phase, and possibly its compatibility with externally normalized matter sectors. An absolute physical calibration can obstruct that scaling without separating the two names inside the unchanged sum in Equation (17.7).

17.5 Linked consistency relations for the kinetic repair

A discrimination proposal should use predictions that are linked by one action rather than count algebraically related outputs as independent discoveries. Consider the canonical-plus-cubic comparison in Chapter 11, on its positive homogeneous branch. Remove the specified constant vacuum contribution when forming excitation density and pressure, and define

$$P(X)=X+\frac{X^3}{M^8}-U_0, x=\frac{X}{M^4}>0,$$
$$w_e=\frac{1+x^2}{1+5x^2}, \tag{17.11}$$
$$\chi=c_\phi^2=\frac{1+3x^2}{1+15x^2}.$$

The scalar propagation formula is established for the local kinetic setting [32]; the two-term action and its vacuum repair were already examined in Chapter 11. Eliminating x yields an additional useful joint consistency form.

Proposition 17.4 (joint kinetic consistency). For this action at finite $x>0$, its excitation equation of state, sound speed, and expansion evolution obey

$$\begin{gathered}(7-5w_e)\chi=1+w_e,\\ \frac{1}{5}<\chi<w_e<1,\end{gathered}\tag{17.12}$$

$$\begin{gathered}w_e'=\frac{3(1+w_e)(5w_e-1)(1-w_e)}{7-5w_e}>0,\\ n_e=-\frac{d\ln\rho_e}{ds}=3(1+w_e).\end{gathered}\tag{17.13}$$

Proof. The first equation follows by cross-multiplying the two rational expressions in Equation (17.11). Their difference is $8x^2/\left[(1+5x^2)(1+15x^2)\right]$, which is positive. The endpoint bounds follow from the same expressions. For a conserved purely kinetic excitation, $p_e'=\chi\rho_e'$ and $\rho_e'=-3(\rho_e+p_e)$. Differentiating $w_e=p_e/\rho_e$ therefore gives $w_e'=3(1+w_e)(w_e-\chi)$. Substitution of Equation (17.12) proves the evolution identity. The final relation is continuity divided by $\rho_e>0$.

Thus the repair follows a constrained curve in the (w_e,χ) plane while its local density slope lies between $18/5$ and 6. At $x=1$ it gives $(w_e,\chi,n_e)=(1/3,1/4,4)$. At $x=0.1$ the corresponding values are approximately $(0.96190,0.89565,5.88571)$. The positive pure-cubic branch instead has $w_e=\chi=1/5$ and a constant density slope $18/5$. These are connected model predictions, not separate observational detections.

A future consistency test would need estimates referring to this same component, the same vacuum convention, and compatible epochs, with their joint uncertainty propagated. Replacing w_e by a total effective cosmic equation of state

changes the test. Moreover, satisfying these relations does not uniquely select this microscopic action: normalization, unvisited action domains, and additional sectors may remain free. The large-x limit also inherits the effective-theory restriction already stated in Chapter 11; proximity to $1/5$ does not establish control of omitted operators.

17.6 Statistical indistinguishability of shared observables

Let an experiment return a vector Y. A theory, its allowed parameters, nuisance quantities, and observation prescription determine a probability law for that vector. If two allowed specifications induce the same law, every statistic and every randomized decision rule has the same distribution at those specifications. This follows directly by integrating the same function against the same probability measure.

For a concrete finite-noise setting, assume

$$Y \sim N_m(\mu, \Sigma), \Sigma > 0, \tag{17.14}$$

with the same known positive-definite covariance under both hypotheses. Equal predicted means then imply equal laws. A test with false-positive probability at most α at the first specification has power at most α at its observationally equivalent competitor. Repeating the experiment independently produces identical product distributions, so this obstruction persists at every sample size.

The equal-law qualification is essential. Equal means with different, physically predicted covariances can be distinguishable. Non-Gaussian distributions can differ in higher moments even when their means and covariances agree. Conversely, adding an identical shared calibration uncertainty cannot create separation; it must be represented consistently in both observation models. A fit that excludes a competitor solely

by fixing its permissible nuisance calibration differently has changed the comparison class.

Applied to Proposition 17.2, a Gaussian distance-only experiment with the same predicted distances, calibration, and covariance cannot select between those matched backgrounds. This conclusion holds for every possible realized data vector, not just for the noiseless central prediction. Additional geometric precision can improve a coefficient estimate within Equation (13.5) while leaving this between-model question unresolved.

17.7 Exact power for two declared Gaussian predictions

For unequal fixed means, known covariance provides a quantitative experimental target. Define the Mahalanobis separation and the directed unit-variance statistic

$$d^2=\left(\mu_1-\mu_0\right)^T\Sigma^{-1}\left(\mu_1-\mu_0\right),$$
$$T=\frac{\left(\mu_1-\mu_0\right)^T\Sigma^{-1}\left(Y-\mu_0\right)}{d}. \tag{17.15}$$

Assume $d>0$, and write $z_q=\Phi^{-1}\left(q\right)$ for a standard-normal quantile. Under the first mean, T is standard normal; under the second it has mean d and variance one. The test rejecting the first mean when $T>z_{1-\alpha}$ consequently has exact size α and power

$$\pi\left(d\right)=\Phi\left(d-z_{1-\alpha}\right). \tag{17.16}$$

Proposition 17.5 (fixed-prediction separation criterion). Among all tests of size at most α for the first Gaussian mean, this test has greatest power at the second. For $\alpha+\beta<1$, power at least $1-\beta$ is achievable exactly when

$$d\geq z_{1-\alpha}+z_{1-\beta}. \tag{17.17}$$

Proof. Expanding the two Gaussian densities gives the log likelihood ratio $d\,T - d^2/2$, which is strictly increasing in T. For the threshold test $\varphi_{¿}$ and any other test φ of no larger null expectation, integrate $(\varphi_{¿} - \varphi)(p_1 - k\,p_0)$, where k is the likelihood-ratio threshold. The integrand is nonnegative on both sides of the threshold. Adding the nonnegative term $k\,E_0(\varphi_{¿} - \varphi)$ proves $E_1\varphi_{¿} \geq E_1\varphi$. Solving Equation (17.16) for the requested power gives Equation (17.17). This is the familiar likelihood-ratio testing argument, included to specify every condition used here.

For size 0.05 and target power 0.90, the required separation is 2.92640519. This is a design separation measured with a stipulated covariance, not a cosmological detection significance. For N independent repetitions with a known common single-repetition covariance, the sample mean has covariance Σ/N and separation $\sqrt{N}\,d$. Shared systematic errors, correlated repetitions, or theory uncertainty do not follow that scaling without their own model.

17.8 Composite prediction sets and certified separation

Physical hypotheses usually predict sets of possible means rather than single points. Let A and B be two nonempty compact sets declared independently of the present data, including the nuisance freedom allowed in each hypothesis. Define

$$d_{¿} = \min_{a \in A,\, b \in B} \sqrt{(b-a)^{T}\,\Sigma^{-1}(b-a)}. \tag{17.18}$$

For arbitrary such sets, applying Proposition 17.5 to their closest pair shows that Equation (17.17), with $d_{¿}$ in place of d, is necessary for uniform power $1-\beta$ at uniform size α. Necessity

alone does not guarantee one decision rule that works well in every possible direction.

Theorem 17.6 (exact convex-set Gaussian discrimination). Suppose additionally that both sets are convex and $d_¿ > 0$. Let $a_¿, b_¿$ be a closest pair, and put

$$u = \frac{\Sigma^{-1}(b_¿ - a_¿)}{d_¿}, \qquad T_¿ = u^T(Y - a_¿). \tag{17.19}$$

The test $T_¿ > z_{1-\alpha}$ has worst-case size α and minimum power $\Phi(d_¿ - z_{1-\alpha})$. No other test with uniform size at most α has greater minimum power over B. Thus the separation criterion is necessary and sufficient under these convexity and covariance assumptions. Gaussian testing by separation of convex prediction sets is established methodology; Goldenshluger, Juditsky, and Nemirovski give the closest-point construction and its antecedents [63, Section 2.3.1].

Proof. The nearest-pair condition and convexity allow first-order variations toward every other point in either set. Differentiating the squared distance along those segments gives

$$u^T(a - a_¿) \le 0 \,(a \in A), \qquad u^T(b - b_¿) \ge 0 \,(b \in B). \tag{17.20}$$

Also $u^T \Sigma u = 1$ and $u^T(b_¿ - a_¿) = d_¿$. Under every null mean, $T_¿$ therefore has variance one and mean at most zero; under every alternative mean its mean is at least $d_¿$. The stated error probabilities follow from the normal distribution and are attained at the closest pair. Any uniformly valid test must be valid at $a_¿$, where Proposition 17.5 bounds its power at $b_¿$. This proves the maximum possible minimum-power statement.

An operational certificate does not require a perfect nearest-pair optimizer. For any predeclared u with $u^T \Sigma u = 1$, rigorous bounds $A_u \geq ¿_{a \in A} u^T a$ and $B_u \leq inf_{b \in B} u^T b$ give the valid statistic $u^T Y - A_u$. If $g = B_u - A_u > 0$, its minimum power is at least $\Phi(g - z_{1-\alpha})$. This sufficient certificate works even for nonconvex sets, provided the support bounds really hold. A local optimizer's candidate distance is not such a lower bound on global separation.

Deterministic uncertainty in predicted means belongs in these sets. For two point predictions enlarged by Mahalanobis balls of radii r_A, r_B, their exact set separation becomes

$$d_{robust} = max(0, d - r_A - r_B). \tag{17.21}$$

The reverse triangle inequality supplies the lower bound, and moving the two ball points along their centers' joining line attains it, including overlap. When this separation is positive, Theorem 17.6 applies. Overlapping sets share an observation law and cannot be uniformly discriminated with power greater than the test size. These radii represent declared bounds, not Gaussian standard deviations. Their validity must be justified by the forward calculation. A deterministic prediction uncertainty must not be averaged down as though it were independent measurement noise.

A sharp nonconvex counterexample shows why the hypothesis-set geometry matters. Let the null be $N(0,1)$ and the alternative be either $N(d,1)$ or $N(-d,1)$. The minimum pairwise separation is d, but the direction is unknown. Symmetrizing any test preserves size and cannot reduce its smaller alternative power. For the symmetric mixture, the likelihood ratio is proportional to $\cosh(dY)$ and increases with $|Y|$. Hence the optimal minimum-power test rejects when $|Y| > z_{1-\alpha/2}$, with

$$\pi_{\pm}(d)=\Phi\left(d-z_{1-\alpha/2}\right) \\ +\Phi\left(-d-z_{1-\alpha/2}\right). \tag{17.22}$$

At size 0.05 and $d=2.92640519$, this maximum minimum power is only 0.83308879, although the fixed-direction criterion predicts 0.90 for its different problem. Reaching 0.90 for the signed alternative requires $d=3.24151499$. Convexifying the signed set would include the null and yield a valid but uninformative separation certificate. It would not establish that the original signed alternatives are undetectable.

17.9 Executed demonstrations and their scope

The accompanying program evaluates the positive-fluid construction at 1001 redshifts in $0\le z\le 3$, with $(\Omega_m,\Omega_q,\Omega_{dr})=(0.30,0.0002,0.0001)$. Direct evaluation of the two algebraic expressions agrees to maximum relative error 8.49×10^{-16}. A separate integration of the four continuity equations agrees with the braneworld expression to within 7.85×10^{-13} in relative error. Luminosity distances calculated from the direct relation and the independently integrated components agree to 6.19×10^{-14} at the five reported redshifts. These errors measure numerical agreement of the constructed backgrounds; they are not experimental uncertainties.

The Gaussian demonstration also includes bounded nuisance means with a correlated covariance:

$$\Sigma=\begin{pmatrix}1 & 0.6\\ 0.6 & 1\end{pmatrix}, \\ A=[-1,1]\times\{0\}, \\ B=[-1,1]\times\{3\}. \tag{17.23}$$

One closest pair is $a_{¿}=(-0.9,0)$, $b_{¿}=(0.9,3)$; its Mahalanobis distance is 3 and the separator is $u=(0,1)$. Thus the exact

minimum power is 0.91231454 at size 0.05. Treating both nuisance coordinates as fixed at zero would instead give point separation 3.75, answering a different, less demanding testing question. The bounded-nuisance calculation exhibits the information lost when the competing specifications may move along their permitted mean sets.

Table 17.2. Exact Gaussian decision probabilities and synthetic replication checks at size 0.05.

Declared comparison	Exact power	Simulated power
Fixed direction, $d = 2.92640519$	0.900000	0.900684
Convex nuisance segments, $d_{ċ} = 3$	0.912315	0.912424
Signed alternative, $d = 2.92640519$	0.833089	0.832420
Point balls: $d = 3, r_A = r_B = 0.2$	0.830248	Analytic only

Each simulated distribution uses 250000 draws from the declared Gaussian law, with PCG64 seed 170012. The convex example's simulated size is 0.050008. All reported replication differences lie within six Monte Carlo standard errors. These simulations check the executed implementation against exact formulas; the formulas and their proofs establish the conditional probabilities. The last table row is calculated analytically and was not assigned a simulated result.

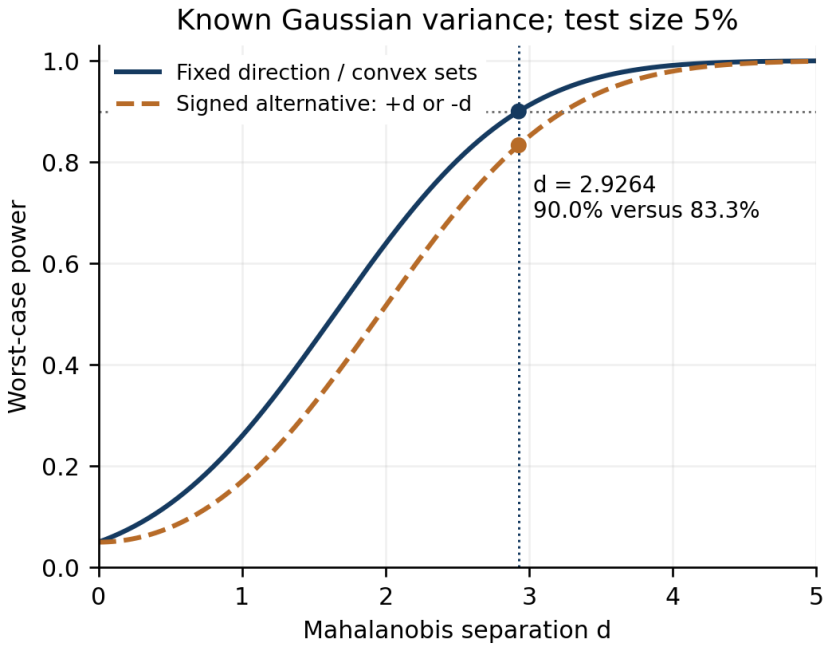

Figure 17.1. Exact Gaussian power for a fixed direction or the convex-set separator, and for the signed nonconvex alternative. Both tests have size 0.05. The same minimum pairwise separation gives different attainable power when the alternative direction is unknown. These are stipulated decision experiments, not a forecast from completed brane perturbation spectra.

Exact rational coefficient checks verify the effective-pressure formula, continuity identity, joint kinetic relation, kinetic evolution, and split-estimation risk identity. The computational directory contains the program, input constants, CSV outputs, figure data, environment versions, verification JSON, and SHA-256 checksums. No observational input from Chapter 13 is read or altered by these demonstrations. Their reproducible contribution is a tested set of background counterexamples and inference calculations.

17.10 The physical information needed for discrimination

Theorems about declared predictions become physical discrimination only after the predictions have been produced. For the brane interpretation, that requires a specified action and background, coupled brane and bulk perturbation equations, admissible initial and boundary conditions, and a controlled solution for the measured quantities. A local principal-part sound speed does not by itself provide transfer functions for matter growth, the metric potentials, lensing, or tensor propagation. The comparison model needs an equally explicit perturbative specification.

Nor does adding a growth observable guarantee universal uniqueness. Kunz and Sapone construct a generalized dark-energy description that reproduces the DGP growth and metric-perturbation behavior in their chosen setting [54]. This antecedent is a reason to declare the allowed entropy and anisotropic stresses, not a claim that every completed theory is indistinguishable. Restricting those freedoms may create separable prediction sets; the restriction must be independently motivated and stated before interpreting the separation.

The normalization must also be tied to the actual local experiment. Garriga and Tanaka derive weak gravitational responses to localized matter in particular Randall-Sundrum settings [41]. Their result supplies a matching antecedent, while a rolling kinetic background can require its own coupled calculation. A coefficient appearing in a homogeneous Friedmann equation cannot be substituted for an independently measured local coupling merely because the dimensions agree.

The practical output of this chapter is therefore precise. Equation (13.5) has an explicit positive four-dimensional

background competitor. The vacuum split has a sample-size-independent estimation obstruction. The kinetic repair predicts a linked consistency curve. Declared Gaussian prediction sets admit exact or certified separation thresholds under the hypotheses proved above. These results identify which questions are already settled within the stated models and which additional physical calculations could change an observationally equivalent comparison into a discriminating experiment.

18 Free Spatial Curvature and Exceptional Sound Histories

The inverse in Chapters 5 and 6 holds spatial curvature fixed. This assumption is observable in principle, but it is not supplied by an expansion history alone. Releasing it adds the template e^{-2s} to the reconstruction. A history that identifies the original four coefficients can then fail to identify the enlarged five-coefficient model. This chapter classifies that failure, constructs a physical example with identical expansion and sound but different bulk geometry, and identifies the calibration that removes the added freedom. All examples in this chapter are synthetic.

The new results extend the conditional inverse developed earlier in the book. They do not alter the junction equation, establish a new gravitational theory, or assert priority over every possible treatment of curvature degeneracy. Their contribution here is an explicit complete classification in the sound coordinate, accompanied by a checked counterexample and a finite-data test. Spatial curvature, bulk curvature and the geometric bulk mass are kept distinct throughout.

18.1 The fifth reconstruction column

Keep the reference scales $a_¿>0$, $S>0$ and the reference coupling fixed, but allow the spatial-curvature amplitude $u=k/\left(a_¿^2 S\right)$ and the effective vacuum intercept to vary. The unknown is the numerical curvature amplitude in this declared coordinate convention. This is different from rescaling the coordinates while describing the same geometry. If an independent assumption fixes the numerical value of u, the four-column problem applies instead.

Let I be a compact interval with nonempty interior, containing $s=0$. A continuous supplied sound derivative $0\le\chi\le1$ determines Q and J through the normalized transport equations of Chapter 5. Put $U=e^{-2s}$ and use $c_U=-u$ for the coefficient of the new column:

$$\begin{aligned} J'=-Q,\,Q'=-3(1+\chi)Q,\,Q(0)=1,\,J(0)=0,\\ h=\beta_0+\beta_1 J+\beta_2 J^2+c_U U+d\,U^2,\,c_U=-u. \end{aligned} \tag{18.1}$$

The sign in $c_U=-u$ follows from Eq. (2.8). The observed quantity in this chapter is the raw dimensionless expansion $h=H^2/S$, before adding any supplied curvature correction. For a fixed common sound history, write V for the span of $1, J, J^2, U, U^2$. Functional rank means the dimension of this span on the entire interval. A numerical sample matrix provides evidence about a chosen finite design, not a definition of this rank.

Since U is strictly monotone, it can itself serve as a coordinate. Direct differentiation gives a useful conversion between the shape of $J(U)$ and the physical sound derivative:

$$\begin{aligned} J_U=\frac{Q}{2U}>0,\,Q=2U\,J_U,\\ \chi=\frac{-1+2U\,J_{UU}/J_U}{3}. \end{aligned} \tag{18.2}$$

For the last identity, differentiate $\log Q=\log 2+\log U+\log J_U$ with respect to s. Because $U'=-2U$, the result is $Q'/Q=-2-2U\,J_{UU}/J_U$. Comparing it with the transport equation proves (18.2). A continuously differentiable Q gives the required twice continuously differentiable J in the U coordinate. The derivative is positive even though both J and U decline as s increases.

18.2 Complete classification of rank failure

Theorem 18.1 — Five-column exceptional histories. Under the preceding hypotheses, the functional rank of V is either four or five. It is four if and only if, throughout the interval, $J(U)$ satisfies at least one of the following relations with constant real coefficients:

$$\begin{aligned} J &= A + B\,U + C\,U^{2}, \\ \text{or } (J - K)^{2} &= A + B\,U + C\,U^{2}. \end{aligned} \tag{18.3}$$

In the second relation, the quadratic is positive on the interval and a single smooth square-root branch is used, except for the affine case excluded by the causal sound condition. The conditions $J_U > 0$, Eq. (18.2), and the reference normalization remain part of the theorem. An arbitrary choice of quadratic coefficients need not define admissible matter.

Proof. Dependence of the five columns means that some nonzero constant vector satisfies

$$a + b\,J + c\,J^{2} + d_{1}\,U + e\,U^{2} = 0. \tag{18.4}$$

The functions $1, U, U^{2}$ are independent on an interval of positive length. Consequently b and c cannot both vanish. If $c = 0$, solve for J to obtain the first relation in (18.3). If $c \neq 0$, completing the square gives the second relation. Conversely, either relation is itself a nonzero dependence among the five columns. This proves the classification of failure of rank five without any use of numerical differentiation or a mesh.

It remains to exclude lower rank and a hidden branch exception. The independent subset $1, U, U^{2}$ shows that rank is at least three. If rank were three, both J and J^{2} would belong to its span. The first statement makes J a polynomial of degree at most two. Its square can have degree at most two only when J

is affine, because a nonzero quadratic leading coefficient would create a nonzero fourth-degree term. Since $J_U>0$, the affine slope is positive, and (18.2) would give $\chi=-1/3$. This contradicts $\chi\geq 0$. Thus any dependence in the causal class has rank exactly four.

Suppose the quadratic in the second relation vanishes at an interior point U_0. Then $J(U_0)=K$, and differentiation of the squared relation gives zero first derivative of the quadratic at U_0. Its second derivative there equals $2J_U(U_0)^2>0$. It is therefore a positive constant times $(U-U_0)^2$. A differentiable strictly increasing J must pass through the zero as one affine function; the same squared identity fixes that affine function on the whole connected interval. This again forces $\chi=-1/3$. The identical argument applies at an endpoint when the stated derivatives extend there. Hence the admissible non-affine branch has a positive radicand and a fixed sign. This completes the proof.

The theorem includes two different shapes of exceptional history. The polynomial case obeys $\chi=(-B+2CU)/(3(B+2CU))$ wherever its slope is positive. A square-root case has a different rational sound law. The Riccati condition in Theorem 5.1 classifies dependence when curvature has already been fixed; it is not by itself a complete test after the curvature column is released. The extra exception is precisely a relation whose coefficient of U is nonzero.

18.3 Constant sound and finite epoch identification

For constant $\chi=c\in[0,1]$, normalization gives $J=(U^p-1)/(2p)$, where $p=3(1+c)/2$. The five columns then have the same span as the five powers below:

$$p=\frac{3(1+c)}{2},\ J=\frac{U^{p}-1}{2p},$$
$$V=span\{1,U,U^{2},U^{p},U^{2p}\}. \tag{18.5}$$

The exponents are distinct throughout the causal constant-sound range except at $p=2$, or $c=1/3$. Distinct powers are independent on a positive interval: setting $x=\log U$ turns them into exponentials with distinct real exponents. Repeated application of Rolle's theorem after dividing out the smallest exponential shows that a nonzero sum of five such terms has at most four distinct zeros. Therefore every five distinct epochs give a nonsingular evaluation matrix in the nonexceptional constant-sound case. At radiation sound, $J=(U^{2}-1)/4$ and the rank is four.

For a general nonconstant sound history, rank five guarantees that some five epochs give full rank. To see this, consider the span of all evaluation vectors. If it had dimension less than five, a nonzero vector orthogonal to that span would supply a functional dependence. This would contradict rank five. The argument does not say that every selection of five epochs works. Epoch design, sound uncertainty and singular values still control useful precision.

Thus five exact expansion values can identify five coefficients for a suitable design, with the supplied exact sound history. A sixth reserved value is the first additional scalar residual that can test this saturated interpolation without an extra parameter restriction. The distinction matters: a five-epoch interpolation can be exact for every five-vector of expansion values and therefore cannot, by that fact alone, validate a five-coefficient model.

18.4 A causal example with changing bulk geometry

Consider the interval $-0.15 \le s \le 0.15$ and the explicitly normalized history

$$U = e^{-2s}, J = \frac{2}{\sqrt{3}}\sqrt{10+U+U^2} - 4,$$
$$Q = \frac{2U(1+2U)}{\sqrt{3}\sqrt{10+U+U^2}}, \tag{18.6}$$
$$\chi = \frac{1}{3}\left[-1+\frac{39U}{(10+U+U^2)(1+2U)}\right].$$

At the reference point $U=1$, these expressions give $J=0$, $Q=1$ and $\chi = 1/36$. They obey the transport identities analytically. The companion verifies the domain with rational inequalities as well as evaluating a dense plotting grid. In particular, $37/50 < U < 27/20$ encloses the complete interval. The numerator that tests $\chi > 0$ is $N(U) = -10+18U-3U^2-2U^3$. It is concave on this interval and positive at both rational endpoints, so it is positive everywhere between them. The polynomial for $\chi < 1$ is $40+45U+12U^2+8U^3$, with positive coefficients for $U > 0$.

The rational enclosure of U is itself certified in the code by bounding the positive exponential series and its tail at 0.3, and then taking a reciprocal. The sampled sound range, approximately 0.0104123 to 0.0298904, is a plot diagnostic. The complete-interval causal claim follows from the inequalities just proved, not from those sampled extrema.

Squaring the definition of J supplies the exact null relation

$$J^2+8J+\frac{8}{3}-\frac{4}{3}U-\frac{4}{3}U^2=0,$$
$$r=\left(\frac{8}{3},8,1,-\frac{4}{3},-\frac{4}{3}\right). \tag{18.7}$$

Theorem 18.1 gives rank four for the five columns. The original four columns $1, J, J^2, U^2$ have rank four as well: if they had a dependence, the five-column nullspace would contain a vector with zero U component. Its one-dimensional nullspace is generated by r, whose U component is nonzero. This is therefore an example that the fixed-curvature inverse identifies exactly, while the free-curvature inverse does not.

Let the coefficient order be $(\beta_0,\beta_1,\beta_2,c_U,d)$. Two members of one exact expansion orbit are

$$\theta_0=(24,10,1,0,1),\theta_1=\theta_0+\frac{1}{10}r,$$
$$\theta_1=\left(\frac{364}{15},\frac{54}{5},\frac{11}{10},-\frac{2}{15},\frac{13}{15}\right). \tag{18.8}$$

Equation (18.7) proves that their expansion histories agree for every epoch in the interval. Their sound histories agree because the same J, Q, χ were used. Nevertheless their geometric coefficients differ. Both admit the physical family of Theorem 6.1. Choosing its normalization $C=1$ gives the exact representatives in Table 18.1.

Table 18.1. Exact physical representatives of one free-curvature expansion orbit. Reference scales are fixed; all entries are dimensionless.

Quantity	Model 0	Model 1
Spatial curvature u	0	$2/15$
Inverse tension η	1	$11/10$
Reference density V	$9/2$	$49/11$

Quantity	Model 0	Model 1
Vacuum intercept b	$-3/4$	$-133/66$
Bulk combination L	1	$74/33$
Bulk coefficient d	1	$13/15$

For each model, $v=V+J$ and $p=-v+Q/3$. Since $J>-4$ and both listed V values exceed four, density is positive throughout the interval. Enthalpy is positive because $Q>0$, inverse tension is positive, and $L>0$ places both representatives on the AdS branch. The expansion is positive as well: the common model-0 expression is $h=24+10J+J^2+U^2=(J+5)^2-1+U^2>0$ when $J>-4$. Substituting the representatives into Eq. (2.8) reproduces the same expansion. A negative b is allowed here; an additional prior on b would define a narrower problem.

At fixed S and $a_{¿}$, the ratio of bulk curvature lengths is $\ell_1/\ell_0=\sqrt{33/74}\simeq 0.66779$, while $\mu_{B,1}/\mu_{B,0}=13/15$. These are differences of physical metric coefficients in the declared ansatz, not a change of units or a vacuum-split relabeling. The finite numerical grid reproduces the expansion identity to about 7.11×10^{-15} in dimensionless double precision. Its exact validity was already established by the rational relation.

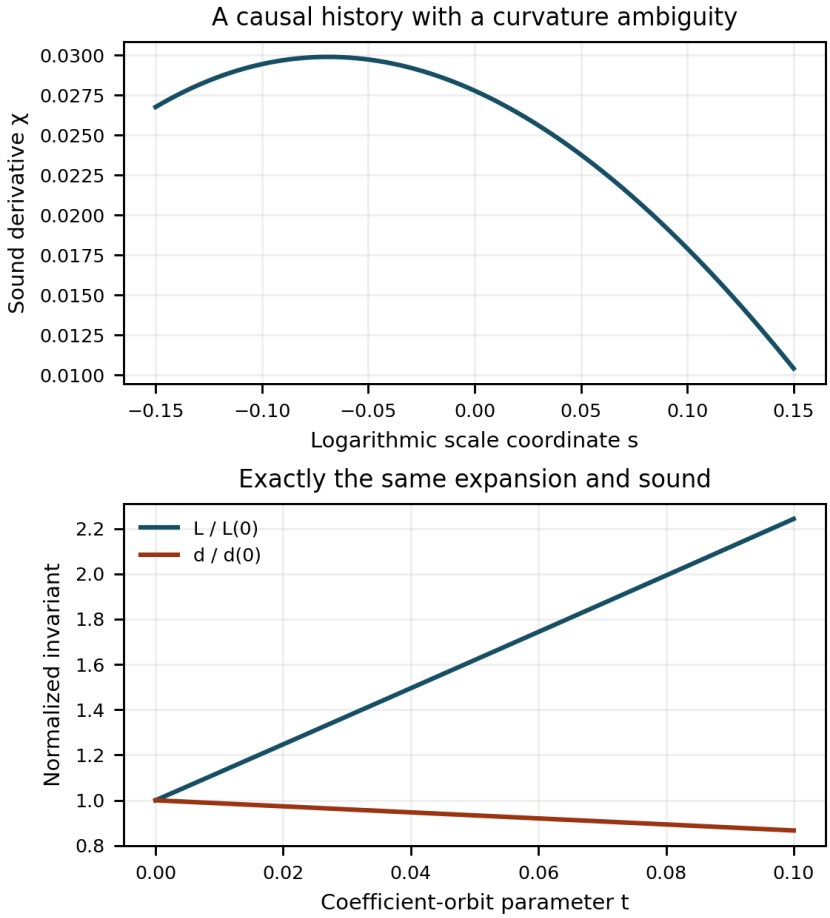

Figure 18.1. A synthetic causal history with a spatial-curvature ambiguity. The lower panel follows the exact coefficient orbit from model 0 to model 1. Expansion and sound remain identical while the bulk curvature combination and geometric mass coefficient vary. Lines visualize the proved identities; they are not fits to cosmological measurements.

This counterexample concerns the input pair (h, χ). It does not assert equality of every cosmological observable. For example, transverse distances depend on spatial curvature as well as the line-of-sight expansion integral, so an appropriately calibrated transverse-distance measurement can distinguish these two

models. That fact supplies a concrete observational route for the next section. It also prevents an expansion-only degeneracy from being overstated as equivalence of complete data distributions.

18.5 The calibration that removes the added freedom

Proposition 18.2 — One transverse coefficient measurement. Suppose the exact common history has rank four, and a nonzero null vector r is known. Every coefficient solution is $\theta(t)=\theta_{¿}+t\,r$. An exact scalar linear measurement $a^T\theta=m$ fixes the remaining coefficient parameter uniquely if and only if $a^T r\neq 0$, provided a physically admissible solution exists. If $a^T r=0$, the measurement is constant on the whole orbit and cannot distinguish its members.

Proof. Along the orbit, the measurement is $a^T\theta_{¿}+t\,a^T r$. A nonzero slope determines one value of t. A zero slope gives either agreement for every member or disagreement for every member. No further inverse argument is required. The admissible domain then decides whether the selected coefficient vector has a physical realization.

For a curvature measurement, a selects $u=-c_U$, so the relevant slope is $-r_U$. A nonzero r_U characterizes the added curvature ambiguity and one exact curvature value removes it. If $r_U=0$, fixing curvature cannot repair the original four-column exception. The theorem also shows why measuring more expansion values of the same exact history fails: all their evaluation vectors annihilate r. The density-normalization family C can still remain after the coefficients are fixed; the recovered bulk invariants survive that separate freedom under Theorem 6.1.

A deterministic measurement error can be propagated without introducing a probabilistic interpretation. If $\left|a^T\theta - m\right| \le \epsilon$, then

$$\left| t - \frac{m - a^T\theta_{¿}}{a^T r} \right| \le \frac{\epsilon}{\left|a^T r\right|}, a^T r \neq 0. \tag{18.9}$$

Intersect this interval with the admissible physical domain before projecting it into L, d, ℓ or any other quantity. A narrow reported coefficient interval is uninformative if its conversion crosses $L=0$ or $\beta_2=0$. This is the same nonlinear domain issue addressed in Appendix F and Chapter 15.

For the exact orbit in (18.7)–(18.8), the formulas simplify to

$$\begin{aligned} u(t) &= \frac{4}{3}t, d(t) = 1 - \frac{4}{3}t, \\ L(t) &= \frac{(10+8t)^2}{4(1+t)} - 24 - \frac{8}{3}t = \frac{40}{3}t + \frac{1}{1+t}. \end{aligned} \tag{18.10}$$

A curvature anchor centered at zero with deterministic halfwidth 0.01 gives $-3/400 \le t \le 3/400$. The derivative $L'(t) = 40/3 - (1+t)^{-2}$ is positive throughout this interval. Its endpoints therefore give the exact extrema in Table 18.2. Even perfect expansion and sound leave a finite geometric interval when the only distinguishing input has finite error.

Table 18.2. Exact projection of the declared curvature-anchor error. These are deterministic allowed ranges under exact expansion and sound, not confidence intervals.

Quantity	Allowed lower value	Allowed upper value
L	3603/3970	4403/4030
d	99/100	101/100
$\ell\sqrt{S}$	0.9567053	1.0496950

The two rational bounds for L are approximately 0.9075567 and 1.0925558. The length bounds are rounded evaluations of inverse square roots of the exact rational endpoints. A real distance analysis must propagate its common covariance, ruler calibration and curvature assumptions before substituting an anchor width. The illustrative width used here is not an estimate of an instrument's precision.

18.6 A sixth epoch as a reserved test

The reserved-epoch contrast of Proposition 5.2 extends to the five-column model by the same linear-algebra argument. This is a conditional Gaussian test with a fixed exact sound design and known joint covariance. It provides a check of the common expansion relation; it does not estimate the sound history or validate a selected design on the data used to select it.

Let X_T be the nonsingular five-by-five training matrix and $x_{¿}^{T}$ the sixth row. Let Y be the six measured expansion values and Σ their known positive-definite covariance. Define

$$a=\begin{pmatrix} -X_T^{-T}x_{¿} \\ 1 \end{pmatrix}, a^T X=0,$$
$$Z=\frac{a^T Y}{\sqrt{a^T \Sigma a}}. \tag{18.11}$$

Under $Y \sim N(X\theta, \Sigma)$, Z is exactly standard normal for every coefficient vector θ. Indeed, the mean vanishes because $a^T X=0$, and the denominator is its exact standard deviation. Thus rejecting when $|Z|>z_{1-\alpha/2}$ has size α. Correlation between training and reserved measurements is allowed because the full joint covariance enters the denominator. Fitting or selecting the sound history with all six measurements changes the statistic and requires a new calibration.

The executed example uses dust sound $\chi = 0$ at six epochs: $(-0.5, -0.3, -0.1, 0.1, 0.3, 0.5)$. Its covariance is $\Sigma_{ij} = 10^{-8} \exp\left(-|s_i - s_j|/0.25\right)$. The first five epochs determine the contrast weights. A single synthetic draw with seed 20261012018 gives a contrast standard deviation of 0.000324166, $Z = 1.59150$ and two-sided $p = 0.11150$. This draw illustrates execution; it is not empirical evidence for the model and is not a simulation estimate of the test's size. The exact size is established by the preceding distributional proof.

The training matrix has an unscaled two-norm condition number of approximately 18457. This is a warning about the chosen interpolation design, even though its rank is exactly five. The contrast explicitly propagates the resulting amplification. The companion saves every epoch, design value, noise realization and contrast weight, so the reported number can be checked without regenerating a larger experiment.

18.7 What the extension changes

The central geometry statement now has an explicit curvature qualification. With supplied curvature and a nonexceptional four-column history, L and d are identified within the declared bulk metric class. With free curvature and a nonexceptional five-column history, the data can identify u together with those coefficients. In the exceptional five-column class, a one-dimensional coefficient orbit remains. Its bulk invariants generally vary, as the exact example demonstrates.

A useful measurement must vary across that orbit. Equation (18.9) quantifies the information carried by a linear calibration; it also identifies calibrations that are exactly blind. Transverse distance or intrinsic-curvature information can supply the missing direction when its forward model and uncertainty are

justified. Additional observations then improve the inverse because they contribute a distinguishable quantity, rather than merely adding more samples of an already identical expansion curve.

The result is a stronger specification of what can be learned, including a larger obstruction where the previous hypotheses were too restrictive. It gives a complete answer to one extended mathematical question and a reproducible example of its practical meaning. It does not settle the brane–bulk perturbation boundary problem, provide new astronomical sound measurements, or convert the retrospective distance calibration of Chapter 16 into an identification of five-dimensional gravity.

19 What the Third Edition Establishes

The third edition extends the inverse from an exact uniqueness statement toward a checkable statement about finite information. It now supplies common-history witnesses and exclusions, preserves coefficient correlations when bounding geometry, quantifies unavoidable reconstruction error, calibrates positive signals on a declared finite grid, and classifies the additional ambiguity created by unknown spatial curvature. It also gives explicit competitors and decision thresholds for asking whether an inferred background selects its physical origin. These achievements have different evidentiary meanings. Their value depends on retaining the hypotheses that make each conclusion valid.

A mathematical obstruction can be a substantive result. It identifies a question that no increase in the precision of the same information can answer. A constructive certificate can be equally substantive: it provides a history, bound or contrast that another calculation can inspect. The book now contains both kinds of result. Its strongest conclusions state exactly which quantities survive the allowed freedoms and how additional information can change that answer.

19.1 The exact inverse after its assumptions are exposed

With exact sound, fixed reference scales and supplied spatial curvature, the expansion belongs to the span of $1, J, J^2, e^{-4s}$. Theorem 5.1 classifies its functional rank failure through the Riccati relation. Away from that class, Theorem 6.1 parameterizes the entire free-vacuum normalization family. The combinations $L = \beta_1^2/(4\beta_2) - \beta_0$ and d survive this family when the physical branch conditions hold. Their dimensional

conversions require the same declared scales and metric ansatz.

Chapter 18 removes one of those assumptions. With curvature free, the additional e^{-2s} column can create a coefficient ambiguity even when the original four columns are independent. Theorem 18.1 completely describes the causal exceptional histories by a quadratic or shifted-square-root relation in $U=e^{-2s}$. The executed example keeps the entire expansion and sound histories fixed while moving L from 1 to $74/33$ and d from 1 to $13/15$. Thus the original geometric invariant is invariant along the specified normalization family, not along every enlargement of the model class.

One exact linear calibration removes a rank-four coefficient freedom precisely when it varies along the null direction. The curvature measurement in Proposition 18.2 supplies such a calibration for the newly introduced curvature ambiguity. Repeating a measurement whose prediction is already constant on the orbit cannot do so. This criterion turns the phrase additional information into an explicit mathematical requirement.

Even after L and d are identified, the result refers to the Schwarzschild–AdS-type homogeneous bulk family used in the book. It does not reconstruct unrestricted five-dimensional topology, all boundary data, a bulk quantum state or a dimensional black-hole mass without its gravitational normalization. The invariant is a well-defined target within its class. Extending the class requires a new identifiability analysis.

19.2 What finite observations can now certify

Chapter 15 supplies a finite representation of the common-path requirement under a fixed Lipschitz budget. A nodal box

encloses a family of sound paths. Analytic transport bounds then produce necessary intervals for all its density ratios and sound windows. A disjoint observation excludes the box. A single accepted interpolant, with its normalization and physical checks, supplies a witness. Remaining overlap is reported as unresolved. This procedure prevents separate successful fits from being mistaken for one compatible history.

The normalized transport bound is sharpened to $\tanh(r/2)$, with an even more informative pointwise interval. Its sharpness concerns the stated multiplicative-envelope class; the more restrictive physical sound class need not attain it. The numerical examples use outward arithmetic and analytic quadrature remainders. The proofs establish the logic of the enclosure; the executed records establish which declared finite examples the implementation resolves.

The correlated coefficient example is a second concrete advance. Its joint polytope gives exactly $37/3000 \le L \le 397/27000$, while the smallest bounding rectangle crosses $L = 0$. The difference arises from retaining the directions allowed by the same information. A rectangular approximation may be valid as an outer set and still be too loose to establish a positive AdS invariant. The convex support certificate supplies a finite way to check the stronger bound.

Upper and lower error bounds now accompany the rank criterion. Proposition 15.5 turns a certified rank margin, sound-design error and observation-noise bound into a finite geometric diameter. Theorem 15.6 constructs one observation compatible with two physical models and proves that every point estimator must be inaccurate for at least one of them by half their invariant separation. Together they separate uniqueness in ideal arithmetic from accuracy in a declared

experiment. An exact rank calculation alone cannot replace either bound.

None of the synthetic error intervals becomes a confidence region by being printed in a table. A simultaneous statistical observation event must be established separately, and every subsequent outer step must retain it. Chapter 9 provides that architecture for its stated experiments. The finite certificates can strengthen the geometric projection on that event when their additional hypotheses and calibration inputs apply.

19.3 What the expanded calibration answers

The observations remain the same thirteen DESI DR2 BAO entries and 1590 selected Pantheon+ light-curve records with the retained covariance matrices. Chapter 13 preserves the original distance fit and the 10,000-draw pointwise null experiment. The third edition adds 43,128 nonlinear simulated fits across eight generating quadratic coefficients and nine nuisance points: 399 calibration and 200 fresh validation vectors for each of the 72 cells. These are additional computational experiments, not additional astronomical measurements.

Chapter 16 separates a positive-signal detection statistic from a one-sided exclusion statistic at a proposed coefficient. Its Monte Carlo rank construction includes the observed rank, handles ties conservatively, and maximizes over the declared nuisance grid. For a frozen procedure with the true coefficient and nuisance point on that grid, the finite-grid coverage argument follows from exchangeability. This is a stronger statistical statement than assigning a universal confidence label to one asymptotic profile crossing. It remains a statement about that explicitly limited experiment. [59; 60; 62]

The historical observations still have $\widehat{\Omega}_q = 0$ and a finite-grid detection p-value of 1. The retrospective upper calculation retains 0 and 10^{-4} on its eight-value grid; its first rejected sampled value is 2×10^{-4}, with maximum nuisance p-value 0.045. This is a discrete acceptance calculation under the displayed rule, not a continuous upper bound. The numerical calibration therefore refines the exclusion question without producing evidence for a positive correction.

The grid was chosen after the historical observations and their baseline fit were available. Accordingly, the observed inversion is retrospective. The finite-grid theorem does not repair unrestricted data-dependent grid selection, extend coverage between untested grid points, or certify a continuous upper endpoint. Fresh validation vectors sharing one calibration bank estimate performance conditional on that bank; their binomial uncertainty differs from the theorem that averages over calibration and observation randomness. Chapter 16 and Appendix D retain these distinctions alongside the results.

The expanded calculation keeps the covariance model, flat dust branch and fixed zero dark radiation of the chosen likelihood. It does not add covariance-construction uncertainty, a nonlinear early-universe likelihood or a second free nonnegative correction. Reusing this calibration for a materially changed fitting procedure would require checking the relevant distributional conditions again. The executed records make the present procedure reproducible and define the scope of its error probabilities.

19.4 What a future positive coefficient would establish

An independently validated positive Ω_q would challenge the zero-correction subfamily of Eq. (13.5) within the observation

model used to establish it. Chapter 17 proves that the same positive background term has an explicit four-dimensional conserved stiff-fluid representation on its stated coefficient domain. Consequently that background detection would not, by itself, identify a five-dimensional origin. The statement is an exact counterexample to uniqueness of origin, not a prediction that a future signal will be absent.

The physical comparison must therefore specify completed models and their observation maps. Equal probability laws make all tests equally unable to distinguish the paired specifications. Unequal predictions can be assessed quantitatively. For known Gaussian covariance, Theorem 17.6 gives an exact closest-set criterion for compact convex mean sets; the signed-alternative example shows why minimum pairwise separation alone is insufficient for an arbitrary nonconvex alternative. A certified support gap can still give a sufficient test when the sets have more complicated shapes. [63]

The action audit supplies another exact limit. If the constants appear only through $\tau = \lambda + U_0$, observing the same unchanged specification cannot distinguish λ from $\lambda + \Delta$ accompanied by the compensating vacuum shift. Proposition 17.3 quantifies this with the lower risk $\Delta^2/4$. A physical restriction or new separate coupling changes the model. An overall action normalization is a different freedom and can be constrained by an appropriately matched absolute calibration.

The canonical repair also has a clearer joint target. Its excitation equation of state, propagation speed and density evolution lie on the linked relations of Proposition 17.4. A measurement would need to refer to that same component and vacuum convention, with common uncertainty. Agreement would test those linked restrictions; it would not make them

independent discoveries or prove uniqueness of every microscopic extension of the action.

19.5 The remaining research question

The next physical calculation has a definite object: a normalized action and background, a conserved matter content, coupled brane and bulk perturbation equations, specified initial and boundary data, and controlled predictions for the measured quantities. The competing model must have a comparably explicit specification. Only then can a growth, lensing, clock or tensor observation be assigned a physically justified prediction set and tested with the correct nuisance and covariance treatment.

The current book does not solve that full boundary problem. It establishes exact and finite-information results that tell the calculation what it must distinguish, which calibrations are needed, and which redundancies remain even with ideal data. This is a completed mathematical and computational extension with an explicitly open empirical task. A stronger future result must add either a proved restriction on the allowed physical descriptions or new discriminating evidence under a justified observation model.

The reader can assess the present claims directly through the theorem statements, full derivations, exact examples, simulation records and contribution map. The success of a later comparison will depend on its physical predictions and evidence. The purpose of this edition is to make that dependence precise enough to test.

Appendix A Units and Convention Crosswalk

A.1 Natural units and derivative conventions

Unless an SI conversion is stated, the book uses $c=\hbar=1$ and signature ¿. Write E for an energy unit; length and time then have units E^{-1}. The scale factor a has dimensions of length because the constant-curvature spatial coordinates have a fixed dimensionless normalization. A convention in which a is dimensionless requires a corresponding change in the curvature and bulk coefficients before numerical values can be compared.

The coordinate $s=\log(a/a_{¿})$ is dimensionless. A prime denotes its derivative, while a dot denotes a derivative with respect to cosmological proper time:

$$\frac{ds}{dt}=H,\dot{f}=Hf',\chi=\frac{dp}{dv}. \tag{A.1}$$

The logarithmic coordinate describes the chosen monotone branch of the cosmology. It is not a replacement for proper time at an expansion turning point. In Chapters 4–9, p is dimensionless pressure, equal to $\kappa_0 P/S$ for physical pressure P. Chapter 2 first denotes this same dimensionless variable by ϖ. Scalar pressures such as p_ϕ in the action analysis carry physical density units when written with their physical Lagrangian.

Table A.1. Dimensions in the braneworld convention. The scalar convention is $X=-h^{\mu\nu}\partial_\mu\phi\,\partial_\nu\phi/2$. A dimensionless logarithmic frequency is distinct from a physical fluctuation frequency, which has energy units. The symbol S in reconstruction is a curvature scale, whereas the full action is dimensionless in natural units.

Quantity	Symbol or definition	Natural units
Radius, scale factor and bulk curvature length	$r, a, a_{¿}, \ell$	E^{-1}
Hubble rate	H	E
Curvature scales	$S, \Lambda_5, \Lambda_4, \Lambda_{eff}$	E^{2}
Bulk metric mass coefficient	μ_B	E^{-2}
Reduced gravitational scales	M_5, M_4	E
Five-dimensional coupling	$G_5=\left(8\pi M_5^3\right)^{-1}$	E^{-3}
Four-dimensional reference or background coupling	$g_{ref}, g_{bg}, \kappa_0$	E^{-2}
Physical density, pressure and vacuum stresses	$\rho, P, \lambda, U_0, \tau$	E^{4}
Scalar field in the adopted convention	ϕ	E
Scalar kinetic variable and physical Lagrangian	$X, F(X)$	E^{4}
Dimensionless reconstruction quantities	$h, v, p, b, u, d, \eta, Q, J$	1
Logarithmic frequencies, widths and sound ratio	$\omega, \Delta, w, s, \chi$	1

A.2 Split tension and total vacuum stress

The bare or split tension is written λ or λ_{bare}. When the matter Lagrangian contains a constant contribution $-U_0$, the total vacuum stress is $\tau=\tau_{vac}=\lambda+U_0$. The two associated linear coefficients and constant expansion terms are

$$\begin{gathered} g_{ref}=g_{split}=\frac{\lambda}{6M_5^6}, g_{bg}=\frac{\tau}{6M_5^6}, \\ \frac{\Lambda_4}{3}=\frac{\lambda^2}{36M_5^6}-\ell^{-2}, \frac{\Lambda_{eff}}{3}=\frac{\tau^2}{36M_5^6}-\ell^{-2}. \end{gathered} \tag{A.2}$$

The density accompanying g_{ref} may include U_0. The excitation density accompanying g_{bg} has that constant subtracted. Replacing Λ_4 by Λ_{eff} while retaining the former density and coupling is therefore not a consistent change of notation. All parts of the split must change together. [4]

The reference quantity $G_{4,ref}$ is defined by $8\pi G_{4,ref}=g_{ref}$. It is not automatically a measured Newton constant. Similarly, $M_4^{-2}=g_{bg}$ defines the vacuum-subtracted background scale; identifying it with local gravity requires the matching conditions discussed in Chapter 10.

A.3 Dimensionless reconstruction and physical conversion

With fixed S, $a_¿$ and $\kappa_0=g_{ref}/3$, the normalization is

$$\begin{gathered} h=H^2/S, v=\kappa_0\rho/S, \\ p=\kappa_0 P/S, b=\Lambda_4/(3S), \\ u=k/(a_¿^2 S), d=\mu_B/(a_¿^4 S), \\ \eta=\frac{S}{2\kappa_0\lambda}, L=\frac{1}{4\eta}-b. \end{gathered} \tag{A.3}$$

The symbol τ is reserved for vacuum stress; η^{-1} always means the inverse of the dimensionless inverse tension. Physical conversion gives

$$\lambda=\frac{S}{2\kappa_0\eta},\ell=(SL)^{-1/2},\\ \mu_B=a_¿^4Sd,\rho=(S/\kappa_0)\nu. \tag{A.4}$$

These expressions require positive finite η and positive L for the stated AdS branch. The limit $\eta=0$ is not a finite positive-tension representative. The conversion of an identified coefficient into energy density also remains conditional on the supplied reference coupling and scales. Changing units is different from independently measuring those scales. [3]

For a local scalar completion written as $P(X)=p$, the physical pressure Lagrangian is $(S/\kappa_0)P(X)$. Naming a coefficient in this representation does not fix an absolute matter normalization. If a convention $F(0)=0$ is used to isolate U_0, the action must first possess a well-defined extension to $X=0$.

A.4 Coordinate normalization and SI restoration

In a planar bulk, a spatial-coordinate rescaling can be accompanied by

$$\tilde{r}=\zeta r,\tilde{a}_¿=\zeta a_¿,\\ \widetilde{T}=T/\zeta,\tilde{x}=x/\zeta,\\ \tilde{\mu}_B=\zeta^4\mu_B,\tilde{\ell}=\ell,\zeta>0. \tag{A.5}$$

Here x denotes the normalized planar coordinates. This relabeling preserves the geometry. The quantities d and $r_h/a_¿$ remain invariant at fixed S, while the numerical coefficient μ_B depends on the declared normalization. A physical bulk mass additionally involves G_5 and the spatial-volume convention. [3]

For SI formulas using energy density ε and tension in joules per cubic metre, restore

$$h=\frac{H^2}{c^2 S},\kappa_{0,SI}=\frac{8\pi G_{4,ref}}{3c^4},\nu=\frac{\kappa_{0,SI}\varepsilon}{S}. \tag{A.6}$$

The remaining dimensionless definitions retain their form with this SI coefficient. Using mass density instead requires its factor of c^2. In an effect estimate containing $H_\rho \ell$, an SI Hubble rate and a length must occur as $H_\rho \ell/c$. Sound means remain averages of the dimensionless χ in s; physical sound speed satisfies $c_s^2=c^2\chi$ under the stated barotropic interpretation. These conversions prevent a unit convention from being mistaken for a physical constraint.

Appendix B Reconstruction Algorithms

B.1 Choose the data problem

Record the interval, reference scales, supplied curvature and vacuum terms, matter class and calibration assumptions before solving an inverse. Distinguish an exact continuous history, finite exact values, deterministic error bounds and a statistical measurement region. Each supplies different information. A finite grid does not become a continuous band merely through interpolation. The procedures below specify mathematical targets; numerical use must record integration errors, rank conventions, physical-domain checks and solver statuses.

Use $s=\log(a/a_{¿})$ on an interval containing zero, with fixed $S, a_{¿}, \kappa_0$ and supplied u. Include positive density, positive enthalpy and the chosen expanding branch among the requirements. Treat $\eta=0$ as a limiting effective case, separately from finite positive tension.

B.2 Exact sound with supplied vacuum

Construct the transport from the supplied sound history:

$$Q(s)=\exp\left[-3s-3\int_0^s \chi(t)\,dt\right], J(s)=-\int_0^s Q(t)\,dt. \tag{B.1}$$

At at least four expansion epochs, assemble

$$A_i=\left(1, J_i, J_i^2, e^{-4s_i}\right), f_i=h_i-b+u\,e^{-2s_i}. \tag{B.2}$$

Check column rank and solve $A\theta=f$. With more than four observations, require consistency of the entire vector. If rank fails, retain the coefficient solution set; a pseudoinverse gives one representative rather than a unique physical solution. Small singular values quantify sensitivity in the declared scaling.

Use a factorization, such as QR or SVD, instead of explicitly inverting the matrix. Record the column scaling and threshold used to assess rank. A small singular value is numerical evidence about conditioning, not an analytic proof of exact dependence. With noisy values, a least-squares solution is a point estimate and belongs to the uncertainty route below rather than to the exact-consistency calculation.

For $\theta=(\alpha_0,\alpha_1,\alpha_2,d)$, use

$$\Delta_\alpha=\alpha_1^2-4\alpha_0\alpha_2,\ C=\sqrt{\Delta_\alpha},$$
$$\eta=\alpha_2/\Delta_\alpha,\ V=\frac{2C\alpha_0}{\alpha_1+C}. \tag{B.3}$$

Require positive $\alpha_0,\alpha_1,\alpha_2,\Delta_\alpha$, nonnegative d, $1/(4\eta)>b$, and positive $v=V+CJ$ and h throughout the interval. Convert units only after these checks. Four consistent samples do not establish agreement with an independently supplied full curve. [18; 19]

B.3 Exact sound with free vacuum

Use the same matrix but solve against $y_i=h_i+ue^{-2s_i}$ for $(\beta_0,\beta_1,\beta_2,d)$. For an identified vector with $\beta_2>0$, calculate

$$\Sigma=\beta_1^2-4\beta_0\beta_2,\ L=\frac{\Sigma}{4\beta_2}, \tag{B.4}$$

¿

Require $L>0$, $C_{max}>0$, $d\geq 0$ and positive common expansion. Return the full family

$$0<C<C_{max},\ \eta_C=\frac{\beta_2}{C^2},$$
$$V_C=\frac{C(\beta_1-C)}{2\beta_2},\ b_C=\frac{C^2-\Sigma}{4\beta_2}. \tag{B.5}$$

Report $\ell=(SL)^{-1/2}$ and $\mu_B=a_¿^4 Sd$ with their normalization. Additional priors restrict the family explicitly. One density anchor requires solving a quadratic and retaining every admissible root. Two distinct density anchors or an absolute enthalpy anchor determine a candidate C, which must still fit all observations. Never apply the fixed-vacuum discriminant inverse after freeing the intercept. [3]

B.4 Finite values with a common matter history

For this route, supply b,u,d and consider each candidate η. Transform positive residual intervals using

$$R_i=h_i-b+u\,e^{-2s_i}-d\,e^{-4s_i},\quad f_\eta(R)=\frac{2R}{1+\sqrt{1+4\eta R}}. \tag{B.6}$$

Use the union of density epochs and sound-window endpoints as the node set. Introduce one density v_i and one rate $q_i>0$ at every node, shared by both adjacent cells. For a sound margin $0\le m<1/2$, set $A_m=3(1+m)$ and $B_m=3(2-m)$. On each cell of length Δ, impose

$$\begin{aligned} e^{-B_m\Delta}q_i\le q_{i+1}\le e^{-A_m\Delta}q_i,\\ q_-(t)=max\left(q_i e^{-B_m t},q_{i+1}e^{A_m(\Delta-t)}\right),\end{aligned} \tag{B.7}$$

¿

The exponential branches integrate exactly. Chapter 4 gives their cone representations. Add sound means as endpoint-rate ratios using (4.19), and impose all proxy-gain inequalities on these same densities. With logarithmic proxy bounds $y^{\pm}_{p,i}$, these are

$$v_j\le\exp\{\delta|s_i-s_j|-y^-_{p,i}+y^{+¿}_{p,j}\}v_i \text{ for every } i,j.¿ \tag{B.8}$$

The sufficient background condition $b-u\,e^{-2s}+d\,e^{-4s}\ge 0$ guarantees positive expansion between nodes. Without it, positivity needs an additional justified check. A positive first-to-

last density separation excludes the constant zero-enthalpy branch.

Return feasibility with a common witness, infeasibility with appropriate evidence, or an unresolved status. Do not interpolate untested parameter gaps or convert solver failure into exclusion. Interval endpoints are justified only where an interval theorem applies. A smooth completion preserves finite constraints with a smaller positive margin; it does not automatically preserve an added derivative budget. [11; 16; 15]

B.5 Propagate a common uncertainty event

Obtain a simultaneous measurement region from the actual observation model. Independent complete Gaussian repeats permit the coordinate Student construction in Chapter 9. Distinct epochs are not substitutes for those repeats. Declare a regularity bound covering the entire sound class and the full windows before deriving a uniform error ε_{χ}.

Integrate the nominal sound curve with justified errors ζ_i for numerical values $\widetilde{J}_i$. Form

$$\begin{aligned} R_i &= \left(\left|\widetilde{J}_i\right| + \zeta_i\right)\left(e^{3\varepsilon_{\chi}|s_i|} - 1\right) + \zeta_i, \\ \widehat{A}_i &= \left(1, \widetilde{J}_i, \widetilde{J}_i^2, E_i\right), \\ B_i &= \left(0, R_i, 2\left|\widetilde{J}_i\right| R_i + R_i^2, 0\right). \end{aligned} \tag{B.9}$$

For fixed vacuum, retain every nonnegative coefficient vector satisfying

$$\left|\widehat{A}\,\theta - f\right| \le e + B\,\theta. \tag{B.10}$$

For free vacuum, replace f by y and allow the intercept to have either sign. Its uncertainty column is zero, so the inequalities remain linear when the other coefficients are nonnegative. The result is an outer set. Enforce physical constraints through all

compatible sound histories, not only the nominal curve, and map every surviving free-vacuum C. Report unbounded outputs as unbounded rather than selecting convenient finite endpoints. [20; 6]

For at least four expansion epochs and a positive diagonal 4×4 scaling W, a useful rank enclosure is

$$\gamma = \sigma_{min}\left(\widehat{A}\, W\right) - \| B\, W \|_F . \tag{B.11}$$

A positive value certifies full column rank for every matrix admitted by the sound bound. A nonpositive value is inconclusive. This check addresses matrix uncertainty; it does not make all permitted histories yield one coefficient vector or remove the free-vacuum family. Account for numerical error in both terms if the reported rank enclosure is intended as a rigorous computational certificate.

B.6 Report the scope of the result

A useful reconstruction record includes the supplied nuisance quantities, measurement event, regularity budget, retained coefficient set, physical conversion and unresolved cases. Distinguish exact identities from floating-point comparisons and distinguish common-history witnesses from outer enclosures. If continuous weak integrals are used, supply continuous expansion and sound bands; four expansion values are insufficient. If a mode was selected statistically, identify the calibrated test and its actual target separately from the physical confidence set. This record makes the result reproducible and exposes which additional measurement would narrow the remaining ambiguity.

Appendix C Scalar–tensor comparison and finite clock references

C.1 A separate four-dimensional model

The scalar–tensor source provides a useful comparison because it develops an explicit inference problem with finite clocks, lensing, and massive tracers. Its action is a four-dimensional canonical scalar coupled universally through a conformal matter metric. With $x^0 = c\,t$, it can be written

$$S_{ST} = \frac{c^3}{16\pi G_0}\int d^4x\sqrt{-g}\left[R - 2(\partial\varphi)^2 - 2\mu_\varphi^2\varphi^2\right] + S_m\left[\tilde{g}, \psi\right], \tilde{g}_{\mu\nu} = e^{2\alpha_{ST}\varphi} g_{\mu\nu}. \tag{C.1}$$

Here φ and α_{ST} are dimensionless, while μ_φ is an inverse length. The source's linear nonmetricity representation is equivalent to this curvature action under its declared matter and boundary conventions. It is an established scalar–tensor class, not an independent observational identification of nonmetricity. [40]

Neither G_0 nor the scalar range μ_φ^{-1} is a renamed five-dimensional coupling or brane tension. A common action embedding these sectors has not been supplied. The comparison concerns the logic of inference and calibration.

C.2 Weak-source potentials and a common mass standard

For a weak, isolated, spherical source, the first-order physical potentials are

$$U(r)=\frac{K}{r}\left[1+B\,e^{-\mu_\varphi r}\right],$$
$$W(r)=\frac{K}{r}\left[1-B\,e^{-\mu_\varphi r}\right], \tag{C.2}$$
$$K=G_0 M,\; B=\alpha_{ST}^2 F(\mu_\varphi).$$

The form factor F depends on the source profile. The sum $U+W=2K/r$ removes the direct conformal scalar from first-order bending at fixed tensor mass. Lensing supplies $K_L=c^2 b_L \theta/4$ at this order, with b_L the light-ray impact parameter, while material acceleration contains the factor $1+B(1+\mu_\varphi r)e^{-\mu_\varphi r}$. A mass already inferred from material motion is not automatically the same calibration. [40]

In the formulas below, a_r is the positive inward acceleration magnitude in this static weak-field model. Kinematic, multipole, and environmental contributions must be handled before interpreting a measured trajectory through that radial quantity.

The approximation order matters. In the source's Solar-scale example, omission of the second-order Schwarzschild bending term creates a 6.25129 ppm mass bias, larger than its assigned 2.94304 ppm scalar dynamical residual. This is a model error-budget example, not a detected signal. Its purpose is to require a sufficiently accurate baseline before applying the inverse.

C.3 Finite-reference identification

Let stationary clocks occupy exterior radii $a<b$. Write $\eta=b/a>1$, $x=\mu_\varphi a$, and let $R_{ab}=d\tilde{\tau}_a/d\tilde{\tau}_b$ be their corrected rate ratio. Measured photon-frequency transfer must first be related to that orientation. Define

$$Z_{ab}=\frac{a c^2}{K_L}\left(1-R_{ab}\right)-\left(1-\frac{a}{b}\right),$$
$$D_a=\frac{a^2 a_r(a)}{K_L}-1. \tag{C.3}$$

At the retained order, $Z_{ab}=B\left(e^{-x}-\eta^{-1}e^{-\eta x}\right)$ and $D_a=B(1+x)e^{-x}$. The common amplitude cancels:

$$\frac{Z_{ab}}{D_a}=h_\eta(x)=\frac{1-\eta^{-1}e^{-(\eta-1)x}}{1+x},$$
$$B=\frac{D_a e^x}{1+x},\ \mu_\varphi=\frac{x}{a}. \tag{C.4}$$

Finite-reference proposition. Given a correctly shared K_L, a resolved $D_a>0$, and the isolated single-range model, a noiseless ratio in $0<Z_{ab}/D_a\le 1-1/\eta$ identifies a unique finite $x\ge 0$. [40]

Proof. The function starts at $1-1/\eta$ and tends to zero. Its derivative has numerator $e^{-(\eta-1)x}\left[1+(\eta-1)x/\eta\right]-1$, which is negative for $x>0$. It is therefore strictly decreasing away from the endpoint. The amplitude then follows from Equation C.4.

At a scalar-free null both residuals vanish and the range is unidentified. Near the long-range endpoint, the expansion is $h_\eta(x)=1-1/\eta-(\eta-1)^2x^2/(2\eta)+O(x^3)$: the linear range response cancels. These are structural limits, not defects repaired by collecting repeated measurements at effectively one radius. Noisy ratios near either boundary require a forward fit to the original observables and their covariance.

C.4 A derivative identity is not a unique signature

For residuals defined from a differentiable potential and its force,

$$C(r)=\frac{r\,U(r)}{K_L}-1,\ D(r)=\frac{r^2 a_r(r)}{K_L}-1,\qquad D=C-r\,C'. \tag{C.5}$$

The last relation follows from differentiation for any such potential. A single exponential requires additional conditions, including a constant logarithmic slope and agreement across radii. A positive sum of several exponentials satisfies the derivative identity but generally has a changing slope. [40]

A common calibration error $\widehat{K}_L=(1+\delta)\,K_L$ gives

$$\widehat{C}=\frac{C-\delta}{1+\delta},\ \widehat{D}=\frac{D-\delta}{1+\delta},\qquad \hat{\mu}_\varphi=\mu_\varphi\frac{C}{C-\delta}. \tag{C.6}$$

The generic derivative identity can survive that bias. Correct identification therefore requires calibration information or nuisance fitting in addition to the closure. This is the methodological connection with the brane normalization problem; it does not equate their actions.

Source structure remains relevant after the exponential range and amplitude have been inferred. For a uniform sphere of radius R,

$$F(z)=\frac{3(z\cosh z-\sinh z)}{z^3},\ z=\mu_\varphi R,\ F(0)=1. \tag{C.7}$$

A general positive spherical density supported inside the same radius obeys $1\le F\le \sinh z/z$. The measured B therefore restricts the microscopic coupling to $B\,z/\sinh z\le\alpha_{ST}^2\le B$ until the density

profile is specified. It does not determine the sign of that coupling, which changes together with the sign convention for the scalar field. Finite test bodies can introduce an additional source factor. The inverse proposition identifies an exterior response under its assumptions, while microscopic interpretation needs these further source inputs. [40]

This is also why the clock and dynamical channels should be fitted together at the observable level. A shared reference clock contributes correlated errors to several links, and the same lens calibration can affect all inferred residuals. Treating every derived residual as independent would assign information that the measurement design has not supplied. A forward covariance model can retain that shared information and fit the nuisance mass without taking unstable ratios near the scalar-free boundary. The source's synthetic studies illustrate such a design; they do not determine the covariance of a future experiment. [40]

C.5 Higher-order clocks and a stellar precision limit

The source completes a specified second-order static exterior clock problem using a scalar amplitude normalized at a finite matching radius. It combines the scalar correction with the physical metric, finite frequency transfer, and reciprocal ranging terms. The relevant special-function particular solution has an explicit antecedent in Schärer et al.; the finite-boundary convention and integration into the source's calculation should retain that attribution. [40] [44]

An exterior amplitude must be fitted as boundary information or obtained by an interior source calculation. Its leading weak-source expression cannot be imposed as an exact strong-body relation. Likewise, isotropic and areal radial coordinates must

be converted before comparing second-order clock coefficients with a Schwarzschild expression used elsewhere in the book.

The stellar examples expose another precision boundary. The scalar–tensor manuscript reports thirty fully coupled static configurations with two published candidate-EOS approximations. At 1.4 nominal solar masses, its GR radii are 11.70606 km for SLy and 11.31968 km for AP4. Read et al.'s rounded tabulated radii and fit errors imply approximately 11.7113544 and 11.325148 km, differences of 5.2944 and 5.468 m. The source acknowledges that this external comparison has not been reconciled across all conventions. [40] [45]

By comparison, two fixed-central-density massless examples with $\alpha_{ST}=0.002$ change their physical radii by only 1.12 and 0.24 mm. These use different matching conditions from the external benchmark; the comparison illustrates the precision scale, not a statistical error distribution. Tiny internal refinement changes cannot establish observable stellar constraints when the external and EOS uncertainties remain unresolved. Static convergence also does not supply radial stability, tidal response, or a population likelihood.

The source's tables and plots remain reported computational evidence; its executable archive was unavailable. The finite-reference proposition is a mathematical result under its assumptions. Further observational claims require the corresponding measurement and numerical support.

Appendix D Reproducible Calculations

Edition convention for reproduction. Sections D.1–D.8 describe preserved second-edition calculations. In the third-edition companion their original package is under baseline/, and those commands are run from that directory. Sections D.9–D.10 describe the new modules and are run from the third-edition package root. The supplied survey files and covariance arrays are unchanged.

D.1 What the companion calculation contains

The original analytical companion program reproduce_book.py generates eight figures, their tabulated data and a machine-readable verification record from analytical examples and benchmark constants. It uses no observational catalogue. The distance-likelihood calculation uses public observations and is documented in Section D.6. Sections D.7–D.8 document the new null-calibration and exact-sound extensions. The analytical program requires Python, NumPy, SciPy, SymPy and Matplotlib:

This A5 companion is an independent reconstruction from the printed equations. It provides the regenerated figures, explicit numerical inputs, tabulated curves and a verification record. Earlier numerical diagnostics quoted in the text retain their historical provenance; they are not asserted to be the outputs of this new run.

```
python reproduce_book.py --output-dir results
```

The output contains a `figures` directory with PNG, PDF and SVG versions; a `data` directory with CSV tables; and `verification.json` with inputs, software versions and individual comparison results. The accompanying README states the run command and evidentiary scope. Vector figure exports support resizing without losing mathematical labels.

The executable checks cover symbolic identities and independent numerical comparisons. The A5 computational companion independently reconstructs the examples and records 25 specified checks. All passed in the archived A5 run. They verify the named expressions or examples; they are not independent empirical confirmations of a cosmological model. The program stops on a failed check. Passing a floating-point tolerance certifies only the declared computation at that tolerance.

D.2 Algebra and evolution checks

The symbolic checks include the constant vacuum split, action-orbit scaling of the two gravitational coefficients, the acceleration equation, the bulk-curvature effect-size relation, the cubic and canonical-plus-cubic energy densities, the cubic quadratic and cubic fluctuation actions, current conservation, the fixed- and free-vacuum discriminants, the stable density inverse, the bulk vertex invariant, the Riccati exceptional family and the paired-window identity.

The canonical-plus-cubic example is computed by two different routes. One integrates the differential equation for $\log x(s)$ from $x(0)=1$. The other solves the conserved-current equation independently at the sampled epochs. Over $-3\le s\le 3$, their largest absolute difference in $\log x$ is approximately 1.48×10^{-11} in the original book run, and the largest relative current drift is approximately 1.91×10^{-11}. These diagnostics concern that background evolution only. They do not test bulk perturbations or an ultraviolet cutoff.

The equivalence-class check uses the exact Chapter 6 benchmark, including $k=u=0$, $(\beta_0,\beta_1,\beta_2,d)=(9.5632,3.216,0.27,10^{-4})$, $\chi=0.2$ and

$-0.5 \le s \le 0.5$. Three distinct normalizations reproduce the same expansion on the numerical comparison grid. The two values $C = 0.216$ and $C = 3$ also share $\nu(0) = 1.2$. Numerical agreement illustrates the algebraic identity; the continuum result follows from the theorem, not from the finite grid.

The covariance figure compares an exact analytical plug-in rejection probability against a separately evaluated F survival function. It is not a new Monte Carlo ensemble. The rank-two calculation assumes independent Gaussian validation vectors and the ordinary unbiased covariance estimator. Its matched Hotelling curve concerns the same experiment.

D.3 Physical-scale inputs and results

The scale calculation fixes $H_0 = 70\, km\, s^{-1} Mpc^{-1}$ and $M_4 = 2.435 \times 10^{18} GeV$. It uses $1\, Mpc = 3.0856775814913673 \times 10^{22} m$, $\hbar = 6.582119569 \times 10^{-25} GeV\, s$ and $\hbar c = 1.973269804 \times 10^{-16} GeV\, m$. These are explicit conversion inputs. The resulting reference density is $3.96594 \times 10^{-47} GeV^4$.

Table D.1. Declared physical-scale calculations.

Declared calculation	Result rounded for reading
Present reference-density ratio at $\tau_{vac}^{1/4} = 1\, TeV$	$\epsilon_{brane} = 1.98297 \times 10^{-59}$
Corresponding upper bound on $\left(H - H_{lin}\right)/H_{lin}$ under Chapter 12's assumptions	9.91484×10^{-60}

Declared calculation	Result rounded for reading
Radiation ratio at $T = 1\,MeV$, $g_{¿} = 10.75$, TeV tension	1.76830×10^{-24}
Tension scale giving radiation ratio 0.1 at that MeV benchmark	$2.05064\,MeV$
Temperature for ratio 0.1, TeV tension and fixed $g_{¿} = 106.75$	$274.708\,GeV$
Temperature for ratio 1 under the same inputs	$488.507\,GeV$
AdS radius at TeV tension and $\Lambda_{eff} = 0$	$1.17696\,mm$
Tension scale corresponding to $\ell = 0.1\,mm$	$3.43068\,TeV$
Tension scale for a present reference-density ratio of 0.01	$6.67312\,meV$
AdS radius for the preceding one-percent example	$0.856550\,Gpc$

The MeV threshold is a scale diagnostic at a stipulated ratio, not a nucleosynthesis likelihood bound. The millimetre conversion uses a specified zero-effective-vacuum relation, not a direct fit of a gravity experiment. The percent correction uses the reference excitation density and does not represent a measured cosmological deviation. Chapter 12 gives the assumptions that connect these calculations to the model.

D.4 Figure provenance and interpretation

Table D.2. Provenance of the scientific figures.

Figure	Calculation and interpretation
1.1	Constant-curvature triangle relation; a geometrical illustration
3.1	QR projection of an exponential design on a fixed 41-epoch layout; conditional information with known noise
4.1	Exact reachable-rate envelopes and the incompatible adjacent-triple example
6.1	The free-vacuum equivalence class from the explicit Chapter 6 coefficients
7.1	Uniform-window transfer functions over a declared finite frequency band
8.1	Exact Gaussian covariance-estimation calibration diagnostic
11.1	Canonical-plus-cubic sound and two-route homogeneous evolution
12.1	Direct quadratic-to-linear ratios from the stated physical benchmarks

The eight original analytical figures were generated from the preserved companion. Figure 5.1 adds the earlier conditioning experiment; Figures 13.1–13.4 show the executed profiles, residuals, null calibration and local comparison. Figures 15.1–15.2 show finite certificates and verified model pairs, Figures 16.1–16.2 show the new calibration, Figure 17.1 displays Gaussian power and Figure 18.1 illustrates the free-curvature ambiguity. Their captions identify observed, simulated and exact analytic inputs separately.

D.5 Earlier numerical results

Some earlier manuscripts report synthetic experiments, nonlinear recovery errors, posterior calculations and larger internal verification totals. Their original executable archives

were not part of the material available for this edition. Those full historical runs were not reproduced here. The present revision independently reconstructs the DESI control likelihood from public inputs and adds a new supernova and positive-quadratic analysis. It does not recreate the source clock posterior, the original 33-check suite, or every Series II simulation.

An independent reproduction of earlier source-reported results would require their original inputs, units, model branch, solver settings, random seeds where applicable and full covariance or likelihood specification. The original analytical companion is complete for its eight figures and twenty-five specified checks. The independently executed extensions have their own archived calculations and verification records; their check counts are not substituted for missing historical runs.

D.6 Executed public distance analysis

The observations directory contains four original data files, selected rows and covariance arrays, fit results, profile tables, sensitivity outputs, residuals, physical-scale calculations and two diagnostic figures. The source directory contains download, likelihood, run and plotting programs. A manifest pins repository commits and hashes. Existing raw files are checked before reuse; fetching is not needed for the supplied archive.

Run the following commands from the package root in the documented Python environment:

python source/run_observational_analysis.py

python source/plot_observational_results.py

The first program rebuilds the selected inputs and all reported fits from the included raw files. It profiles calibration nuisances rather than fixing them. The second generates profile and

whitened-residual plots in PNG, PDF and SVG, together with a compact fit CSV. No random seed is needed for this deterministic analysis. The recorded environment is Python 3.12.14, NumPy 2.3.5 and SciPy 1.17.0; environment and requirements files accompany the code.

The observational audit contains sixteen passed numerical checks, separate from the twenty-five analytical companion checks. Its log preserves the failed initial Pantheon-summary tolerance and the resolved Powell boundary issue. The numerical checks verify implementation at stated tolerances, not repeated-sampling coverage, completeness of the cosmological model, or the collaboration's entire analysis pipeline. The README identifies the remaining external-summary and perturbation limitations.

The package retains the pre-observational Word/PDF input, the approved cover assets and production scripts so that the revision can be traced and rebuilt. It is complete for the calculations executed for this book. It does not contain unavailable original archives or undistributed raw telescope observations, and does not claim to reproduce them.

Data and code access

The QR code retains the author-designated data and code folder used for the earlier editions. The new third-edition production records, scripts and reproduction guide are in the companion distributed with this edition. Their inclusion here does not assert that this external folder has been updated to contain them.



https://drive.google.com/drive/folders/
13W45ooLMzd5DXBnbmXl4mldbUWwZamYy?usp=sharing

D.7 Reproducing the pointwise null experiment

From the complete package root, run:

```
python statistics/source/run_null_calibration.py \
  --package-root . --output-dir statistics \
  --replicates 10000 --seed 20261012
python statistics/source/audit_null_calibration.py \
  --package-root . --statistics-dir statistics
python statistics/source/plot_null_calibration.py \
  --statistics-dir statistics
```

The statistics directory includes the analysis specification, every fitted simulation row, numerical and optimizer audits, a local-information record, threshold and plotting CSVs, and figures in PNG, PDF and SVG. Each figure is designed at 112 mm width. The input checksums, software versions, Gaussian scale, seed and random generator are recorded in null_calibration_summary.json. No network access, survey refetch or modification of the original raw files is required. A

fresh 10,000-draw run produces the same numerical experiment; the production run's successful first 5,000-draw prefix was continued with the same random stream after a timing-based increase in the target count. The design was not externally preregistered or blinded.

D.8 Exact-sound prediction, completion and conditioning

The scientific-revision archive includes the algebraic reserved-epoch example, the twenty-one-epoch conditioning calculation and supplementary checks of the finite-constraint constructions. All these inputs are synthetic. The proofs in Appendix F stand independently of their numerical illustrations. Run from the archive root:

```
python geometry/reproduce_geometry_extension.py
python math/verify_extensions.py
```

The geometry program records the known synthetic covariance, design normalization, singular values, invariant gradient and prediction contrast. Its six checks verify the stated identities and their numerical implementation. The mathematical validation program checks the explicit finite-constraint correction, transport bounds, fixed-error example and finite coefficient enclosures; the input and output record states every tolerance. A passed implementation check is distinct from a theorem proof or an astronomical measurement.

The archive also contains the final insertion text, the bibliography evidence register, the document assembly program and a revision log. The original raw catalogues and likelihood code are retained with their checksums. The new simulation and geometry outputs can therefore be recomputed from the delivered archive, with no new survey download. Use the accompanying 12 October 2026 scientific-revision archive

for these additions; the earlier author-designated access link records the original package location.

D.9 Reproducing the positive-signal calibration

D.9.1 Inputs, identities and deterministic streams

The source experiment is the unchanged background-distance likelihood archived with the second edition. Four raw survey files define the numerical inputs: desi_dr2_mean.txt, desi_dr2_cov.txt, Pantheon+SH0ES.dat and Pantheon+SH0ES_STAT+SYS.cov. Their full SHA256 values and the checksums of the baseline likelihood and prior null-calibration source appear in statistics/run_v11_clean/verification/input_hashes.json. The original download manifest records the upstream repository commits. The third-edition calculation reads these files and never rewrites them.

The frozen protocol is statistics/PROTOCOL.json, with an identical copy in statistics/run_v11_clean/PROTOCOL.json. Its implementation amendment records a correction to the numerical statistic, not a change in the generating grid, random seeds, sample counts, test direction or decision threshold. Superseded and interrupted implementation records are preserved in statistics/verification/excluded_run_records.zip and are excluded from all production summaries. The final audit checks that the protocol and every input hash remain unchanged over the production run.

Each stream is determined by the tuple $\left(202610120316, i_q, i_m, i_A, s\right)$ passed through NumPy SeedSequence to PCG64. The indices are the zero-based positions in the protocol lists; stage $s=0$ generates 399 calibration vectors and stage $s=1$ generates 200 independent

validation vectors. The vectors contain 1603 Gaussian coordinates in the same BAO-then-supernova order as the likelihood. A stored SHA256 of every realized coordinate vector allows regeneration to be checked without duplicating a large uncompressed noise matrix. The pseudorandom generator, software versions and seed rule are part of the reproducible numerical experiment; the mathematical theorem assumes ideal independent Gaussian draws.

D.9.2 Profiling and numerical coordinates

The optimizer uses fixed coordinates $u=(m-0.30)/0.01$ and $v=q/0.0003$. The fixed reference amplitude 30 and intercept 23.8 make the coordinate origin independent of the historical-data fit. They are computational reference values, not parameter priors. The complete nonlinear means are evaluated with 64-node Gauss–Legendre integration, while analytic derivatives supply gradients. The original full covariance factorizations are reused. BAO amplitude and supernova-intercept minimization is analytic at every nonlinear parameter evaluation.

The physical lower matter boundary at a fixed positive correction is handled directly. Combining positive effective vacuum with the AdS inequality gives $(m+2q)^2>4q$ for the relevant branch. The restricted optimizer therefore enforces the original matter bound together with $m>2\sqrt{q}-2q$. The artificial numerical upper bounds and the positive-vacuum condition remain those of the baseline. Their inactivity at the realized fits is an audited output, not an assumed property of every possible future data vector.

L-BFGS-B uses the recorded tolerances and a projected-gradient check. The prescribed bounded Nelder–Mead fallback is used when the status or stationarity criterion requires it. The zero

edge is retained as a nested candidate for the global alternative. The global and zero fits do not depend on which positive correction is being tested. Restricted fits produce only the positive upper statistic. Small negative differences caused by roundoff are clipped to zero; larger nesting failures would fail the audit. Additional multistarts evaluate selected draws without replacing the production records silently.

D.9.3 Ranks, validation decisions and uncertainty

The raw U and D values are stored together with integer ranks obtained with a rounding unit of 10^{-8} for each nonnegative statistic. The rank convention is the same for the observations, calibration draws and validation draws. Upper-tail comparisons use greater-than-or-equal, so ties are treated conservatively. Rejecting at $p \le 0.05$ means that at most 19 of 399 calibration statistics exceed or tie the test statistic at every one of the nine nuisance points. No simulated p-value is set to zero.

For a validation cell, the coverage count is the number of its 200 fresh vectors for which the maximum upper p-value exceeds 0.05. The detection count is the number for which the maximum p-value against the nine zero-signal banks is at most 0.05. The fixed-reference comparison records $U_q \le 2.705543454$. Statistics, ranks and decisions are preserved separately, so a reviewer can reconstruct every reported count without reoptimizing distances.

If k successes occur in $n = 200$ independent validation draws conditional on fixed banks, the reported two-sided 95% interval for that conditional success probability is [61]

$$p_L = B^{-1}_{k,n-k+1}(0.025), \quad p_U = B^{-1}_{k+1,n-k}(0.975). \tag{D.1}$$

Here $B_{a,b}^{-1}$ is the beta-distribution quantile; set $p_L = 0$ when $k = 0$ and $p_U = 1$ when $k = n$. These intervals are pointwise across the 72 cells. There is no pooled binomial interval pretending that validation outcomes from different generating cells share one common success probability. There is also no claim that the minimum of the displayed pointwise lower limits is a simultaneous bound over the grid.

D.9.4 Reproduction and evidence hierarchy

Run statistics/source/run_positive_calibration.py with the archived baseline directory and statistics/run_v11_clean as the output directory. The protocol fixes all scientific choices; the worker count changes scheduling only. Completed JSONL prefixes are resumed only after their sequential replicate identifiers and regenerated noise hashes agree. Then run statistics/source/audit_positive_calibration.py, followed by the plotting and chapter-building scripts. The summary, validation and inversion records are generated from the complete checkpoints, not manually transcribed into tables.

There are three useful audit levels. File integrity verifies that the observations and protocol have not changed. Numerical agreement checks the objective, derivatives, quadrature, optimization and equality of statistical maps. Inferential validity concerns the stated Gaussian experiment, exchangeability, nuisance inclusion and historical selection. Passing the first two levels cannot establish a physical model, validate a survey covariance outside its assumptions or remove the third level's restrictions. Conversely, a mathematically valid rank rule still requires reliable source data and a consistently computed statistic.

The primary result is the frozen finite-grid procedure and its verified implementation. Fresh conditional validation is an

empirical check on its realized banks. The historical table is a retrospective application of that procedure. Continuous nuisance coverage, a continuous upper endpoint, unknown covariance, additional active boundaries and independent future data are outside the delivered calibration. Their absence is explicit so that the next extension has a checkable target rather than an ambiguous confidence label.

D.10 Reproducing the new mathematical and physical certificates

The companion separates the preserved second-edition calculation under baseline/ from the third-edition modules math/, statistics/, physics/ and curvature/. Commands printed in Sections D.1–D.8 refer to the preserved baseline root. Commands in the new sections refer to the third-edition package root. This distinction prevents files with similar names from different editions being mistaken for one experiment.

The finite-observation program math/reproduce_certificates.py generates the seventeen-node sound inputs, overlapping windows, density intervals, explicit witnesses, exclusions, correlated polytope and two-model forward checks. Its verification records separate exact rational arithmetic, outward interval calculation and ordinary plotting diagnostics. The proof-status file states the scope of the executable certificate and the analytical claims.

```
python math/reproduce_certificates.py
```

The physics module contains the independent effective-fluid integration, exact Fraction coefficient identities, Gaussian power calculations and synthetic validation draws. The Chapter 18 script produces the free-curvature history, rational interval checks, physical representatives and six-epoch contrast. Neither module reads astronomical observations.

```
python physics/compute_chapter17.py
python curvature/reproduce_free_curvature.py
```

The independent Chapter 18 audit uses higher precision and a separate singular-value construction of the reserved contrast. Numerical agreement does not replace the displayed proof, but it checks algebraic transcription, physical representatives and reported values. The independent Chapter 15 review distinguishes the rigorously executed examples from unresolved cases and checks the preprocessing assumptions needed for outward inclusion.

The manuscript integration uses archived JSON blocks and Pandoc to create editable native Office Math in Word. Its integrity record verifies retention of every original numbered equation, the section geometry and page-reference targets. Final pagination is regenerated from the rendered book. The cover illustrations remain conceptual artwork; only the scientific plots in the text encode calculated values.

The distributed package manifests specify every file required by the chosen reproduction command and its SHA-256 checksum. The edition history and earlier supplied manuscripts remain available in the preserved Editions 1–2 archive. A file included for provenance is not counted as a second independent confirmation. A simulation row excluded during implementation review is not included in the production sample count.

Appendix E Source Register and Result Map

E.1 The manuscript sequence

This edition draws on 27 supplied research manuscripts: twelve articles in the first collected volume, twelve separate Series II papers, a separate four-dimensional scalar–tensor study, the predecessor bulk-geometry paper and the final dynamical-completion paper. The source collection thus contains both a sustained braneworld inverse program and an independent comparison model. A source label identifies a manuscript; it does not imply journal publication or peer review. Published primary references are listed separately by their bibliographic records in the References.

The book reorganizes the material by logical dependency. It does not present the sequence of source papers as a sequence of independent empirical confirmations. Repeated formulas and synthetic examples are consolidated, conventions are reconciled, and distinct assumptions are retained where the source problems differ.

Table E.1. Source manuscripts and their destinations.

Source	Main contribution used in the book	Main destination
Series I, I	Finite geometrical information and the operational inverse	Chapters 1–3
Series I, II	Finite-epoch expansion design and conditioning	Chapter 3
Series I, III	Matter calibration and normalization freedom	Chapters 3–4
Series I, IV	Bounded calibration drift and compatible gains	Chapter 4
Series I, V	Complete-curve matter restrictions	Chapter 4

Source	Main contribution used in the book	Main destination
Series I, VI	Shared finite histories and exact counterexamples	Chapter 4
Series I, VII	Smooth completion and conic representations	Chapter 4
Series I, VIII	Point sound anchors and regularity limits	Chapter 4
Series I, IX	Integrated sound windows and common reconstruction	Chapter 4
Series I, X	Sound coordinates and column dependence	Chapters 5–6
Series I, XI	Exceptional Riccati sound histories	Chapters 5–6
Series I, XII	Synthesis of the first inverse sequence	Chapters 1–6 and 14
Series II, I	A stipulated golden-scale sound family	Chapter 7
Series II, II	Window transforms, offset and gain calibration	Chapter 7
Series II, III	Algebraic recovery of two frequencies	Chapter 7
Series II, IV	Blind spots and a third window	Chapter 7
Series II, V	Joint sound–expansion local rank	Chapter 7
Series II, VI	Weak information and observational design	Chapter 7
Series II, VII	Shared-parameter goodness-of-fit calibration	Chapter 8
Series II, VIII	Selected-space validation and leakage	Chapter 8
Series II, IX	Conservative finite-sample regions	Chapter 8
Series II, X	Unknown covariance and validation replicates	Chapter 8
Series II, XI	Uniform sound uncertainty and outer inversion	Chapter 9

Source	Main contribution used in the book	Main destination
Series II, XII	Statistical synthesis and scope corrections	Chapters 8–9 and 14
Predecessor bulk paper	Free-vacuum equivalence classes and bulk invariants	Chapter 6
Final dynamical paper	Covariant normalization, kinetic audit and scale limits	Chapters 10–14
Separate scalar–tensor study	Clock, lensing and dynamics comparison in another action	Appendix C

The complete bibliographic titles appear in the References. [1; 2; 12; 10; 13; 11; 16; 17; 15; 18; 19; 5; 21; 23; 22; 24; 25; 26; 27; 28; 29; 30; 20; 6; 3; 4; 40]

E.2 Relation to the final dynamical paper

The final paper, *Dynamical Completion and Observational Limits of Identifiable Bulk Geometry*, supplies the principal action-level development. Its 26 numbered equations are incorporated through the covariant and normalization discussion of Chapter 10, the kinetic construction and fluctuation audit of Chapter 11, and the hierarchy, acceleration and varying-tension analysis of Chapter 12. The observation interfaces are developed in Chapter 13 and the combined conclusions in Chapter 14. The book also restores the earlier reconstruction results needed to understand what that final paper is completing.

The most consequential convention is the separation between the split reference coefficient and the vacuum-subtracted background coefficient. The background coefficient depends on the total constant vacuum stress: moving a constant

contribution between the split brane term and the matter vacuum leaves that total and the background coefficient unchanged. The distinct classical scaling of Chapter 10 changes the background coefficient while preserving the split reference coefficient. The direct quadratic-to-linear correction therefore uses the total constant vacuum stress after the vacuum subtraction has been specified. A corresponding local Newton coupling requires a localized-source matching calculation under the chosen matter standards.

This edition integrates the source program with consistent notation, complete finite-constraint proofs, a reserved-epoch test, conditioning figures, explicit evidence categories and a reproducible computational record. The proof labels identify statements proved under the specified assumptions in this volume. Historical priority for a new result remains a separate literature question; the source register makes the closest verified connections explicit.

The observational revision additionally supplies Sections 13.7–13.13 and their downloadable calculation. References 46–48 identify the Pantheon+ publication and the two public input repositories. References 49–50 establish relevant prior braneworld distance and nucleosynthesis work. This extension is an application with an explicit evidence boundary, not a new claim to the origin of the background equations.

The 12 October scientific revision adds Sections 5.5–5.6, 13.14–13.15, 14.6 and Appendix F. References 51–58 document close precedents for dark-sector and tension degeneracies, information splitting, boundary likelihoods and kinetic-scalar brane models. These citations narrow the contribution claim to the hypotheses and results actually developed here.

E.3 Verification and documentary boundaries

The scientific review checked the final source against the relevant earlier derivations, examined sign and normalization conventions, and compared the book's central formulas across chapters. It explicitly separates full-history results from finite sampling, structural rank from numerical conditioning, and local scalar stability from stability of the coupled brane–bulk system. It also retains the source's reported statistical shortcomings when later diagnostic experiments address a different question.

The References use supplied-document status for the research manuscripts unless an independently identifiable publication record is available. The book author is Mohammed F. A. Alghenaim. Bibliographic authorship of earlier supplied sources is retained only when their documents explicitly establish it. No academic affiliation, degree, institutional endorsement or biographical history has been inferred for this edition.

E.4 Relation to established literature

The starting background is the established braneworld junction and effective-gravity framework. The density-squared term and dark-radiation integration constant are inherited ingredients, and earlier work already used supernova distances to test brane backgrounds. The observational addition in this edition is a documented fit to specified public DESI and Pantheon+ inputs, together with numerical controls and a physical-scale interpretation; it is not the first distance test of a braneworld. [7–9; 49]

Kunz formulates a dark degeneracy in which gravitational information constrains total stress-energy while the

decomposition into dark components remains underdetermined. Liddle and Taylor exhibit an inflationary reconstruction degeneracy between the potential and brane tension. These are direct antecedents to the motivation for studying equivalence classes. The present analysis has a different input and target: a conserved barotropic sound history defines J, and the book proves rank criteria and a free-vacuum orbit for the resulting four-column background representation. Its candidate contribution is that explicit classification and its geometric invariants under the declared assumptions, rather than the general observation that cosmological parameters can be degenerate. [51; 53]

The fluid and scalar constructions also have close precedents. Arroja and Sasaki give conditions for equivalence between an irrotational barotropic perfect fluid and a k-essence scalar; Quercellini, Bruni and Balbi study affine equations of state; Perković and Štefančić reconstruct purely kinetic descriptions from sound-speed information. Chimento and Richarte analyze kinetic-scalar brane cosmologies in a different construction, including a dynamically incomplete atypical model. The contribution of Chapters 10–11 is the integration of local realization, action normalization and vacuum consistency with this inverse. The pure-cubic zero-gradient defect established here must not be identified with a different model's incompleteness merely because both concern kinetic actions. [33–35; 58]

The statistical machinery likewise has a prior foundation. Gaussian randomization into independent components is a special case of data fission and information splitting. Accordingly, Equation (8.6) should be credited to this established construction. The scientific application developed here concerns selected sound subspaces, bounded primary

leakage and propagation into physical inverse sets. Gaussian independence requires the specified covariance; adding noise does not estimate an unknown covariance or create an independent cosmological measurement. The asymptotic interpretation of a likelihood ratio at a physical boundary belongs to the established nonregular likelihood literature and must be matched to the actual nuisance structure. [52; 55–57]

Adding perturbation data also requires a defined comparison class. Kunz and Sapone show that an appropriately generalized dark-energy description can reproduce modified-gravity perturbative behavior in the setting they study. Consequently, a new growth or sound observable does not by itself guarantee unique discrimination of extra dimensions. A useful extension must declare the permitted effective stresses, entropy and anisotropic stress, gravitational couplings, bulk boundary conditions and calibration assumptions. Within those choices, the book's rank conditions and invariants provide explicit targets for testing and for identifying which additional information removes which freedom. [14; 54]

E.5 Contribution map and evidentiary categories

The categories describe the support for each statement. A proof, a constructed example and a likelihood evaluation answer different questions, and may appear in the same chapter. The unpublished manuscript sequence records provenance; its repeated treatment of a result does not constitute independent external confirmation.

Established relation. A relation or method adopted from prior literature, whether or not rederived here.

Theorem proved in this volume. A statement accompanied by a proof under stated hypotheses. This label concerns auditability and does not assert worldwide priority.

Synthetic example or benchmark. A constructed input, analytic illustration or chosen numerical scale; it supplies no new cosmological observation.

Observed likelihood result. A computation using specified public measurements and their observation model, conditional on the fitted model and calibration choices.

Proposed test. A defined experimental or computational extension whose physical measurement or full forward analysis has not been executed here.

Table E.2. Contribution map with evidence and audit locations.

Item	Evidence, contribution and scope
Junction law and scalar sound formula	**Established relation.** The quadratic-density and dark-radiation background terms, and $c\varphi^2 = F_X/\left(F_X+2XF_{XX}\right)$, are established ingredients. The book fixes conventions and tracks their implications for the inverse. **Location:** Chs. 2, 10–11; [7–9; 14; 32]
Dark-sector and reconstruction degeneracy	**Established relation.** The general possibility of gravitational degeneracy and an inflationary potential–brane-tension degeneracy predate this volume. They motivate a precise classification of what the present data assumptions identify. **Location:** Related-literature section; [51; 53–54]
Exceptional sound histories	**Theorem proved in this volume.** The equivalence between dependence of $\{1,J,J^2,\exp(-4s)\}$ and the Riccati condition $D\chi \equiv 0$ is proved for the declared interval and regularity class. Pointwise failure, functional failure and finite-design conditioning remain distinct. **Location:** Theorem 5.1; §§5.2–5.4

Item	Evidence, contribution and scope
Finite-constraint completion and recovery	**Theorem proved in this volume.** Appendix F proves exact completion with a relaxed positive sound margin, finite sound anchoring, compatible-set contraction with shrinking error, density-difference calibration and finite invariant enclosures. **Location:** §§4.5–4.6, 6.4, 6.6; Appendix F.
Free-vacuum family and surviving geometry	**Theorem proved in this volume.** The complete admissible C-family is explicitly parameterized. Rank-four coefficients determine L and d under the stated model and sign conditions, although density normalization and split tension vary. **Location:** Theorems 6.1–6.2; §§6.2–6.6
Barotropic and purely kinetic realization	**Established relation.** Fluid–scalar equivalence, affine equations of state and sound-based kinetic reconstruction have direct precedents. The book supplies a local realization in its conventions and audits the visited field range, vacuum and normalization. **Location:** Chs. 10–11; [33–35; 58]
Known-covariance information split	**Established relation.** The independent Gaussian training and validation construction is established information splitting/data fission. Its use here targets selected sound components with declared projection and leakage assumptions. **Location:** §8.3, Eq. (8.6); [52; 55]
Conditional validation and inverse sets	**Theorem proved in this volume.** The volume gives proofs for its specified-null and selected-subspace experiments and develops sound-uncertainty propagation for the inverse. These are restricted guarantees, not a new general theory of post-selection inference. **Location:** Props. and constructions in Chs. 8–9; [52; 55–57]
Reserved-epoch prediction and conditioning	**Conditional proposition and synthetic calculation.** A fixed Gaussian contrast predicts a fifth expansion epoch from four training epochs. A constructed design quantifies the loss of precision near the Riccati exception. **Location:** Proposition 5.2; §§5.5–5.6.

Item	Evidence, contribution and scope
Two-normalization orbit illustration	**Synthetic example or benchmark.** The $\chi = 0.2$ example constructs identical expansion and sound histories. The split-tension ratio is about 193; the corresponding whole-action normalization factor is about 13.89. The example is a counterexample to uniqueness under its inputs. **Location:** §§6.4–6.5 and computational companion
Cubic sound and radiation temperatures	**Synthetic example or benchmark.** The value 1/5, exponent −18/5 and the temperatures 274.7/488.5 GeV follow from declared kinetic and radiation inputs. Their algebra is reproducible; they are not measured universal constants or observed transition energies. **Location:** Chs. 11–12; §14.5
DESI and Pantheon+ Ω_q profile	**Observed likelihood result.** A defined dust-background fit gives a zero-boundary optimum and positive profile crossings. The result concerns the retained compressed distances, covariance and nuisance treatment; a confidence label requires the specified calibration. **Location:** §§13.7–13.13; [43; 46–48; 56–57]
Pointwise nonlinear null calibration	**Synthetic calibration experiment for an observed-data statistic.** Ten thousand Gaussian vectors are refitted at one fitted zero-correction control. Null-tail calibration and local sensitivity are reported; upper-endpoint coverage is not inferred. **Location:** §§13.14–13.15; D.7.
Joint sound, expansion and absolute-matter experiment	**Proposed test.** A closed perturbation and measurement model would allow the rank, representation and normalization conditions to be tested on common observations, with boundary and selection calibration where required. **Location:** §§13.13, 14.4–14.5; testability register

This map makes a bounded contribution claim. A finding that no closer paper was retrieved would not establish novelty. Any

stronger priority statement requires a separate, comprehensive comparison of mathematical hypotheses and conclusions.

E.6 Contributions and boundaries of the third edition

Chapters 15–19 are additions to the second-edition text. The original chapters and display equations remain traceable to their preserved source, while the front matter and result register now describe the expanded scope. The new mathematical statements are identified as proofs included in this edition. This wording does not assert that no equivalent result has appeared in a different formulation.

The finite-mesh transport and normalization arguments extend the common-history and recovery framework already used in Chapters 4–9 and Appendix F. The convex invariant projection applies standard convexity and Schur-complement reasoning to the particular geometric combination. Its exact rational example and the verified near-exception model pairs are new executed companion studies. The rank and curvature classification in Chapter 18 is derived directly for the enlarged five-column inverse and independently checked in the companion.

The calibration method has direct statistical antecedents. Dufour develops Monte Carlo tests with nuisance maximization, including finite-sample and discrete-statistic issues [59]. Cowan and collaborators distinguish detection and one-sided exclusion statistics in likelihood-based testing [60]. Clopper and Pearson supply the classical binomial-tail interval used to report simulation uncertainty [61]. Phipson and Smyth explain the discrete Monte Carlo rank treatment and the need to include the observed rank [62]. Chapter 16 applies those principles to the retained likelihood and its declared grid; it does not claim invention of a general calibration method.

The background comparison is connected to the established dark degeneracy and effective-stress reasoning [51; 54]. Chapter 17 gives the explicit positive-component representation for Eq. (13.5), the identical-action estimation bound, the linked kinetic consistency relation, and a complete Gaussian discrimination argument under stated assumptions. Convex prediction-set testing has the antecedent recorded in [63]. Its exact fixed-size Gaussian specialization is proved in the chapter, and its nonconvex limitation is demonstrated explicitly.

Table E.3. Third-edition result map. The evidence category belongs to each stated result and its assumptions.

Addition	Evidence	Principal scope
Finite common-path certificates	Proofs and outward checks	Fixed sound class and calibrated finite data; Ch. 15
Correlated geometric bounds	Exact convex and rational certificates	Positive quadratic coefficient; Ch. 15
Finite recovery obstruction	Verified physical model pairs	Declared deterministic noise norm; Ch. 15
Positive-signal calibration	43,128 nonlinear simulated fits	Frozen discrete grid and retained likelihood; Ch. 16
Observable-equivalence analysis	Proofs and synthetic calculations	Specified effective fluids and observation laws; Ch. 17
Free-curvature classification	Complete proof and exact example	Causal exact sound and fixed reference scales; Ch. 18

The observational evidence has not multiplied with the number of simulated data vectors. All new nonlinear calibration vectors are generated from the same retained survey observation model. The physical-comparison and curvature examples are constructed. The finite-grid procedure was chosen retrospectively and is not an externally preregistered cosmological measurement. No new experimental

confirmation, unrestricted continuous-parameter coverage, full bulk perturbation solution, external peer review or global priority is asserted by the new calculations.

AI tools assisted drafting, calculation, document preparation and internal cross-checks. The proof and code record is inspectable, but internal agreement is not independent scientific peer review. Author approval for subsequent publication, source verification and responsibility for the scientific claims remain distinct from the fact that a document and its companion can be reproduced.

Appendix F. Finite-constraint completion and recovery certificates

The results in this appendix make explicit three distinctions used in the main text: a weak history versus a smooth completion, refinement of a measurement mesh versus reduction of measurement uncertainty, and algebraic identification versus stable physical conversion. The gravitational model, the vacuum split, and the supplied background coefficients remain those of Chapters 4–6. None of the arguments selects a microscopic matter law or establishes a higher-dimensional origin for an observed expansion.

F.1. A right inverse for the finite constraints

Let $I=¿$ have positive length, and let

$$s_{-}=s_0<s_1<\cdots<s_N=s_{+¿¿} \tag{F.1}$$

be the ordered union of the density epochs and all sound-window endpoints. Repeated endpoints are merged. For a positive absolutely continuous rate q, define

$$\begin{aligned} v(s)&=v(s_{-})-\int_{s_{-}}^{s} q(t)\,dt,\\ p&=-v+\frac{q}{3},\ \chi=-1-\frac{q'}{3q}. \end{aligned} \tag{F.2}$$

The sound relation is understood almost everywhere for a weak history. Set $A_m=3(1+m)$ and $B_m=3(2-m)$. The margin $m\le\chi\le 1-m$ is equivalent to

$$q'+A_m q\le 0,\ q'+B_m q\ge 0. \tag{F.3}$$

All densities below have a positive terminal value, so positivity of q also guarantees positive density throughout the interval.

Lemma F.1 — Independent correction of node values and cell integrals. On any open neighborhood of I, the map from smooth functions to the $N+1$ node values and N cell integrals has a linear right inverse whose image is finite dimensional. In particular, corrections tending to zero in these $2N+1$ measurements can be realized by corrections tending to zero in the $C^1(I)$ norm.

Proof. Choose smooth functions φ_i with disjoint small neighborhoods of the nodes as supports and $\varphi_i(s_j)=\delta_{ij}$. At an endpoint, the support is allowed to extend outside I. For each cell choose a smooth function ψ_j supported strictly inside (s_{j-1},s_j), with integral one. Write

$$M_{ji}=\int_{s_{j-1}}^{s_j}\varphi_i(s)\,ds.$$

For prescribed node corrections a_i and integral corrections b_j, set

$$\begin{aligned} r(s)&=\sum_{i=0}^{N} a_i\varphi_i(s)\\ &+\sum_{j=1}^{N}\left(b_j-\sum_{i=0}^{N}M_{ji}a_i\right)\psi_j(s). \end{aligned} \tag{F.4}$$

The second sum vanishes at every node, and its integral over a cell corrects precisely the integral left by the first sum. Thus $r(s_i)=a_i$ and $\int_{s_{j-1}}^{s_j} r=b_j$. Because the basis is fixed and finite, its C^1 norms give a finite bound for the norm of this right inverse. This bound depends on the mesh and the chosen supports; no mesh-independent bound is asserted. ▫

The construction identifies the required independence of the finite constraints. An arbitrary assertion that small local corrections exist would not by itself establish it.

F.2. Smooth completion with exact finite data

Theorem F.2 — Completion with a relaxed positive sound margin. Suppose $q>0$ is absolutely continuous on I and satisfies Equation F.3 almost everywhere for $0<m<1/2$. For every $0<m'<m$, it has smooth positive approximants $\tilde{q}$ with

$$\begin{gathered}\tilde{q}(s_i)=q(s_i),\\ \int_{s_{j-1}}^{s_j}\tilde{q}(s)\,ds=\int_{s_{j-1}}^{s_j}q(s)\,ds,\\ m'<-1-\frac{\tilde{q}'}{3\tilde{q}}<1-m'(s\in I).\end{gathered}\tag{F.5}$$

Their uniform distance from q can be made arbitrarily small. The reconstructed densities converge in $C^1(I)$, retain every density node exactly, and have one smooth barotropic pressure law on the visited density interval. Every uniform sound mean whose endpoints are among the nodes is retained exactly.

Proof. The differential inequalities and compactness imply that q is bounded and has a bounded weak derivative. Extend it continuously beyond the two endpoints by exponential pieces with logarithmic slopes in $[-B_m,-A_m]$. Continuity prevents a point-mass contribution to the weak derivative at the joins, so Equation F.3 continues to hold almost everywhere on the extended interval.

Convolve this extension with a nonnegative smooth compactly supported kernel of integral one. For a sufficiently small kernel width ε, the resulting q_ε is smooth, positive, and satisfies

$$\begin{aligned} q_\varepsilon' + A_m q_\varepsilon \le 0, \\ q_\varepsilon' + B_m q_\varepsilon \ge 0 \end{aligned} \tag{F.6}$$

on I. These inequalities follow by convolving the corresponding distributional inequalities; they do not require convergence of the original derivatives. Also $q_\varepsilon \to q$ uniformly. In particular, if $q_{min} = min_I\, q > 0$, then $min_I\, q_\varepsilon \ge q_{min}/2$ for small ε.

Apply Lemma F.1 to the differences between the original and smoothed node values and cell integrals. It produces $r_\varepsilon \to 0$ in $C^1(I)$ such that $\tilde{q} = q_\varepsilon + r_\varepsilon$ satisfies the first two lines of Equation F.5 exactly.

Put $\Delta_m = 3(m - m') > 0$. Before this correction, the inequalities at the relaxed margin have the strict reserves

$$\begin{aligned} q_\varepsilon' + A_{m'} q_\varepsilon \le -\Delta_m q_\varepsilon, \\ q_\varepsilon' + B_{m'} q_\varepsilon \ge \Delta_m q_\varepsilon. \end{aligned} \tag{F.7}$$

Choose ε small enough that

$$\begin{aligned} \| r_\varepsilon \|_\infty < \frac{1}{2} \min_I q_\varepsilon, \\ \| r_\varepsilon' \|_\infty + B_{m'} \| r_\varepsilon \|_\infty < \Delta_m \min_I q_\varepsilon. \end{aligned} \tag{F.8}$$

Positivity and both strict relaxed inequalities then survive the correction. This proves the third line of Equation F.5.

Integration constructs $\tilde{v}$ with the original initial value. Its cell integrals give all original density nodes, and its positive rate makes it strictly decreasing. The terminal density remains positive. Smooth inversion of $s \mapsto \tilde{v}(s)$ therefore defines one smooth pressure function $\tilde{p}(\tilde{v})$. Uniform convergence of the rates implies C^1 convergence of the densities.

Finally, for any included endpoints $a < b$,

$$\int_a^b \widetilde{\chi}(s)\,ds = -(b-a) - \frac{1}{3}\log\frac{\widetilde{q}(b)}{\widetilde{q}(a)} \quad \text{¿} \int_a^b \chi(s)\,ds. \tag{F.9}$$

Thus exact uniform means, and hence any intervals containing those means, are preserved. ▫

Finite calibration restrictions that depend only on the retained node densities can be retained with the same node gains. The theorem does not preserve a supplied residual or proxy curve between nodes. Nor does it preserve the original sound function pointwise or provide a derivative bound on the completed sound.

Why the relaxed margin is necessary

The requirement $m' < m$ is substantive. Take a cell of length Δ, constants $A < B$, and endpoint rates strictly satisfying

$$e^{-B\Delta} q_0 < q_1 < e^{-A\Delta} q_0.$$

The lower envelope

$$q_-(t) = \max\{q_0 e^{-Bt}, q_1 e^{A(\Delta - t)}\} \tag{F.10}$$

switches branches at an interior point. Its left and right derivatives there are $-Bq_-$ and $-Aq_-$, which differ. If the density drop equals $\int_0^\Delta q_-$, every admissible continuous rate must equal q_-: the nonnegative continuous difference from this envelope has zero integral. Consequently no C^1 rate preserves these endpoint rates, this extremal drop, and the same differential bounds. This counterexample also applies when $A = A_m, B = B_m$ for a positive $m < 1/2$.

At the physical boundary $m=0$, relaxation to a smaller positive margin is unavailable. A general smooth-completion claim within $0\le\chi\le1$ is therefore false without additional slack. Likewise, a continuous nonnegative sound profile with an exactly zero mean on a window must vanish on that whole window; an arbitrary positive point anchor cannot be inserted there.

F.3. Point sound anchors without a derivative budget

Proposition F.3 — Finite point anchors can be imposed in an interior class. Under the hypotheses of Theorem F.2, prescribe $\chi(z_j)=a_j$ at finitely many distinct interior points, with $0<a_j<1$. There is a smooth completion retaining all the density nodes, node rates and sound means of Theorem F.2, attaining these point values, and satisfying some strictly positive sound margin. No fixed bound on χ' is imposed.

Proof. First obtain a smooth completion $\acute{q}$ with a positive margin and sound $\acute{\chi}$. Around the z_j, choose disjoint smooth cutoffs θ_j equal to one at their centers, taking values in $[0,1]$, and supported in intervals of width tending to zero. Define

$$\chi_\delta=\Big(1-\sum_j\theta_j\Big)\acute{\chi}+\sum_j\theta_j a_j. \tag{F.11}$$

This convex interpolation has a common positive margin $\mu_0=min\{\text{margin of }\acute{\chi},a_j,1-a_j\}>0$, and it takes the prescribed values. Its L^1 distance from $\acute{\chi}$ tends to zero. Solve

$$q_\delta(s)=\acute{q}(s_-)\exp\big[-3(s-s_-)\big]\times\exp\left[-3\int_{s_-}^{s}\chi_\delta(t)\,dt\right]. \tag{F.12}$$

It follows directly that $q_\delta \to \acute{q}$ uniformly, so the errors in the finite rate and integral constraints tend to zero.

These errors must now be corrected without changing the imposed sound values. Require each correction to satisfy

$$r'(z_j)+3(1+a_j)r(z_j)=0. \tag{F.13}$$

The right inverse in Lemma F.1 can be constructed in this restricted space. All cell-integral bumps are placed away from the finitely many anchors. A node bump is also placed away from them unless its node is itself an anchor. At such a coincident point $s_i=z_j$, multiply an even cutoff, equal to one at the node, by $\exp\left[-3(1+a_j)(s-s_i)\right]$. This gives the prescribed unit node value and derivative $-3(1+a_j)$. Supports exclude all other nodes and anchors. Formula F.4 still corrects all the measurements and now also satisfies Equation F.13. Fix this correction basis independently of the shrinking sound-patch width. Its operator norm is then finite and constant throughout the limiting argument.

The correction tends to zero in C^1. As in Equation F.8, a final margin smaller than μ_0 preserves positivity and the differential bounds. At each anchor, Equation F.13 preserves the exact relation between the corrected rate and its derivative, so the sound value is unchanged. ▫

The cutoff derivatives grow as their supports shrink. The proposition consequently supplies no result for a class with a fixed Lipschitz bound on χ. The envelopes and three-node criterion in Section 4.5 concern that different, more restrictive class.

The three-node criterion with a fixed Lipschitz budget

For completeness, take $s_0<s_1<s_2$, densities $v_0>v_1>v_2>0$, and the class $m\le\chi\le 1-m$ with Lipschitz constant at most L_χ. Suppose the finite sound anchors satisfy their range bounds and the pairwise Lipschitz inequalities. The envelopes $\chi_-, \chi_{+¿¿}$ in Equation 4.18, with $L=L_\chi$, then belong to this class, attain all the anchors, and bound every admissible sound profile pointwise. Let Q_χ be normalized at s_0, and define

$$R[\chi]=\frac{\int_{s_1}^{s_2} Q_\chi(s)\,ds}{\int_{s_0}^{s_1} Q_\chi(s)\,ds}.$$

With no independently prescribed rate normalization, the three densities admit a history in this class if and only if

$$R¿$$

To prove the ordering, if $\chi_a\ge\chi_b$, the ratio Q_{χ_a}/Q_{χ_b} is nonincreasing. Its average with weight Q_{χ_b} on the later cell is no larger than its average on the earlier cell, giving $R[\chi_a]\le R[\chi_b]$. This proves necessity. The convex family $(1-t)\chi_{+¿+t\chi_-¿}$, $0\le t\le 1$, retains the anchors, range bounds and Lipschitz budget. Its continuous ratio covers the interval between the two envelope ratios. For a profile attaining the required ratio, choose $C=(v_0-v_1)/\int_{s_0}^{s_1} Q_\chi>0$ and integrate $q=CQ_\chi$. Both density drops then match and the density remains positive. This proves sufficiency. The argument does not extend by applying separate triple tests with separately chosen profiles when more nodes are supplied.

F.4. Dense sound windows identify the fixed-vacuum parameter

Keep $b, u, d, S, \kappa_0, a_¿$ fixed. Let a true history have parameter $\eta_¿ \geq 0$, positive strictly decreasing density $v_¿$, positive absolutely continuous rate $q_¿ = -v_¿'$, and $\chi_¿ = -1 - q_¿'/(3q_¿) \in [0,1]$ almost everywhere. Its residual is

$$R = v_¿ + \eta_¿ v_¿^2 > 0,$$
$$f_\eta(R) = \frac{2R}{1+\sqrt{1+4\eta R}}. \tag{F.14}$$

Let K be a fixed compact subset of ¿, containing $\eta_¿$, on which the separately required background conditions hold. Including $\eta = 0$ here means adjoining the infinite-tension boundary, not adding a finite-tension model.

For each mesh, let $F_n \subset K$ consist of the parameters admitting a positive absolutely continuous rate with $0 \leq \chi \leq 1$, a density agreeing with $f_\eta(R)$ at every mesh node, and the prescribed adjacent sound means. Between nodes the candidate residual need not equal the true residual. All constraints are imposed on one history.

Theorem F.4 — Contraction of the compatible sets. Suppose the largest cell width δ_n tends to zero and the residual samples are exact. Every prescribed adjacent-mean interval is assumed to contain the true mean and to have width at most ϵ_n, where $\epsilon_n \to 0$. Then

$$¿_{\eta \in F_n} |\eta - \eta_¿| \to 0. \tag{F.15}$$

The compatible sets contain the true parameter under these hypotheses. For nested meshes with exact means, they are nested. No assertion that they are intervals is needed. If a reported mean has a valid symmetric error radius e_n, its

interval has width $2e_n$, so one may take $\epsilon_n = 2e_n$; the interval radius and the candidate-to-truth bound must not be confused.

Proof. Normalize the transport at the left endpoint for this proof:

$$Q_¿(s) = \exp\left[-3(s - s_-) - 3\int_{s_-}^{s} \chi_¿(t)\,dt\right], \qquad Z_¿ = \int_{s_-}^{s_+¿ Q_¿(s)\,ds.¿} ¿ \tag{F.16}$$

This differs from the Chapter 5 normalization only by a constant factor. For any feasible rate q, put $C = q(s_-)$ and

$$\zeta(s) = \log \frac{q(s)}{C\,Q_¿(s)}.$$

Since $\zeta' = -3(\chi - \chi_¿)$, its Lipschitz constant is at most three. Exact adjacent means give $\zeta(s_i) = 0$ at every node. Therefore, within a cell,

$$|\zeta(s)| \le 3\,min\{s - s_i, s_{i+1} - s\} \le \frac{3}{2}\delta_n. \tag{F.17}$$

With mean errors bounded by ϵ_n, summing their integrals first gives $|\zeta(s_i)| \le 3¿$. Taking the nearer endpoint of each cell then gives

$$\|\zeta\|_\infty \le r_n := 3¿ \tag{F.18}$$

The estimate requires no derivative of a measured residual.

For $\eta \in K$, define the positive endpoint drop and the normalized cumulative density drop

$$D_\eta = f_\eta\left(R\left(s_-\right)\right) - f_\eta ¿$$
$$F_\eta(s) = \frac{f_\eta\left(R\left(s_-\right)\right) - f_\eta\left(R(s)\right)}{D_\eta}, \tag{F.19}$$
$$F_Q(s) = \frac{1}{Z_¿}\int_{s_-}^{s} Q_¿(t)\,dt.$$

The denominators are bounded away from zero on K: $R\left(s_-\right) > R¿$, f_η is strictly increasing in R, and K is compact. Matching the endpoint densities determines $C = D_\eta / \int_I Q_¿ e^\zeta$. At every mesh node, matching the other densities consequently gives

$$F_\eta\left(s_i\right) = \frac{\int_{s_-}^{s_i} Q_¿(t) e^{\zeta(t)}\,dt}{\int_{s_-}^{s_{+¿}} Q_¿(t) e^{\zeta(t)}\,dt}. ¿ \tag{F.20}$$

The bounds $e^{-r_n} \le e^\zeta \le e^{r_n}$ imply

$$\left|F_\eta\left(s_i\right) - F_Q\left(s_i\right)\right| \le e^{2r_n} - 1. \tag{F.21}$$

Moreover, $F_\eta(s)$ is jointly continuous on the compact set $K \times I$; this follows from continuity of R, f_η, and the positive lower bound on D_η. Thus this family is uniformly equicontinuous. If ω_K is a common modulus of continuity for the F_η, and ω_Q is one for F_Q, then Equation F.21 extends between the nodes:

$$\begin{aligned} &\| F_\eta - F_Q \|_\infty \\ &\le e^{2r_n} - 1 + \omega_K(\delta_n) + \omega_Q(\delta_n) \to 0 \end{aligned} \tag{F.22}$$

uniformly over feasible η.

It remains to prove that $F_\eta = F_Q$ selects one parameter. The true density also has normalized drop F_Q. Such an equality therefore implies $f_\eta(R) = a_0 + k\, v_{¿}$ for a constant a_0 and $k = D_\eta / D_{\eta_{¿}} > 0$. Substitution into the common residual gives a polynomial identity on the nontrivial interval of values visited by $v_{¿}$. Its coefficients obey

$$a_0 + \eta\, a_0^2 = 0,\; k\left(1 + 2\eta\, a_0\right) = 1,\; \eta\, k^2 = \eta_{¿}. \tag{F.23}$$

If $\eta = 0$, these equations give $a_0 = 0, k = 1, \eta_{¿} = 0$. If $\eta > 0$, the alternative $a_0 = -1/\eta$ would require $-k = 1$, contradicting $k > 0$. Hence $a_0 = 0, k = 1, \eta = \eta_{¿}$ in every case.

If Equation F.15 failed, compactness of K would provide a sequence of feasible parameters bounded away from $\eta_{¿}$, with a subsequence converging to some $\acute{\eta} \neq \eta_{¿}$. Joint continuity and Equation F.22 would imply $F_{\acute{\eta}} = F_Q$, contradicting Equation F.23. For nested exact meshes, each coarser mean is a length-weighted average of the finer means, so every fine-mesh history also satisfies the coarse constraints. This proves the nesting statement. ▫

This is a consistency theorem within a fixed model and a fixed compact parameter search. It supplies neither a universal convergence rate in η nor a finite-sample confidence level. In particular, it does not permit b, u, or d to change with the mesh, and it does not address residual errors that remain nonzero.

Proposition F.5 — A fixed sound error can preserve an interval of parameters. Assume additionally that $R \in C^2(I)$, $R' < 0$, the true sound lies in $[m, 1-m]$ for some $m > 0$, and K contains an open interval around $\eta_{¿}$ on which the other physical inequalities are strict. On every mesh, use mean intervals centered on the true means with a fixed half-width

$\epsilon>0$, intersected with $[0,1]$. A nontrivial neighborhood of $\eta_{¿}$ then remains compatible on every mesh.

Proof. For the complete candidate curve $v_{\eta}=f_{\eta}(R)$, Equation 4.8 gives

$$\chi_{\eta}=-1-\frac{R''}{3R'}+\frac{2\eta R'}{3(1+4\eta R)}. \tag{F.24}$$

On a sufficiently small compact neighborhood of $\eta_{¿}$, this function is jointly continuous in η, s and therefore converges uniformly to $\chi_{¿}$ as $\eta \to \eta_{¿}$. Choose the neighborhood so that $\| \chi_{\eta}-\chi_{¿} \|_{\infty}<min\{\epsilon, m/2\}$ and all other physical inequalities persist. Each such candidate reproduces the residual at every epoch, has a positive sound margin, and has every window mean within the tolerance. The same neighborhood therefore survives every mesh. ▫

The proposition is an existence statement for an interior class. It does not claim that every fixed error model, boundary history, or additional observation leaves the same ambiguity.

F.5. A minimal calibration of the free-vacuum orbit

Theorem 6.1 writes every allowed representative as

$$v_C(s)=\frac{C(\beta_1-C)}{2\beta_2}+C\,J(s),$$
$$0<C<C_{max}.$$

Proposition F.6 — One calibrated density difference suffices. With the identified coefficients and the sound history fixed, one absolutely calibrated difference $D=v(s_a)-v(s_b)$ at $s_a<s_b$ determines at most one representative:

$$A_{ab}=J(s_a)-J(s_b)=\int_{s_a}^{s_b} Q(s)\,ds>0,$$
$$C=\frac{D}{A_{ab}}. \tag{F.25}$$

The separate absolute values of the two densities are unnecessary for selecting C. A common unknown additive offset cancels. A common unknown multiplicative gain does not.

Proof. Subtract the two expressions for v_C. The constant term cancels, leaving $D=C\,A_{ab}$. Positivity of Q makes $A_{ab}>0$. The identified coefficients then fix V_C,η_C,b_C through Equation 6.3. A candidate outside $0<C<C_{max}$, or inconsistent with other data, is rejected rather than replaced by another branch. ▫

For rectangular deterministic enclosures $0\le D_-\le D\le D_{+¿¿}$ and $0<A_-\le A_{ab}\le A_{+¿¿}$, the guaranteed outer interval is

$$\frac{D_-}{A_{+¿}}\le C\le\frac{D_{+¿}}{A_-}.¿¿ \tag{F.26}$$

These bounds are attained over the rectangle itself. Correlations with the expansion fit, or additional physical restrictions, can make its projection smaller. An uncertain physical conversion from density to v belongs in the same joint enclosure.

If the Chapter 5 normalization is used and a valid uniform bound $|\hat{\chi}-\chi|\le\varepsilon_\chi$ holds between the reference epoch zero and both anchors, then, with $R_s=max\{|s_a|,|s_b|\}$,

$$\hat{A}_{ab}e^{-3\varepsilon_\chi R_s}\le A_{ab}\le\hat{A}_{ab}e^{3\varepsilon_\chi R_s}. \tag{F.27}$$

This follows by bounding the integrated sound error in the exponential defining Q, then integrating the resulting positive

functions. It gives one explicit way to propagate sound uncertainty into Equation F.26. It does not turn a fitted sound curve without a valid error bound into calibrated data.

F.6. Finite-error certification of the geometric invariant

The free-vacuum invariant is

$$L=\frac{\beta_1^2}{4\beta_2}-\beta_0,\beta_2>0. \tag{F.28}$$

Its first differential is

$$\begin{aligned} dL=&-d\beta_0+\frac{\beta_1}{2\beta_2}d\beta_1\\ &-\frac{\beta_1^2}{4\beta_2^2}d\beta_2. \end{aligned} \tag{F.29}$$

This expression supports local sensitivity calculations, but a first-order approximation can be inadequate when L is small or the uncertainty approaches $\beta_2=0$. The following enclosure remains valid for finite errors.

Proposition F.7 — An exact rectangular enclosure. Suppose $\beta_i\in\left[l_i,u_i\right]$ for $i=0,1,2$, with $l_2>0$. Define

$$\begin{aligned} q_{min}&=dist\left(0,\left[l_1,u_1\right]\right)^2,\\ q_{max}&=max\left\{l_1^2,u_1^2\right\}. \end{aligned}$$

The minimum and maximum of L over this rectangle are

$$\begin{aligned} L_-&=\frac{q_{min}}{4u_2}-u_0,\\ L_{+¿=\frac{q_{max}}{4l_2}-l_0.¿}& \end{aligned} \tag{F.30}$$

If L_->0, the whole rectangle lies on the AdS side and, at supplied exact S>0,

¿¿ (F.31)

Proof. The square of β_1 has the stated extrema on its interval. Division by positive β_2 decreases the quotient as β_2 increases; subtracting β_0 decreases it as β_0 increases. The independent endpoint choices attain Equation F.30. The map $L \mapsto (SL)^{-1/2}$ is decreasing for $L>0$, proving Equation F.31. ▫

If $L_- \le 0 < L_{+¿¿}$, the rectangle alone does not certify a finite upper bound on ℓ: its positive-L part approaches zero. A correlated joint set or further physical constraints might remove that approach and must be examined directly. If $L_{+¿\le 0¿}$, the rectangle contains no model on the stated AdS branch. If the enclosure reaches $\beta_2 = 0$, Proposition F.7 is inapplicable and the full nonlinear identified set must be retained.

The example in Equation 6.16 illustrates the cancellation:

$$L = 9.576533333\ldots - 9.5632 = \frac{1}{75}. \tag{F.32}$$

A one-percent change of β_0 alone changes L by 0.095632, over seven times its reference value. This is a perturbation of a constructed coefficient example, not an observational error model. A covariance can constrain different directions much more strongly than a rectangle. The example shows why exact rank and a fixed algebraic invariant do not by themselves establish a precise AdS radius.

All the enclosures in this appendix are deterministic. They acquire a confidence interpretation only when the joint input event has the stated coverage, as in Chapter 9. Finally, a certificate for L and ℓ does not certify a bulk mass in absolute units: the coordinate convention for μ_B, the value of G_5, and the spatial-volume convention remain separate requirements.

Glossary

Action normalization. The overall scale multiplying an action. A constant positive scale leaves classical stationary equations unchanged but need not leave quantum predictions unchanged at fixed $\hbar$.

AdS radius. The length ℓ setting the negative bulk curvature in the stated Einstein-bulk model.

Anchor. An independent matter value or difference used to constrain a reconstruction family. Its units and calibration are part of the input.

Barotropic fluid. A fluid with pressure specified as a function of its density on the relevant branch. Additional entropy or anisotropic-stress degrees of freedom require a broader description.

Bulk. The higher-dimensional spacetime in which the brane is embedded.

Calibration drift. An allowed change of a measurement gain across epochs, restricted here by a stated Lipschitz bound on log gain.

Classical scaling orbit. A parameter transformation that multiplies the complete specified action by one positive constant.

Common history. A single matter evolution satisfying all finite values, windows, conservation and calibration restrictions together.

Conditional inverse. A reconstruction made while declared nuisance parameters or background terms are held fixed.

Confidence region. A random set whose repeated-sampling coverage is guaranteed under a stated observation experiment and model class.

Dark radiation. The a^{-4} term induced by the geometric bulk mass coefficient in the homogeneous background; the name does not identify it with a measured thermal species.

Effective vacuum. The constant term in the chosen background Friedmann representation after its convention has been stated.

Enthalpy density. The sum of density and pressure; it determines the density decline under conservation in an expanding universe.

Equivalence class. A collection of distinct parameter descriptions yielding the same declared information. Equivalence is always relative to what is observed and to the model.

Identifiability. Uniqueness of a target quantity from ideal information within a declared class. It is distinct from the precision attainable with finite noisy data.

Information projection. Removal of nuisance directions from a local signal derivative using the specified noise metric.

Kinetic completion. A scalar pressure Lagrangian constructed to realize a specified conserved barotropic history on its visited kinetic interval.

Leakage. A residual projection of an allowed primary signal into a selected space used to search for an additional component.

Local stability. Positivity of the relevant quadratic kinetic and gradient coefficients on a specified background; it does not establish all-sector stability.

Look-elsewhere effect. The change in a test's null behavior when a frequency or other parameter is selected by a search over the data.

Outer confidence set. A set guaranteed to include the target identified set on a common coverage event, possibly also including points excluded by a sharper joint model.

Physical mass. A mass obtained after fixing the gravitational normalization, distinct from a metric's geometric mass coefficient.

Point identification. Identification of one value, in contrast to identification of a nontrivial set or continuous family.

Riccati exception. The classified sound histories for which the dark-radiation function belongs to the quadratic span of the sound coordinate.

Selection. A data-dependent choice of a frequency, direction or model component. Its use in later inference requires an appropriate calibration.

Sound coordinate. The integrated transport function J that turns a conserved density into the affine form $v = V + C\,J$.

Sound window. A specified average of the sound history over an interval, including the coordinate and weighting used in the average.

Split brane tension. The constant assigned to the brane term separately from a constant matter vacuum in a chosen decomposition.

Structural rank. Independence of the design functions or columns in exact arithmetic, without a claim about their numerical conditioning.

Total vacuum stress. The sum of the split brane constant and constant matter vacuum; this sum enters the vacuum-subtracted background normalization.

Training and validation. Independent data blocks used respectively to select a target and to perform a calibrated check of it.

Uniform coverage. A probability guarantee applying throughout the declared parameter or function class; it depends on every stated bound being valid.

Vacuum subtraction. Rewriting the stress as a constant vacuum contribution plus excitations, with the resulting background coefficients transformed consistently.

Window blind spot. A frequency at which a measurement window has zero response. Several windows can reduce exact blind spots without ensuring stability at every frequency.

Terms Added in the Third Edition

Certificate. A finite mathematical or numerical object whose checked conditions establish a specified witness, exclusion or bound. Its assumptions and numerical error treatment are part of the claim.

Coefficient polytope. A compact convex region specified by finitely many vertices or linear inequalities. Correlations in this region can be lost by replacing it with separate coordinate intervals.

Finite-grid inversion. A set of accepted parameter values on an explicitly enumerated grid, obtained by inverting tests at those values. It is not automatically a continuous interval.

Frozen procedure. A fully specified observation-to-statistic and decision rule held fixed for the probability statement being

made. Choosing it using the same data requires separate selection reasoning.

Mahalanobis separation. The distance between mean predictions in the metric of a declared positive-definite covariance. It has a testing interpretation only under the accompanying distributional assumptions.

Observable equivalence. Equality of the probability laws generated by the complete specified observation maps, including calibrations and noise. Equality of background expansion alone is a weaker condition.

Transverse calibration. A measurement whose prediction changes along a remaining coefficient null direction. Here transverse describes the algebraic direction; a transverse astronomical distance can be one physical source of such information.

Unresolved certificate. A retained computational case for which the executed necessary tests and witness search establish neither existence nor exclusion. It is not an accepted model.

References

The supplied research manuscripts are distinguished below from published primary literature. Existing reference numbers are retained. References 46–50 document the distance-analysis revision; references 51–58 document the related-literature, information-splitting and boundary-calibration additions.

[1] Geodesic triangles as curvature probes in relativity and braneworld cosmology. Unpublished research manuscript, Series I, Paper I, 30 September 2026.

[2] Geodesic curvature and finite epoch consistency tests in braneworld cosmology. Unpublished research manuscript, Series I, Paper II, 30 September 2026.

[3] Identifiable Bulk Geometry with Uncertain Brane Vacuum Energy: Exact equivalence classes and limits of cosmological reconstruction. Unpublished research manuscript, research draft for independent assessment, 9 October 2026.

[4] Dynamical Completion and Observational Limits of Identifiable Bulk Geometry: Gates 1 and 2 on Action Normalization and Dynamical Consistency. Unpublished research manuscript, first research memorandum for independent assessment, 9 October 2026.

[5] From curvature measurements to brane and bulk black hole identification: A unified framework of data assumptions and inference limits. Unpublished research manuscript, Series I, Paper XII, 30 September 2026.

[6] From Logarithmic Sound Modulation to Calibrated Braneworld Inference: Synthesis of Series II Papers I to XI. Unpublished research manuscript, Series II, Paper XII, version 1.0, 9 October 2026.

[7] T. Shiromizu, K. Maeda, and M. Sasaki (2000). The Einstein Equations on the 3-Brane World. Physical Review D 62, 024012. DOI: https://doi.org/10.1103/PhysRevD.62.024012; arXiv: https://arxiv.org/abs/gr-qc/9910076

[8] P. Binétruy, C. Deffayet, U. Ellwanger, and D. Langlois (2000). Brane cosmological evolution in a bulk with cosmological constant. Physics Letters B 477, 285–291. DOI: https://doi.org/10.1016/S0370-2693(00)00204-5; arXiv: https://arxiv.org/abs/hep-th/9910219

[9] P. Kraus (1999). Dynamics of Anti-de Sitter Domain Walls. Journal of High Energy Physics 1999(12), 011. DOI: https://doi.org/10.1088/1126-6708/1999/12/011; arXiv: https://arxiv.org/abs/hep-th/9910149

[10] Sharp brane tension bounds under bounded density calibration drift. Unpublished research manuscript, Series I, Paper IV, 30 September 2026.

[11] Finite epoch reconstruction of barotropic brane cosmologies: Exact common curve tests with uncertain density calibration. Unpublished research manuscript, Series I, Paper VI, 30 September 2026.

[12] Density calibration and brane tension reconstruction from cosmological geometry. Unpublished research manuscript, Series I, Paper III, 30 September 2026.

[13] Matter stability and sound speed constraints on brane tension: A conditional extension of four companion studies. Unpublished research manuscript, Series I, Paper V, 30 September 2026.

[14] D. Langlois, R. Maartens, M. Sasaki, and D. Wands (2001). Large-scale cosmological perturbations on the brane. Physical Review D 63, 084009. DOI: https://doi.org/10.1103/PhysRevD.63.084009; arXiv: https://arxiv.org/abs/hep-th/0012044

[15] Finite window sound constraints in brane cosmology: Global consistency and sharp tension bounds. Unpublished research manuscript, Series I, Paper IX, 30 September 2026.

[16] Smooth scalar completions of finite epoch brane cosmologies: Sound margins, exact interpolation, and limits of identification. Unpublished research manuscript, Series I, Paper VII, 30 September 2026.

[17] Sound data and regularity in brane cosmology: No-go interpolation and sharp tension intervals from three epochs. Unpublished research manuscript, Series I, Paper VIII, 30 September 2026.

[18] Brane tension and bulk black hole identifiability: Exact degeneracies and reconstruction from cosmological sound data. Unpublished research manuscript, Series I, Paper X, 30 September 2026.

[19] Identifying bulk black holes from cosmological sound data: Complete degeneracy classification and weak reconstruction in brane cosmology. Unpublished research manuscript, Series I, Paper XI, 30 September 2026.

[20] Confidence Sets for Brane Tension and Bulk Mass under Sound Uncertainty: Calibrated inverse inference and separation from cosmological degeneracy. Unpublished research manuscript, Series II, Paper XI, version 1.0, 9 October 2026.

[21] Golden Ratio Modulation in Braneworld Cosmology: Sound dynamics and identification inspired by rolled geometry. Unpublished research manuscript, Series II, Paper I, version 1.0, 1 October 2026.

[22] Testing Multiple Sound Modes in Braneworld Cosmology: Three averaging widths and the limits of gravitational reconstruction. Unpublished research manuscript, Series II, Paper III, version 1.0, 1 October 2026.

[23] Recovering Logarithmic Sound Modulation in Braneworld Cosmology: Paired window measurements, unknown frequency and parameter stability. Unpublished research manuscript, Series II, Paper II, version 1.0, 1 October 2026.

[24] Designing Sound Windows for Braneworld Reconstruction: Hidden modes finite frequency bounds and the role of the golden ratio. Unpublished research manuscript, Series II, Paper IV, version 1.0, 1 October 2026.

[25] Joint Sound and Expansion Reconstruction in Braneworld Cosmology: Hidden modes nuisance parameters and limits of local recovery. Unpublished research manuscript, Series II, Paper V, version 1.0, 8 October 2026.

[26] Unknown Sound Frequencies in Braneworld Reconstruction: Local information weak modes and calibrated frequency searches. Unpublished research manuscript, Series II, Paper VI, version 1.0, 8 October 2026.

[27] Calibrating Nonlinear Mode Searches in Braneworld Cosmology: Monte Carlo tests, nuisance envelopes and limits of detection. Unpublished research manuscript, Series II, Paper VII, version 1.0, 8 October 2026.

[28] Validating Selected Sound Modes in Braneworld Cosmology: Gaussian information splitting and exact tests with unknown nuisance parameters. Unpublished research manuscript, Series II, Paper VIII, version 1.0, 8 October 2026.

[29] Testing Sound Modes with an Uncertain Primary Frequency in Braneworld Cosmology: Derivative projection and analytical bounds over a continuous frequency interval. Unpublished research manuscript, Series II, Paper IX, version 1.0, 8 October 2026.

[30] Validating Sound Modes with Unknown Covariance in Braneworld Cosmology: Replicated measurements and nuisance adjusted Hotelling inference. Unpublished research manuscript, Series II, Paper X, version 1.0, 8 October 2026.

[31] L. Randall and R. Sundrum (1999). An Alternative to Compactification. Physical Review Letters 83, 4690–4693. DOI: https://doi.org/10.1103/PhysRevLett.83.4690; arXiv: https://arxiv.org/abs/hep-th/9906064

[32] J. Garriga and V. F. Mukhanov (1999). Perturbations in k-inflation. Physics Letters B 458, 219–225. DOI: https://doi.org/10.1016/S0370-2693(99)00602-4; arXiv: https://arxiv.org/abs/hep-th/9904176

[33] F. Arroja and M. Sasaki (2010). A note on the equivalence of a barotropic perfect fluid with a k-essence scalar field. Physical Review D 81, 107301. DOI: https://doi.org/10.1103/PhysRevD.81.107301; arXiv: https://arxiv.org/abs/1002.1376

[34] C. Quercellini, M. Bruni, and A. Balbi (2007). Affine equation of state from quintessence and k-essence fields. Classical and Quantum Gravity 24, 5413–5426. DOI: https://doi.org/10.1088/0264-9381/24/22/006; arXiv: https://arxiv.org/abs/0706.3667

[35] D. Perković and H. Štefančić (2021). Purely kinetic k-essence description of $c_s^2(w)$ barotropic fluid models. Physics of the Dark Universe 32, 100827. DOI: https://doi.org/10.1016/j.dark.2021.100827; arXiv: https://arxiv.org/abs/2009.08680v4

[36] P. Brax, J. A. R. Cembranos, and P. Valageas (2020). K-essence scalar dark matter solitons around supermassive black holes. Physical Review D 101, 063510. DOI: https://doi.org/10.1103/PhysRevD.101.063510; arXiv: https://arxiv.org/abs/2001.06873

[37] J. G. Lee, E. G. Adelberger, T. S. Cook, S. M. Fleischer, and B. R. Heckel (2020). New Test of the Gravitational $1/r^2$ Law at Separations down to 52 μm. Physical Review Letters 124, 101101. DOI: https://doi.org/10.1103/PhysRevLett.124.101101; arXiv: https://arxiv.org/abs/2002.11761

[38] R. Allahverdi, A. Mazumdar, and A. Pérez-Lorenzana (2001). Final reheating temperature on a single brane. Physics Letters B 516, 431–438. DOI: https://doi.org/10.1016/S0370-2693(01)00967-4; arXiv: https://arxiv.org/abs/hep-ph/0105125

[39] L. Á. Gergely (2008). Friedmann branes with variable tension. Physical Review D 78, 084006. DOI: https://doi.org/10.1103/PhysRevD.78.084006; arXiv: https://arxiv.org/abs/0806.3857

[40] From Curvature to Nonmetricity: An Operational Finite-Reference Clock–Lensing–Dynamics Reconstruction in Massive Scalar–Tensor Gravity. Unpublished research manuscript, submission-oriented revision, version 6, 3 October 2026.

[41] J. Garriga and T. Tanaka (2000). Gravity in the Randall-Sundrum Brane World. Physical Review Letters 84, 2778–2781. DOI: https://doi.org/10.1103/PhysRevLett.84.2778; arXiv: https://arxiv.org/abs/hep-th/9911055

[42] J. Ke, J. Luo, Q. Li, Y.-J. Tan, and C.-G. Shao (2026). Testing the equivalence principle with lunar laser ranging residuals from different planetary and lunar ephemerides. Physical Review D 114, 084008. DOI: https://doi.org/10.1103/94kl-p7dd; arXiv: https://arxiv.org/abs/2609.15303v1

[43] DESI Collaboration (2025). DESI DR2 Results II: Measurements of Baryon Acoustic Oscillations and Cosmological Constraints. Physical Review D 112, 083515. DOI: https://doi.org/10.1103/tr6y-kpc6; arXiv: https://arxiv.org/abs/2503.14738v3

[44] A. Schärer, R. Angélil, R. Bondarescu, P. Jetzer, and A. Lundgren (2014). Testing scalar-tensor theories and PPN parameters in Earth orbit. Physical Review D 90, 123005. DOI: https://doi.org/10.1103/PhysRevD.90.123005; arXiv: https://arxiv.org/abs/1410.7914

[45] J. S. Read, B. D. Lackey, B. J. Owen, and J. L. Friedman (2009). Constraints on a phenomenologically parameterized neutron-star equation of state. Physical Review D 79, 124032. DOI: https://doi.org/10.1103/PhysRevD.79.124032; arXiv: https://arxiv.org/abs/0812.2163

[46] D. Brout et al. (2022). The Pantheon+ Analysis: Cosmological Constraints. Astrophysical Journal 938, 110. DOI: https://doi.org/10.3847/1538-4357/ac8e04; arXiv: https://arxiv.org/abs/2202.04077

[47] Cobaya BAO data repository. DESI DR2 Gaussian BAO means and covariance, desi_bao_dr2 directory. Commit bb0c1c9009dc76d1391300e169e8df38fd1096db. Retrieved 10 October 2026. https://github.com/CobayaSampler/bao_data

[48] Pantheon+ and SH0ES Data Release. Distance table, statistical-plus-systematic covariance and SN-only likelihood code. Commit c447f0fea703fcd0fff57de5000947b5ca81286b. Retrieved 10 October 2026. https://github.com/PantheonPlusSH0ES/DataRelease

[49] M. P. Dąbrowski, W. Godłowski, and M. Szydłowski (2004). Brane universes tested by supernovae. International Journal of Modern Physics D 13, 1669–1702. DOI: https://doi.org/10.1142/S0218271804005213; arXiv: https://arxiv.org/abs/astro-ph/0210156v2. Cited as prior work on distance tests, without adopting its historical numerical constraints.

[50] J. D. Bratt, A. C. Gault, R. J. Scherrer, and T. P. Walker (2002). Big Bang Nucleosynthesis Constraints on Brane Cosmologies. Physics Letters B 546, 19–22. DOI: https://doi.org/10.1016/S0370-2693(02)02637-0; arXiv: https://arxiv.org/abs/astro-ph/0208133v2.

[51] M. Kunz (2009). The dark degeneracy: On the number and nature of dark components. Physical Review D 80, 123001. DOI: https://doi.org/10.1103/PhysRevD.80.123001; arXiv: https://arxiv.org/abs/astro-ph/0702615

[52] J. Leiner, B. Duan, L. Wasserman, and A. Ramdas (2025). Data Fission: Splitting a Single Data Point. Journal of the American Statistical Association 120(549), 135–146. DOI: https://doi.org/10.1080/01621459.2023.2270748; arXiv: https://arxiv.org/abs/2112.11079

[53] A. R. Liddle and A. N. Taylor (2002). Inflaton potential reconstruction in the braneworld scenario. Physical Review D 65, 041301. DOI: https://doi.org/10.1103/PhysRevD.65.041301; arXiv: https://arxiv.org/abs/astro-ph/0109412

[54] M. Kunz and D. Sapone (2007). Dark Energy versus Modified Gravity. Physical Review Letters 98, 121301. DOI: https://doi.org/10.1103/PhysRevLett.98.121301; arXiv: https://arxiv.org/abs/astro-ph/0612452

[55] D. García Rasines and G. A. Young (2023). Splitting strategies for post-selection inference. Biometrika 110(3), 597–614. DOI: https://doi.org/10.1093/biomet/asac070; arXiv: https://arxiv.org/abs/2102.02159

[56] S. G. Self and K.-Y. Liang (1987). Asymptotic Properties of Maximum Likelihood Estimators and Likelihood Ratio Tests under Nonstandard Conditions. Journal of the American Statistical Association 82(398), 605–610. DOI: https://doi.org/10.1080/01621459.1987.10478472

[57] H. Chernoff (1954). On the Distribution of the Likelihood Ratio. The Annals of Mathematical Statistics 25(3), 573–578. DOI: https://doi.org/10.1214/aoms/1177728725

[58] L. P. Chimento and M. G. Richarte (2011). k-essence and tachyons in braneworld cosmology. International Journal of Modern Physics D 20(9), 1705–1712. DOI: https://doi.org/10.1142/S0218271811019736; arXiv: https://arxiv.org/abs/0905.3780

[59] J.-M. Dufour, Monte Carlo tests with nuisance parameters: A general approach to finite-sample inference and nonstandard asymptotics, Journal of Econometrics 133 (2006), 443–477. DOI: https://doi.org/10.1016/j.jeconom.2005.06.007

[60] G. Cowan, K. Cranmer, E. Gross and O. Vitells, Asymptotic formulae for likelihood-based tests of new physics, European Physical Journal C 71 (2011), 1554; corrected arXiv:1007.1727v3 (2013). DOI: https://doi.org/10.1140/epjc/s10052-011-1554-0; arXiv: https://arxiv.org/abs/1007.1727

[61] C. J. Clopper and E. S. Pearson, The use of confidence or fiducial limits illustrated in the case of the binomial, Biometrika 26 (1934), 404–413. DOI: https://doi.org/10.1093/biomet/26.4.404

[62] B. Phipson and G. K. Smyth, Permutation p-values should never be zero: Calculating exact p-values when permutations are randomly drawn, Statistical Applications in Genetics and Molecular Biology 9 (2010), Article39. DOI: https://doi.org/10.2202/1544-6115.1585; arXiv: https://arxiv.org/abs/1603.05766

[63] A. Goldenshluger, A. Juditsky, and A. Nemirovski (2015). Hypothesis testing by convex optimization. Electronic Journal of Statistics 9(2), 1645-1712. DOI: https://doi.org/10.1214/15-EJS1054; arXiv: https://arxiv.org/abs/1311.6765

Subject Index

Page numbers refer to the Arabic-numbered text. Entries identify substantive discussions; the glossary also defines the principal terms.

Acceleration....110,147
Action normalization....54,91–92,96,145
AdS radius....12,48,106,239
Anchors, density....29,51,243
BAO distance likelihood....124
Barotropic fluid....8,26,35,97
Brane tension....9,20,35,49,105
Bulk curvature....12,36,49,144
Calibration drift....24–25,242
Canonical kinetic term....100,102
Coefficient polytope....167
Common histories....24,26,34,82,244
Common path certificates....159,163
Confidence regions....21,73,82,84
Conservation....9,26,35,91,112
Covariance estimation....18,73,76
Cubic kinetic law....97–98,146
Curvature calibration....225
Dark radiation....12,37,39,48,85
Density normalization....20,35,48,51
Distance sensitivity....133
Effective vacuum....10,47,84,92,105
Enthalpy....26,35,91
Equivalence classes....48–49,53,144
Finite clock references....247,251
Finite epochs....15,27,39
Finite grid inversion....177
Free spatial curvature....216,218
Frequency recovery....58–59,62,64
Gaussian validation....71,77

Geodesic triangles....2–3
Geometric diameter....170
Geometric mass....12,50,239
Golden ratio....57,61,96
Horizon....13,50
Hotelling calibration....75
Identifiability....6,15,36,47,144
Information projection....17,64
Kinetic completion....31,91,100,145
Kinetic consistency relation....204
Lensing calibration....117,247,250
Lipschitz bounds....26,31,59,81
Local gravity....93,106,115,149
Mahalanobis separation....207–208
Matter calibration....22,24,49,97
Monte Carlo rank tests....177
Nucleosynthesis....109,148,256
Observable equivalence....197,206
Observational data....123
Outer confidence sets....79,82,84
Pantheon supernovae....126
Perturbations....14,98,116,147
Physical mass....50,239,247
Planck scales....9,93,107,239
Positive signal calibration....177
Profile likelihood....126
Quadratic density constraints....126
Rank and conditioning....15,17,39,63,85
Reproducibility archive....258
Riccati exception....35,39,55,57
Scalar–tensor comparison....117–118,247,252
Selection and validation....64,67,70,77
Sharp transport enclosure....161
Short intervals....18,64
Signed alternatives....208

Sixth epoch contrast..... 227
Sound coordinates..... 35,38,57
Sound windows..... 32,57,60,80
Stability..... 26,98,102
Total vacuum stress..... 92,95,105,239
Training data..... 71
Two model accuracy bound..... 170
Ultraviolet control..... 31,104,147
Vacuum split estimation risk..... 202
Vacuum subtraction..... 92–93,105,239
Varying tension..... 12,111,150
Weak reconstruction..... 40,85
Window blind spots..... 61–62
Witness and exclusion..... 163,165

IDENTIFIABLE BULK GEOMETRY

What can cosmic history reveal about hidden geometry?

Cosmological histories can constrain a model while leaving some of its physical parameters undetermined. This book asks which features of a higher-dimensional bulk remain identifiable when matter calibration and vacuum normalization are uncertain.

The third edition adds verified finite-data certificates, positive-signal calibration, tests of observational equivalence and a complete classification with free spatial curvature. Worked examples distinguish mathematical identification from observational evidence and quantify the limits of the inverse.

Nineteen chapters, six appendices, scientific figures, a glossary and a subject index support the analysis. The computational companion includes proofs, code, numerical results and simulation records prepared for this edition.

GEOMETRY / DYNAMICS / LIMITS OF INFERENCE

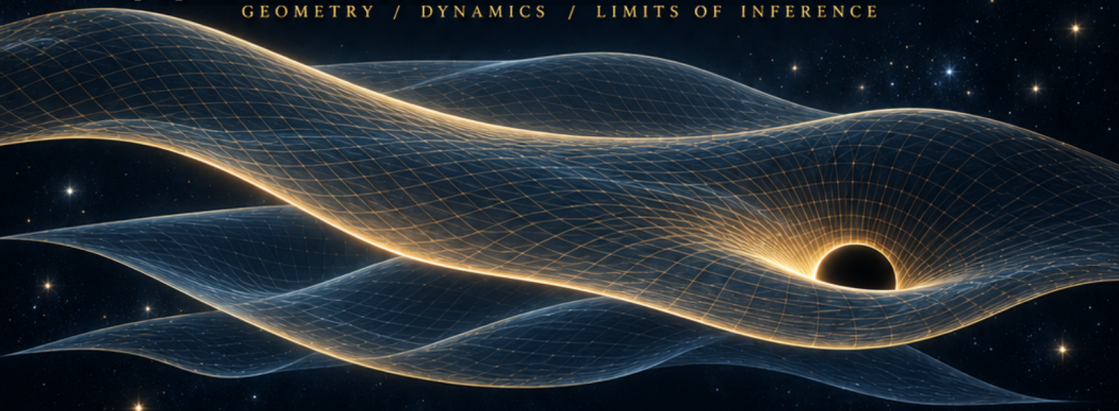

Mohammed F. A. Alghenaim

DATA & CODE

THIRD EDITION • 2026